THE FATIGUE PERFORMANCE OF ADHESIVELY BONDED FIBRE-COMPOSITE JOINTS

by

STEPHEN OLUSEGUN OSIYEMI

A thesis submitted to the University of London for the degree of Doctor of Philosophy and for the diploma of Imperial college

Strength of Materials Section
Department of Mechanical Engineering
Imperial College of Science Technology and Medicine
London SW7 2BX

1992

BIBL. LONDIN. UNIV.

ABSTRACT

This thesis discusses an investigation of the mode I fatigue performance of adhesively bonded fibre-composite joints. Two adhesives were studied. One was "FM73M", a hot-cure rubber-modified epoxy-film adhesive and the other was "9309.3NA", a two-part cold-cure rubber-modified epoxy-paste adhesive. The substrates were "913C XAS-5-47%", a carbon epoxy composite and "APC-2", a carbon PEEK composite.

Firstly, a test method was developed for assessing the fatigue performance of bonded joints. The test method corrects for the problems of inconsistency of fracture energy values obtained from the beam theory method of analysis, compared to values obtained using the "area" and "compliance" methods. Furthermore, the values of the specimen modulus obtained from the "corrected beam theory" are not dependent on the crack length, as was previously observed for the "uncorrected beam theory" analysis. Static test results were generated for use as control data for the fatigue tests. The static test result revealed that mode I fracture energy of the bonded joint using the "FM73M" adhesive is lower (2.93 $\pm$0.08kJ/m^2) than that using "9309.3NA" adhesive (5.7 $\pm$0.2kJ/m^2). It was also found that the thickness of the substrate, as well as the type of substrate has no significant effect on the fracture energy of the adhesive provided there was a cohesive failure through the adhesive layer.

Secondly,the Fatigue test results revealed that the bonded joint using the "FM73M" adhesive performs better than the "9309.3NA" adhesive in fatigue even though the latter has the higher fracture energy. Surface examination using the scanning electron microscopy (SEM), of the fracture surfaces when the locus of failure was cohesive through the adhesive layer revealed that the influence of the mat-carrier in the "FM73M" adhesive is a major factor and is responsible for the good fatigue resistance of the adhesive. Indeed the presence of the mat-carrier may account for the observation that the fatigue performance of this adhesive is superior to that of "9309.3NA" even though the latter has a higher fracture energy than the former. It was also found that the specimen displacement ratio did have a significant influence on the fatigue performance of the joints. However, no dependence is found on the frequency of loading (1Hz - 5Hz), specimen mean displacement (1.5mm - 7.2mm), the composite substrate thickness (24 - 48 plies) and the type of composite substrate used.

Thirdly an investigation into the effect of fatigue cycling in hot/wet environment showed that the adhesives possess good resistance to attack by moisture and that there was negligible hydrolysis of the adhesive at temperatures below 50 °C. However, it was observed that, as the temperature of testing increased towards 50 °C in the hostile environment (distilled water), the interface of the bonded structure was weakened resulting in interlaminar failures being observed.

Finally, a model to predict the service life of bonded components by using the material constants, obtained from fitting empirical equations to the growth rate curves generated from the fatigue tests using DCB bonded joints, has been proposed. Results from the proposed model are in good agreement with experimental results obtained from real bonded structures earlier tested. Also, in order to verify that the material constants obtained from the proposed model are independent of the specimen geometry, and to further test the predictive model, these constants have been successfully used to predict the service life of joints made from a different geometry (i.e single lap joints). The predicted results were also found to be in good agreement with experimental observations.

ACKNOWLEDGMENTS

I am most greatful to my supervisor, Professor A. J. Kinloch, for his sustained encouragement, guidance and advice throughout the duration of this research work. Working with him has tremendously improved my logical approach to science.

I will like to thank my past and present colleagues in the strength of materials section, in particular Dr A. Ivankovic, Maria Chalarambides, B. Blackman, Tom Robinson, Nick Tailor and Hugh MacGillivray for their useful discussions and technical assistance throughout the period of this research.

I will also wish to express my gratitude to the Ministry of Defence for providing funds that were needed to carry out this research work and Dr G. Durtnall for his support and encouragement.

Last, but not the least, I would like to express my indebtedness to all members of my family, in particular my dearest uncle, Professor F. O. Osiyemi on whose idea I embarked on this project and on whose moral guidance I have been able to complete it. This has been a very humbling experience. However, I have no regrets because a humbled man is a very wise man indeed.

it is only a
beginning
always

He opened the book and read from Roosevelt's diary about the death of his first wife: "And when my heart's dearest died, the light went from my life forever."

He closed the book. The room was full of the sound of the weeping, of muffled sobbing. Some people held handkerchiefs to their faces, others clutched their arms, a few held hands. Many were stunned and immobile.

"That was T. R. in his twenties," Nixon said. "He thought the light had gone from his life forever—but he went on. And he not only became president, but as ex-president he served his country always in the arena, tempestuous, strong, sometimes wrong, sometimes right, but he was a man."

He talked about other, similar disappointments—failure to pass the bar exam, the death of someone close, the loss of an election. "We think, as T. R. said, that the light had left his life forever. ***Not true. It is only a beginning always."***

from the book "The Final Days"
by
Bob Woodward
&
Carl Bernstein

CONTENTS

Title Page 1

Abstract 2

Acknowledgment 3

Dedication 4

Contents 5

List of symbols 13

List of Abbreviations 17

CHAPTER ONE : INTRODUCTION 18

1.1 GENERAL 18

1.2 THE AIMS OF THE PROJECT 20

1.3 LAYOUT OF THESIS 22

CHAPTER TWO : FRACTURE MECHANICS: BASIC CONCEPTS 23

2.1 INTRODUCTION 23

2.2 LINEAR ELASTIC FRACTURE MECHANICS (LEFM) 24

2.2.1 Energy Balance Approach 24

2.2.2 Stress Intensity Factor Approach 26

2.2.3 G and K relations 27

2.2.4 Limitations of LEFM 28

2.3 APPLICATION OF LEFM TO DELAMINATION FRACTURE 29

2.4 APPLICATION OF LEFM TO FATIGUE CRACK GROWTH 29
2.4.1 Introduction 29
2.4.2 Fatigue Crack Growth under Constant Amplitude Loading 30
2.4.3 Fatigue Crack Growth under Variable Amplitude Loading 36
2.5 APPLICATION OF LEFM TO FATIGUE CRACK GROWTH IN BONDED JOINTS 38
2.6 CONCLUSIONS 40

CHAPTER THREE : EXPERIMENTAL DETAILS 42
3.1 INTRODUCTION 42
3.2 MATERIALS USED 42
3.2.1 The Composites 42
3.2.2 The Adhesives 44
3.3 SURFACE TREATMENT 44
3.4 MODE I TESTING 45
3.5 SPECIMEN GEOMETRY 45
3.6 PREPARATION OF BONDED DCB JOINT 46
3.7 STATIC TEST EXPERIMENTS 47
3.8 FATIGUE TEST EXPERIMENTS 48
3.9: MEASUREMENT OF THE FATIGUE CRACK LENGTH 49
3.9.1 Travelling Microscope 49
3.9.2 Compliance Method 49
3.9.3 Electrical Potential Method 49
3.9.4 Photographic Method 50
3.9.5 Ultrasonic Scanning Method 50
3.9.6 Discussion of Measurement Techniques 50

3.10 CRACK FRONT CURVATURE IN DCB SPECIMEN 51
3.11 TESTING OF THE JOINTS 53
3.11.1 Constant Crosshead Rate Tests 53
3.11.2 Fatigue Tests 53
3.12 CONCLUDING REMARKS 54

CHAPTER FOUR : CONSTANT RATE OF DISPLACEMENT TESTS 55
4.1 INTRODUCTION 55
4.2 THEORETICAL METHODS FOR CALCULATING G_{1c} 55
4.2.1 'Area' Method 55
4.2.2 'Compliance' Method 56
4.2.3 The 'Beam Theory' Method 58
4.2.3.1 'Load' Method 59
4.2.3.2 'Displacement' Method 60
4.2.3.3 "Corrected Beam Theory" Analyses 61
4.3 RESULTS AND DISCUSSION 64
4.3.1 Introduction 64
4.3.2 Analysis of the DCB Tests 65
4.3.3 Influence of Adhesive Type 69
4.3.4 Influence of the Type and Thickness of the Substrate 70
4.3.5 Reinforcement of the Composite Substrate 73
4.4 CONCLUSIONS 75

CHAPTER FIVE : FATIGUE TESTS CONDUCTED IN AIR 76
5.1 INTRODUCTION 76
5.2 POSSIBLE VARIABLES IN FATIGUE TESTING 76
5.3 METHODS OF PRESENTATION OF FATIGUE DATA 77

5.3.1 Introduction 77
5.3.2 S-N Curves 78
5.3.3 Fatigue Damage Plots 79
5.3.4 G_{max} -N Curves 80
5.3.5 da/dN versus G (or K) Curves 82
5.4 ANALYSIS OF THE FATIGUE EXPERIMENTS 84
5.4.1 Methods of Estimating da/dN 84
5.4.1.1 The Graphical Method 85
5.4.1.2 The Secant Method 85
5.4.1.3 Incremental Polynomial Method 85
5.4.1.4 Discussion of Methods for Estimating da/dN 86
5.4.2 Methods of Estimating G_{max} of an Adhesive in a DCB joint 88
5.5 RESULTS AND DISCUSSION 90
5.5.1 Introduction 90
5.5.2 Effect of Frequency 90
5.5.3 Effect of Displacement Ratio, δ_R 92
5.5.4 Effect of Mean Displacement 94
5.5.5 Comparison of the Fatigue Performance of the Cold Cure Epoxy Paste Adhesive with the Hot Cure Epoxy Film Adhesive 96
5.5.6 Influence of Substrate Thickness and Type 100
5.6 LINEAR REGION II CONSTANTS 103
5.7 THRESHOLD VALUES OF THE MAXIMUM STRAIN ENERGY RELEASE RATE, G_{th} 105
5.8 CONCLUSIONS 106

CHAPTER SIX : FATIGUE TESTING WITHIN A HOSTILE ENVIRONMENT (WATER) 109

6.1 INTRODUCTION 109

6.2 RESULTS AND DISCUSSION 112

6.2.1 Introduction 112

6.2.2 Fatigue Performance of the Cold-Curve Epoxy Paste Adhesive in Water at 25 °C and 50 °C 112

6.2.3 Fatigue Performance of the Hot-Cure Epoxy Film Adhesive in Water at 25 °C and 50 °C 117

6.2.4 Influence of the Substrate Employed on the Fatigue Performance of the Hot-cure Film Adhesive Tested in Dry Air and in Water at 25 °C and 50 °C 120

6.3 CONCLUSIONS 126

CHAPTER SEVEN : SCANNING ELECTRON MICROSCOPY STUDIES 128

7.1 INTRODUCTION 128

7.2 EXPERIMENTAL TECHNIQUE 129

7.3 RESULTS AND DISCUSSION 130

7.3.1 Cold Cure Epoxy Paste Adhesive ("9309.3NA") 130

7.3.2 Hot Cure Epoxy Film Adhesive with a Mat-Carrier 135

7.4 CONCLUSIONS 141

CHAPTER EIGHT : PREDICTION OF THE SERVICE LIFE OF BONDED JOINTS 143

8.1 INTRODUCTION 143

8.1.1 Background 143

8.1.2 Service Life Design Philosophies 144

8.1.3 Selection of Minimum and Maximum Permissible Crack Sizes for the Prediction of Service Life 145

8.1.4 Fatigue Crack Initiation and Propagation Lifetimes 145

8.2 PREDICTION OF THE SERVICE LIFE USING THE CRACK GROWTH RATE MODEL 147

8.3 MODELLING AND PREDICTING THE FATIGUE BEHAVIOUR OF THE DCB JOINTS 148

8.3.1 Adaptation of the Crack Growth Rate Model to the DCB Specimen Geometry 148

8.3.2 Variables Affecting the Compliance Curve of a DCB Joint 151

8.3.3 Modelling the Fatigue Crack Growth Law 155

8.3.3.1 The Hot Cure Epoxy Film Adhesive Bonding the Thermosetting CFRP 155

8.3.3.2 The Cold Cure Epoxy Paste Adhesive Bonding the Thermosetting CFRP 160

8.3.4 Predicting the G_{max} versus N Relationship 161

8.4 THE PREDICTION OF FATIGUE FAILURE IN SINGLE LAP JOINTS 162

8.4.1 Introduction 162

8.4.2 Estimating the Value of $(G_{max})_{SLJ}$ for Single Lap Joints 162

8.4.3 Prediction of the Service Life of Single Lap Joint using the Crack Growth Rate Model 165
8.4.3.1 Introduction 165
8.4.3.2 Estimating the Initial Flaw Size 165
8.4.3.3 Estimating the Final Flaw Size 167
8.4.4 Crack Growth Rate Equations for Predicting the Service Life of Single Lap Joints 168
8.4.5 Experimental Investigation of the Fatigue Performance of Single Lap Joints 169
8.4.6 Comparison of the Experimental Observations from SLJ Tests with the predicted Results 169
8.4.6.1 Predicted Lifetimes Using the Linear Region II Model 170
8.4.6.2 Predictions Using the 'Full Characteristics Model' 171
8.5 FURTHER PREDICTIONS OF THE FATIGUE LIFETIME OF SINGLE LAP JOINTS 173
8.5.1 Introduction 173
8.5.2 Effect of the Overlap Length 173
8.5.3 Effect of Substrate Thickness 175
8.5.4 Effect of Adhesive Thickness 175
8.6 CONCLUSIONS 176

CHAPTER NINE : SUMMARY OF MAIN CONCLUSIONS 179

CHAPTER TEN : PROPOSALS FOR FUTURE WORK 183

APPENDIX 186

Appendix A Experimental data (Static and Fatigue Tests) 187

Appendix B Effective Modulus of a DCB Bonded Joint 211

Appendix C Speed of Water Along the Direction of Crack Propagation 213

Appendix D Estimation of SERR from a Single Lap Joint 216

REFERENCES 220

LIST OF SYMBOLS

a	:	crack length
a_i	:	initial crack length in a DCB joint
a_f	:	final crack length in a DCB joint
a_o	:	intrinsic flaw size
a_{si}	:	initial crack length in a single lap joint
a_{sf}	:	final crack length in a single lap joint
A	:	surface area
B	:	width of specimen
C	:	specimen compliance
D	:	material constant obtained from of the power law used to describe the linear region II part of fatigue crack growth
D_1, D_2	:	constants obtained from fitting empirical equations into regions I and III part of the fatigue crack growth curve
E	:	modulus
E_a	:	modulus of the adhesive
E_f	:	fatigue modulus
E_s	:	modulus of the substrate
E_{11}	:	axial modulus
f	:	frequency
F	:	correction factor required in simple beam analysis method of calculating G_{1c}
G	:	strain energy release rate
G_{1c}	:	fracture energy due to mode I loading

G_{max} : maximum stain energy release rate due to mode I loading

$(G_{max})_{SLJ}$: maximum value of strain energy release rate obtained from loading a single lap joint

G_{th} : threshold value of the maximum strain energy release rate due to mode I loading

ΔG : strain energy release rate range

ΔG_I : strain energy release rate range due to mode I loading

ΔG_{II} : strain energy release rate range due to mode II loading

ΔG_{III} : strain energy release rate range due to mode III loading

ΔG_T : total strain energy release rate range

h : thickness of the substrate

I : second moment of area

K : stress intensity factor

K_{1c} : fracture toughness

K_{max} : maximum value of the stress intensity factor due to fatigue cycling

K_{min} : minimum value of the stress intensity factor due to fatigue cycling

ΔK : stress intensity factor range

n : material constant obtained from of the power law used to describe the linear region II part of fatigue crack growth

N : number of cycles of fatigue testing

N_f : number of cycles to complete failure of specimen

M : bending moment

$P_{critical}$: load required to fracture specimen

P_{1c} : load required to fracture specimen

P : load on specimen

P_{max} : maximum load applied to specimen during fatigue cycling

Q	:	amount of damage due to fatigue loading
R_s	:	stress ratio
S	:	applied stress
T	:	applied load per unit width
t_a	:	thickness of the adhesive
U	:	available elastic energy stored in body
W	:	external work done
W_A	:	thermodynamic work of adhesion
W_{Al}	:	thermodynamic work of adhesion in the presence of a liquid
X	:	flexural rigidity
Y	:	geometric factor
Z	:	correction factor required in simple beam analysis method of calculating G_{1c}
γ	:	surface free energy
γ^D	:	dispersive component of the surface free energy
γ_{lv}	:	surface free energy of a liquid
γ^P	:	polar component of the surface free energy
δ	:	displacement applied to specimen
δ_{max}	:	maximum displacement applied to specimen during fatigue cycling
δ_m	:	mean displacement applied to specimen during fatigue cycling
δ_{min}	:	minimum displacement applied to specimen during fatigue cycling
δ_R	:	displacement ratio
ς	:	half the length of the bonded overlap in a single lap joint
μ	:	Poissons ratio
σ_a	:	tensile strength of the adhesive
σ_{amp}	:	stress amplitude
σ_{ij}	:	component of stress tensor

σ_m : mean stress

σ_{max} : maximum stress applied during fatigue loading

σ_{min} : minimum stress applied during fatigue loading

σ_R : stress ratio

σ_{TS} : mean value of ultimate tensile strength

σ_y : yield stress

$\Delta\sigma$: stress range

χ : correction factor required in simple beam analysis method of calculating G_{1c}

LIST OF ABBREVIATIONS

913C XAS-5-47%	:	carbon fibre/epoxy composite (manufactured by Ciba-Geigy)
9309.3NA	:	two-part cold-cure rubber modified epoxy adhesive
APC-2	:	carbon Fibre/PEEK composite (manufactured by ICI)
ASTM	:	American society for testing and materials
CFRP	:	carbon fibre reinforced plastic
CT	:	compact tension test specimen geometry
DCB	:	double cantilever beam
E - U	:	Uncorrected modulus values (see Equation 4.14)
E - C	:	corrected modulus values (see Equation 4.19)
EPFM	:	elastic plastic fracture mechanics
FM73M	:	one -part hot-cure rubber modified epoxy adhesive
G_c (area)	:	G_{1c} values obtained using the area method (i.e Equ. 4.1)
G_c (comp)	:	G_{1c} values obtained using the compliance method (i.e Equ. 4.3)
Gc - U - L	:	G_{1c} values from the uncorrected load method (i.e Equ. 4.11)
Gc - U - D	:	G_{1c} values from the uncorrected displacement method (i.e Equ. 4.13)
Gc - C - L	:	G_{1c} values from the corrected load method (i.e Equ. 4.15)
Gc - C - D	:	G_{1c} values from the corrected displacement method (i.e Equ. 4.16)
LEFM	:	linear elastic fracture mechanics
NDI	:	non-destructive testing
R.H	:	relative humidity
SEM	:	scanning electron microscope
SERR	:	strain energy release rate
SLJ	:	single lap joint

CHAPTER ONE

INTRODUCTION

1.1 GENERAL

The major industries of most developed nations have been undergoing a dramatic change. The heavy metal production and fabrication industries are being replaced by the light manufacturing industries of electronics, sporting goods, medical disposables, consumer products and similar products. These light manufacturing industries use light metal alloys, plastics and fibre reinforced composites and the traditional use of mechanical joining techniques are often no longer a technical or an economic option. Unfortunately the design engineer in his search for lighter and cheaper structures is often unaware that structural adhesives may be a viable option. Table 1 highlights the advantages of using adhesive bonding in the aircraft, automobile, construction and building industries compared with the traditional methods of joining such as welding, riveting bolting etc.

Table I: Advantages of adhesive bonding

Advantage	Example
A more even stress distribution is attainable (resulting in a high fatigue life)	-helicopter blades
Dissimilar substrates may be joined	-GRP/metal bonding in sports car
Improved appearance of joints	-automobile bonnets
High strength-to-weight ratio may be achieved	-aircraft control surfaces
Reduce points for corrosion to occur	-automobile hemming flange
Fabrication of complex shapes is possible	-aerospace components
Good sealing and insulation properties are possible	-shipping containers

However as with any advancement of technology, there are some disadvantages:

(1) difficulty in disassembling of bonded structures without component damage;

(2) tedious surface preparation techniques are often required for substrates to be bonded;

(3) abnormal inspection problems to determine the integrity of bonded structures;

(4) there is often a lack of information on the durability of bonded joints;

(5) heat and pressure are usually required for curing the adhesive;

The driving force for the development and continual growth of the adhesive market is that the advantages they offer over other traditional joining methods are much greater than their disadvantages. A good example to illustrate this is found in the aircraft industry where Hart-Smith (1985) found that better performance was obtained by replacing rivets with adhesive bonding. It was found that by using adhesive bonding, it was possible to dramatically reduce the number of sites where fatigue cracks could start. As a result, the aircraft became much safer for passengers and the aircraft's weight and maintenance costs were greatly reduced. Lower aircraft weight meant less fuel was required and therefore more passengers could be carried. In another example, (Palmer 1980) showed that a more uniform stress distribution could be achieved by using adhesive bonding. A comparison was made between bomber aircraft test panels constructed from spot-welding, riveting and adhesive bonding. The results showed that adhesive bonding gave a fatigue life about twenty two times greater than spot welding and fifteen times greater than riveting.

Also, from an economic point of view, cost studies justify the use of adhesives. Palmer (1980) showed that in a major commercial aircraft project the cost of a centre engine inlet duct was reduced from $20,000 to $8,000 when a honeycomb bonded assembly was used in place of a riveted one. Apart from this advantage of saving cost, the other reason for their choice of adhesive bonding was a higher fatigue resistance combined with a reduction in weight. Some forward looking companies in the motor industry have been involved in very similar research programmes. One company (Palmer 1980) discovered that by bonding

fibre-glass polyester body of a sports car to a steel frame, it was possible to achieve a better designed structure with a more even stress distribution, a higher fatigue life and reduced production cost. Many examples like those discussed above have tremendously increased the market potential of adhesives, indeed some market research carried out by Chemark Consulting Group Inc. (Broxterman 1989) estimated the 1988 market for adhesives to be more than $550 million and predicted the growth rate to exceed the rate anticipated for the United States GNP by 250% by the 1990s.

1.2 THE AIMS OF THE PROJECT.

Dynamic fatigue is the failure or fracture of a component under repeated or oscillatory loading. The importance of fatigue is that under such fluctuating loads, components fail at stresses much lower than they can withstand under monotonic loading. This is true for all materials and all types of joining methods. It has been established (Bascom 1977) that dynamic fatigue is responsible for at least 75% of in-service failures. Since fatigue failure often gives no warning, it is of paramount importance for designers to have a good understanding of the phenomenon and to prevent its occurrence. Hence, experimental data are usually obtained from test specimens and used as a guide to the most effective methods to improve the fatigue life of components.

The major problems encountered in generating a fatigue data on adhesively bonded joints are (i) the specification of suitable and relevant test methods and (ii) the specification of the in service performance conditions which should not be exceeded if the joint is to meet the required design criteria. In addition, exposure to hot/wet environment can severely affect adhesive joints (Kinloch 1987). It is most likely that when an adhesive joint is subjected to cyclic stresses in a hot/wet environment, then these two conditions can act synergistically to produce an extremely severe test condition.

Therefore, the aims of the present project were:

(1) To develop test methods based upon continuum fracture mechanics approach for assessing the fatigue performance of adhesively-bonded fibre-composite joints.

(2) To use the test method developed to study the effect of test parameters such as frequency, displacement ratio, mean displacement, the type of adhesive and type of substrate, upon the fatigue performance.

(3) To investigate the presence of any minimum fatigue threshold limit below which no fatigue failures would be observed.

(4) To study the effects of fatigue cycling in hot/wet environments

(5) To establish the mechanisms of fatigue damage and environmental attack on the adhesive

(6) To investigate whether it is possible to use the fatigue data generated to predict the lifetime of a bonded component.

(7) The above work should enable both the development of a soundly based quality control test method and a method for quantitatively predicting the lifetime of a bonded component.

1.3 LAYOUT OF THESIS

The thesis is divided into nine main chapters. Chapter Two reviews the application of fracture mechanics concepts to the study of fracture and fatigue. Chapter Three discusses the materials used and the development of a test method for assessing the fatigue performance of bonded joints. Experimental details considered include the specimen geometry, the materials employed, the surface treatment techniques and the techniques for measuring the crack growth rate. Chapters Four, Five and Six discuss the experimental results. In Chapter Four the results from the constant rate of displacement tests are discussed. Chapter Five then discusses the results from the fatigue tests conducted in dry air and Chapter Six discusses the results from the fatigue tests conducted in hot/wet environments. In Chapter Seven the mechanisms of fatigue damage on adhesive joints is described. Chapter Eight is concerned with using the fatigue data which has been generated to predict the lifetime of a bonded joint. Finally Chapter Nine states the main conclusions and outlines recommendations for future work.

CHAPTER TWO

FRACTURE MECHANICS: BASIC CONCEPTS

2.1. INTRODUCTION

Adhesive joints usually fail by the initiation and propagation of flaws (Kinloch 1987). Hence the application of fracture mechanics concepts to adhesive joints has received considerable attention. Several authors (Ewalds 1984, Broek 1986, Kinloch 1983, Williams 1984) have shown that fracture mechanics can be particularly useful for characterising the toughness of materials, identifying the mechanisms of failure and estimating the service life of structures. There are three different modes by which a crack in a solid may be stressed. These are the tensile opening mode (mode I), the shearing mode (mode II) and the tearing mode (mode III) and these are illustrated in Figure 2.1. The three modes may appear in their pure form or in various combinations with one another.

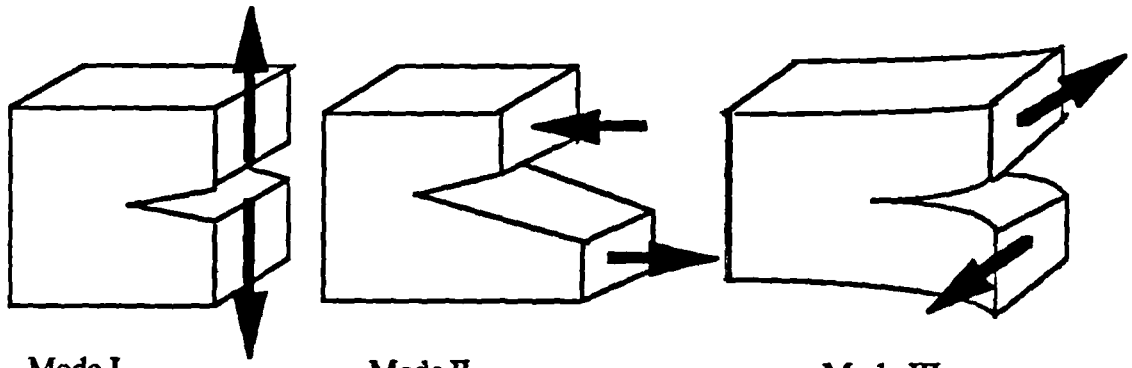


Figure 2.1. An illustration of the three modes of loading

In general, the fracture behaviour of a material is based on the assumption of linear elastic behaviour (LEFM) for a brittle material, elastic-plastic behaviour (EPFM) for relatively ductile (i.e semi-brittle) materials and total plastic collapse for highly ductile materials. For

many polymers, including adhesives and in particular the epoxy based ones which are relatively brittle, the LEFM model has been found (Williams 1984) to describe accurately many experimental observations. There is of course a zone of plastically deformed material in the vicinity of the crack tip, but this is allowable as long as the plastic zone is relatively small compared with the other dimensions of the specimen. The two main approaches to characterising the fracture behaviour of materials are the energy-balance approach and the stress-intensity factor approach. The use of the energy-balance approach has two advantages over the stress-intensity factor approach. Firstly, an unambiguous value of fracture energy, G_{1c}, may be deduced since the stored elastic energy or the potential energy of the loading system can in principle be calculated from any type of test piece while the calculation of the fracture toughness, K_{1c}, is not always straightforward because it requires a knowledge of the geometric factor of the test specimen. Secondly, by using a thermodynamic approach, the value of G_{1c} may be directly related to the intrinsic bonding forces in the material while there is no direct link in the case of K_{1c}. Both approaches are briefly discussed below.

2.2 LINEAR ELASTIC FRACTURE MECHANICS (LEFM)

2.2.1 Energy Balance Approach:

Griffith (1921) laid down the foundations of linear elastic fracture mechanics. He proposed that every engineering material contains a distribution of flaws or imperfections and that failure occurs when the flaw size reaches a critical size. Furthermore, he noted that when a flaw grew in a stressed material there was a decrease in potential energy of the body and so energy was released and available to form the new surfaces of the growing flaw. According to Griffith, a crack would grow when

$$\frac{\partial}{\partial a}(W-U) \geq \gamma \frac{\partial A}{\partial a} \qquad (2.1)$$

where W = external work done

U = available elastic energy stored in the body

γ = surface free energy of the material

∂a = increment in crack growth

∂A = increment in surface area associated with crack growth

For a crack propagating through a laminar of thickness B, the Griffith criterion becomes

$$\frac{\partial}{B\,\partial a}(W - U) \geq 2\gamma \qquad (2.2)$$

Griffith derived his equation for glass which is a very brittle material. Thomas (1953) examined the above criteria with respect to crosslinked polymers and commented that greater energy was usually required to cause crack growth than the free surface energy, 2γ. Two main reasons were suggested for this theory. Firstly, the value of 2γ only reflects the energy required to rupture the secondary bonds, e.g van der waals forces, while the crack growth in polymers generally necessitates the rupture of stronger covalent bonds. Secondly, fracture in most brittle polymers involve localised viscoelastic and/or plastic energy dissipative processes occurring in the vicinity of the crack tip or elsewhere in the specimen. Such mechanisms usually represent the main source of energy absorption in the material during crack growth. Provided the assumptions of LEFM applies, 2γ may be replaced in Equation 2.2 by strain energy release rate, G, which encompasses all the energy losses incurred around the crack tip and therefore is the energy per unit area required per crack growth. Hence the fracture criteria becomes:

$$\frac{\partial}{B\,\partial a}(W - U) \geq G \qquad (2.3)$$

If the cracking of the material is quasi-static (i.e stable), then the value of G becomes equal to its critical value G_{1c} just enough to balance the crack resistance of the material, R. If G > R unstable fracture occurs and if G < R no fracture occurs. G_{1c} is a material property and in this work will be referred to as fracture energy of the material.

2.2.2 Stress-Intensity Factor Approach:

LEFM can also be viewed from another perspective, as an analytical procedure which relates the magnitude and distribution of the stress-field in the vicinity of the crack tip to the normal stress applied to the structure and also the size, shape and orientation of a flaw or any other crack-like discontinuity. Westergaard (1939) developed certain solutions which relate the local stress concentration σ_{ij} to the crack tip applied stress σ_o. He showed that

$$\sigma_{ij} = \sigma_o \left(\frac{a}{2r}\right)^{1/2} f_{ij}(\theta) \qquad (2.4)$$

In which r and θ are the polar coordinates at a point with the crack tip as the origin and 2a is the length of the crack (Figure 2.2). Irwin (1964) modified this solution to give

$$\sigma_{ij} = \frac{K}{(2\pi r)^{1/2}} f_{ij}(\theta) \qquad (2.5)$$

The parameter K is the stress-intensity factor and relates the magnitude of the stress-intensity local to the crack in terms of the applied load and the geometry of the structure in which the crack is located. After further modification the fracture stress σ_c at any cracked body of the material was found to be (Irwin 1964).

$$\sigma_c = \frac{K}{Y\sqrt{a}} \qquad (2.6)$$

where

a = crack length and Y = geometric parameter.

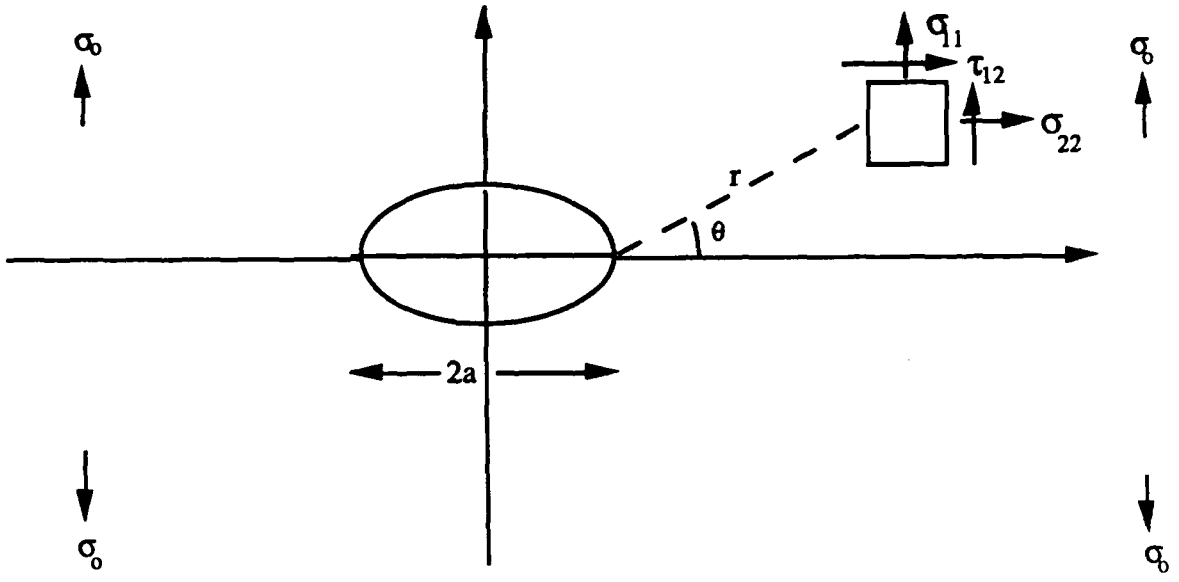


Figure 2.2. Stresses at a point ahead of the crack tip.

2.2.3. G and K relations

The parameter governing fracture may therefore be stated either as a fracture toughness K_{1c} or a fracture energy value G_{1c}. For tensile loading the relationship between K_{1c} and G_{1c} are for plane stress conditions;

$$K_{1c} = (EG_{1c})^{1/2} \tag{2.7}$$

and for plane strain conditions;

$$K_{1c} = \left(\frac{EG_{1c}}{1-\mu^2}\right)^{1/2} \tag{2.8}$$

where μ = Poissons ratio and E = modulus of elasticity of the material

2.2.4. Limitations of LEFM

LEFM can only be applied if the extent of the plasticity at the crack tip is small compared with the test piece dimensions. In addition the test piece must be sufficiently thick so that most of the deformation that occurs at the crack tip is under plane strains conditions. For these LEFM conditions to be met, the ASTM E-399 standard (1981) recommends that:

$$a, B, h \geq 2.5\left(\frac{K_{1c}}{\sigma_y}\right)^2 \tag{2.9}$$

where

K_{1c} = fracture toughness of the material

a = crack length

B = specimen width

h = thickness of the specimen

σ_y = yield stress of the material

Although the ASTM standard was recommended for metals, it has been found by many authors (e.g Williams 1987, Kinloch 1983) to be successful for use in polymers and adhesives.

2.3. APPLICATION OF LEFM TO DELAMINATION FRACTURE

The delamination process in fibre-polymer composites may be regarded as a crack propagation phenomenon and it can be characterised using fracture mechanics concepts. These composites are usually designed to be stiff, elastic materials so that they behave in a linear elastic manner (Williams 1990). Hence one may use LEFM to derive the value of the interlaminar fracture energy, G_{1c}. Several approaches have been developed for estimating the value of G_{1c} for delamination fracture in fibre-polymer composites (e.g Williams 1990). The three most common approaches are referred to as the "area", "compliance" and "beam theory" methods. Basically these approaches are interrelated and are extensions of the fundamental equation for G (i.e Equation 2.3). The three approaches are discussed in full detail in section 4.2.

2.4. APPLICATION OF LEFM TO FATIGUE CRACK GROWTH

2.4.1 Introduction

As was mentioned earlier in section 1.2, failure by fatigue crack growth in materials typically occurs at much lower load levels than they do under monotonic loading. Thus, crack growth occurs at values of K_{1c} and G_{1c} where the latter values are monotonic loading conditions. The cyclic loads are applied repeatedly and can be at constant amplitude or variable amplitude. Although constant amplitude loading does occur in practice the vast majority of structure subjected to fatigue loading actually experience variable amplitude loading that is often fairly random. The next two sections discusses the application of the principles of LEFM to the characterisation of fatigue crack growth under these two forms of repeated loading.

2.4.2 Fatigue Crack Growth under Constant Amplitude Loading.

Historically, it was McEvily et al (1959) who first noticed that the stress at the crack tip had some control over the rate of fatigue crack growth in a material. Much later, Liu et al (1961) noticed that the applied stress range and crack length had effects on the fatigue crack growth rates in materials.

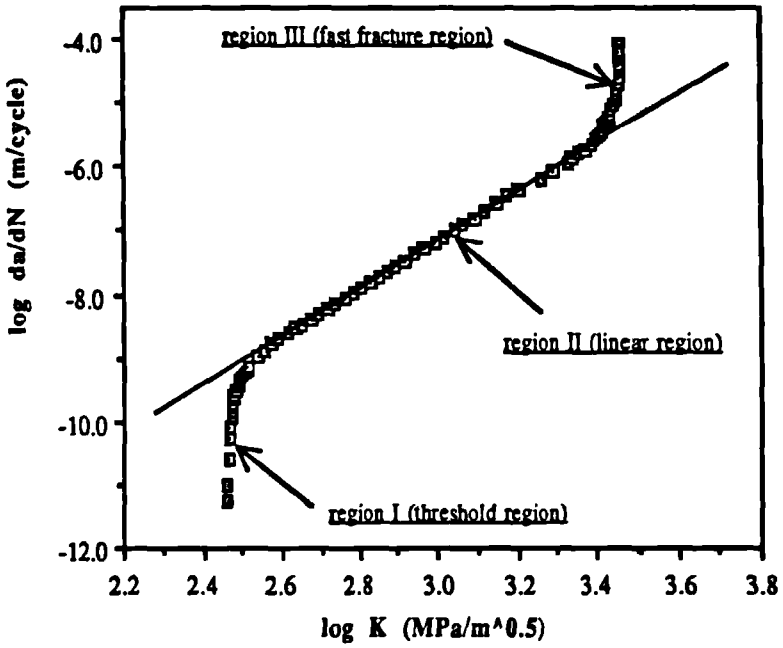


Figure 2.3. Characteristic shape of the plot of log da/dN versus log K.

However, it was Paris and his co-workers (1963) who received the credit for a major breakthrough on an improved method of characterising fatigue crack growth. Paris showed that the crack growth rate in a material could be related to a fracture mechanics parameter, such as the stress-intensity factor which defines the stress field in the zone ahead of the crack tip and controls the fracture process. In most cases for metallic and ceramic materials and components the fatigue data are presented as plots of log (da/dN) against log ΔK. The resulting shape of such a curve is sigmoidal as shown in Figure 2.3. Three regions can be distinguished and are referred to as regions I (the near threshold region), Region II (the linear region) and region III (the near fracture region).

Region I is the region where the crack growth rate decreases rapidly and then ceases or at least becomes negligible. It occurs at relatively low values of ΔK and the curve tends towards an asymptote known as the threshold value of the stress-intensity factor, ΔK_{th}. In recent years, a number of investigators including Paris (1972) and Backlund (1982) have suggested that the threshold value of fatigue crack propagation may be considered as a material property in a similar way to the fracture toughness K_{1c}. Region II of the curve in Figure 2.3 characterises the stable fatigue crack growth region. In this region, there is often a linear relationship (on a logarithmetic plot) between the crack growth rate da/dN and the ΔK. Region III is the region where the crack growth rate increases rapidly to an asymptote as the corresponding maximum stress intensity factor K_{max} increases to become equal to its critical value K_{1c} and the specimen fractures. This region is not very important in the engineering sense since it occurs at a very high crack growth rate and the associated time to failure for this region is negligible in comparison to the total lifetime.

Ever since the shape of the crack growth curve in regions I, II and III had been known, attempts have been made by many authors to describe the curve empirically. Several such empirical crack growth laws exist. In fact there are probably as many growth laws as there are researchers in the field and examples are presented in Table 2.1. The values of the material constants D and n obtained from one empirical equation are usually different from those obtained from another, since these equations are derived from curve-fitting and do not have any physical significance. For this reason, Broek (1989) has recommended that the source of the relevant curve-fitting equation as well as the units of these constants should be specified before quoting the values of D and n as material constants. An indiscriminate use of these material constants without due regard to their source can be very misleading. The differences among the growth laws listed in Table 2.1 are not very large and none of them have any general applicability. Each law may be found reasonably satisfactory in a limited region or a limited set of data. The most widely used crack growth law is Equation 2.10 and it is referred to as the Paris law (1963). Although the Paris law has been found to describe

most of the crack growth data adequately, the law fails to model the deceleration of crack growth to negligible rates which occurs at low values of ΔK (i.e region I) and the acceleration of crack growth that can occur at very high values of ΔK (i.e region III).

Table 2.1. Proposed equations for describing fatigue crack growth.

Equation	Reference	Eqn. no.
$\frac{da}{dN} = D(\Delta K)^n$	(Paris 1963)	(2.10)
$\frac{da}{dN} = D\frac{\Delta K^n}{(1-R)K_c - \Delta K}$	(Forman 1967)	(2.11)
$\frac{da}{dN} = D\frac{\Delta K^4}{K_c^2 - K_{max}^2}$	(Weertman 1966, 1969)	(2.12)
$\frac{da}{dN} = D(\Delta K^n - \Delta K_{th}^n)$	(Klesnil 1972)	(2.13)
$\frac{da}{dN} = D(\Delta K - \Delta K_{th})^2\left(1 + \frac{\Delta K}{K_c - K_{max}}\right)$	(McEvily 1983)	(2.14)
$\frac{da}{dN} = D(K_{max}^2 - K_{min}^2)^n$	(Arad 1971)	(2.15)
$\frac{da}{dN} = DK_{max}^{n_1}\Delta K^{n_2}$	(Walker 1970)	(2.16)
$\frac{da}{dN} = D\left((0.5 + 0.4R_s)\Delta K\right)^n$	(Elber 1971)	(2.17)

where a = crack length

N = the number of cycles

K_{1C} = critical value of stress intensity factor (i.e the fracture toughness)

K_{max} = maximum value of stress intensity factor during fatigue cycling

K_{min} = minimum value of stress intensity factor during fatigue cycling

ΔK = stress intensity factor range (i.e K_{max} - K_{min})

ΔK_{th} = threshold value of stress intensity factor during fatigue cycling

R_s = stress ratio (minimum stress/maximum stress)

and

D, n, n_1 and n_2 are material constants.

As a result, many modifications have been applied to the Paris law to account for these two regions. The most popular modifications were from a standard produced by the Central Electricity Generating Board, (CEGB 1986). The standard recommended that separate expressions could be used to describe growth over these three regions. It was suggested that for the near fracture region (region (III)) where the monotonic loading value of K (i.e K_{1c}) dominates the overall crack growth rate the following equation could be used to describe the crack growth relationship:

$$\frac{da}{dN} = \frac{D(\Delta K)^n}{\left(\frac{K_c}{K_{max}} - 1\right)} \qquad (2.18)$$

For the linear region (region II) the equation proposed was:

$$\frac{da}{dN} = D(\Delta K)^n \qquad (2.19)$$

For the the near threshold region (region I), the equation proposed was:

$$\frac{da}{dN} = D(\Delta K - \Delta K_{th})^n \qquad (2.20)$$

The disadvantage of the above proposal is that Equations 2.18 to 2.20 can only be used if the

relevant region of crack growth is known or can be clearly seen on a graph similar to Figure 2.3. In most practical situations, the regions of crack growth are not all known. In such circumstances, Equation 2.19 which describes the linear region (region II) is the most frequently used. This frequent use of Equation 2.19 is then justified by making assumptions which tend to ignore the effects of regions I (near threshold) and region III (near fast fracture). In the document (CEGB 1986) it is assumed that the crack growth rate in region III plays an insignificant effect on the number of cycles to failure, N_f. This was because the number of cycles to failure when the material was undergoing fatigue cycling in the near fracture region was usually less than 1000 cycles. If this was compared with the experimental results for the cases where the value of N_f was over 100000 cycles the effect of ignoring the near fracture region by using Equation 2.19 was insignificant.

For the near threshold region (region I), the situation is not that simple. Firstly, a practical definition is yet to be universally accepted to define the near threshold region. So far, no acceptable standards exist for actually modelling the near threshold fatigue crack growth. The British Standards Institution published a document, PD 6493 (BSI 1980) which admits the existence of ΔK_{th} but tends to ignore its use when making recommendations on the prediction of service life. The document recommends the use of the Paris law for all the three regions and only suggests that if the value of ΔK during fatigue testing is less than ΔK_{th} then it should be assumed that no extension of the defect will occur and the material should continue to last until a new value of ΔK greater than ΔK_{th} is reached. The standard recommended by the Japanese Welding Engineering Society (JWES, 1980) is similar to the BSI standard because it specifies that the threshold region should be ignored and assumes that all values of ΔK greater than zero should be used in the Paris equation (i.e Equation 2.19).

However, in the document published by European Convention for Constructional Steelwork (ECCS, 1985), the threshold value of fracture energy ΔK_{th} was defined as the

corresponding value of ΔK when the value of da/dN, obtained by extrapolation from a plot of log (da/dN) versus log ΔK in the linear region, was about 10^{-11} m/cycle. It was suggested that if this definition for $\Delta K = \Delta K_{th}$ was used then the crack growth rate could be assumed to be negligible. Another definition of ΔK_{th} is provided in the ASTM E 647.88 standard as: "that asymptotic value of ΔK at which da/dN approaches zero". The standard recommends that ΔK_{th} may be taken as that value of ΔK which corresponds to fatigue crack growth rate of 10^{-10} m/cycle.

The above review of existing crack growth laws leads to the conclusion that a relationship which fully characterises the fatigue behaviour of materials in regions I, II and III will be very useful as it eliminates the shortfalls in the assumptions made when using only the Paris equation to describe the fatigue crack growth curve. A very good form of such an expression would be one in which the straight line graph resulting from the log-log plot of the value of da/dN vs ΔK obtained from the linear region II is modified into the shape of the material response as observed experimentally from regions I (near fast fracture) and III (near threshold). Such an expression has been suggested by Ewalds (1984) to be of the form:

$$\frac{da}{dN} = D(\Delta K)^n \left(\frac{1 - \left(\frac{\Delta K_{th}}{\Delta K}\right)^{n_1}}{1 - \left(\frac{K_{max}}{K_{1c}}\right)^{n_2}} \right)^{n_3} \qquad (2.21)$$

where

K_{max} = maximum value of stress intensity factor

ΔK = stress intensity factor range

ΔK_{th} = stress intensity factor range at near threshold region

K_{1c} = critical value of stress intensity factor

D and n are material constants obtained from Equation 2.19

n_1, n_2 and n_3 are empirically adjusted exponents.

Equation 2.21 was later modified by Martin (1990) by replacing ΔK with the maximum fracture energy, G_{max}, and adjusting the exponent $n_3 = 1$ give the expression;

$$\frac{da}{dN} = D(G_{max})^{n} \left(\frac{1 - \left(\frac{G_{th}}{G_{max}}\right)^{D_1}}{1 - \left(\frac{G_{max}}{G_{1c}}\right)^{D_2}} \right) \qquad (2.22)$$

where

G_{max} = maximum value of the strain energy release rate

G_{th} = the value of the strain energy release rate at the near threshold region

G_{1c} = the fracture energy , and

D_1 and D_2 are material constants

From Equation 2.22, it can be seen that as G_{max} tends to G_{th}, da/dN tends towards zero and as G_{max} tends towards G_{1c}, da/dN tends towards infinity. These observation are in good agreement with the expected growth rates in the near threshold and near fast fracture regions. Also the constants D and n are obtained from a modified form of the Paris law as will be described in Chapter Five. The value of G_{1c} and G_{th} are found and will be described in detail in Chapters Four and Five. The constants D_1 and D_2 can be found by fitting Equation 2.22 to the experimental data as will be described in Chapter Eight.

2.4.3 Fatigue Crack Growth Under Variable Amplitude Loading

As was mentioned in the previous section, the logic of using LEFM indicates that cracks in a given material subjected to the same K history, will grow at the same rate. Since engineering structures are usually subjected to complex fluctuating loads, a thorough understanding of

fatigue crack growth, particularly under variable amplitude load fluctuations is absolutely essential to the development of accurate fatigue life predictions of these structures. Many investigators (e.g Schijve 1967, McMillan et al 1967, vonEuw at al 1972, Wei et al 1974), have observed that the fatigue crack growth rate in any engineering material will be accelerated or retarded if there is any change in the amplitude of the applied cyclic load. For example, vonEuw (1972) observed that the crack growth rate in metallic materials previously under constant amplitude loading did not return immediately to its original value following the application of a single higher tensile cyclic load and that the growth rate decelerated gradually to its original value. This phenomenon was termed delayed retardation and it occurs due to the combined effects of the mechanisms of crack closure, residual stresses and crack tip blunting (Wheeler 1972, Willenborg 1971, Elber 1976). Extensive investigations are currently being conducted to develop methods to predict the fatigue lives under variable amplitude load fluctuations. Presently, a model suggested by Barsom (1973) appears quite promising. The model advocates that fatigue crack growth rate during variable amplitude loading and can be related to an effective stress intensity factor range, ΔK_{rms}, resulting from the load variations and to an equivalent stress intensity factor range, ΔK, that might have been obtained from constant amplitude loading by the expression:

$$\frac{da}{dN} = D(\Delta K_{rms})^n = D(\Delta K)^n \qquad (2.23)$$

where

$$\Delta K_{rms} = \left(\frac{\Sigma \Delta K_i^2}{\Sigma N_i}\right)^{1/2} \qquad (2.24)$$

and

ΔK_i = stress intensity factor for the i^{th} cycle

N_i = number of cycles corresponding to ΔK_i

Although the above model has been supported by experimental data (Barsom 1973), further research is necessary in this area of work.

2.5. Application of LEFM to Fatigue Crack Growth in Bonded Joints

Roderick et al (1975) and Mostovoy et al (1975) were among the first to study fatigue crack growth in bonded joints using fracture mechanics concepts. Roderick et al studied fatigue crack growth in metal-to-composite joints under mode I and mixed-mode loading at constant amplitude while Mostovoy et al investigated pure mode I dynamic fracture. These early studies showed that the relationship between the crack growth rate and the corresponding range of strain energy release rate, ($\Delta G = G_{max} - G_{min}$), on a log-log plot resulted in the same sigmoidal shape that was previously observed in the study of fatigue crack growth rate in metals (see Figure 2.3). For the values of strain energy release rate above a certain threshold value, G_{th}, and below the fracture energy, G_{1c}, of the adhesive, a modified form of the Paris law was used to characterise the fatigue performance of the adhesive. The modified equation was expressed as:

$$\frac{da}{dN} = D(\Delta G)^n \qquad (2.25)$$

Many investigators have used Equation 2.25 to characterise crack growth in bonded joints. Mall et al (1989) showed that there was a linear relationship between da/dN and ΔG when they tested DCB specimens made from graphite epoxy substrates bonded with an epoxy adhesive ("EC3445"). Liechti et al (1987) also showed that there was a linear relationship between log da/dN and log ΔG when they tested cracked lap shear specimens and single lap joints made from aluminium substrates bonded with a hot cure epoxy adhesive ("FM73M"). Similar findings were reported by Johnson et at (1988), Luckyram and Vardy (1988), Mall and Yun (1987) and Schmueser (1991).

Later on, Mall et al (1982, 1986 & 1988) and Liechti et al (1987) suggested that it was better to characterise fatigue crack growth in bonded joints by relating the crack growth rate (da/dN) to the total strain energy release rate range, ΔG_T (i.e $\Delta G_{Tmax} - \Delta G_{Tmin}$) instead of to just ΔG. They suggested an expression of the form:

$$\frac{da}{dN} = D(\Delta G_T)^n \qquad (2.26)$$

The total strain energy release rate range for an adhesive joint was defined by Mall et al (1988) to consist of three components, namely the opening mode, ΔG_I, the sliding mode, ΔG_{II} and the tearing mode, ΔG_{III}. However, in most of the cases involving practical adhesive joints, only ΔG_I and ΔG_{II} and their mixed-mode combinations are usually encountered. The practical significance of using ΔG_T is that it simplifies the analysis procedures, since the total strain energy release rate in a mixed-mode test is easier to determine than the individual components G_I and G_{II}.

Recent research work (Whitcomb 1985, Martin 1990) has found that Equation 2.25 is not applicable to the fatigue of composites and bonded joints. The is because during the unloading part of the fatigue cycling, the debonded surfaces come into contact resulting in facial interference (Martin 1990). For adhesively bonded joints, facial interference is a combination of effects which include the rubbing of debonded surfaces and collection of adhesive debris at the crack tip. If fatigue experiments are carried out under constant displacement amplitude, then these defects aid in artificially opening the delamination during the unloading cycle. Facial interference has the largest effect on G_{min} (or P_{min}) as the displacement ratio (i.e $\delta_{min}/\delta_{max}$) approaches zero. Hence the value of G_{min} may be higher than its actual value so that the value of ΔG is lower. Thus, it was suggested (Martin 1990) that in order to eliminate the effect of facial interference, the ΔG in Equation 2.25 could be replaced with G_{max} such that the new equation for characterising fatigue growth now becomes:

$$\frac{da}{dN} = D(G_{max})^n \qquad (2.27)$$

where D and n are material properties.

It should be noted that the form of Equations 2.25 to 2.27 are essentially empirical and are not based upon any theoretical models and as mentioned earlier, the values of D and n obtained from one empirical equation are different from those obtained from another. Hence in all cases, it is recommended that the source of the relevant equation and the units of these constants (i.e D and n) should be specified.

2.6. CONCLUSIONS

The main conclusions from this chapter are:

(1) The basic concepts of Linear Elastic Fracture Mechanics (LEFM) have been discussed from two main approaches namely the stress-intensity factor approach and the energy balance approach. The relationship between these two approaches have been defined. The application of LEFM to delamination fracture have been described.

(2) A literature review on the application of LEFM to constant amplitude and variable amplitude fatigue crack growth revealed that the crack growth rate da/dN could be related to a fracture mechanics parameter such as K or G. Such relationship has led to the formulation of several crack growth laws. The most widely used law is the Paris law (or in its modified form) in which the resulting shape of plots of log da/dN against log ΔK (or ΔG) is sigmoidal in shape with three distinguishable regions (i.e regions I, II and III). Several crack growth laws formulated to describe each region

(or combination of these regions) have been discussed. These laws are essentially empirical and are not based on any theoretical models and therefore it is recommended that the source of the relevant law and the units of the linear region II constants (i.e D and n) should be specified. Also, the existing standards recommended for analysing fatigue data were reviewed.

(3) The available literature on the use of LEFM concepts to characterise the fatigue growth in bonded joints were reviewed. The review showed that little work has been done on gaining a fundamental understanding of the fatigue performance of adhesives, mechanisms involved, establishing design criteria and developing quantitative methods for establishing the service life of adhesively bonded joints. The following chapters will be concerned with contributing towards a better understanding of the above problems.

CHAPTER THREE

EXPERIMENTAL DETAILS

3.1 INTRODUCTION

This chapter describes the materials used together with the sequence of steps taken to achieve the initial aims of this research work, which were to recommend a test method for assessing the fatigue performance of bonded joints.

3.2 MATERIALS USED

3.2.1: The Composites:

The composites used were:

APC-2: A thermoplastic composite manufactured by ICI. It consists of a matrix of thermoplastic polymer, poly(ether-ether ketone), reinforced with 61% by volume of unidirectional carbon fibres. The composite laminates were made from the unidirectional prepreg. The prepregs were laid into a ply stack, the ply direction being [0°]. The number of prepregs in a stack determined the thickness of the laminate. The laminates were cured by compression moulding which was carried out according to the manufacturer's specifications (ICI 1988). The process involved moulding in a hot press at 380 °C for 5 minutes at a pressure of 1.4MPa (200psi) and post-consolidation cooling at a pressure of 2 MPa (300 psi).

913C XAS-5-47%: A thermosetting epoxy composite manufactured by Ciba-Geigy. It consists of a thermosetting matrix of modified-epoxy reinforced with 66% by weight of unidirectional carbon fibres. The composite laminates are also laid into a ply stack with ply direction being [0°]. Similar, the laminates were cured by compression moulding which was carried out in accordance with manufacturers specification (Ciba Geigy 1988). The process involved moulding at 150 °C for 20 minutes under a pressure of 2MPa. In most cases the thermosetting composite was used as a trial specimen in cases where there were experimental problems to first overcome. The reason being that it is cheaper and more readily available. To

cure both composites a special mould was designed to give accurate control of temperature and pressure as well as maintaining uniform temperature across the platens. The order of stacking and the dimensions of the mould are shown in Figure 3.1.

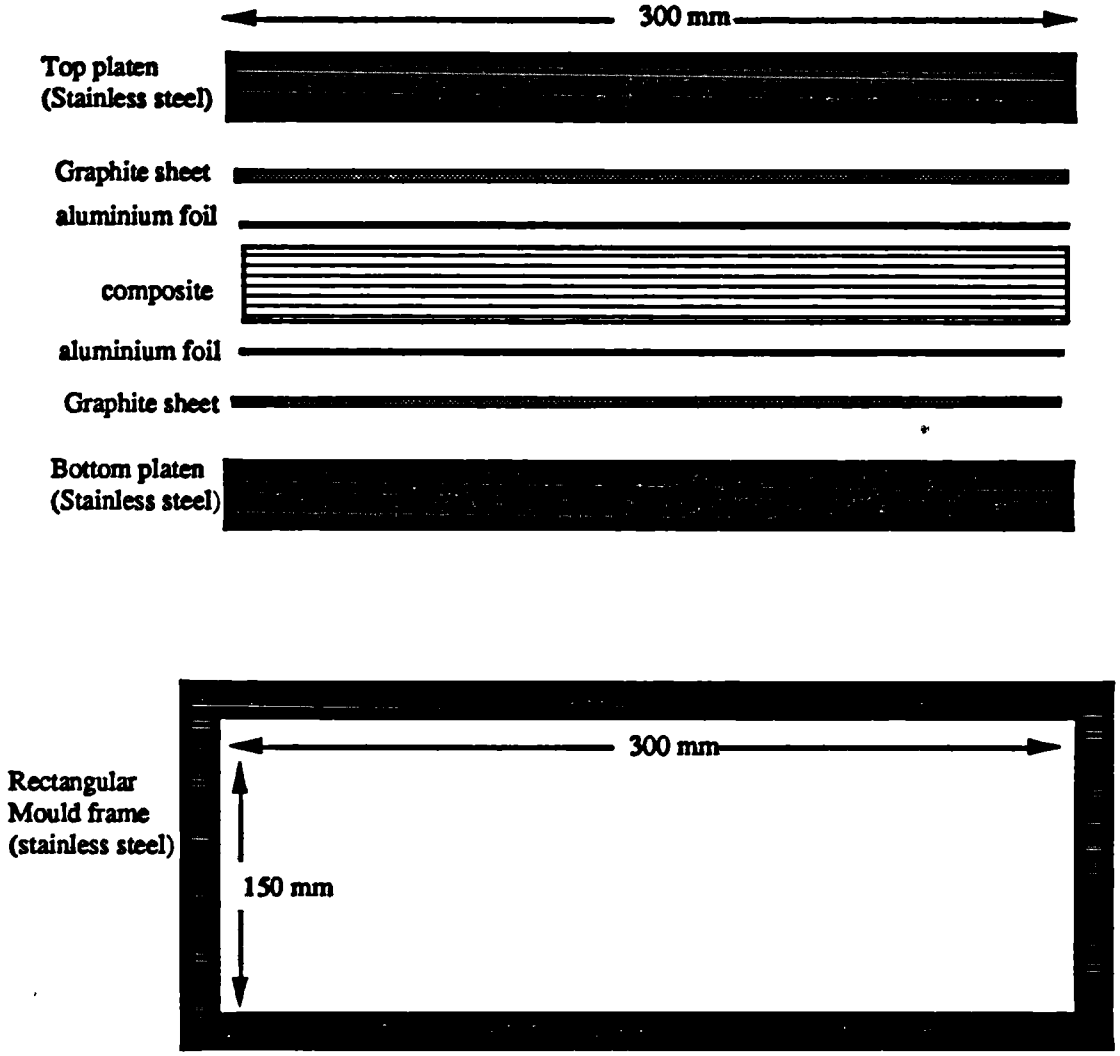


Figure 3.1. Order of stacking and dimensions of the mould

With the exception of the composite, all the contents stacked in the mould were coated with a mould releasing agent. The releasing agent used in this work was Freekote 44 supplied by Hysol Dexter (Hysol 1988). The graphite sheets were place next to the top and bottom platens to distribute the curing pressures evenly thereby ensuring uniform thickness of the laminate. The release coated aluminium foil was placed on the top and bottom of the composite to ensure smooth surface finish.

3.2.2 The Adhesives

The adhesives used were:

FM73M: A hot-cure epoxy film adhesive. The cure cycle may vary from 95 °C to over 175 °C, with minimum pressures which ensure proper mating of the substrates to be bonded.The cure cycle chosen was:

(1) The adhesive was placed between the bonded substrate and the joint was heated up from room temperature (Cyanamid 1988) to 120 °C in 30 minutes.

(2) The bonded parts were held at 120±3 °C for 60 minutes at a pressure of 0.028MPa (4psi). It was convenient to use relatively low pressure because the geometry of the specimen used permitted easy mating of the substrates.

EA 9309.3 NA: This is a room temperature two-part epoxy paste adhesive consisting of a pink paste (part A) and a blue paste (part B) mixed in the ratio of 100:22 by weight (Hysol 1988) and had been chosen because it is a tough adhesive curing at room temperature. A sprinkling of a small volume fraction (less than 0.1%) of glass beads of an average diameter of 0.35mm were used to control the glue line thickness. The bonded parts were held in contact by a pressure of about 4psi. The adhesive was left to fully cure at room temperature for 5 days.

3.3 SURFACE TREATMENT

Before any substrate can be joined by adhesive bonding it is necessary to ensure that any weak boundary layers and releasing agent transferred to the surface while processing are reduced to a minimum. The surface treatment technique recommended (Parker 1982, Pocius 1985) for the themosetting epoxy based composite (i.e. the 'XAS') consisted of simply grit-blasting the surface, then cleaning it with methyl-ethyl ketone and allowing it to dry.

For the thermoplastic 'APC-2', a 'corona' surface treatment was recommended (Kinloch et al 1989) as a necessary additional treatment to the surface after it had been grit-blasted and cleaned. This treatment involved the use of an atmospheric plasma to pretreat the surface of the polymer. Experimental results (Kodokian 1989) using this treatment have shown that it is very successful for thermoplastic materials. The results also showed that for a corona treatment level of 10.0 kJ/m^2 a cohesive locus of failure occurs when both the above adhesives are used to bond 'APC-2'.

3.4 MODE I TESTING

In general, there exist three modes of testing a specimen. These are the opening mode (mode I), the sliding mode (mode II) and the tearing mode (mode III). In an adhesive joint, various combinations of loading modes can occur at the crack tip ranging from pure mode I to combinations of modes I/II, to pure mode II. In rubber-modified adhesives, the value of the adhesive fracture energy, G_{1c}, under different modes of loading show that the order of magnitude of the strain energy release rate is mode I < mode II < mode III (DeVries 1977). In this work, emphasis is placed on mode I fatigue crack growth for two main reasons.

Firstly, because the mode I fracture energy is the most important of the three modes; i.e the majority of cracks will tend to propagate in pure mode I or in a mixed mode having a high proportion of mode I. Although genuine modes II and III are also possible they do not occur frequently. Secondly, the fracture and crack growth analysis procedures for each of the modes are very similar, although different numerical values may apply.

3.5 SPECIMEN GEOMETRY

Ripling et al (1971) was the first to suggest the use of the double cantilever beam (DCB) specimen geometry for the pure mode I testing of adhesive joints. The specimen is shown in Figure 3.2. The DCB has been found to be more acceptable than the conventional compact tension specimen (ASTM E399). There are three main reasons for this:

(i) Composites laminates are cured from their prepregs at recommended temperatures and pressures, hence there will always be the problem of ensuring a low temperature gradient during the curing. Since compact tension specimens are much thicker than DCB specimen, this problem becomes more important, and would require the use of highly precise temperature controllers.

(ii) The crack growth analysis procedure for the DCB is based on an energy balance, G_{1c}, approach which has advantages over the fracture toughness, K_{1c}, approach used in the analysis of compact tension specimen. These advantages include the fact that G_{1c} may be related to the intrinsic bonding forces of the adhesive (Kinloch 1987) and that the determination of K_{1c} for a joint is not always straight forward since it usually requires a knowledge of the geometric factor which may be a complex function of the moduli of the adhesive and the substrates.

(iii) By using the DCB advantage is taken of some recent analysis developed by Williams et al (1990) for the interlaminar failure of composite materials which allows

for the assumption of zero compliance at the crack root and large displacements of the DCB specimen.

For reasons of economy (i.e material costs, specimen preparation time, testing machine size etc) it was desirable for the specimen chosen to generate the fracture data were as small as possible, although care was taken to ensure that the specimen size was not too small as to invalidate the use of linear elastic fracture mechanics, as was discussed earlier in section 2.2.4. The width of the specimen was chosen to minimise edge effects. A minimum width of 20mm is recommended (Kinloch 1989). For unidirectional carbon-fibre composites, which are mainly to be used in this work, the substrate thickness was determined by the number of plies stacked together when making the composite laminates from the prepregs. The prepreg thickness used for both types of composite was 0.125mm, and was as supplied by the manufacturers.

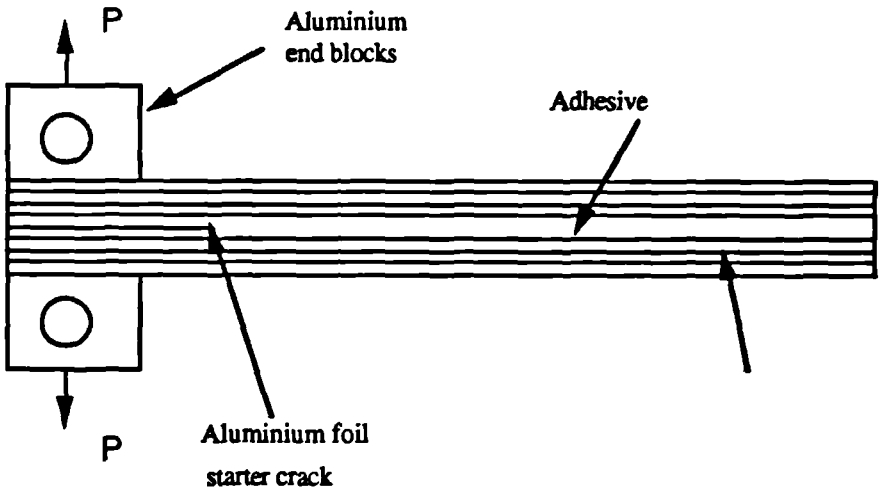


Figure 3.2 The double cantilever beam (DCB) joint specimen

3.6 PREPARATION OF BONDED DCB JOINT

The DCB joint were prepared by cutting rectangular strips from the laminates with fibres running parallel to the subsequent direction of crack growth. The relevant surface treatment technique was next applied (section 3.3). The adhesive was then applied to the two strips to be bonded. A release-coated aluminium foil, about 50mm in length, was then placed between the mating parts before they were brought together. This foil acts as a crack starter. The bonded parts were then subjected to the appropriate consolidating pressure and curing temperature, as

recommended by the manufacturers. After curing, aluminium alloy tabs were bonded at one end of the DCB specimen to allow the application of the loading forces. To monitor the position of the crack front, the side of the specimen was be painted white with typewriter correction fluid, and marked at 5mm intervals. It was important to apply only a thin coating, so that the crack length measured was the actual crack in the specimen and not due to the cracking of the correction fluid either ahead or behind the actual crack tip.

3.7 STATIC TEST EXPERIMENTS

Static tests (constant crosshead rate tests) were also performed on bonded composite joints. These tests were considered necessary for the following reasons. Firstly, the load and displacement values obtained from the constant crosshead rate tests as the crack propagated cohesively through the adhesive layer could be used as a reference point for determining the maximum and minimum loads, or displacements, to be applied to the specimen during cyclic fatigue testing. In the present studies when the fatigue tests were conducted in displacement control mode, the maximum displacement used for the fatigue cycling was chosen to be between 70 - 90% of the displacement obtained in static loading. A similar approach to fatigue experiments was adopted by Whitcomb (1985) et al.

Secondly, as will be discussed in Chapter Four, the values of the fracture energy, G_c, obtained using the double cantilever beam specimen and assuming the simple beam theory were in error due to the assumptions of zero compliance at the crack root and large displacements of the double cantilever beam. An investigation of the above problem has recently been reported for interlaminar failure of composites and correction factors suggested (Williams 1990). As will be shown later, (section 4.4.1), these correction factors are applicable to the fracture energy calculations for adhesively bonded DCB joints.

Thirdly, the results obtained from static experiments provided an opportunity to investigate whether changes in some material parameters such as the type of substrate, thickness of substrate and type of adhesive have a significant effect on the adhesive fracture energy, G_c, when a cohesive fracture occurs through the adhesive. It also served as a way of comparing results obtained in the static tests with those obtained in subsequent fatigue tests. The fourth reason was that in section 3.8, attention was focussed on the need to stiffen the DCB specimen by either increasing the specimen thickness or reinforcing the specimen with aluminium or steel plates. The static test experiments provided a means of ensuring that there was no yielding in the stiffening strips used for the DCB specimen. It should be noted that that bulk yielding of the DCB arm invalidates the LEFM approach which is the basis for the analysis of the DCB specimen geometry.

3.8 FATIGUE TEST EXPERIMENTS

The fatigue tests were carried out under displacement control. The two main reasons for this were:

(i) In load control the crack growth rate increases as the crack grows, whereas in displacement control the crack growth rate decreases with crack. The relevance of this is that the fatigue threshold region would be easier to locate in the displacement control mode compared to load control.

(ii) The servo-hydraulic machines generally used for these experiments are designed to produce relatively high loads and low displacements. It was observed during the earlier part of this work that such machines were not well suited for testing composites and adhesives where the loads applied to the specimen were small in comparison to the forces required to accelerate the moving parts of the machine and, more importantly, the displacements obtained from the DCB specimen geometry may become too large for the machine to cope with at higher frequencies than 1Hz. This limitation therefore results in the maximum displacement of the specimen to be held constant as oppose to the load during fatigue testing of the bonded composites.

In order to successfully carry out the fatigue test under constant displacement amplitude, the the specimen displacement must be fixed and must be high enough so as to ensure that tests were started at a G_{max} value close to G_{1c}. Thus as the crack grows the value of G_{max} decreases and eventually the crack arrests. This is only possible if the value of the displacement is fixed at between 70-90% of the value of the required applied displacement obtained during static testing. Again, if the DCB specimen is not stiff enough, this value may be too high for the testing equipment to cope with.

This limitation brings about the need to reduce the displacement of the specimen during testing. Two solutions were considered to minimise specimen displacement, both of which made the specimen stiffer. One was by increasing the thickness of the composite substrate and the other was by reinforcing the composite substrate by bonding aluminium or steel plates to the composite. The results obtained are discussed in the next chapter, but the former solution was found to be the best solution and the thickness of the composite substrates were nominally 6 mm.

3.9: MEASUREMENT OF THE FATIGUE CRACK LENGTH

Five techniques have been considered as practicable for measuring crack lengths in adhesively bonded fibre-composites joints. These are:

(1) the use of a travelling microscope,
(2) an electrical potential method,
(3) a compliance method,
(4) a time lapse photography method and
(5) a ultrasonic scanning method.

These techniques are briefly discussed below.

3.9.1 Travelling Microscope

A frequently used method for following crack propagation is by using a travelling microscope mounted on a platform fixed to the base of the machine. This technique may give very accurate results and it involves direct visual observation of the growing crack (Martin 1990, Everett 1987, Laskimi 1985).

3.9.2 Compliance Method

This method involves recording the load and displacement on the specimen and using a compliance calibration curve to estimate the corresponding crack length (Mall 1988, Prel 1989, Radon 1984). The compliance calibration curve (compliance vs crack length) was obtained in two ways. One was from static tests in which the crack length corresponding to a given load and displacement was measured using a travelling microscope. The other was by using finite element analysis in which the material properties and loading conditions were used to estimate the specimen displacement for a corresponding crack length (Mall 1989). The crack length in the fatigue test was then indirectly obtained from estimating the compliance from the fatigue test and using the calibration curve generated from the two methods described above.

3.9.3 Electrical Potential Method

This technique involves bonding an electrically conductive foil gauge to the side of the specimen (Spicer 1990, Gibala 1982). When current passes through the conductor, the electrical potential changes as the crack length increases and fractures the gauge. The change in the potential can be measured continuously or at predetermined intervals on the specimen using sensing leads. Finally the potential difference measured across the leads is then related to the crack length by a calibration curve, and hence crack length values can be obtained. The conductive foil required is in the order of 5 microns thick.

B LONDIN. UNIV

3.9.4 Photographic Method

This is a method that uses a novel automated photographic process to measure the crack length. It consist of using a camera ("Canon T70") equipped with a "Canon 70" command back which can be programmed to take pictures at any set of time between zero and 23hrs 59secs and at any interval between zero and 23hrs 59 secs. The number of frames to be taken can also be set. The camera prints on each frame the date and time at which it was taken. This feature enables the number of cycles to be estimated at the instant the picture was taken. An extension tube is used on the camera which gives a field of view of about 120mm. Lighting is provided by means of a flash gun which is switched on and off by the time switch, at the instant the pictures are taken. When pictures have been taken, the film is removed and developed. The negatives are then mounted on to slides, after which they are projected on to a screen and the crack length can be measured.

3.9.5 Ultrasonic Scanning Method

This method of crack length measurement involves sending an electrical signal from a pulse receiver to a transducer which converts it to ultrasonic signals (Whitcomb 1981, Liechti 1987, Everett 1985). The ultrasonic signals are made to interact with the test specimen and the reflected waves are sent back to a transducer for amplification. The amplified signal are then transferred to a time gate so that only reflections from the crack front is kept. The amplitude of the signals from the time gate are then transferred to a computer which has software that specifies the crack length. All ultrasonic techniques require some couplant to transmit the ultrasound from the transducer to the specimen. In many cases water is used as the couplant by immersing the specimen in a water tank.

3.9.6 Discussion of Measurement Techniques

The measurement of crack growth in fatigue tests is a prime candidate for automation. The experiments are tedious, require continuous monitoring and must be performed with a high degree of accuracy. In addition some fatigue experiments, such as threshold testing, can last for weeks and even months. The automation of fatigue crack growth experiments therefore offers the possibility of a large return on the initial investment both in terms of a reduction in man hours to conduct the experiments and the accuracy of results.

From this point of view, the ultrasonic scanning method appears to be the most attractive for automation because of its accuracy and convenience. However, the method was not used in this work for two main reasons. Firstly, it is a very new technique still at its development stages with very little information available on its successful application. A commitment to such an idea after about one year into this research work was considered a risk that might cause considerable deviation from the initial aims of the work. Secondly, setting up the equipment

would require a substantial amount of funds which was thought not to be readily available within the time allowed for this research work. The electrical potential method also appears very attractive for automation. However the main objection to this method was that since the crack would be propagating through two media (i.e an adhesive and a conductive foil), there was no way of ensuring that the foil would not crack ahead or behind the crack tip. Thus false readings of crack length might be possible.

The compliance calibration method is a reliable method for measuring crack length in bonded structures. However, the method was not used in this work because it was thought that a calibration curve for a particular R ratio (i e a given stress or displacement ratio) could not be used to describe crack propagation at a different R ratio and that a compliance calibration curve established under static loading conditions could not be used to predict reliably the crack length during fatigue crack growth. However experimental results from the later part of this work has proved that this method may have been used and the results are discussed in Chapter Eight. The photographic method is feasible for automation but it is considered that the advantages gained from the ability to take pictures of the cracked specimen in the absence of the researcher has to be weighed against the man-hours involved in developing the films and taking measurements.

In view of the above discussions, it is believed that the most convenient and accurate method of crack length measurement is by visual observation with the aid of a travelling microscope. The method is used throughout the present work. Nevertheless, the need to record crack lengths manually has the obvious disadvantage of requiring the operator to be present at any time of the day or night particularly when rapid crack propagation is expected. Thus, the possibility of using automated techniques merits serious consideration in an establishment where cheap reliable labour is not readily available.

3.10 CRACK FRONT CURVATURE IN DCB SPECIMEN

Experimental studies conducted by Schapery et al (1987) on carbon fibre composites have shown that the crack front in a DCB specimen was shaped like a thumbnail. Davidson (1990) tried to find an explanation for the shape of the crack front by performing a three dimensional finite element analysis of the DCB specimen assuming an initially straight crack front. His analysis showed that the distribution of strain energy release rate, G, across the width of a DCB specimen is such that G is highest at the centre of the specimen and lowest at the edges. His analysis suggested that the distribution of available strain energy causes crack growth to first occur in the central region of the specimen before occurring at the edges. For this reason the crack front changes from being initially straight to being shaped like a thumbnail. When

this thumbnail shape of the crack front has been formed it was found (Schapery et al 1987) that the delamination front will remain curved and will not change in shape with crack length.

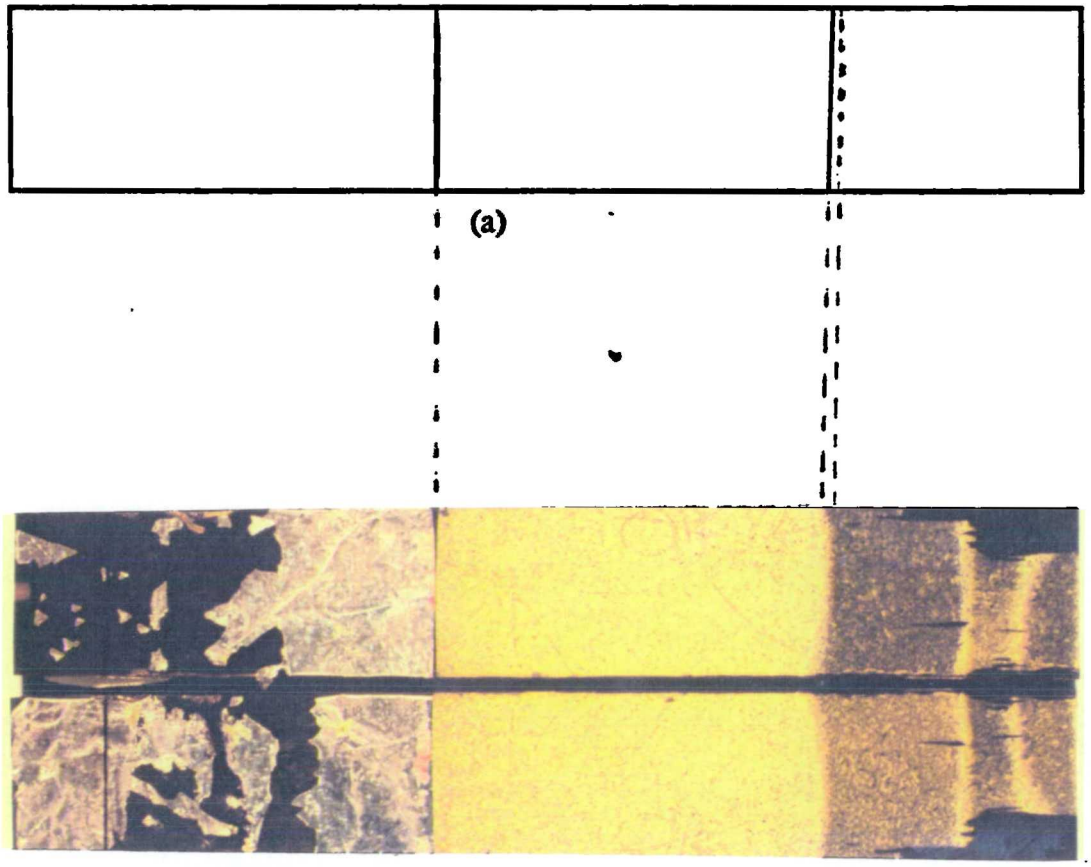


Figure 3.3 (a) Perceived area created for a straight crack front.
(b) True area created by actual crack growth accounting for crack curvature.

The problem of the crack front curvature is that the perceived cracked area estimated using the crack length measured from the side of the specimen is different from the actual cracked area created due to crack growth (Figure 3.3). Thus there will be an error in the value of G estimated using the perceived area instead of the actual area and Davidson (1990) suggested that the error is given by:

$$\text{ERROR} = \frac{G^{\text{perceived}}}{G^{\text{true}}} - 1 = \frac{\Delta A^{\text{true}} - \Delta A^{\text{perceived}}}{\Delta A^{\text{perceived}}} \qquad (3.1)$$

where

ΔA^{true} = true area created during crack growth.

$\Delta A^{perceived}$ = perceived area created during crack growth.

$G^{perceived}$ = value of strain energy release rate estimated using the perceived area.

G^{true} = value of strain energy release rate estimated using the true area and accounting for crack front curvature.

Davidson (1990) found out that for DCB specimens these errors are relatively small, for example, for unidirectional composite, it was found to be about 1.6%. In the present investigation the maximum error due to crack front curvature was estimated using Equation 3.1 and found to be 2.88%, whilst the minimum was 0.96%. Since these errors are much smaller than the error due to experimental scatter (about 10%), the effects of crack front curvature on the calculation of strain energy release rate have been ignored in this work.

3.11 TESTING OF THE JOINTS

3.11.1 Constant Crosshead Rate Tests

All constant crosshead rate tests were performed using an Instron "model 1186" tensile testing machine. The loads applied to the specimen under tension or compression are detected by a highly sensitive electronic force measuring system equipped with load cell strain gauges. A set of load cell amplifiers controls provide an adjustment and the calibration measuring system to give reliable and accurate test data. The specimens to be tested were fastened between grips and the tensile loading were applied with the crosshead moving away from the load cell. Test results were presented on a strip-chart recorded in which a basic single pen recorder system provided a trace showing load versus crosshead position.

3.11.2 Fatigue Tests

All fatigue tests were carried out using a Mayes servohydraulic testing machine (Mayes 1988) equipped with a closed loop control system. Load cells were available from which load ranges could be selected from the control panel. A digital voltmeter displayed the feedback signal from the load, strain and crosshead modules as a percentage of the selected range and the range provided a high precision for any value of load. The control unit incorporated a function generator and the square, triangular and sine waveforms could be selected with frequency ranges from 0.01 to 100Hz. The sine waveform was used in this work since it is well defined and easily standardised. The machine was designed to cycle the specimen under either load or displacement control.

3.12 CONCLUDING REMARKS

In this chapter, the adhesives and composites employed in the present studies have been described. The approach to the experiments have been discussed and the main points are:

(1) The fatigue testing will be conducted using mode I loading and using the double cantilever beam.

(2) Test will be carried out under a constant displacement amplitude.

(3) A travelling microscope will be used to monitor crack propagation.

(4) The effect of crack front curvature will be ignored since earlier findings (Davidson 1990) and results from this work have shown that it has a negligible effect on the calculated value of strain energy release rate.

(5) Static testing will be undertaken to decide the maximum and minimum loads, or displacements, of the specimen during cyclic fatigue testing.

CHAPTER FOUR

CONSTANT RATE OF DISPLACEMENT TESTS

4.1 INTRODUCTION:

In section 3.7 the need to obtain test data from constant rate of displacement (i.e static) tests was explained. This chapter discusses the work undertaken to generate such data. Firstly, the theoretical methods for calculating the adhesive fracture energy, G_{1c}, in the DCB specimen geometry are reviewed. Secondly, the experiments which were carried out to determine the values of G_{1c} obtained from the various theoretical methods are considered. Finally the effects of parameters such as adhesive type, substrate type and thickness, on the performance of the bonded joints are presented.

4.2 THEORETICAL METHODS FOR CALCULATING G_{1C}

In section 2.3, the three main methods for calculating the value of G_{1c} due to delamination fracture in fibre-polymer composites were described. They are the 'area' method the 'compliance' method and the 'beam theory' method. Although these methods have been found to be suitable for fibre-polymer composites (Williams 1990), they should be equally applicable to adhesively bonded fibre-composite joints.

4.2.1 'Area' Method

The first approach is the 'area' method, where for elastic behaviour the value of G_{1c} may be defined by:

$$G_{1c} = \frac{\Delta U}{B\,\Delta A} \qquad (4.1)$$

where B is the width of the DCB specimen, and for example, ΔU_1 is the area under the load versus displacement trace and Δa is the increase in crack length from a_1 to a_2 (see Figure 4.1).

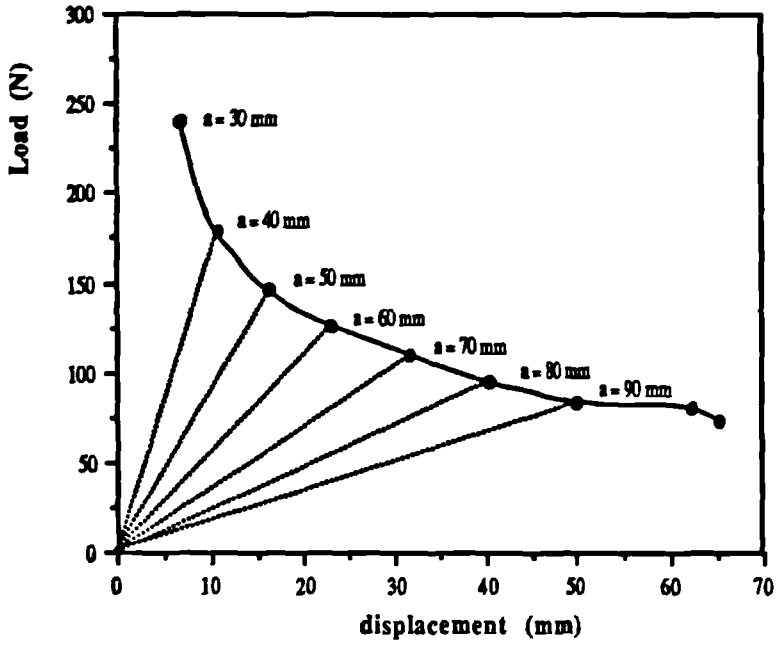


Figure 4.1. A typical load displacement diagram obtained from a DCB bonded joint.

Now when the loading and unloading relations are linear, the LEFM approach may be used and, for example:

$$\Delta U_1 = U_2 - U_1 = 0.5(P_1\delta_2 - P_2\delta_1) \qquad (4.2)$$

where P_1 and δ_1 are the load and displacement at a crack length a_1, and P_2 and δ_2 are the respective values at a crack length a_2.

4.2.2 'Compliance' Method

The second approach is the 'compliance' method where the value of the fracture energy, G_{1c}, from an LEFM test is given by:

$$G_{1c} = \frac{P^2}{2B} \cdot \frac{dC}{da} \tag{4.3}$$

where P is the load and C is the compliance, given by:

$$C = \frac{\delta}{P} \tag{4.4}$$

where δ is the displacement corresponding to a load P.

To evaluate G_{1c} via the "compliance" method, a plot of C versus crack length, a, may be constructed as illustrated in Figure 4.2. The plot of C against a is then curve-fitted using an appropriate polynomial function and differentiated. Then, knowing the values of the load, P, and the differential, dC/da, at a given crack length, the value of G_{1c} as a function of crack length, a, may be evaluated using Equation 4.3.

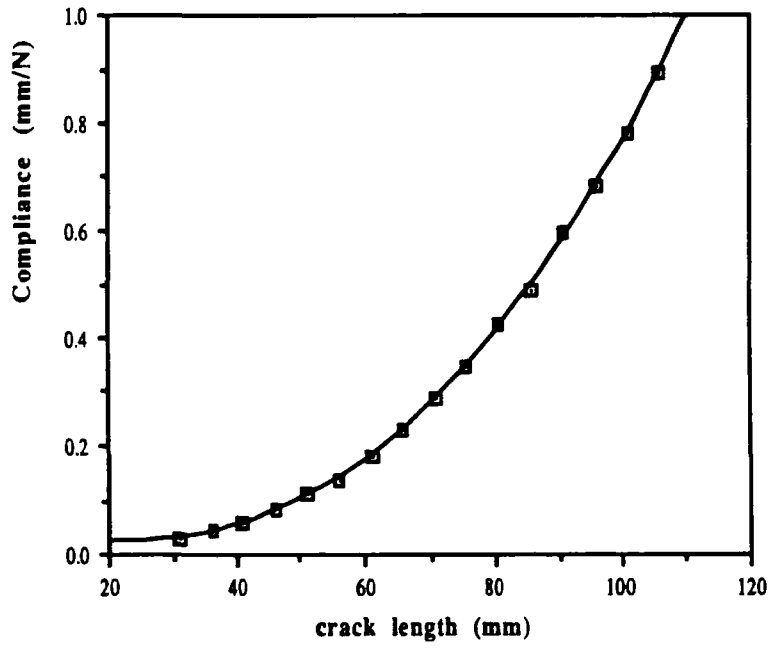


Figure 4.2. A typical compliance versus crack length curve obtained from a DCB bonded joint.

4.2.3 The 'Beam Theory' Method

The third approach is the 'simple beam theory' method, based upon the assumption of small displacement and elastic behaviour of a built-in cantilever beam. Williams (1988) proposed a very powerful method by which the energy release rate, G, that causes the delamination in fibre-composite can be found from the crack tip values of the applied bending moment, M, the specimen's axial modulus, E_{11}, and the second moment of area, I.

Williams stated that:

$$G = \frac{1}{16\,B\,E_{11}\,I}\left(\frac{M_1^2}{\varepsilon^3} + \frac{M_2^2}{(1-\varepsilon)^3} - (M_1 + M_2)^2\right) \qquad (4.5)$$

where

$$\varepsilon = \frac{h_1}{h_1 + h_2} \qquad (4.6)$$

where h_1 and h_2 are the thicknesses of the upper and lower arms of the debonded sections of the composite laminate (see Figure 4.3).

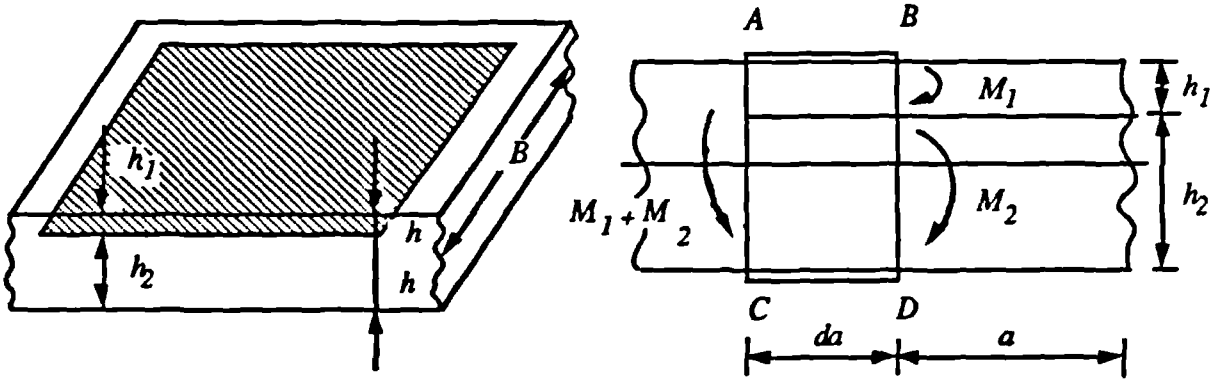


Figure 4.3. Delamination in fibre-polymer composite under bending (Williams 1988).

Equation 4.5 is concerned with the calculation of G and not the criteria for fracture. It becomes a fracture criteria when the value of G is such that the circumstances allow crack growth to occur (e.g when $G = G_{Ic}$), and when fracture occurs, Equation 4.5 can be partitioned into different modes of fracture. For the special case of pure mode I fracture, the equation becomes:

$$G_I = \frac{6}{B^2 E_{11}} \frac{h_1^3}{h_2^3(h_1^3 + h_2^3)} \left(M_2 - \left(\frac{h_2}{h_1}\right)^3 M_1\right)^2 \tag{4.7}$$

and for pure mode II fracture:

$$G_{II} = \frac{6}{B^2 E_{11}} \frac{3h_1 h_2}{(h_1 + h_2)^2 (h_1^3 + h_2^3)} (M_2 + M_1)^2 \tag{4.8}$$

and for the case of mixed mode fracture:

$$G = G_I + G_{II} \tag{4.9}$$

According to Williams (1988) Equation 4.5 conveniently covers most of the test geometries used in testing composite laminates which usually involve elastic behaviour and slender beams. The equation can also be applied to the analysis of compression failure and transverse cracking problems in composite laminates. Equation 4.7 has been adapted to the DCB specimen (Williams 1990) and and the resulting equations are referred to as the 'load' and 'displacement' methods. The two methods are briefly discussed below.

4.2.3.1 'Load' Method

If a DCB bonded joint is subjected to symmetrical loading, the bending moments M_1 and M_2 in each arm of the DCB joint are equal so that:

$$M_1 = -M_2 = Pa \tag{4.10}$$

where

P = applied load

a = crack length

Substituting equation 4.10 into 4.7 and noting that $h_1 = h_2$ the resulting equation, which is generally referred to as the 'load' method is given as:

$$G_{1c} = \frac{12P^2a^2}{B^2h^3E_s} \tag{4.11}$$

where E_s is the flexural moduli of the fibre-composite substrate arms, which are now assumed to act as simple built-in beams and where E_a, the modulus of the adhesive layer, is assumed to be much less than E_s. This is because the effective modulus of the DCB bonded joint has been shown (Appendix B) to differ from that of the substrate by only about 1.18% so that the energy stored in the joint due to loading is mainly carried by the composite substrate. The three approaches are briefly discussed below.

4.2.3.2 'Displacement' Method

Equation 4.11 can be rearranged by substituting the relationship between the specimen displacement, δ, and compliance, C, in the place of the load, P, where C is obtained from:

$$C = \frac{\delta}{P} = \frac{8a^3}{BE_sh^3} \tag{4.12}$$

The resulting equation, referred to as the 'displacement method' is given as:

$$G_{1c} = \frac{3P\delta}{2Ba} \tag{4.13}$$

Now, as long as the load versus displacement relationships for the specimen are linear for loading and unloading at any given crack length, which is true for all the present work, then any of the four methods of calculation (i.e equations 4.1, 4.3, 4.11 and 4.13) should give identical results for a given experiment. Further, another cross-check on the analysis methods is provided by calculating the value of the modulus, E_s, of the substrate arms. This is given by:

$$E_s = \frac{8Pa^3}{Bh^3\delta} \tag{4.14}$$

and the value of E_s calculated from equation 4.14 may obviously be compared to the value obtained by direct experimental measurements.

4.2.3.3 "Corrected Beam Theory" Analyses

Now, compared to metallic substrates, the use of polymeric fibre-composite substrates may give rise to several sources of error upon analysing the data employing Equations 4.11.4.13 and 4.14. Firstly, the relatively low shear modulus of the fibre-composite substrate arms leads to rotations and deflections occurring at the crack tip. Such effects are ignored in the simple beam analyses, which assume that the compliance at the crack root is zero, i.e. the arms act as built-in cantilever beams. Secondly, substrate arms prepared from fibre-composites tend to be slender beams and often undergo large, albeit linear, displacements during the fracture test. Thirdly, the end-blocks which are bonded to the composite substrate arms, through which the loads are applied, tilt as the arm is bent. Both of these effects lead to an effective shortening of the composite beam. Finally, a correction is also required for the stiffening effects due to the presence of the metal end-blocks.

From the work of Williams (1990) on the interlaminar fracture of composites using the DCB

specimen, the corrections for the above effects may be expressed for the "corrected" load method as:

$$G_{1c} = \frac{12P^2(a + \chi h)^2}{B^2 E_s h^3} . F \qquad (4.15)$$

and for the "corrected displacement" method as:

$$G_{1c} = \frac{3P\delta}{2B(a + \chi h)} . \frac{F}{Z} \qquad (4.16)$$

where F, Z and χ are the various correction factors which are discussed below.

Firstly,the correction factor, χ, allows for all the necessary shear corrections in the DCB specimen and may be ascertained experimentally from the relationship between the measured compliance, C, of the specimen and the crack length, a. The relationship between these parameters is given by the equation:

$$C = Z\frac{8\,(a + \chi h)^3}{Bh^3 E_s} \qquad (4.17)$$

Hence:

$$\left(\frac{C}{Z}\right)^{1/3} = \left(\frac{8}{Bh^3 E_s}\right)^{1/3} (a + \chi h) \qquad (4.18)$$

Thus, from Equation 4.18 the measured compliance, $(C/Z)^{1\,3}$, may be plotted against the corresponding value of crack length, a, and the intercept yields the value of the correction factor, χ. Also, from the gradient of the line, the value of the modulus, E_S, may be obtained.

Note, that the modulus may also be ascertained from the expression:

$$E_s = \frac{P}{\delta}\frac{8Z(a+\chi h)^3}{Bh^3} \qquad (4.19)$$

Secondly, large displacements in the specimen cause the arm to effectively shorten. In addition, the bonded end-blocks give rise to further changes if the load-point is above the beam, since the block tilts as the arm is distorted. This shortening of the crack length may be expressed in the form of a multiplying factor which may be applied to the measured crack length, a. Thus:

$$F = 1 - k_1\left(\frac{\delta}{a}\right)^2 - k_2\left(\frac{\delta L_1}{a^2}\right) \qquad (4.20)$$

The values of k_1 and k_2 are 0.3 and 1.5 respectively and L_1 is defined as the distance of the load point above the beam axis, as shown in Figure 4.4.

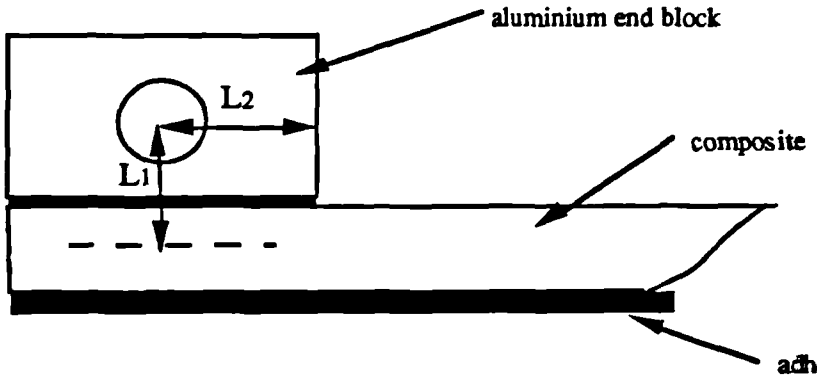


Figure 4.4. Arrangement of the end block bonded to the composite substrate arms.

Thirdly, since the test specimens are loaded via end-blocks bonded to the specimen arms, a correction factor is also required to account for the stiffening effect caused by the metal end-blocks. This correction factor is most conveniently expressed in the form of a correction

factor Z by which the displacement, δ, may be divided. In this form the correction factor Z also includes (in the last two terms) the corrections needed for the large displacement and the end-block tilting effects. Thus:

$$Z = 1 - k_3\left(\frac{L_2}{a}\right)^3 - k_4\left\{1-\left(\frac{L_2}{a}\right)^2\right\}\frac{\delta L_1}{a^2} - k_5\left(\frac{\delta}{a}\right)^2 \qquad (4.21)$$

where L_2 is obtained from the dimensions of the end block as shown in Figure 4.4. The values of K_3, K_4 and K_5 are 1, $9/8\{1 - (L_2/a)^2\}$ and 9/35 respectively. The effectiveness of these corrections will be discussed later in section 4.3.2.

4.3 RESULTS AND DISCUSSION

4.3.1 Introduction

As discussed earlier in section 3.11, the constant crosshead rate tests were performed using an "Instron" tensile testing machine (model 1186). The two adhesives tested were a heat cure epoxy film adhesive ("FM73M") and a cold cure epoxy paste adhesive ("9309.3NA"). The substrates were thermoplastic CFRP (APC-2) and thermosetting CFRP (913C XAS-5-47%).

The bonded DCB specimens were tested at a displacement rate of 2 mm/min. The load versus displacement trace was linear up to the start of crack propagation and stable crack growth was observed. The crack was monitored using a travelling microscope and as the crack propagated and crossed the markers this event was recorded on the load versus displacement trace, as shown in Figure 4.1. Hence, values of the adhesive fracture energy, G_{1c}, could be determined as a function of crack length, a. The following results were obtained from the constant rate of displacement tests.

4.3.2 Analysis of the DCB Tests

Table 4.1 shows the fracture data for the bonded PEEK based composites (i.e. APC-2) using the two-part cold-cure adhesive (i.e. "9309.3NA"). As may be seen from the values of G_{1c} deduced using the "area" and "compliance" methods (Equations 4.1 and 4.3 respectively) there is good correlation between these two basic analytical results. However, when the "load" and "displacement" methods based upon the assumptions of simple beam theory are employed, i.e. Equations 4.11 and 4.13, then the agreement between these two methods is very poor and, furthermore, the agreement with the former two methods is also poor.

TABLE 4.1. Values of the adhesive fracture energy, G_{1c} (kJ/m^2), and substrate modulus, E_s

	adhesive fracture energy calculated using:						Es (GPa)		F and Z	
crack length (4.21)	area (4.1)	comp. (4.3)	displ. (4.11)	load (4.13)	corr displ (4.15)	corr load (4.16)	uncorr modulus (4.14)	corr modulus (4.19)	F (4.20)	Z
35		5.72	6.55	4.91	5.33	5.47	90.77	128.91	0.82	0.85
40	5.86	5.68	6.52	5.11	5.38	5.43	94.75	126.81	0.82	0.85
45	5.08	5.45	6.10	5.12	5.11	5.31	101.55	130.54	0.82	0.86
50	5.18	5.28	5.91	5.18	5.01	5.23	106.11	131.24	0.82	0.86
55	5.43	5.43	6.15	5.55	5.24	5.40	109.25	129.49	0.81	0.85
60	4.92	5.14	5.77	5.45	4.96	5.23	114.35	132.31	0.81	0.85
65	5.24	4.93	5.62	5.42	4.87	5.08	116.61	131.18	0.80	0.84
70	5.83	5.66	6.60	6.43	5.70	5.69	117.78	125.42	0.77	0.81
75	5.65	6.09	7.06	7.13	6.09	6.06	122.09	125.05	0.75	0.80
80	5.96	6.59	7.57	7.92	6.52	6.46	126.55	124.50	0.73	0.78
90	6.15	5.77	6.65	7.29	5.78	5.87	132.76	127.59	0.73	0.78
95	5.80	5.69	6.58	7.36	5.73	5.80	135.46	127.32	0.72	0.77
100	5.28	5.15	5.93	6.80	5.20	5.41	138.72	130.62	0.73	0.78
105	5.63	5.47	6.36	7.38	5.54	5.59	140.43	126.82	0.70	0.75
110	5.60	5.43	6.33	7.36	5.51	5.53	142.75	126.04	0.69	0.74

Notes: Substrate: corona treated APC-2, laminate thickness 12 ply (1.62mm).
Adhesive: Hysol 9309.3NA, joint failure was cohesive through the adhesive layer.
The numbers under headings indicate the equation number employed in the calculation.

Also, the "load" method results in an significant increase in the value of G_{1c} with increasing crack length, a; which suggests that a rising "R-curve" (i.e resistance curve) is recorded for this joint. However the other methods of calculation do not suggest an "R-curve" is present. The results comparing the values of G_{1c} obtained using all the four methods (i.e Equations 4.1, 4.3, 4.11 and 4.13) are shown graphically in Figure 4.6. It should be recalled that all these

values of G_{1c} have been deduced from the same experimental load versus displacement curve and, therefore, discrepancies from using the simple beam approach cannot be attributed to experimental error. The fact that the values of G_{1c} based upon simple (uncorrected) beam theory are in error is further revealed from a consideration of the values of the substrate modulus, E_s, also calculated using simple beam theory, i.e. from Equation 4.14, which are shown in Table 4.1 and Figure 4.9. These data show that the value of E_s so deduced appears to vary with crack length, obviously this conclusion cannot be correct.

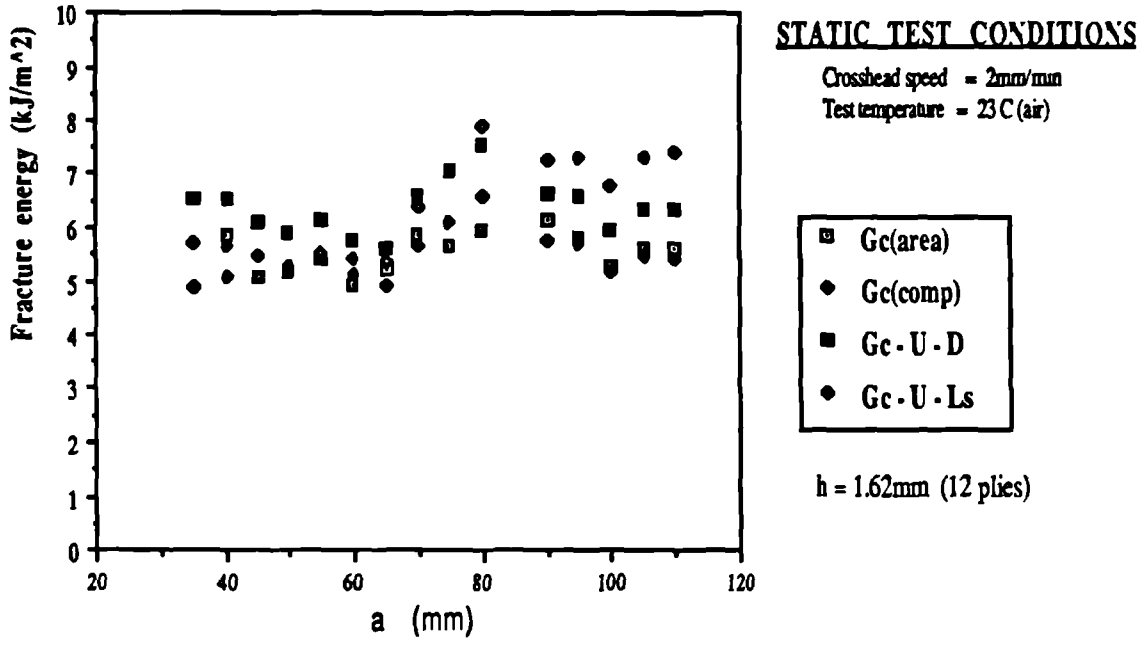


Figure 4.6. Variation of the fracture energy with crack length when beam analysis corrections were not applied. (Composite: "APC-2" Adhesive: "EA9309.3NA").

The values of G_{1c} deduced using the corrected beam theory analyses are also shown in Table 4.1; values from using both the "corrected load" (Equation 4.15) and "corrected displacement" methods (Equation 4.16) are included. In these equations the values of the correction factors F and Z were calculated from Equations 4.20 and 4.21 respectively and values of these terms are quoted in Table 4.1. It should be noted that for relatively long cracks these correction factors make a significant difference, particularly to the "load" method (see Equation 4.15). The value of the crack-tip rotation and deflection correction term, χ, was ascertained using Equation

4.18. The plot of $(C/Z)^{1/3}$ versus the corresponding value of the crack length, a is shown in Figure 4.7 As may be seen, an excellent linear fit to the data exists with a correlation coefficient of 0.999. The intercept yields a value of χ of 4.03, so that $\chi h = 6.53$. The values of G_{1c} deduced using the "corrected load" (Equation 4.15) and "corrected displacement" methods (Equation 4.16) are in good agreement with one another, and are also in good agreement with the values from the "area" and "compliance" methods (which are, of course, unaffected by the correction factors).

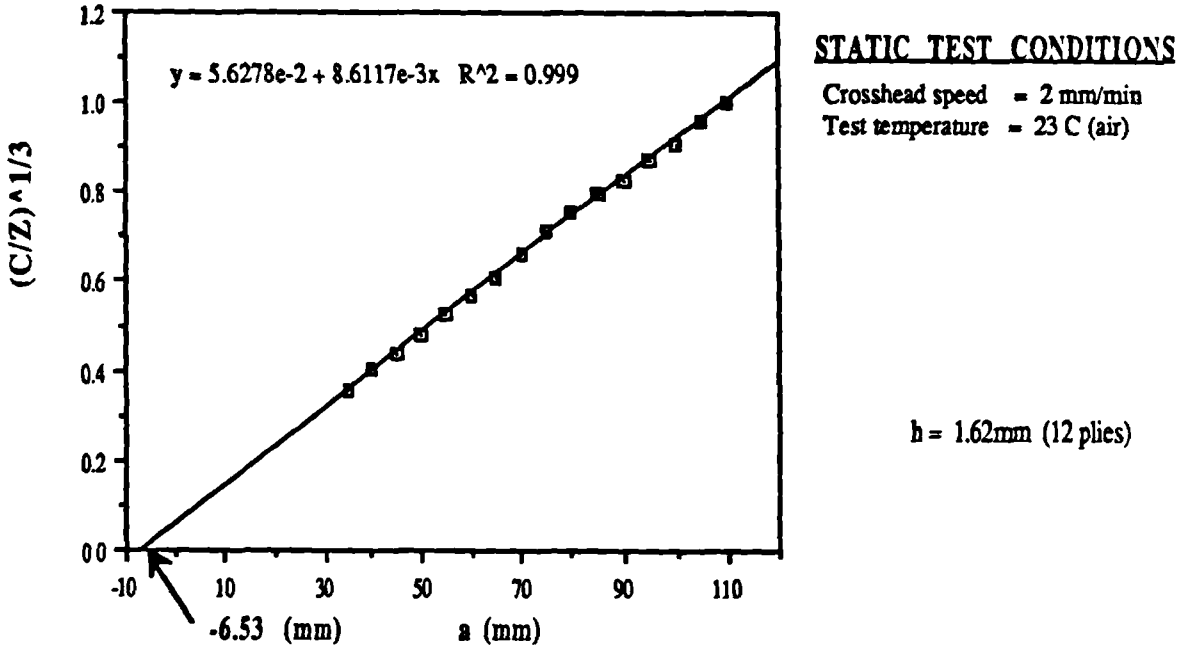


Figure 4.7. (C/N)^1/3 vs "a" for "APC-2" bonded with "EA9309.3NA" adhesive. Intercept = crack length correction.

A graphical representation of the G_{1c} values obtained when the necessary corrections have been applied (i.e Equations 4.1, 4.3, 4.15 and 4.16) is shown in Figure 4.8. Furthermore, the use of the "corrected load" method reveals that, in fact, no "R-curve" actually exists for these joints. The values of E_s calculated from the corrected beam theory method (i.e. using Equation 4.19) are now no longer dependent upon the crack length and the average value is 128.2±2.5 GPa. (It should be noted that this average value may also be calculated by measuring the gradient of the slope from a plot such as shown in Figure 4.7 and using Equation 4.18). This

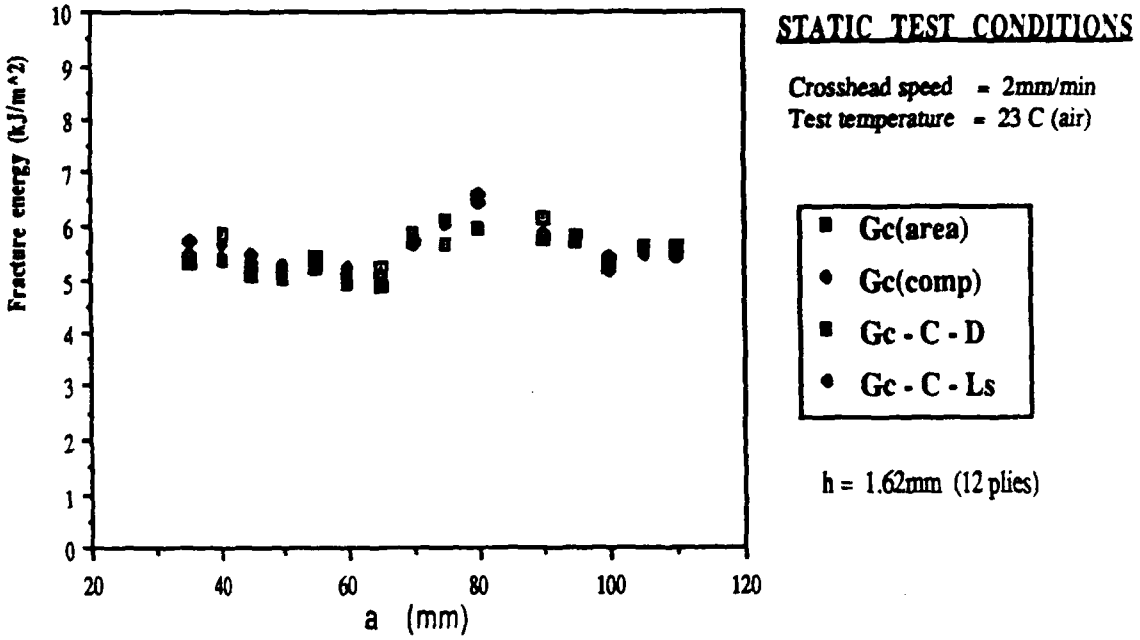


Figure 4.8. Variation of the fracture energy with crack length when beam analysis corrections were applied. (Composite: "APC-2" Adhesive: "9309.3NA").

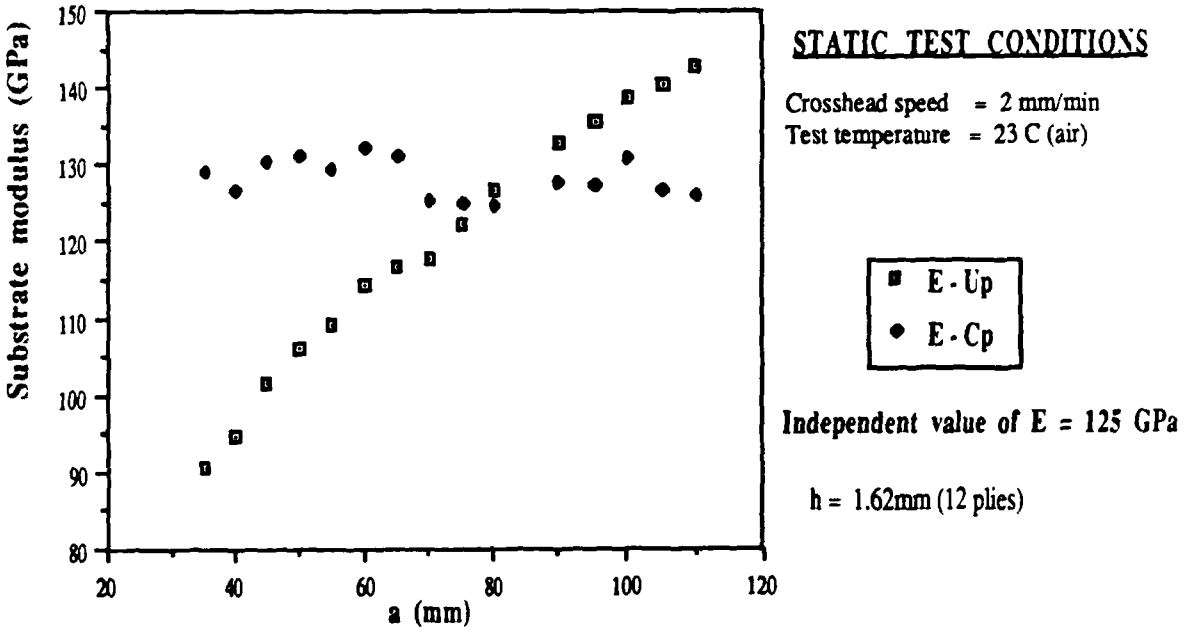


Figure 4.9. Comparison of modulus values when no corrections applied (E - Up) with when corrections were applied (E-Cp). (Composite: "APC-2" Adhesive: "9309.3NA").

value is in excellent agreement with the independently measured value of 125 GPa for this fibre-composite having the same volume fraction of fibres (i.e. 0.65%). Figure 4.9 illustrates the effect of the corrected beam theory on the values of E_s. Similar trends were observed from the complete range of different fibre-composite substrate adhesive combinations: that is "913C XAS-5-47/Hysol 9309.3NA", "913C XAS-5-47/FM73M" and "APC-2/FM73M".

4.3.3 Influence of Adhesive Type

Figure 4.10. shows that the cold cure adhesive (i.e "9309.3NA") has a higher fracture energy, G_{1c}, compared with the hot cure adhesive (i.e "FM73M"). Further, Figure 4.11. shows that the values of G_{1c} obtained are independent of any of the four methods of calculation (i.e Equation 4.1, 4.3, 4.15 and 4.16), provided that the necessary corrections have been applied to the simple beam theory methods (i.e to the "load" and "displacement" methods).

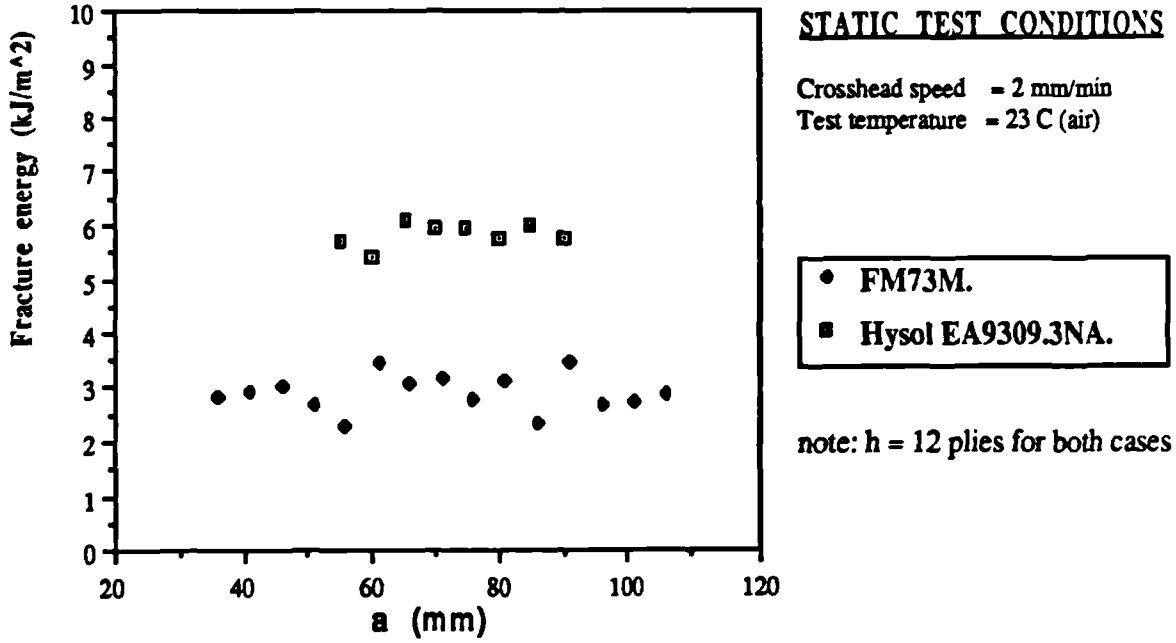


Figure 4.10. Comparison of the fracture energy of "FM73M" with "9309.3NA" using the area method of calculation. (Composite: 913C XAS-5-47%)

The results reveal that the mode I fracture energy, G_{1c}, of the bonded composites using "FM73M" is 2.93 ± 0.3 kJ/m^2 whilst that using "9309.3NA" is 5.7 ± 0.4 kJ/m^2 with the joints

failing by crack growth through the adhesive layer in all cases. This observation is in good agreement with earlier work by Luckyram and Vardy et al (1988) where they found that the cold cured adhesive was tougher than the hot cure adhesive when the bulk properties of the adhesives were tested using compact tension specimens. An interesting part of this work will be to investigate whether a similar trend is observed from the fatigue tests conducted on the joints. These results will be discussed later in chapter five.

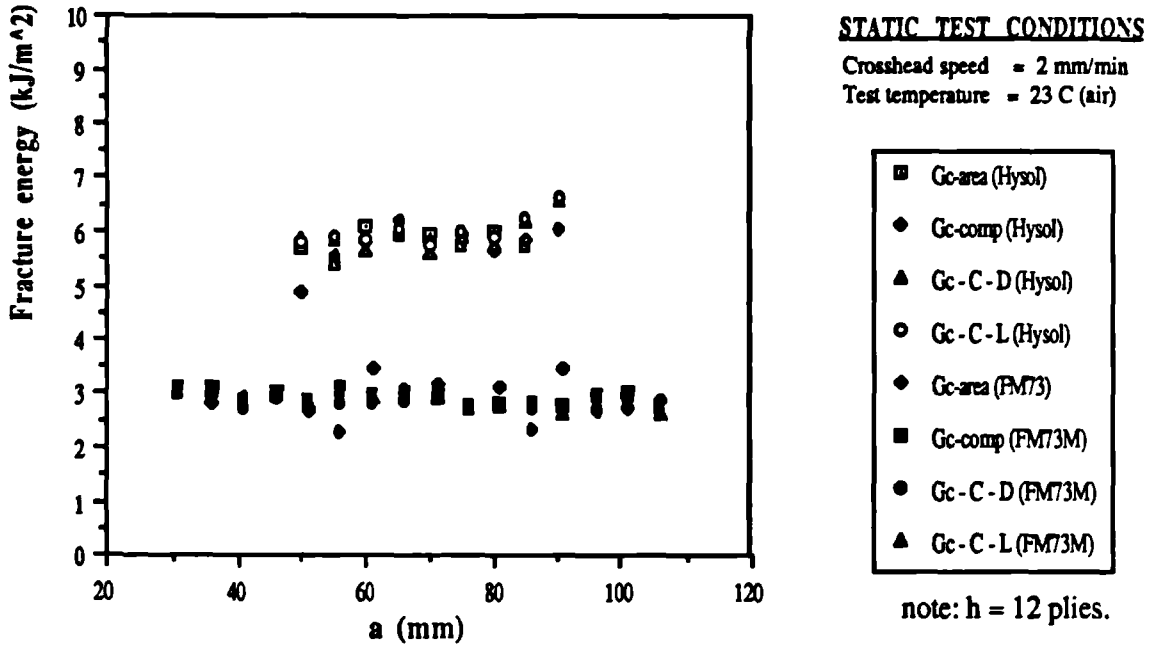


Figure 4.11. Comparison of the fracture energy of "FM73M" with "Hysol 9309.3NA" using all the four methods of calculation. (Composite: 913C XAS-5-47%).

4.3.4 Influence of the Type and Thickness of the Substrate

As discussed earlier in section 3.8, the limitations of the fatigue testing machine brings about the need to reduce the displacement of the specimen during testing. One way of achieving low displacement is to increase the thickness of the substrate, provided it can be ensured that any changes in the substrate thickness will not affect the value of G_{1c} for the adhesive. The information that is to be found in the literature on the influence of the thickness and type of substrate on the fracture energy of an adhesive is contradictory. While some authors (e.g Everett et al, 1987) claim that any changes in the thickness of the substrate should significantly

affect the value of G_{1c}, others (e.g Young 1978) have found that the value of G_{1c} is independent of the substrate thickness. Hence in the present work, it was considered necessary to examine how changes in the thickness and type of the substrate bonded with an adhesive will influence the value of G_{1c} for the adhesive.

Figure 4.12. shows the influence of the type of substrate when the cold cure adhesive ("9309.3NA") was used in bonding "APC-2" and "913C XAS-5-47%" composites. From the figure, it may be concluded that within experimental scatter, the type of substrate has no significant effect on the strain energy release rate of an adhesively bonded joint provided the locus of failure is cohesive through the adhesive.

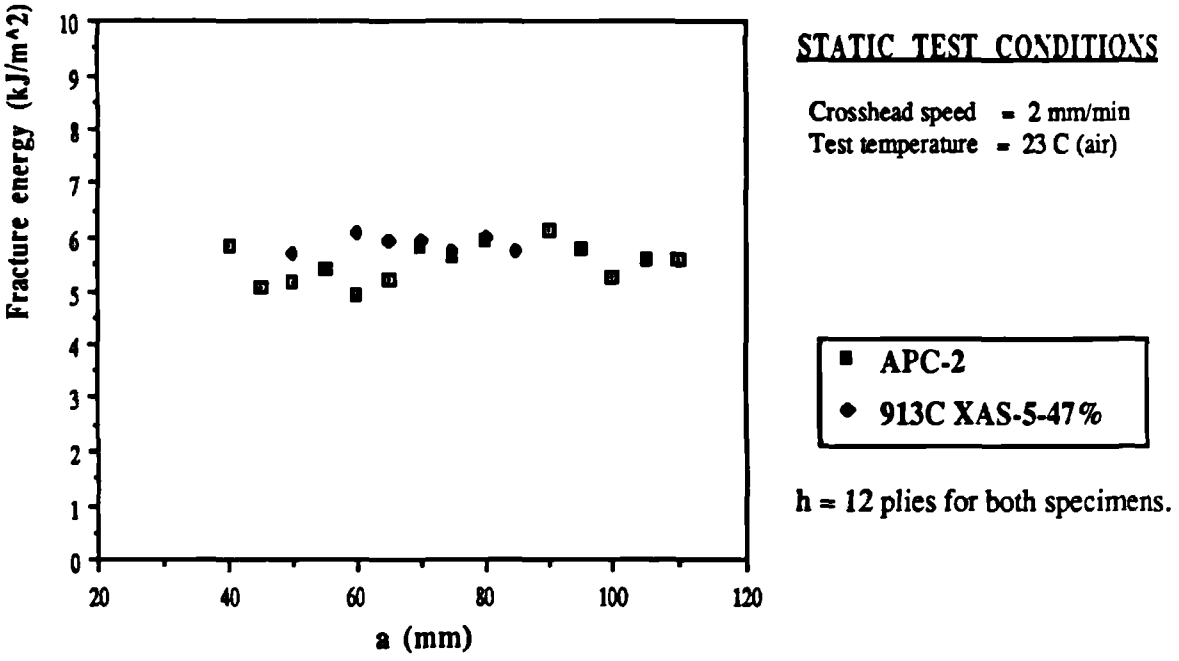


Figure 4.12. Influence of the type of substrate on the fracture energy of "9309.3NA" adhesive using the area method of calculation.

Figure 4.13 shows the variation of the G_{1c} values with crack length obtained using the area method (i.e Equation 4.1) for bonded "913C XAS-5-47%" composite with "FM73M" adhesive with substrate thicknesses of 1.49 mm, 1.81 mm and 3.71 mm. Figure 4.14 shows a plot using all the four methods of calculation (i.e equations 4.1, 4.3, 4.15 and 4.16). As can be

seen, for each method of calculation the overlapping of the data points is such that it may be concluded that there is no significant effect of the substrate thickness on the value of G_{1c} for the adhesively-bonded composite joints. This is an important information for several reasons. Firstly, from the fracture mechanics view point, G_{1c} is a material property and its value for cohesive fracture through the adhesive layer should be independent of the thickness of the substrate. Secondly, the observations from Figure 4.13 leads to the conclusion that the works reported by Bradley et al (1980) and Everett et al (1987) needs further clarification. Bradley et al tested 8, 12 and 16 ply specimens (i.e thicknesses of 1, 1.5 and 2mm), and found that the average value of G_{1c} for the adhesive were 831, 873 and 904 J/m^2 respectively. However, these values of G_{1c} differ by less than 9%, which is low, and could as well be assumed to be within the range of experimental scatter.

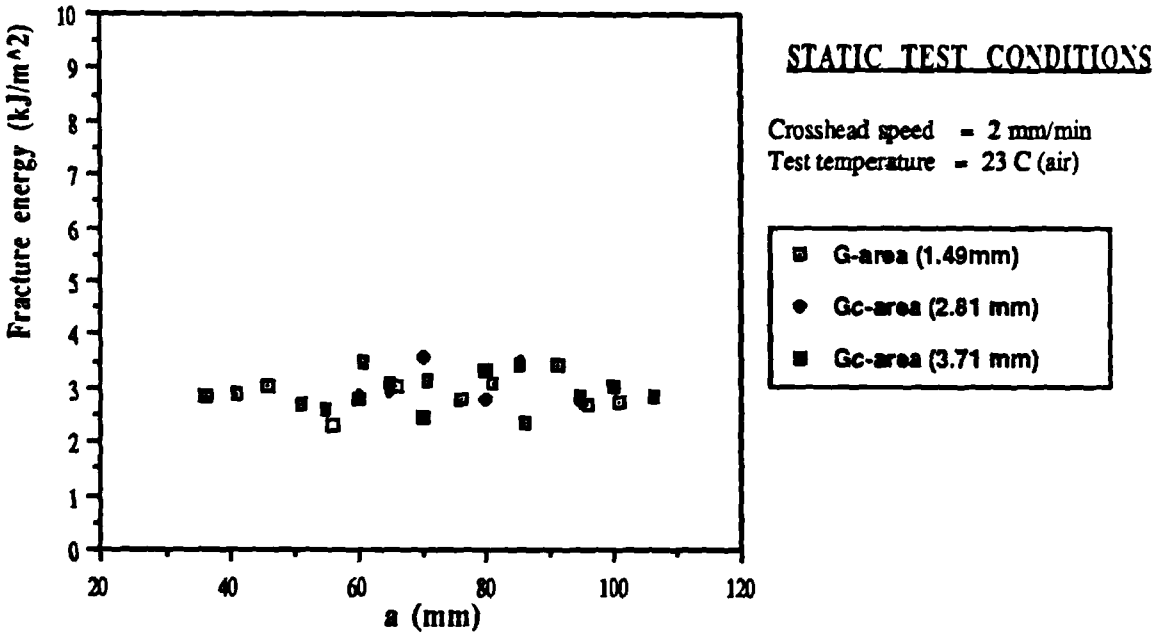


Figure 4.13. Influence of substrate thickness on the fracture energy of "FM73M" adhesive using the area method of calculation.

Everett et al (1987) stated that that increase in the value of G_{1c} could be as much as 20% as the substrate thickness was increased from 8 to 16 up to 24 ply (i.e thicknesses from 1 to 3mm). They suggested that G_{1c} increased with the substrate thickness due to the size of the plastic

zone increasing and hence more energy being dissipated. However Kinloch (1987) explained that the plastic zone size will only increase due to the influence of the substrate if the thickness of the adhesive layer is less than the plastic zone diameter. In this case the rigid composite substrates will impose a constraint upon the adhesive layer and increase the local tensile stresses at the crack tip. Reanalysing the data from the work of Everett et al (1987), then the plastic zone diameter was calculated to be 0.0561mm and this was less than the adhesive layer thickness (0.1mm). Thus the explanation provided by Everett et al (1987) for why G_{1c} increases with adhesive thickness is incorrect. Indeed the scatter in the results from Everett et al (1987) actually invalidates their conclusion that the G_{1c} value is dependent upon the thickness of the specimen.

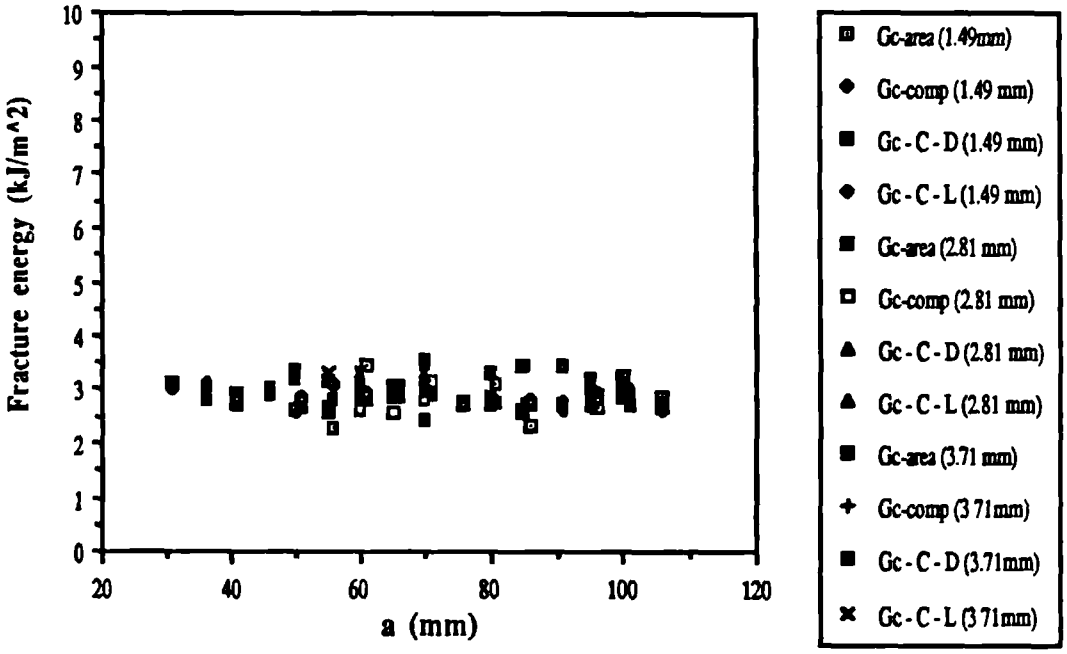


Figure 4.14. Influence of substrate thickness on the fracture energy of "FM73M" adhesive using all the four methods of calculation

4.3.5 Reinforcement of the Composite Substrate

In the previous section and in section 3.8 attention was focussed on the need to reduce the displacement of the arms of the specimen. As shown in section 4.3.4, using relatively thick composites substrate did reduce the displacement. However, due to the difficulty involved with

the manufacture of thick composites and the high cost of materials, an alternative method of reducing the specimen displacement such as reinforcing the fibre-polymer composite substrates by bonding aluminium or steel plates to the composite was considered.

However, before reinforced specimens could be considered adequate for fatigue testing, it was necessary to ensure, from constant crosshead rate testing, that the substrate reinforcement did not have a significant effect on the fracture energy, G_{1c}, when the crack propagated through the precracked adhesive layer. The results obtained showed that when the composite substrate were reinforced with steel, that the surface treatment technique employed (which involved grit blasting and solvent cleaning) were insufficient to prevent debonding at the composite/steel interface during the tests. This problem was observed even when stronger adhesives such as "FM73M" and "9309.3NA" were used in preference to "Permabond E38". However, when the composite substrate was reinforced with aluminium, the surface treatment technique which involved grit lightly blasting, then degreasing and then using the Forest Product Laboratory chemical treatment was sufficient to ensure no debonding at the composite/aluminium interface (Davis 1990).

Nevertheless, in the constant crosshead rate experiment performed to generate static data, there was noticeable yielding of the aluminium reinforcement as the crack grew through the adhesive layer. The problem persisted even when the thickness of the aluminium reinforcement was increased to as much as 19mm. When the grade of aluminium used was changed from "HE30TS" to "HE15TS" (*note: these codes names are from BS 1474*) which has a higher yield stress, then interlaminar failure of the composite substrate was observed. The reason for this is most likely to be a change in the stress distribution in the joint such that the transverse tensile stress that exists surpasses the interlaminar tensile fracture stress of the composite.

As a result of the above problems, the idea to reinforce the thin composite substrate with steel and aluminium beams was abandoned and the fatigue experiments were carried out using "thicker" composite substrates.

4.4 CONCLUSIONS

The main conclusions from this chapter are:

(1) Data has been generated from constant rate of displacement tests to establish the maximum and minimum loads, and displacements, of the specimens for the subsequent fatigue tests.

(2) The correction factors developed for the DCB specimen (Williams 1990) to correct for the assumptions of zero compliance at the crack root and large displacement of the double cantilever beam have been successfully applied to the fracture energy calculations for the adhesively-bonded joints.

(3) Fracture mechanics concepts have been successfully employed to measure the fracture energies of the two adhesives as cracks propagate cohesively through the adhesively-bonded joints. The results revealed that the fracture energy, G_{1c}, of the bonded composite using "FM73M" is 2.93 ± 0.3 kJ/m^2 whilst that using "9309.3NA" is 5.7 ± 0.4 kJ/m^2.

(4) The fracture energy, G_{1c}, of adhesive joints was found to be independent of the thickness of the substrate between 12 and 24 plies (i.e thickness between 1.5 and 3mm) and the type of substrate (i.e the thermoplastic composite "APC-2" and thermosetting composite "913C XAS-5-47%").

(5) Attempts were made to reinforce the relatively thin composite substrates with steel or aluminium plates in order to minimise the displacement undergone by the specimen. This would enable fatigue testing at higher frequencies. However, this work was not successful and it was decided to simply use relatively thick composite substrates for the fatigue testing.

CHAPTER FIVE

FATIGUE TESTS CONDUCTED IN AIR

5.1 INTRODUCTION:

This chapter discusses the fatigue performance of the bonded fibre composite joints made from the materials described in section 3.2. Firstly, the various methods for analysing and presenting the fatigue data are reviewed, and recommendations are made as to the best methods. Secondly the fatigue tests were performed under displacement control as discussed in section 3.8 and the parameters which may influence the fatigue behaviour are discussed; these parameters include frequency, displacement ratio, mean displacement, type of adhesive and the type of substrate.

5.2 POSSIBLE VARIABLES IN FATIGUE TESTING:

Before any predictions of fatigue crack growth rate can be made, data should be available which are relevant to service conditions. Such data are hard to find, since the fatigue behaviour of any engineering material is dependent upon many factors which contribute in different ways to the fatigue crack propagation process. Hence, complex fatigue conditions are usually approximated by simplified laboratory experiments in which the effect of one variable is studied in turn, whilst all the other variables are held constant. The most important of these factors are (Kinloch 1987):

(i) a periodically varying stress with stress amplitude, σ_{amp}, ($\sigma_{amp} = 1/2(\sigma_{max} - \sigma_{min})$;

(ii) a correspondingly fluctuating strain amplitude, ε_a, ($\varepsilon_a = 1/2(\varepsilon_{max} - \varepsilon_{min})$;

(iii) a stress range, $\Delta\sigma$ ($\Delta\sigma = (\sigma_{max} - \sigma_{min})$);

(iv) a mean stress level, σ_m ($\sigma_m = 1/2(\sigma_{max} + \sigma_{min})$;

(v) a stress ratio, σ_R, or displacement ratio δ_R ($\sigma_R = \sigma_{min}/\sigma_{max}$ or $\delta_R = \delta_{min}/\delta_{max}$);

(vi) a frequency, *f*;;

(vii) a characteristic waveform for both stress and strain (e.g sinusoidal, square, etc);

(viii) environmental effects;

(ix) details of the specimen geometry.

The above list presents a tremendous task to the experimentalist since fatigue tests are expensive by nature and the generation of a single set of data points can take a long period of time.

5.3 METHODS OF PRESENTATION OF FATIGUE DATA

5.3.1 Introduction

The aim of generating fatigue data is to use the information to rank and predict the service life of an engineering material and to understand the material or joint behaviour under fatigue loading. Fatigue data are conveniently displayed in different forms. The most commonly encountered forms in which these data are presented are:

(i) A plot of the maximum applied stress versus the number of cycles to failure (i.e S-N curves).

(ii) The use of time dependent changes in residual properties of the material such as the modulus, compliance or strength (which might occur during fatigue cycling) to predict the service life.

(iii) A plot of the maximum applied strain energy release rate versus the number of cycles to failure (i.e G_{max} -N curves).

(iv) A plot of the crack growth rate versus the applied strain energy release rate or stress intensity factor (da/dN versus G_{max} curves).

These methods are discussed in the next four sections.

5.3.2. S-N Curves

In many publications including the handbook for mechanical engineers (Kutz 1986) and a document produced by the British Standard (BSI PD 6493, 1980), it is recommended that fatigue data be presented on a plots of the maximum applied stress, S, versus the number of cycles to failure, N_f. These plots are usually referred to as S-N curves. The standard method of generating these plots is to test no less than five specimens at each of several different stress amplitudes and then simply record the maximum stress, stress amplitude and the number of cycles to failure. The philosophy is that from the S-N curves the service life of any structure can be predicted by simply reading from the curve the number of cycles that corresponds to the applied stress amplitude. In the document BSI PD 6493 (1980) it is suggested that S-N curves should be adequate for the assessment of the fatigue performance of materials, since it offers a simplified procedure which requires no calculation by the design engineer.

However, other authors (e.g Barsom et al (1987) have found that when two samples with different geometries are involved the S-N curve obtained from one geometry does not necessarily provide accurate information regarding the service life of another. Three main reasons were given for this conclusion. Firstly, the surface irregularities in the component may be different from those of the test specimen used in generating the S-N curve. Secondly, the fatigue crack growth is governed by the magnitude of stresses at the tip of the propagating crack, and not by the applied stresses at a distance much further away. Thirdly, It is understood that the material properties that govern the growth of a crack are the critical stress intensity factor K_{1c} (or the fracture energy G_{1c}) at the crack tip. Obviously since different

specimen geometries may have different geometrical factors, the value of G and K governing the crack growth will be different for the same testing conditions. Hence, the cracks in these specimens will propagate at different rates. Thus, simply a knowledge of the S-N curve is really inadequate to understand and predict the fatigue behaviour of an engineering component.

5.3.3. Fatigue Damage Plots.

During a fatigue test many material properties such as modulus, compliance, residual strength and residual strain may change with the number of fatigue cycles. In such circumstances, models can be developed which define the fatigue damage as a function of any of these materials properties. For example, Hwang et al. (1986, 1989) studied the fatigue behaviour of reinforced plastics and introduced the "fatigue modulus concept" in which a relationship is established between an observed gradual fall in the fatigue modulus as the amount of fatigue damage increased. By defining the fatigue modulus, E_f, at the n^{th} loading cycle as the value of the applied stress divided by the resultant strain, they suggested that the service life of the composite may be predicted from the relation:

$$\frac{dE_f}{dN} = A\frac{CN^{C-1}}{BE_f^{B-1}} \qquad (5.1)$$

where A, B and C are material constants and N is the number of fatigue cycles. Similar concepts were introduced by Reifsnider (1986) using changes in residual strength, and Lee (1991) using changes in residual stiffness.

A more comprehensive model was introduced by Beaumont (1986b which relates changes in residual properties of a material during fatigue cycling (such as the elastic stress amplitude, $\Delta\sigma$, and stress ratio σ_R and the amount of damage growth, Q) to the damage growth rate, dQ dN, and is expressed as:

$$\frac{dQ}{dN} = f(\Delta\sigma, \sigma_R, Q) \tag{5.2a}$$

To measure the amount of damage an empirical relationship was established between the damage growth rate and the rate of change in the axial modulus, E, of the composite as:

$$\frac{dQ}{dN} = b_1\left(\frac{1}{E}\frac{dE}{dN}\right) \tag{5.2b}$$

and the service life was predicted from an empirical relationship of the form:

$$N_f = b_2\left(\frac{\Delta\sigma}{\sigma_{TS}}\right)^{b_3}\left(b_4\frac{1-\sigma_R}{1+\sigma_R}\right)^{b_5}\left(1-\frac{\Delta\sigma}{(1-\sigma_R)\sigma_{TS}}\right) \tag{5.2c}$$

where σ_{TS} = mean value of the ultimate tensile strength of the composite and b_1, b_2, b_3, b_4 and b_5 are empirical constants. However all these models are based on the concept of changes in residual properties of a material during fatigue cycling and are at a relatively early stage of development. Indeed, the agreement with experimental observation is only moderate compared with the well established crack growth rate model (section 5.3.5), and further improvements are needed before they can be used to obtain more accurate predictions of the service life.

5.3.4. G_{max} -N Curves

A novel suggestion for a method of locating accurately the threshold value G_{th} was made by O'Brien et al (1989). They found that fatigue data for composites and adhesives could be represented by a plot of G_{max}-N, curve analogous to S-N curves in metals and proposed that by choosing a suitable value of N, it was possible to specify a suitable value of the threshold value, G_{th}.They assumed that when a test was performed in displacement control, in which the

crack growth rate decreases as the crack grew, a point is reached when the G_{max}-N curve will be seen to be approaching an asymptote. If at that point no crack is seen to grow further for another one million cycles, then this lower bound value of G_{max} could be considered as the threshold value, G_{th}. From these curves it is therefore possible to obtain this threshold value of the strain energy release rate, G_{th}, which is a very useful property for quality assurance and design purposes. An example of a G_{max} versus N plot for an epoxy film adhesive bonding a thermosetting CFRP is given in Figure 5.1.

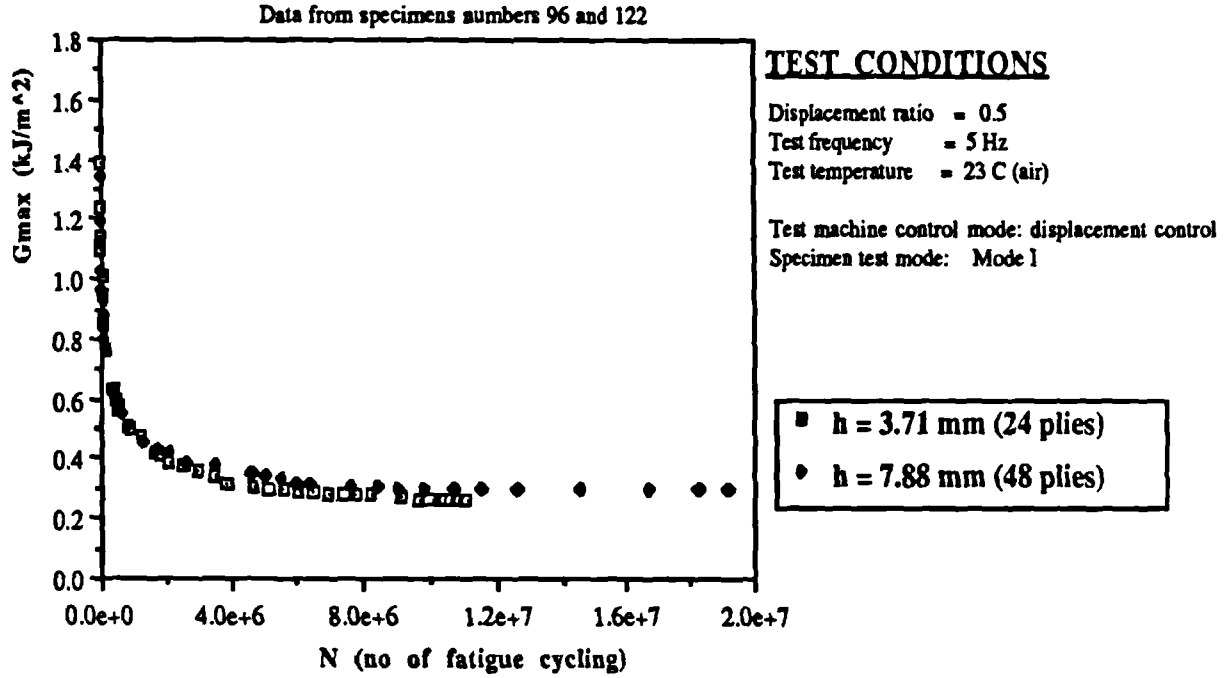


Figure 5.1. Typical Gmax versus N curve showing the influence of substrate thickness on the fatigue performance of a bonded joint (Note: Substrate 913C XAS-5-47%, adhesive FM73M).

Secondly, as mentioned earlier in section 2.5, the use of $\Delta G = (G_{max} - G_{min})$ in characterising fatigue crack growth has some disadvantages when the DCB specimen is used. This is due to the uncertainty in the value of G_{min} as a result of the effects of counter-face interference. Such interference of the opposite faces of an adhesive joint may be due to the rubbing of rough debonded surfaces, the collection of adhesive debris and the effect of the plastic zone at the crack tip. These defects keep the crack tip open during the minimum fatigue cycle and result in

an over-estimation of ΔG values. This problem is avoided by using the G_{max} value in place of ΔG, and support the idea of plotting G_{max} versus N and obtaining the value of G_{th} as described above. As a final comment on this method, the specimen geometry and test method used should obviously be such that the value of G_{max} decreases as the fatigue crack grows. If for example, the value of G_{max} is constant as the fatigue crack grows then the curve of the form shown in Figure 5.1 will obviously not be obtained.

5.3.5. da/dN versus G (or K) Curves

As discussed in section 2.4, crack growth rate data are typically generated under constant amplitude conditions and are plotted in the form:

$$\frac{da}{dN} = f(G \text{ or } K) \qquad (5.3)$$

where da/dN is the crack growth rate per cycle and G (or K) is either the strain energy release rate range, ΔG, (or ΔK) or the maximum applied strain energy release rate, G_{max}, (or K_{max}). In general, the use of the energy balance approach is preferred to the stress intensity factor approach because an unambiguous value of strain energy release rate, G, may be obtained while the determination of the stress intensity factor , K, is not always straightforward. As was discussed above (section 5.3.4), for characterising adhesively bonded joints, the use of G_{max} is often preferred to ΔG. Some other reasons why the use of G_{max} is preferred can firstly be seen by illustrating the difference between the two curves. Figures 5.2a and 5.2b show comparisons of the da/dN versus ΔG curves with the same data replotted as da/dN versus G_{max} curves. As can be seen from Figure 5.2a, when the tests were carried out at a relatively high displacement ratio (e.g $\delta_R = 0.5$) the da/dN versus G_{max} curve differs from a da/dN versus ΔG curve by a shift along the horizontal axis of the curve, and the shift factor has a magnitude equal to (G_{max} - ΔG). This implies that at relatively low displacement ratio (e.g $\delta_R = 0.1$), when G_{min} is very small and ΔG tends to G_{max}, the two curves will tend to be

equivalent to one another as illustrated in Figure 5.2b.

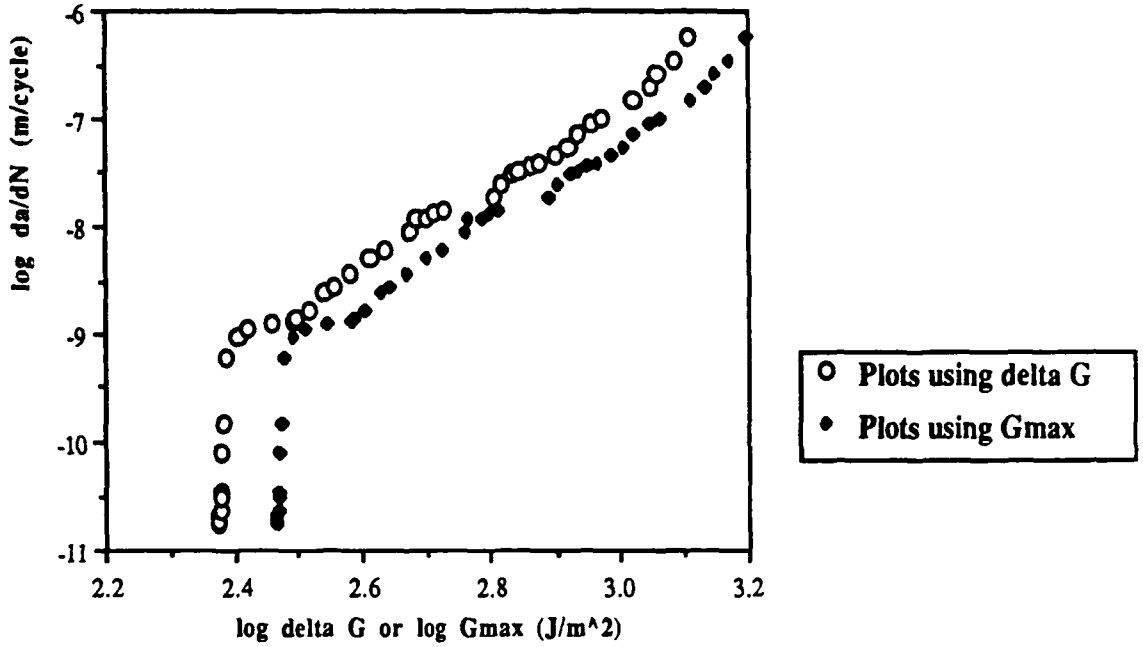


Figure 5.2a. Comparison of the characterisation of a fatigue data by using a da/dN versus delta G curve and using a da/dN versus Gmax curve, when the tests were performed at a relatively high displacement ratio (0.5).

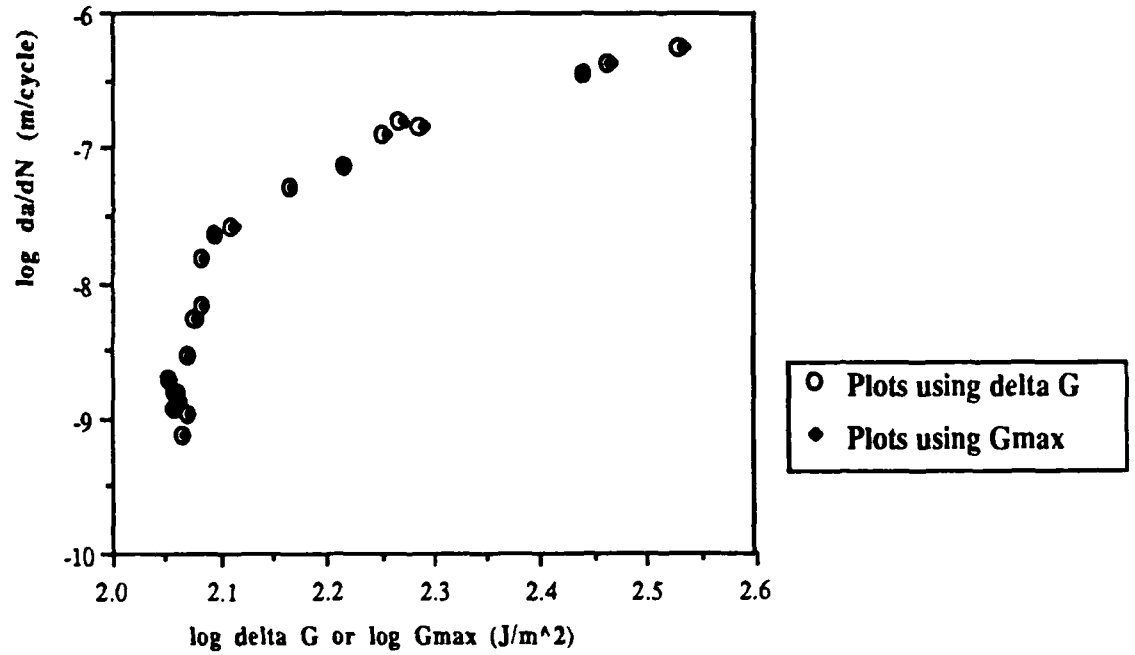


Figure 5.2b. Comparison of the characterisation of fatigue data by using a (da/dN versus delta G) curve with by using a (da/dN versus Gmax) curve when the tests were performed at a relatively low displacement ratio (0.1).

Now it is easier to deduce the extent of loading from a da/dN versus G_{max} curve, than from a da/dN versus ΔG curve. This is because from a knowledge of G_{max} and the displacement ratio, δ_R, G_{min} can easily be calculated by simple multiplication. Whereas, from a knowledge of ΔG and δ_R, the designer has the harder task of solving a simultaneous equation to obtain the values of G_{max} and G_{min}. It should also be noted that while G_{max} can be immediately seen as the maximum strain energy release rate applied to the material, ΔG is just a numerical value which is useless unless the value of δ_R is also known.

Now, not only do plots of da/dN versus Gmax represent material property data (i.e are independent of test geometry), but by the integration of Equation 5.3, the lifetime of any joint geometry can be estimated. This is discussed in detail in Chapter Eight.

5.4 ANALYSIS OF THE FATIGUE EXPERIMENTS

In section 5.3, it was concluded that the best method for characterising the fatigue crack growth in adhesive joints was by relating the crack growth rate da/dN to the corresponding maximum value of the strain energy release rate, G_{max}. This section reviews the methods of analysing the experimental data in order to estimate the values of da/dN and G_{max}.

5.4.1 Methods of Estimating da/dN

The first step in the analysis of test results was to obtain the crack growth rate da/dN from measurements of the crack length and the corresponding number of cycles of testing. The basic experimental data consist of a set of discrete and finite crack length measurements and cycle count values (i.e N_i and a_i measurements). Hence, care must be exercised in defining the crack growth rate to ensure that the calculated values are consistent with the basic assumption of continuity in the fatigue crack growth process which the growth curve is representing. Various techniques have been used to analyse the form of data, and a brief description of the relevant

techniques is presented below.

5.4.1.1 The Graphical Method

This method involves plotting the crack length, a_i, versus the number, N_i, of fatigue cycles and the fitting of a polynomial equation to the experimental data points. The equation for the crack growth rate may be estimated by differentiating the polynomial equation. From the differentiated equation the value of da/dN for each experimental point may then be estimated. Alternatively, instead of fitting an equation to the plot of a versus N the value of da/dN for each data point could be obtained by measuring the slope of the tangent to the a versus N curve at the data point. However, the graphical method has it shortcomings which are discussed in section 5.4.1.4.

5.4.1.2 The Secant Method

The secant method is recommended in the ASTM E647-88 standard and is a commonly used method. The method involves calculating the slope of the straight line connecting two adjacent data points (a_i, N_i) and (a_{i+1}, N_{i+1}) on the a versus N curve. It is formally expressed as:

$$\frac{da}{dN} = \frac{a_{i+1} - a_i}{N_{i+1} - N_i} \tag{5.4}$$

The ASTM standard also recommends that since the computed da/dN is an average over the values of crack lengths between a_{i+1} and a_i, the average value of both lengths (i.e $a_{i+1} + a_i$) is normally used to calculate the corresponding value of G_{max}. For reasons discussed in section 5.4.1.4, the secant method has been found unsuitable for adhesive joints.

5.4.1.3 Incremental Polynomial Method

This method has also been recommended in the ASTM E647-88 standard. It involves estimating the crack growth rate by fitting a second order polynomial (i.e a parabola) to sets of

(2g+1) successive data points, where g is usually 1, 2, 3 or 4. In the present investigation 'g' is assumed to be 3. The form of the equation for a local fit is as follows:

$$a_i = b_o + b_1\left(\frac{N_i - C_1}{C_2}\right) + b_2\left(\frac{N_i - C_1}{C_2}\right)^2 \qquad (5.5)$$

where

$$-1 \le \left(\frac{N_i - C_1}{C_2}\right) \le 1 \qquad (5.6)$$

and b_o, b_1 and b_2 are regression parameters that are determined by the least squares method over the range of crack length values between $a_{i-3} \le a \le a_{i+3}$. The value of a_i is fitted to the value of the crack length N_i. The parameters $C_1 = 1/2(N_{i-3} - N_{i+3})$ and $C_2 = 1/2(N_{i+3} - N_{i-3})$ are used to scale the input data. The crack growth rate is then obtained by differentiating Equation 5.5 with respect to N_i. to give the expression:

$$\frac{da}{dN} = \frac{b_1}{C_2} + 2b_2\left(\frac{N_i - C_1}{C_2^2}\right) \qquad (5.7)$$

For ease of calculation, a computer program was written in the ASTM E647-88 standard to solve Equation 5.7 and obtain the values of da/dN for each data point.

5.4.1.4 Discussion of methods for Estimating da/dN

The choice of any of the three methods described above depends on the degree of variability in the raw experimental data. The graphical method may yield repeatable results when all the data points lie on a smooth curve, but this is not the case in most instances. For example, Fedderson et al (1973) attempted to presented their experimental data using the polynomial curve-fitting equations but observed that the fitted curve oscillated about the experimental data in such a way that the gradient estimated by differentiation was seriously in error. Another

disadvantage they found with the graphical method was the difficulty in obtaining a satisfactory curve fitting equation from the data points. This difficulty arises because the degree of the polynomial needed to accurately fit the curve may range from about 2 to 10 and its correct value can only be known from trial and error.

Hence, the graphical method was abandoned in this present work. The use of the secant method resulted in very large scatter of the data points when used to analyse the results. As a result, the linear region II constants (from Equation 2.27) which were obtained from the slopes and intercepts of the growth curves had very low correlation coefficients. However, when the same set of data were analysed using the incremental polynomial method, the scatter in the graphs were considerably reduced.

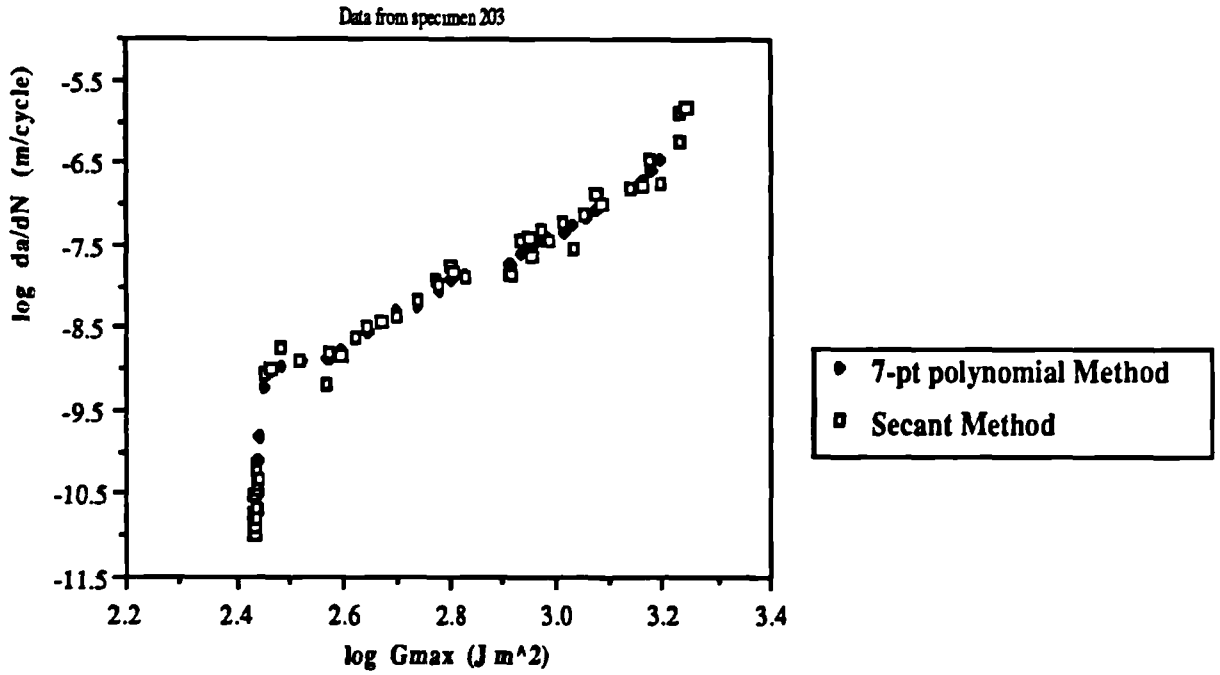


Figure 5.3. Comparison of data analysis using the incremental polynomial method and the secant method. (Note: Substrate 913C XAS-5-47%, adhesive FM73M).

Figure 5.3 shows a comparison of the two methods using the same set of data points. From the graph, It can be seen that the incremental polynomial method is far superior to the secant

method. Thus the incremental polynomial method is recommended as the best method for analysing the crack growth rate in adhesively bonded joints.

5.4.2 Methods of Estimating G_{max} of an Adhesive in a DCB Joint

The four principal equations described in section 4.2 (i.e Equations 4.1, 4.3, 4.15 and 4.16) may be used to evaluate the maximum value of the strain energy release rate G_{max} as follows:

area method

$$G_{max} = \frac{(P_{1max}\delta_{2max} - P_{2max}\delta_{1max}}{2B(a_{2max} - a_{1max})} \tag{5.8}$$

compliance method

$$G_{max} = \frac{P_{max}^2}{2B}\frac{\partial C}{\partial a} \tag{5.9}$$

load method

$$G_{max} = \frac{12P_{max}^2 (a + \chi h)}{B^2 E_s h^3} F \tag{5.10}$$

displacement method

$$G_{max} = \frac{3P_{max}\delta_{max}}{2B(a + \chi h)} \cdot \frac{F}{Z} \tag{5.11}$$

where all variables are as defined in section 4.2. Now, any of the four equations above could be used to plot the growth curve. For example, as can be seen from Figure 5.4 there is good correlation between the curves when the value of G_{max} was calculated using the compliance and displacement methods (section 4.3.2).

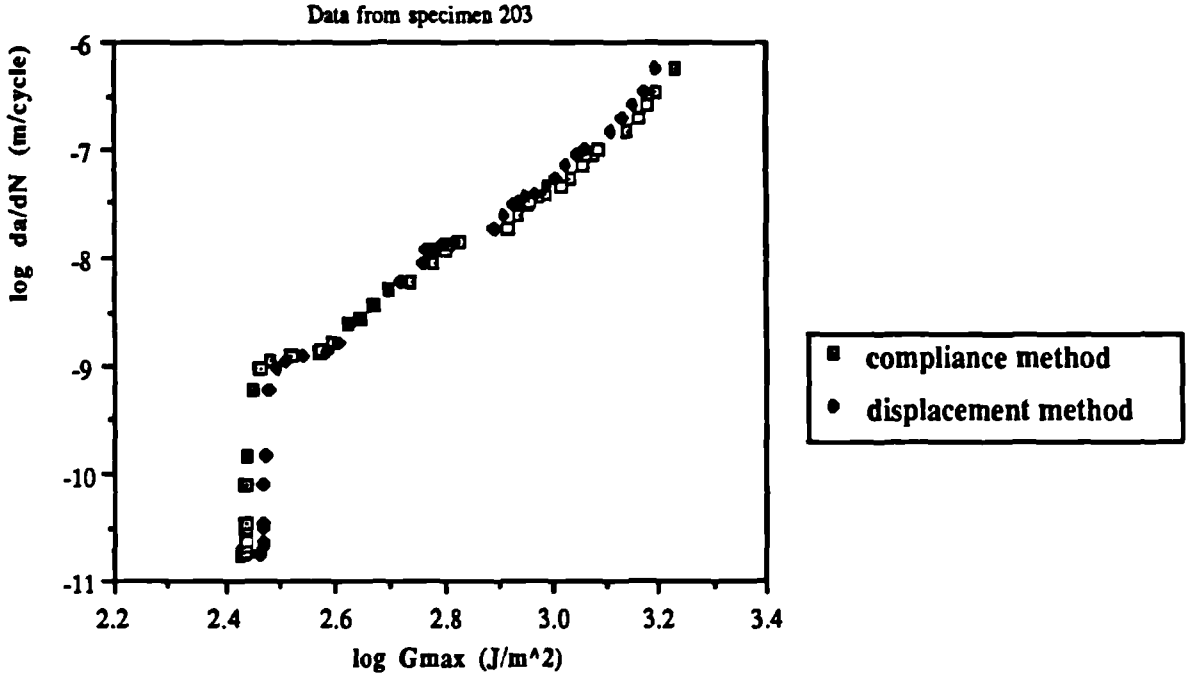


Figure 5.4. da/dN versus Gmax plots where the values of Gmax have been calculated using equations 5.9 and 5.11. (Note: Substrate 913C XAS-5-47%, adhesive FM73M).

In the present investigation, the compliance method was used because it is a simple and powerful method of obtaining G_{max} directly from the load versus displacement values recorded from the fatigue tests, without any calculation of correction factors.

5.5 RESULTS AND DISCUSSION

5.5.1 Introduction

As was discussed in section 3.11, the fatigue tests were carried out using a servo-hydraulic testing machine under displacement control. The two adhesives tested were a hot cure epoxy film adhesive ("FM73M") and cold cure epoxy paste adhesive ("9309.3NA"). The substrates were thermoplastic CFRP ("APC-2") and a thermosetting CFRP ("913C XAS-5-47%"). These materials were made into DCB joints as described in section 3.6, which were mounted in the testing machine. The crack length was measured with the aid of a travelling microscope mounted on a platform fixed to the base of the testing machine. The values of the maximum and minimum loads and displacements, crack length and the number of cycles of testing the specimen were recorded and were used to calculate the values of da/dN and G_{max}, as described in section 5.4. The crack growth curves are presented in two forms. One form is to plot curves of da/dN versus G_{max} while the other is to plot G_{max} -N curves. The locus of failure was always via cohesive fracture through the adhesive layer.

5.5.2 Effect of Frequency

Figure 5.5 shows the effect of frequency on the fatigue performance of the bonded joint. The data shows that there is no significant effect on the crack growth rate as the frequency of cycling is increased from 1 to 5 Hz. The figure also reveals that the threshold value, G_{th}, for the joints bonded using the hot cure epoxy film adhesive at the specified testing conditions is 0.26 ± 0.03 kJ/m^2. The G_{max} -N curve shown in Figure 5.6 supports the above observation that the frequency does not affect the rate of crack growth or the value of G_{th}.

This observation is in agreement with earlier findings (e g Bathias et al 1985, Mall et al 1986, Adams et al 1987, Luckyram and Vardy 1988). Bathias et al (1985) showed that there was no significant effect on the crack growth rate in glass epoxy composites tested at frequencies between 2 and 15 Hz. Mall et al. (1986) showed that the crack growth rate in graphite epoxy

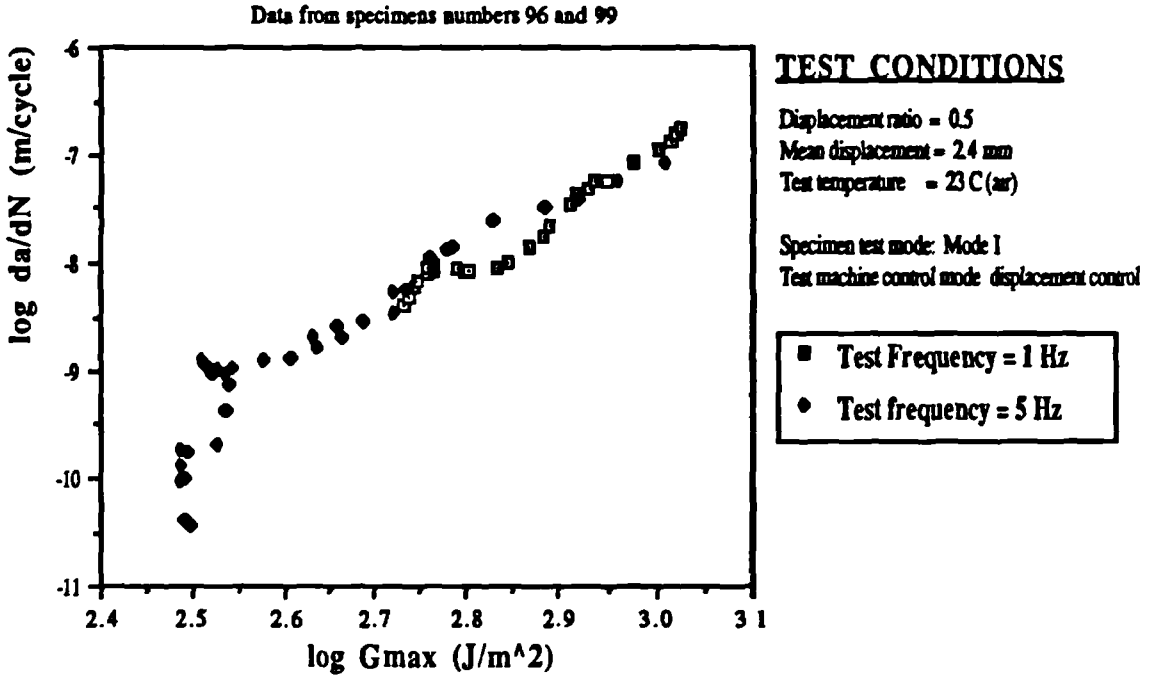


Figure 5.5. Influence of frequency on the fatigue performance of a bonded joint. (Note: Substrate 913C XAS-5-47%, adhesive FM73M).

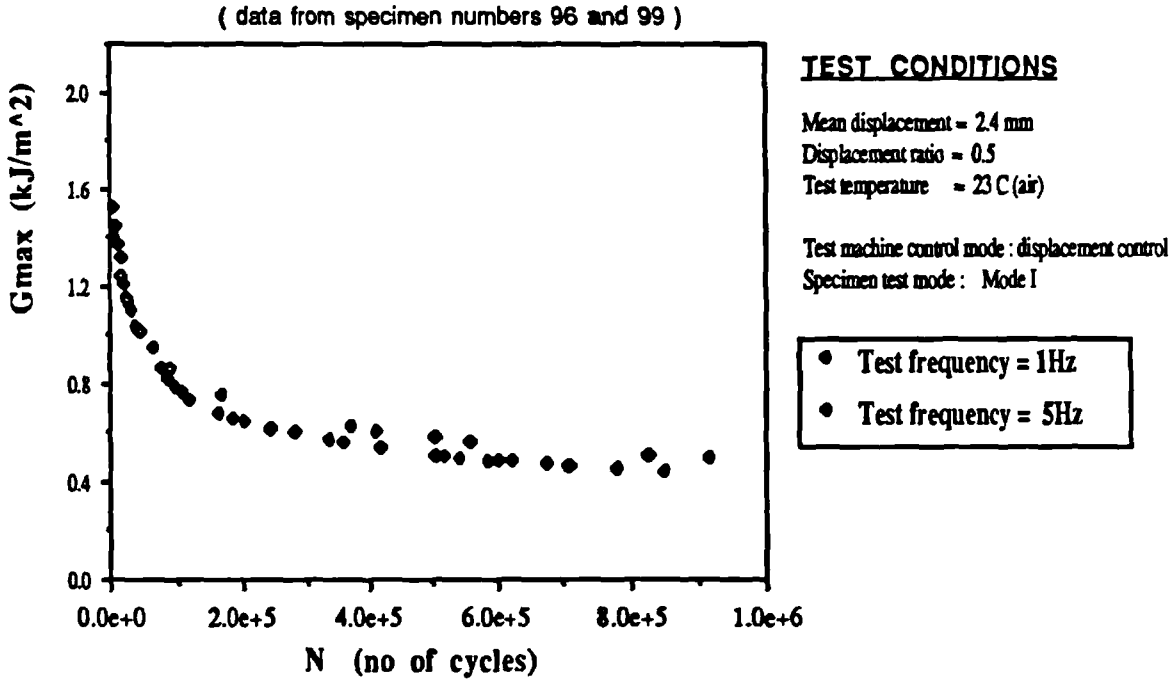


Figure 5.6. Influence of frequency on the fatigue performance of a bonded joint. (Note: substrate: 913C XAS-5-47%, adhesive: FM73M)

substrates bonded with a hot cure epoxy film adhesive (FM300) were not affected by frequency between 3 and 10 Hz and Adam et al (1987) showed that test frequencies between 2 and 10 Hz had no effect on the crack growth rate in graphite epoxy composite. Finally, Luckyram and Vardy et al (1988) studied the fatigue performance of two structural adhesives and also found that the crack growth rate was not affected between frequencies of 0.5 and 5 Hz.

Thus, the results from this work and from the above earlier findings indicate that any change in frequency in the ranges between 0.5 and 15 Hz would not affect the fatigue performance of the adhesive. However, it is possible that a different result may be obtained at more extreme frequencies. For example, Knauss (1973) reported that the cyclic frequency can affect the crack growth rate in glassy polymers as the glass transition temperature of the polymer is approached. He predicted that glassy polymers can soften extensively because of the heat build up at the crack tip as a result of of energy dissipation due to cyclic loading. However, recent investigation on bonded structural adhesives using cyclic frequencies up to 40 Hz (Jablonski 1980), and 66.7 Hz (Kilik et al. 1989), revealed that the temperature rise in the adhesives are negligible. For example, Jablonski reported a temperature rise of about 0.02 °C at the crack tip of a tapered double cantilever beam specimen bonded with a hot cure epoxy adhesive ("EA9649").

5.5.3 Effect of Displacement Ratio, δ_R

The da/dN vs G_{max} curve in Figure 5.7a shows the effect of displacement ratio (i.e. $\delta_R = \delta_{min}/\delta_{max}$) on the fatigue performance of a thermosetting CFRP bonded using the hot cure epoxy film adhesive. It is evident from this comparison that the results differ substantially for the two different displacement ratios. The crack growth rates are higher at a displacement ratio of 0.1 than at 0.5, for the same value of maximum strain energy release rates, G_{max}. The data

also shows that the threshold value, G_{th}, increases as the displacement ratio increases. (Although it is acknowledged that more data points are needed in order to obtain an absolute comparison for the case when the displacement ratio was 0.1). The G_{max} -N curves from Figure 5.7b show that for the same value of G_{max}, the adhesive will last longer under fatigue cycling at a displacement ratio of 0.5 that at 0.1.

These observations on the effects of displacement ratio are consistent with those previously reported by Martin et al (1990) and Donaldson et al (1989). Martin et al (1988) found that, for both mode I and mode II failure, the delamination growth rate in a thermoplastic CFRP ("APC-2") increases as the displacement ratio decreases. Donaldson et al worked on the mode III delamination of graphite-epoxy composite and again observed that the crack growth rates were higher for tests conducted at a displacement ratio of 0.1 compared with that of 0.5.

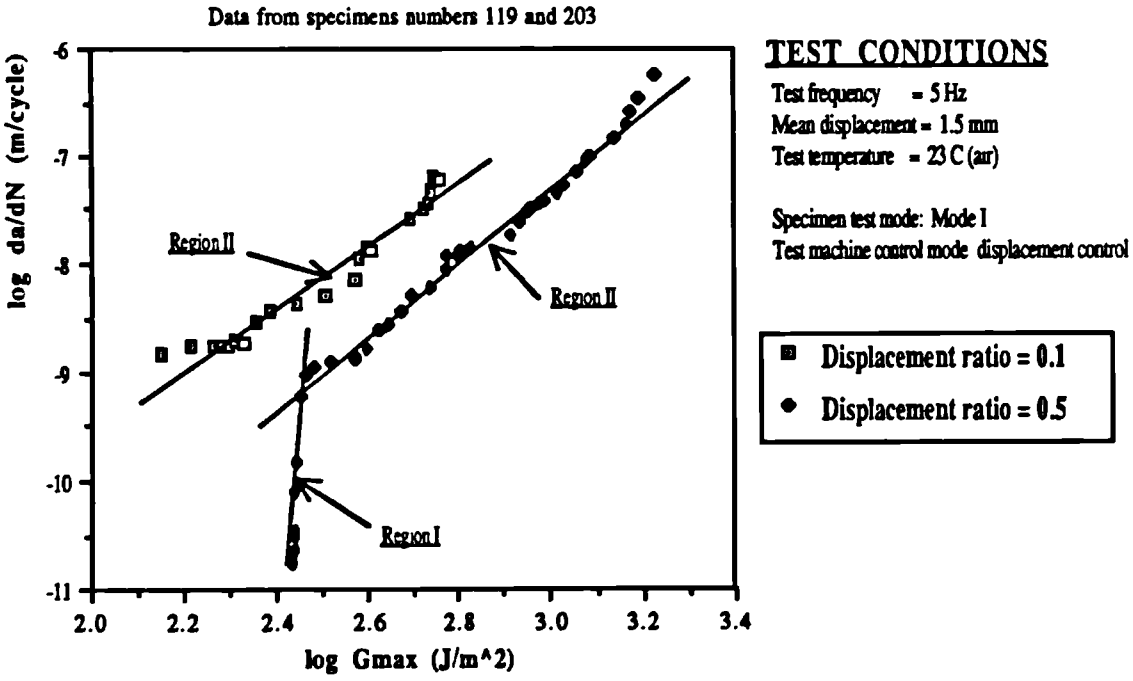


Figure 5.7a. Influence of displacement ratio on the fatigue performance of bonded joints. (Note: Substrate 913C XAS-5-47%, adhesive FM73M).

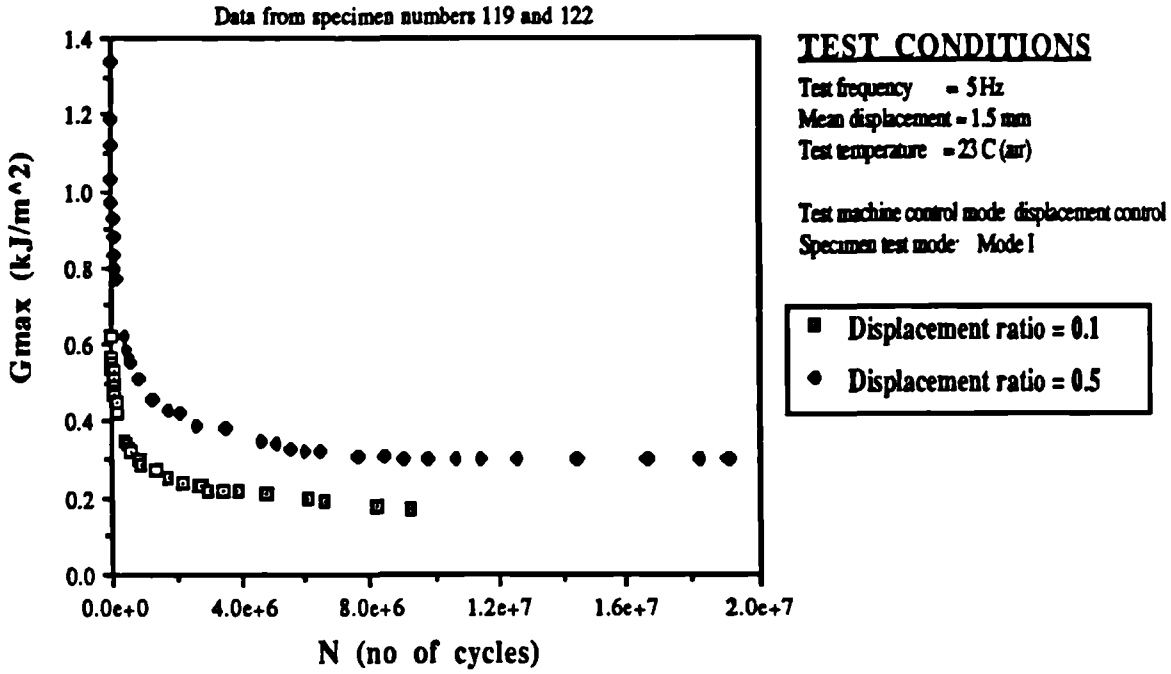


Figure 5.7b. Influence of displacement ratio on the fatigue performance of bonded joints. (Note: Substrate 913C XAS-5-47%, adhesive FM73M).

These observation arise because, as mentioned earlier, experiments in displacement control involved fixing a δ_{max} of about 90% of the corresponding static test value, and then using a predetermined displacement ratio to estimate the value of the δ_{min}. Thus the higher the displacement ratio, the smaller the difference between the maximum and minimum displacements of the specimen and the lower the extent of crack opening. Since it is the extent of crack opening which results in fatigue damage and crack growth, then the lower the extent of crack opening, then the lower the cyclic crack growth rate for a given G_{max} value and the higher the threshold value, G_{th}.

5.5.4 Effect of Mean Displacement

Figure 5.8a shows the effect of mean displacement (i e. $\delta_{mean} = (\delta_{max} + \delta_{min})/2$) on the fatigue performance of a thermosetting CFRP bonded with a hot cure epoxy film adhesive. The specimens were tested under the same test conditions, but at mean displacements of 2.4 mm, 4.8mm and 7.2 mm. The da/dN vs G_{max} curve, shows that, within experimental scatter, the

mean displacement has no effect on the crack growth rate of the bonded joints at either high

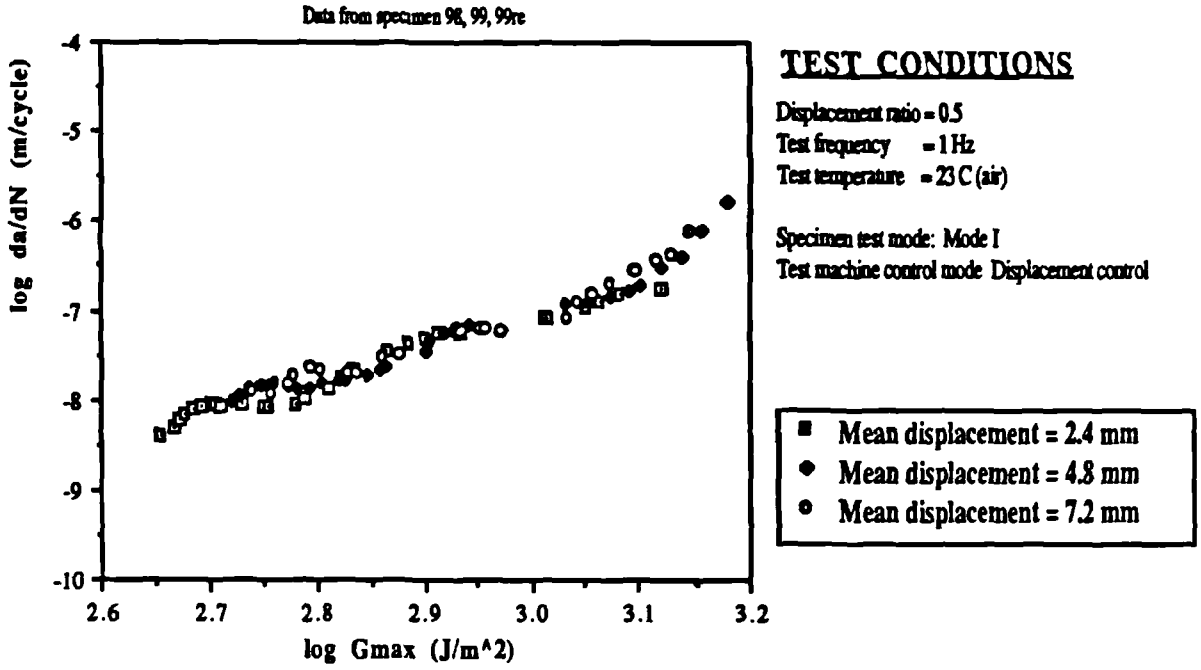


Figure 5.8a. Effect of mean displacement on the fatigue performance of a bonded joint. (Note: Substrate 913C XAS-5-47%, adhesive FM73M).

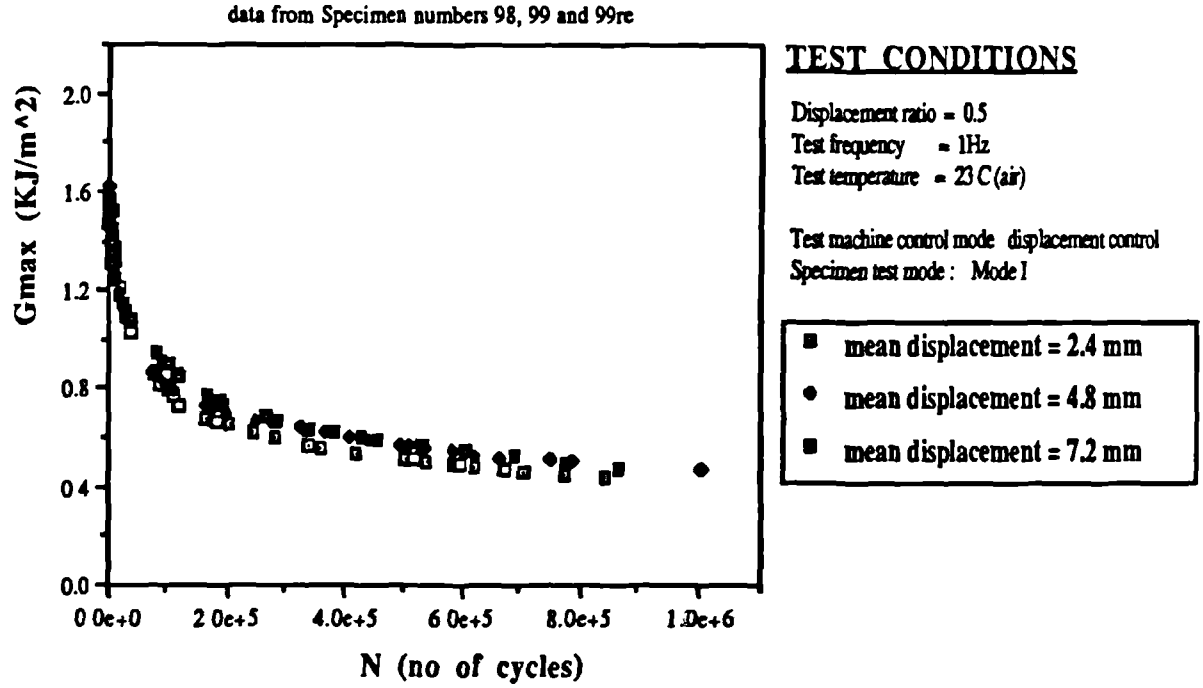


Figure 5.8b Effect of mean displacement on the fatigue performance of bonded joints. (Note: Substrate 913C XAS-5-47%, adhesive FM73M)

or low crack growth rates. The experiments were not conducted for sufficient time to establish conclusively whether the value of G_{th} is independent of the mean displacement. However, in agreement with the results indicated in Figure 5.8a, the G_{max} -N curve shown in Figure 5.8b suggests that the threshold is independent of δ_{mean}.

Knott et al (1973) has examined the effect of mean stress on the fatigue crack growth rate in low alloy steels. However, most probably because the tests were conducted without keeping the stress ratio constant, they found that the crack growth rate increased with increasing mean stress. The investigation should have been conducted keeping all other parameters including the stress ratio, constant. (Since a change in the stress ratio might itself significantly influence the crack growth rate). Thus, it is incorrect for Knott et al to assume that a significant effect of the mean stress has been conclusively demonstrated.

Barsom et al (1987) explained that the effect of 'mean load' on fatigue crack growth rate could be studied using the 'load ratio parameter'. However similarly, they investigated the effect of mean stress on the fatigue performance of ASTM A514 grade B steel without keeping the stress ratio constant.

5.5.5 Comparison of the Fatigue Performance of the Cold Cure Epoxy Paste Adhesive with the Hot Cure Epoxy Film Adhesive

Figure 5.9a shows the fatigue behaviour of the thermosetting CFRP when bonded using the cold cure epoxy paste adhesive with that using the hot cure epoxy film adhesive. The da/dN versus G_{max} curves show that the results differ substantially for these two adhesives. The crack grows faster in two part, cold-cure epoxy paste adhesive (i.e "9309.3NA") than in the one-part hot-cure epoxy film adhesive (i.e "FM73M"). The results also show that the threshold value of the hot cure film adhesive is much higher ($G_{th} = 0.30 \pm 0.02$ kJ/m^2) than the cold cure epoxy paste adhesive ($G_{th} = 0.15 \pm 0.02$ kJ/m^2).

The superior fatigue performance of the one-part hot cure epoxy film adhesive over the cold cure epoxy paste adhesive is in direct contrast to the static fracture energy results obtained in section 4.3.3 which showed that the cold cure epoxy paste adhesive has a higher fracture energy value (G_{1c} = 5.70±0.02 kJ/m^2) compared to the one-part hot-cure epoxy film adhesive (G_{1c} = 2.93±0.03 kJ/m^2). These observations are in agreement with those reported by Luckyram and Vardy (1988) when a one part hot -cure and a two part cold-cure epoxy adhesives were tested in bulk using the compact tension test geometry. Their static tests results showed that that the cold cure epoxy paste adhesive had a higher fracture energy value (G_{1c} = 5.45 kJ/m^2), compared to the one-part hot-cure epoxy film adhesive (G_{1c} = 2.82 kJ/m^2) whilst in contrast their fatigue tests results showed that the crack growth rates in the cold cure paste adhesive were lower than in the hot cure film adhesive.

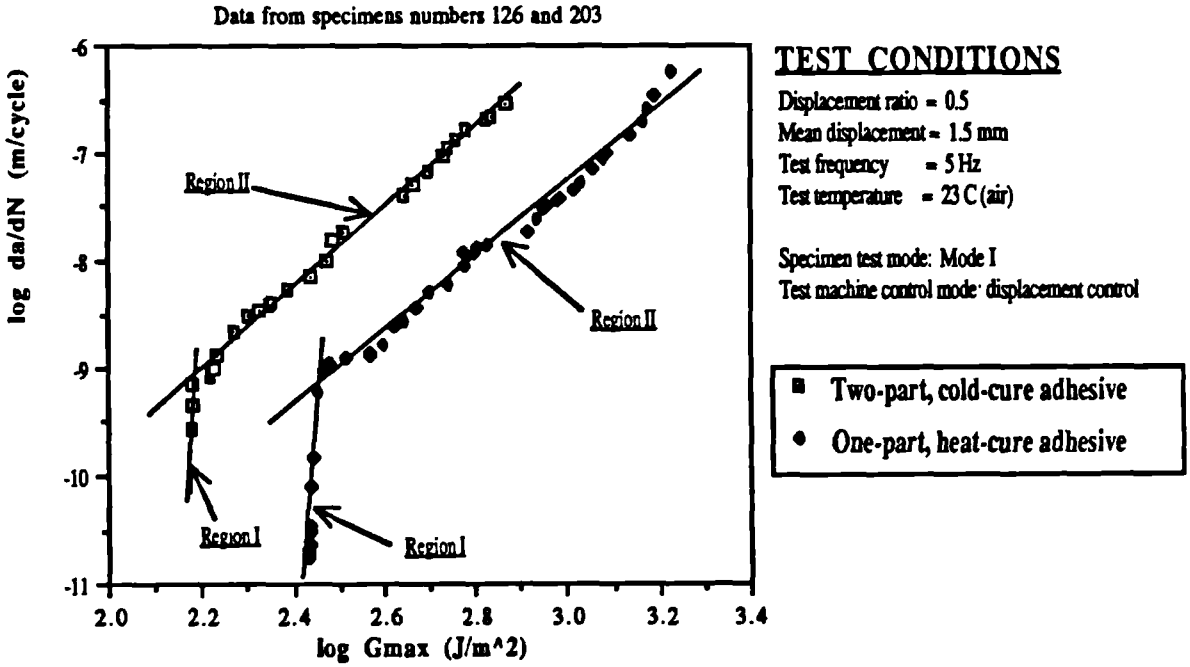


Figure 5.9a. Comparison of the fatigue performance of the two stuctural adhesives used in the bonded composite joints (Note: Substrate 913C XAS-5-47%).

The above experimental results for values of G_{th} and G_{1c} do appear somewhat puzzling since it might be expected that the adhesive with the higher fracture energy in static tests should have

the superior fatigue characteristics, and so also possess a higher G_{th} value. Luckyram and Vardy (1988) tried to speculate on the possible implication of the above results by associating the higher fatigue resistance observed from the hot cure adhesive (which contained a mat carrier) to be due to the effects of localised shear yielding at the crack tip. In the case of the cold cure adhesive (which possessed no mat carrier) they associated the lower fatigue resistance with multiple crazing occurring at the crack tip. Kinloch (1989), however disagreed with the above interpretation, since there was no positive evidence whatsoever of crazing being a possible mechanism of failure in thermosetting epoxy polymers, because these highly crosslinked polymers do not possess the chain mobility and extensibility necessary for craze structures to be formed. Kinloch's remarks were accepted by Luckyram and Vardy (1989).

However, results from previous work (Kenig et al 1989, Sancaktar 1980) has revealed that the trends observed from this investigation could be due to the presence of the polyester mat carrier in the hot cure epoxy film adhesive (i.e "FM73M"). No such carrier was present in the cold cure epoxy paste adhesive ("9309.3NA"). According to the manufacturers of the adhesive, the polyester mat carrier was included to serve as a control for the adhesive bondline thickness and to improve its handling characteristics during use. However, Kenig et al (1989) have conducted test at a constant rate of displacement (2 mm/min) on a series of adhesives (including FM73). The adhesives with mat-carriers had higher strength and modulus than those without the mat-carrier. Further, Sancaktar et al (1980) showed that a modified epoxy adhesive with carrier cloth (i.e Metlbond 1113) had a slower fatigue crack growth rate compared with the adhesive that had no carrier (i.e Metlbond 1113.2). Mall and Johnson (1985) also showed that a hot cure epoxy film adhesive with a carrier (FM300) had superior fatigue resistance compared with a hot cure thermosetting polymer adhesive with no mat carrier (EC-3445).

The most useful support for the trends observed in the present investigation has been from the previous work of Jablonski et al. (1980), where they showed that a mat-carrier improved the

fatigue resistance of a rubber modified epoxy film adhesive in comparison with another without a mat carrier. They used SEM techniques to study the debonded surfaces obtained from fatigue experiments. The SEM photomicrographs revealed the presence of fatigue cracks in the mat-carrier which indicated that the carrier itself also carried some fatigue loading. To avoid the possibility that the cracks were in the carrier before fatigue loading, the debonded surfaces due to static loading were examined carefully to check for signs of cracks but none were found. The SEM work on the debonded surfaces from this investigation will be discussed in Chapter Seven.

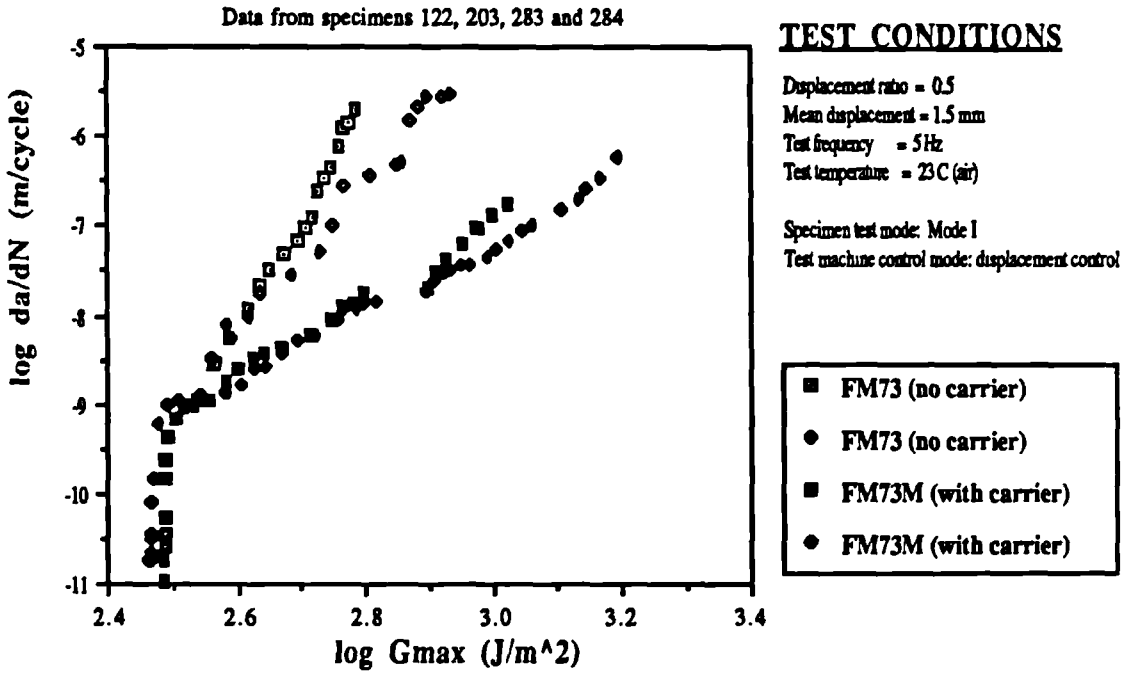


Figure 5.9b. Influence of the polyester mat-carrier on the fatigue performance of bonded joints. (Note: Substrate 913C XAS-5-47%).

Furthermore, by using arguments based on the crack opening displacement criterion, Sancaktar et al. (1980) and Brinson et al (1975) explained that the adhesive with a mat carrier will undergo less strain compared with that containing no mat carrier, when both adhesives are subjected to the same stress levels. As a result, the crack opening displacements are smaller in

the presence of a mat carrier. Hence the presence of a mat carrier increases the fatigue resistance of an adhesive bond.

In the present study, experiments were carried out to investigate the effect of the mat carrier on the fatigue performance of bonded joints. Figure 5.9b shows the influence of the mat-carrier on the fatigue performance of a thermosetting CFRP bonded with the hot cure epoxy film adhesive. The data confirms that the fatigue crack grows slower in the adhesive with the mat-carrier compared to one without a mat carrier.

5.5.6 Influence of Substrate Thickness and Type.

The da/dN versus G_{max} curves shown in Figure 5.10a show that the thickness of the substrate has no significant effect on the fatigue performance of a bonded joint, provided the locus of failure is cohesive through the adhesive. The G_{max} -N, curve on Figure 5.10b also supports this observation. From both figures, it appears that the fatigue crack growth rates are not significantly affected by the substrate thickness in the linear region (region II) of the curve.

Considering the value of G_{th} then the values of the threshold obtained from the curves are 0.26 ± 0.02 kJ/m^2 for the 24 plies thickness and 0.30 ± 0.02 kJ/m^2 for the 48 plies. These results are not significantly different within experimental scatter (i.e are within 8% of the mean value 0f 0.28 kJ/m^2). Indeed, the results obtained from the static testing (i.e at a constant crosshead rate test) shown in Figures 4.13 and 4.14 confirm that the thickness of the composite has no significant effect. Considering the type of substrate, (i.e "APC-2" and "9309.3NA") then the trend of results obtained from Figures 5.11a and 5.11b are very similar to those of Figure 5.10a and 5.10b. The curves show that the type of substrate does not have any significant effect on the fatigue performance of the bonded joint again provided the locus of failure is cohesive.

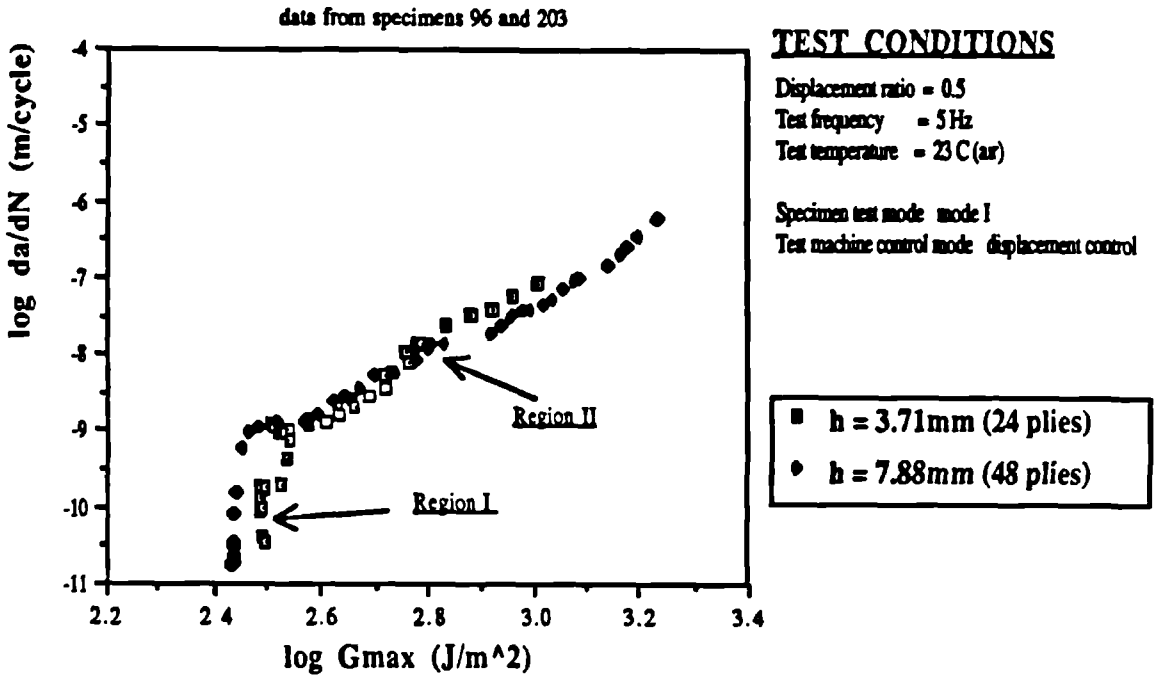


Figure 5.10a. Influence of substrate thickness on the fatigue performance of bonded joints. (Note Substrate 913C XAS-5-47%, adhesive FM73M).

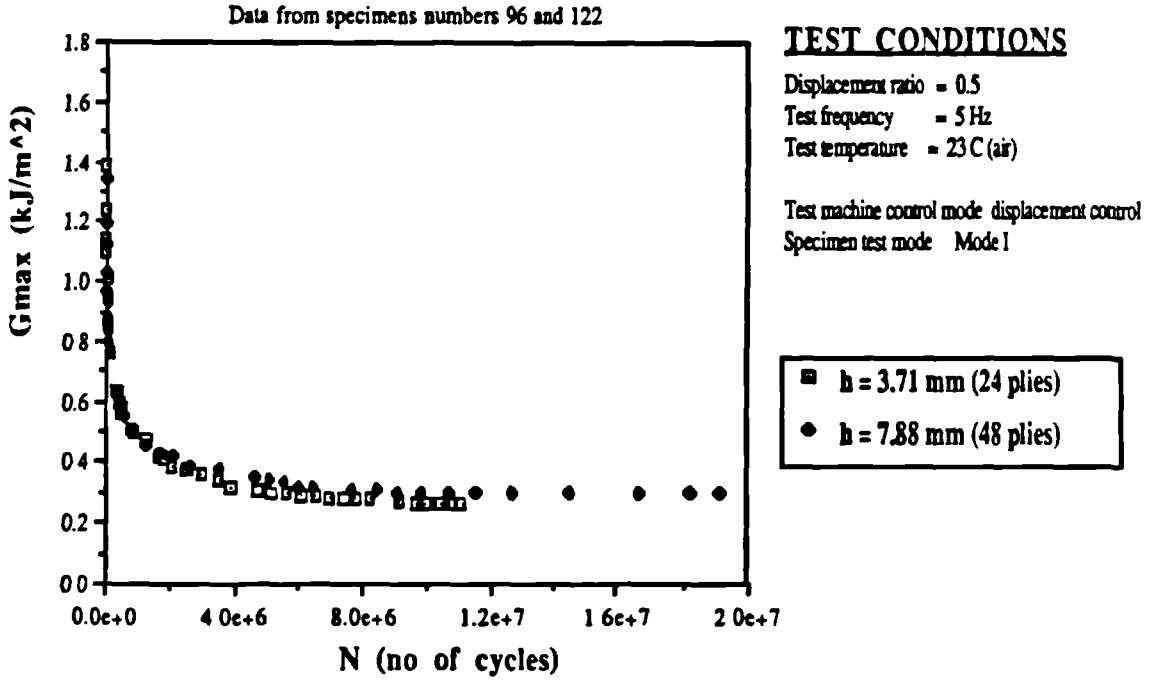


Figure 5.10b Influence of substrate thickness on the fatigue performance of bonded joints (Note Substrate 913C XAS-5-47%, adhesive FM73M)

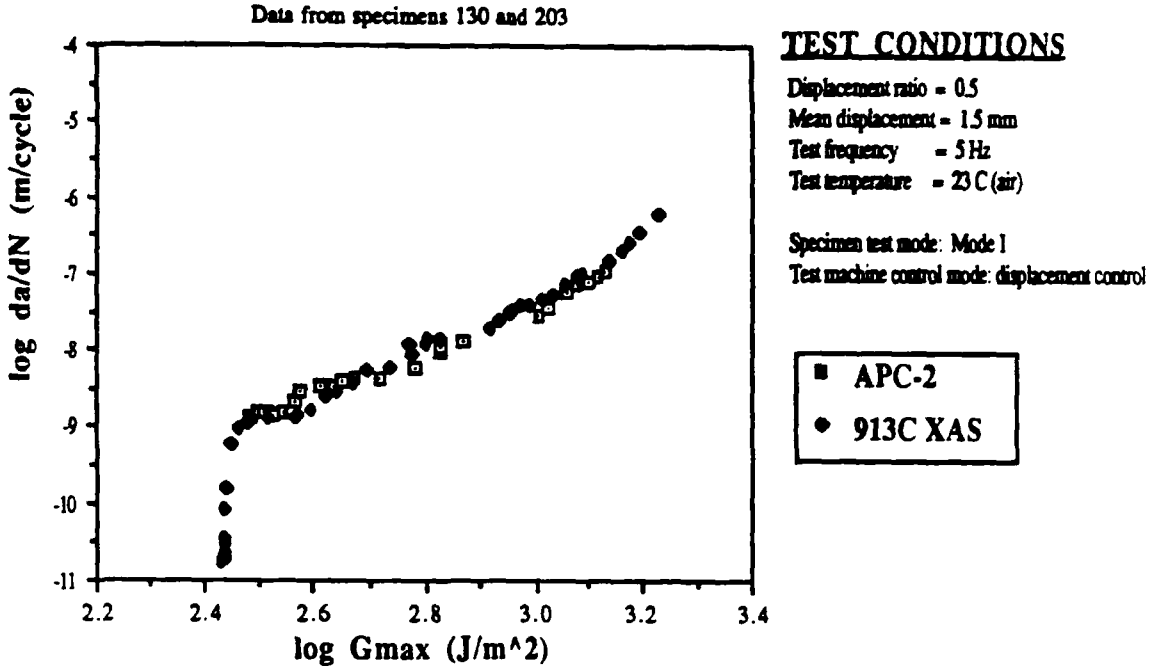


Figure 5.11a. Influence of the type of substrate on the fatigue performance of bonded joints. (Note: Adhesive FM73M).

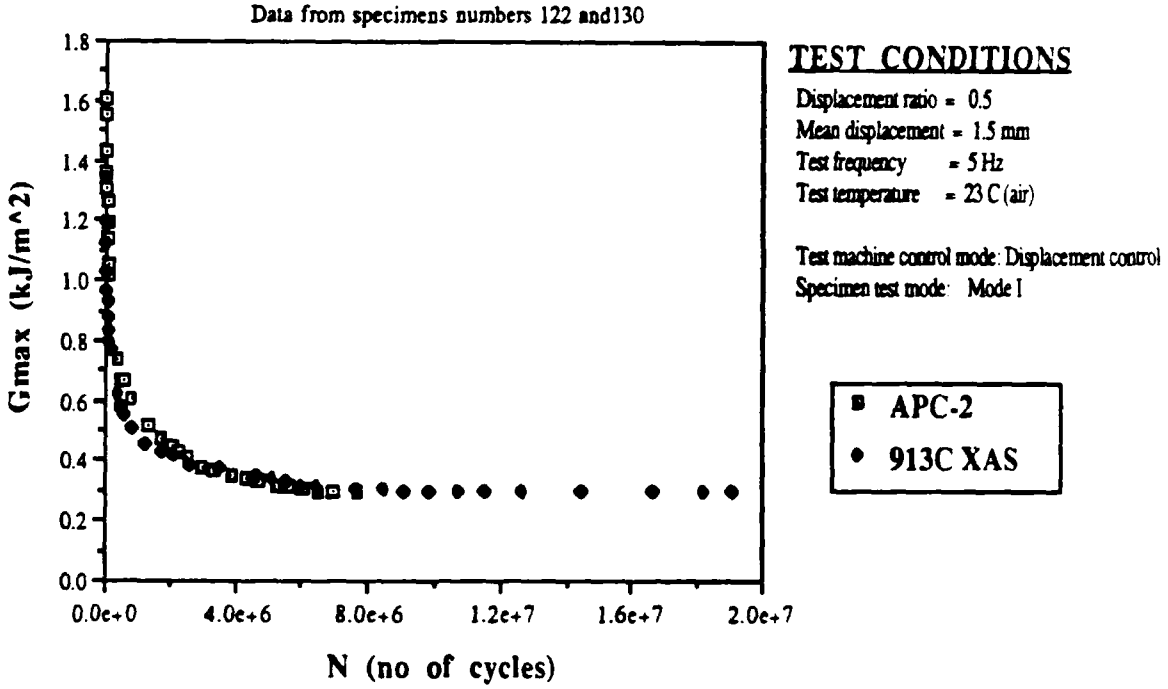


Figure 5.11b. Influence of the type of substrate on the fatigue performance of bonded joints. (Note: Adhesive FM73M).

5.6 LINEAR REGION II CONSTANTS

As was mentioned earlier in section 2.4, the linear region (region II) of the crack growth curve characterises the stable region where the relationship between the crack growth rate, da/dN, and G_{max} is linear on a log-log plot. From the linear region, two material constants, D and n can be obtained. The values of D and n can be obtained from the intercept and slope of the straight line fitted to the data in the linear region.

However, because a typical fatigue curve is divided into three regions (Figure 2.3), it is always necessary to ensure that only the data points that fall into the linear region (region II) part of the da/dN versus G_{max} curve are used to obtain the values of D and n using a linear regression analysis method. From experimental results in the present investigation, and from results from previous studies (Donaldson 1989, Martin 1990), it was observed that a linear relationship usually exist on plots of da/dN versus G_{max} on a log-log scale when the crack growth rate, da/dN, is between $10^{-8} < da/dN < 10^{-5}$ m/cycle. Values of D and n for the two adhesive studied in the present investigation have been obtained and are presented in Table 5.1 below.

As can be seen from Table 5.1. the average value of n for the hot cure epoxy film adhesive ("FM73M") is greater than for the cold cure epoxy paste adhesive ("9309.9NA"). The values of n ranges from 3.41 to 3.86 for the " FM73M" adhesive, while for the "9309.3NA" it ranges from 3.15 to 3.41. In both cases, this value is independent of the displacement ratio. However, the value of D is dependent on the displacement ratio and it decreases as the displacement ratio increases. As can be seen from the table, for the same displacement ratio, the value of D for the hot cure epoxy film adhesive ("FM73M") is greater than for the cold cure epoxy paste adhesive ("9309.9NA").

These observations are in good agreement with earlier findings. For example, Luckyram and Vardy (1988) found that the value of n for the one part hot cure epoxy adhesive was about 3.99

and is greater than for the two part cold cure epoxy adhesive, i.e about 2.2. Martin and Murri (1990) found that for mode I fatigue crack growth in "APC-2" the value of D decreased from 1.36×10^{-12} m/cycle to 9.44×10^{-16} m/cycle as the displacement ratio increased from 0.1 to 0.5. Similarly, Donaldson et al (1989) found that for mode III fatigue crack growth in graphite/epoxy composite, the value of D decreased from 9.56×10^{-25} m/cycle to 2.75×10^{-41} m/cycle as the displacement ratio increased from 0.1 to 0.5.

Table 5.1 Linear region II constants for the adhesives from individual tests

Sp. no	Adhesive type	Displacement ratio	D (m/cycle)	n (m^3/J cycle)	correlation coefficient*
92	FM73M	0.1	5.97×10^{-17}	3.24	0.738
119	FM73M	0.1	9.01×10^{-18}	3.61	0.985
96	FM73M	0.5	2.94×10^{-18}	3.48	0.987
98	FM73M	0.5	2.82×10^{-19}	3.86	0.959
99	FM73M	0.5	4.04×10^{-18}	3.44	0.943
130	FM73M	0.5	2.06×10^{-18}	3.41	0.975
203	FM73M	0.5	2.86×10^{-19}	3.78	0.967
104	9309.3NA	0.1	9.16×10^{-16}	3.41	0.919
105	9309.3NA	0.1	2.15×10^{-15}	3.38	0.950
106	9309.3NA	0.5	2.42×10^{-16}	3.15	0.992

Notes: (1) The units of D and n should be stated as discussed earlier in section 2.4.

(2) Linear regression analysis of data are between limits of $10^{-8} < da/dN < 10^{-5}$.

(3) * : Correlation coefficient obtained from a linear regression analysis of the data points between limits of $10^{-8} < da/dN < 10^{-5}$.

5.7. THRESHOLD VALUES OF THE MAXIMUM STRAIN ENERGY RELEASE RATE, G_{th}

In section 5.3.4, the advantages of defining a threshold value of the maximum fracture energy, G_{th} were discussed. In this work, the threshold values were located using the da/dN versus G_{max} plots and were defined as the lower bound of G_{max} when the crack was observed not to grow significantly (i.e by less than 20 mm) over one million cycles. In the initial experiments, the location of the threshold value was found to be very time consuming. This was because the fatigue tests were performed at a low frequency of 1 Hz. This means that it takes twelve days to generate one million cycles. However, when experiments were performed at 5 Hz, the threshold region was successfully located after only 10 days (i.e over 8 million cycles) but the experiment was continued for more than 20 days in order to ascertain the accuracy of the results. The results obtained were as shown in Table 5.2.

Table 5.2 Threshold values for the adhesives (kJ/m^2)

Sp. no	Adhesive type	Displacement ratio	no of cycles to end of test	G_{th} (displ)	G_{th} (comp)	G_{1c}
96	FM73M	0.5	11,011,294	0.26	0.30	2.93
122	FM73M	0.5	19,113,400	0.30	0.33	2.93
203	FM73M	0.5	23,998,164	0.29	0.27	2.93
126	9309.3NA	0.5	24,378,958	0.15	0.15	5.70

Notes: Substrate: 913C XAS-5-47%

(displ = displacement method (Equation 5.11, comp = compliance method (Equation 5.9)

As was mentioned earlier, any of the four equations (Equations 5.8 to 5.11) could have been used to calculate G_{max} . Although these equations give results that are in good agreement, the values estimated are not exactly the same. For this reason one may conclude that the slight variation in the values of G_{th} shown in Table 5.2 may be due to differences in the equations used for the calculation. Consequently, it is reasonable to draw the conclusion that within experimental scatter the threshold value of the maximum strain energy release rate, G_{th}, for the hot cure epoxy film adhesive (i.e FM73M) from the fatigue tests performed at a displacement ratio of 0.5 are within about 8% of the mean value of 0.28 kJ/m^2.

This value of 0.28 kJ/m^2 appears quite low compared with the value of fracture energy, G_{1c}, obtained for the hot cure epoxy film adhesive (i.e 2.93 ± 0.08kJ/m^2) and may, at a first glance, appear to represent a major problem when designing for adhesive joints possessing long fatigue lives. However, for the purpose of bonding fibre reinforced composites, this may not be the case. This is because, as an example, from fatigue testing of "APC-2" composite, Martin and Murri (1990) found that the threshold value of the strain energy release rate was about 0.175 kJ/m^2. This value is much lower than that obtained for the hot cure epoxy film adhesive (i.e "FM73M") adhesive for the same displacement ratio of 0.5. This implies that the crack will grow in the composite, rather than the adhesive, for the same flaw size. Thus, any structure that permits the use of the composite will definitely permit the use of the above adhesive.

Similarly, the threshold value for cold cure epoxy paste adhesive (i.e "9309.3NA") tested at a displacement ratio of 0.5 is about 0.15 kJ/m^2. This value may be stated with considerable confidence since there was negligible crack growth over five million cycles (i.e 11 days at a test frequency of 5 Hz) and may be compared with the static G_{1c} value of 5.7 kJ/m^2. Thus, the threshold value of the hot cure epoxy film adhesive is about twice as high as that of the cold cure epoxy paste adhesive for the same value of displacement ratio (i.e when δ_R = 0.5). Although of course, the static toughness is much lower for the hot cure epoxy film adhesive.

5.8 CONCLUSIONS

The main conclusions from the results presented in this chapter are:

(1) The procedure which characterises fatigue crack growth curves using S-N or G_{max} -N curves should be treated with caution. This is because the two curves are dependent on the geometry of the test specimen. However, provided the specimen geometry is kept constant, these two curves can be used as a quick assessment method to investigate the effects of testing variables on the fatigue behaviour of bonded joints.

(2) The fatigue crack growth curves in adhesively bonded joints are best represented by curves relating the crack growth rate, da/dN, to the maximum strain energy release rate,

G_{max}. There are two reasons for this statement. Firstly, because the fatigue curves generated from such a form of presentation are independent of the geometry of the test specimen and can be considered as a material property for the specified testing conditions. Secondly, the use of G_{max} in preference to $\Delta G = (G_{max} - G_{min})$ helps to eliminate the uncertainties, due to counter-face interference, involved in estimating G_{min}.

(3) In order to obtain curves that relate da/dN to G_{max} with a minimum scatter due to the analysis of experimental data, the value of da/dN should be estimated using the incremental polynomial method as recommended by the ASTM E 647-88.

(4) The investigations into the influence of parameters such as the cyclic test frequency, displacement ratio and mean displacement on the fatigue performance of 913C XAS-5-47/FM73M bonded composite joints revealed that:

(i) The cyclic test frequency has no significant influence on the fatigue performance of bonded joints between frequencies of 1 and 5 Hz.

(ii) As the displacement ratio increases the fatigue crack growth rate decreases for a given G_{max} value and the G_{th} value increases.

(iii) The mean displacement of the specimen appears to have no significant effect on the fatigue crack growth.

(iv) The type and thickness of the substrate does not have a significant effect on the fatigue performance of a bonded composite joint, providing the locus of failure is cohesive through the adhesive.

(5) The crack growth rate in the hot cure epoxy film adhesive ("FM73M") is slower than in the cold cure epoxy paste adhesive ("9309.3NA") at a given G_{max} value. For fatigue

testing at a displacement ratio of 0.5, the average values of the linear region II constants, D and n, for the "FM73M" adhesive are 1.903×10^{-18} and 3.59 respectively whilst for the "9309.3NA" adhesive, the average values of D and n are 2.42×10^{-16} and 3.15 respectively.

(6) The threshold value, G_{th}, for the "FM73M" adhesive is higher than for the "9309.3NA". The threshold value of G_{max} for "FM73M" is 0.28 ± 0.02 kJ/m^2 while for "9309.3NA" is 0.15 kJ/m^2. The superior fatigue properties of the "FM73M" adhesive compared with the "9309.3NA" are in contrast to the static fracture energy results, which showed that the "9309.3NA" has a higher fracture energy than the "FM73M".

CHAPTER SIX

FATIGUE TESTING IN A HOSTILE ENVIRONMENT (WATER)

6.1 INTRODUCTION

In many adhesive applications, the joints are subjected to potentially damaging hostile environments. One of the most commonly encountered hostile environment is water. and a most important requirement of adhesively bonded joints is to retain a significant part of their strength at elevated temperatures and under high relative humidities for long periods of time. Water may easily penetrate into the bond line causing (i) swelling and deformation of the adhesive (Weitsman 1977), (ii) breaking of chemical bonds in the adhesive (Comyn 1989) and (iii) the rupture of secondary bonds formed across the adhesive/substrate interface (Kinloch 1979). The ability of water to displace the adhesive from the substrate can be assessed by an argument advanced by Kinloch et al (1974) in terms of the thermodynamic work of adhesion, W_A, between two materials. The term W_A was defined as the energy required to separate a unit area of interface into two separate surfaces. The value of W_A can be evaluated from (Kinloch 1987):

$$W_A = 2(\gamma_a^D \gamma_s^D)^{1/2} + 2(\gamma_a^P \gamma_s^P)^{1/2} \qquad (6.1)$$

where γ^D and γ^P are the dispersion and polar force components respectively of the surface free energy and subscripts 'a' and 's' stands for the adhesive and substrates respectively. In the presence of a liquid environment, the expression in equation 6.1 can be modified to give:

$$W_{Al} = 2\left(\gamma_{lv} - \left(\gamma_s^D\gamma_{lv}^D - \gamma_a^P\gamma_{lv}^P - \gamma_s^D\gamma_{lv}^D - \gamma_s^P\gamma_{lv}^P + \gamma_a^D\gamma_s^D + \gamma_a^P\gamma_s^P\right)^{1/2}\right) \quad (6.2)$$

where γ_{lv} is the surface free energy of the liquid. The values of the surface free energies for water and for the adhesives and substrates used in the present study have been calculated (Kodokian 1989, Kinloch 1987) and are presented in Table 6.1 while the values W_A and W_{Al} for water and the relevant adhesive/substrate combination are presented in Table 6.2.

Table 6.1: Surface free energy values for water, test substrates and adhesives.

Material	$(\gamma_s)^D$ (mJ/m^2)*	$(\gamma_s)^P$ (mJ/m^2)**	References
"APC-2"	39.0	2.0	Kodokian (1989)
"913C XAS"	31.3	7.2	Kodokian (1989)
"9309.3NA"	41.1	2.8	Kodokian (1989)
"FM73M"	37.5	2.2	Kodokian (1989)
WATER	22.0	50.2	Kinloch (1987)

Notes: *$(\gamma_s)^D$: Dispersive component of free surface energy

**$(\gamma_s)^P$: Polar component of free surface energy

A positive value of W_{Al} indicates that the interface is thermodynamically stable. A negative value indicates that the interface is unstable, in which case there will be a strong driving force for the displacement of the adhesive from the substrate in the presence of water thus changing the locus of failure from cohesive, to interfacial between the adhesive and the substrate. However, because the thermodynamic analysis does not take into account the interfacial forces arising from primary bonds, acid-base interactions or mechanical interlocking, the use of equations 6.1 and 6.2 should be seen only a limiting guide to interfacial stability.

Table 6.2: Thermodynamic work of adhesion for the adhesively bonded joint.

Substrate	Adhesive	$W_A(mJ/m^2)^*$	$W_{Al}(mJ/m^2)^{**}$
913 C XAS	FM73M	76.5	51.8
APC-2	FM73M	92.7	26.9
913C XAS	9309.3NA	80.7	51.7
APC-2	9309.3NA	98.8	25.0

Notes: *W_A: thermodynamic work of adhesion in an air (equation 6.1)

**W_{Al}: thermodynamic work of adhesion in an i water (equation 6.2)

As far as the adhesive layer of the bonded joint is concerned, combined moisture with relatively high temperatures may be detrimental to the mechanical properties of the adhesive due to susceptibility of the polymer to hydrolysis and degradation resulting in loss in molecular weight and strength (Kinloch 1987). Apart from the irreversible effect of hydrolysis, the ingressing moisture may cause reversible effects, such as plasticization of the adhesive.

Observations from fracture mechanics tests have revealed that joints exposed to wet environments tend to have increased toughness due to plasticization at the crack tip region (Ripling et al 1971), providing significant interfacial attack does not occur. It is also believed that the absorbed moisture may decrease both the glass transition temperature, T_g, and the complex dynamic modulus of the adhesive (Kinloch 1987). A decrease in the adhesive modulus will decrease the stress concentration at the tip of any crack or local stress raiser in the joint and, all other factors being equal, lead to an increase in joint strength.

Whether plasticization and hydrolysis of the adhesive layer by ingressing water, and/or the displacement of the adhesive at the adhesive substrate interface, actually affects the fatigue behaviour of the joint during fatigue loading will be discussed in the present chapter. Also, the

effects of environmental attack on parameters such the type of adhesive and substrate will be studied and compared to the results obtained from the test conducted in a relatively dry environment (about 50% R.H) at 23 °C.

6.2. RESULTS AND DISCUSSION

6.2.1 Introduction:

To assess the extent of water attack on the bonded joint during fatigue loading, the tests were carried out using a servo-hydraulic testing machine under displacement control mode. A specially built environmental chamber consisting of a Grant FH15 (1988) thermostatic controlled flow heater, connected to a perspex water tank was designed to fit onto the "Mayes" fatigue machine (Mayes 1988).

The specimens were tested in water at predetermined temperatures and the influence of moisture and temperature on the crack growth rates were monitored while all other testing variables were kept constant. The crack length was measured with the aid of a travelling microscope mounted on a platform fixed to the base of the testing machine. The values of load, displacement, crack length and the number of fatigue cycles were recorded and used to calculate the values of da/dN and G_{max} as described in section 5.4. The crack growth curves are presented in the form of plots of da/dN versus G_{max}.

6.2.2. Fatigue Performance of the Cold-Cure Epoxy Paste Adhesive in Water at 25 °C and 50 °C.

Figure 6.1 shows the influence of the hostile environments on the fatigue performance of a joint made from thermosetting CFRP (913C XAS-5-47%) bonded with a cold cure epoxy paste adhesive ("9309.9NA"). The figure compares the results from tests carried out in air with those

in distilled water at a temperatures of 25 °C and 50 °C. It can be seen from the region II part of the curve (i.e between $10^{-8} > da/dN > 10^{-5}$), that the crack grew at the same rate for the same value of G_{max} in all three environments.

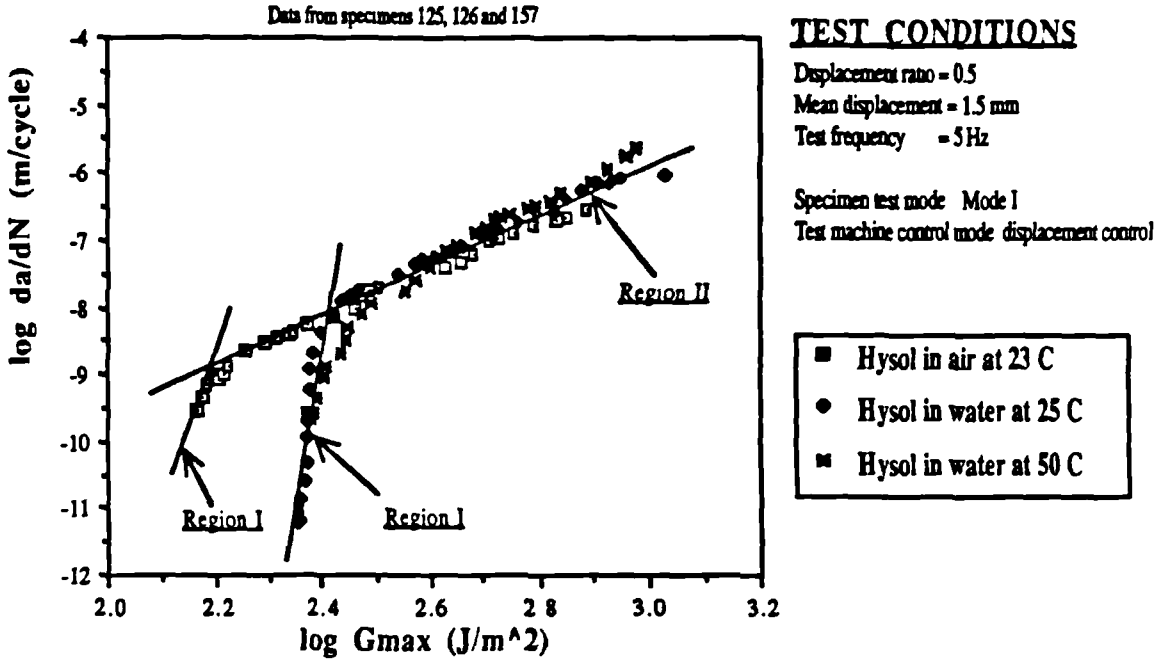


Figure 6.1a. Influence of hot/wet environment (water) on the fatigue performance of a bonded joint. Note: Substrate: thermosetting CFRP (i.e "913C XAS"), adhesive: cold-cure epoxy ("9309.3NA").

An inspection of the fracture surfaces (see Figures 6.1b, 6.1c and 6.1d) showed that the locus of failure was cohesive through the adhesive in all cases. As a guide to interfacial stability, equations 6.1 and 6.2 were used to check for the stability of this adhesive/substrate combination with values of 80.7 mJ/m^2 and 51.7 mJ/m^2 being calculated for W_A and W_{Al}, respectively. These positive values indicate that the locus of failure should be cohesive through the adhesive, as was indeed observed. However, the results of prolonged testing (2 days) show that there is an interaction between water and the bonded joint.

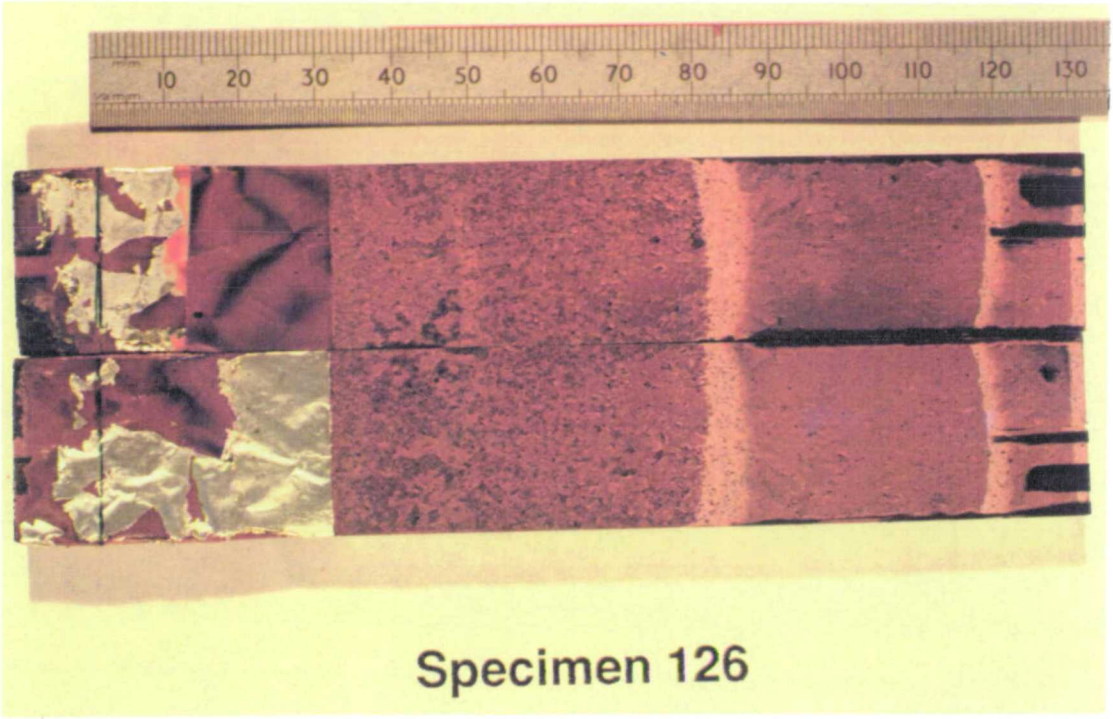


Figure 6.1b. Typical appearance of the fracture surfaces due to a fatigue crack propagating cohesively through a cold cure epoxy paste adhesive (i.e "9309.3NA") bonding a thermosetting composite substrate. The joint was tested in air at 23 °C and 50% R.H.

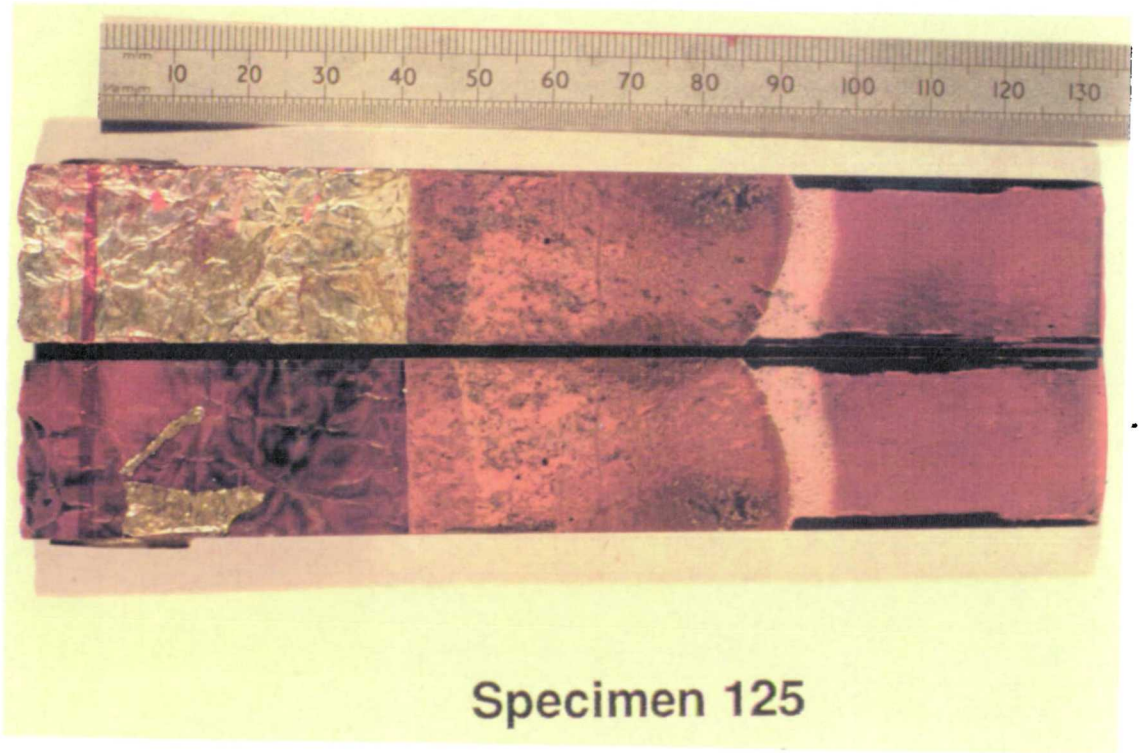


Figure 6.1c. Typical appearance of the fracture surfaces due to a fatigue crack propagating cohesively through a cold cure epoxy paste adhesive (i.e "9309.3NA") bonding a thermosetting composite substrate. The joint was tested in water at 25 °C.

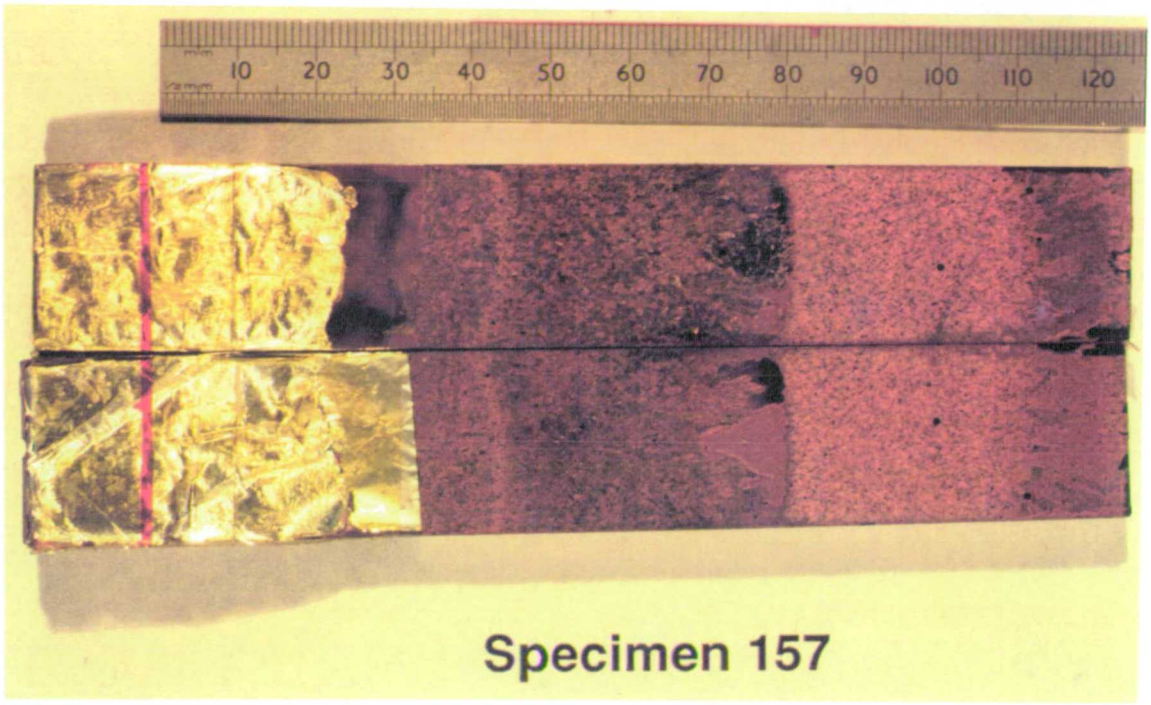


Figure 6.1d. Typical appearance of the fracture surfaces due to a fatigue crack propagating cohesively through a cold cure epoxy paste adhesive (i.e "9309.3NA") bonding a thermosetting composite substrate. The joint was tested in water at 50 °C.

The effect of this interaction is that higher values of threshold fracture energy, G_{th}, are observed from testing the joints in water at 25 and 50 °C compared with testing in air at 23 °C. Since the locus of failure was cohesive through the adhesive, the possible ways by which the ingressing water could have influenced on the adhesive were either by hydrolysis or by plasticization of the adhesive layer. In these particular circumstances, the probability of hydrolysis occurring is minimal since most thermosetting adhesives, in particular the epoxy based ones, are stable in the presence of most organic solvents, water and moderate strength acid and bases (Kinloch 1987). Also, such hydrolysis invariably leads to a decrease in toughness, as opposed to an increase.

Hence the above observations from testing in water are due to the effect of plasticization of the adhesive. There are three competing mechanisms that occur upon plasticization of the adhesive.

Firstly, plasticization lowers the glass transition temperature, T_g, of the adhesive resulting in a decrease in adhesive yield stress and blunting of the crack. As an example, Kenig et al (1989) showed that the T_g for a two part cold-cure adhesive (Hysol "EA 9628") was lowered from 100 °C to 92 °C after exposure to moisture at a relative humidity of 95% for 90 days and as a result the tensile strength of the adhesive was lowered from about 38 MPa to about 26 MPa.

Secondly, Gorbatkina (1991) explained that plasticization might decrease the effect of residual stresses in the adhesive that arise during the curing of the adhesive, thereby increasing the strength of the adhesive.

Thirdly, plasticization might result in further blunting of the crack tip due to the swelling of the adhesive as water is absorbed into it thereby apparently increasing the apparent toughness of the adhesive. Davis (1990) observed that such blunting of the crack tip as a result of water absorption resulted in an increase in the adhesive fracture energy.

Thus as a result of these three mechanisms, the value of the adhesive strength can vary in a very complicated manner. The observed increase in the value of G_{th} due to the effects of plasticization could be because the combined effect of the blunting of the crack tip and decrease in residual stresses which results in an increase in the toughness of the adhesive offset any decrease in strength that might have occurred due to a lowering of the glass transition temperature.

Evidence in support of the suggestion that the ingressing water may result in a change in the mechanical properties of the cold-cure adhesive may be found from the manufacturers data sheet (Hysol 1988). It was observed that the lap shear strength of the adhesive was 33.09 MPa for dry samples tested in air at 23 °C and this value slightly decreased to 32.4 MPa for samples aged in water at 25 °C for 30 days before testing, and then increased to 35.16 MPa for samples aged in water at 50 °C for 30 days before testing. Thus, the results from this section

indicate that the process of plasticization occurs after prolonged testing in water and not immediately after immersing the bonded joint in water.

One possible reason for this interesting observation could be that during the early stages of the fatigue testing of the joint in water at a constant displacement amplitude, the crack may be moving cohesively through the adhesive layer at a faster rate than the rate of water ingression into the crack tip plastic zone.

Unfortunately, the above speculation could not be justified because when attempts were made to calculate the rate of water ingression into the crack tip, dx/dt, (see Appendix C), the results obtained showed that dx/dt was greater than da/dt even at the beginning of the fatigue test when da/dt is highest (i.e $dx/dt = 5.67 \times 10^{-6}$ m/sec, $da/dt = 4.55 \times 10^{-6}$). At the moment, no other possible explanation can be found for this most interesting observation. This is obviously an area where further work is needed.

6.2.3. Fatigue Performance of the Hot-Cure Epoxy Film Adhesive in Water at 25 °C and 50 °C.

Figure 6.2a shows the da/dN versus G_{max} curves obtained when a thermosetting CFRP (i.e "913C XAS") was bonded with the hot-cure epoxy film adhesive ("FM73M"). The tests carried out in dry air at 23 °C were compared with those in water at 25 °C and 50 °C. As can be seen from the figure, for the same value of G_{max}, the crack growth rate in the region II part of the curve (i.e between $10^{-8} < da/dN < 10^{-5}$) was not affected when the test conducted in air was compared with the test in water at 25 °C. However, when the test was carried out at 50 °C, the figure shows that the crack growth rate was higher compared with the test in water at 25 °C and in air at 23 °C. A visual observation of the fracture surfaces of the specimen tested at 50 °C showed that about 60% of the fracture surface was by interfacial failure (see Figure 6.2b) unlike the cohesive locus of failure observed when tests were performed in air at 23 °C

and in water at 25 °C (see Figures 6.2c and 6.2d).

After prolonged testing in water at 25 °C for about 2 days, there was physical interaction between the water and the adhesive resulting in the plasticization of the adhesive. As has already been explained in section 6.2.2, the plasticization of the crack tip region by moisture lowers the adhesive yield stress but blunts the crack tip and so increases the apparent toughness of the joint. Again, it can be seen from Figure 6.2a, that the resultant effect of plasticization was that a higher value of threshold fracture energy was observed from testing in water at 25 °C compared with testing in air at 23 °C. The performance of the adhesive in the near threshold region for the test carried out in water at 50 °C was difficult to assess because of the interfacial failure observed at the adhesive/substrate interface.

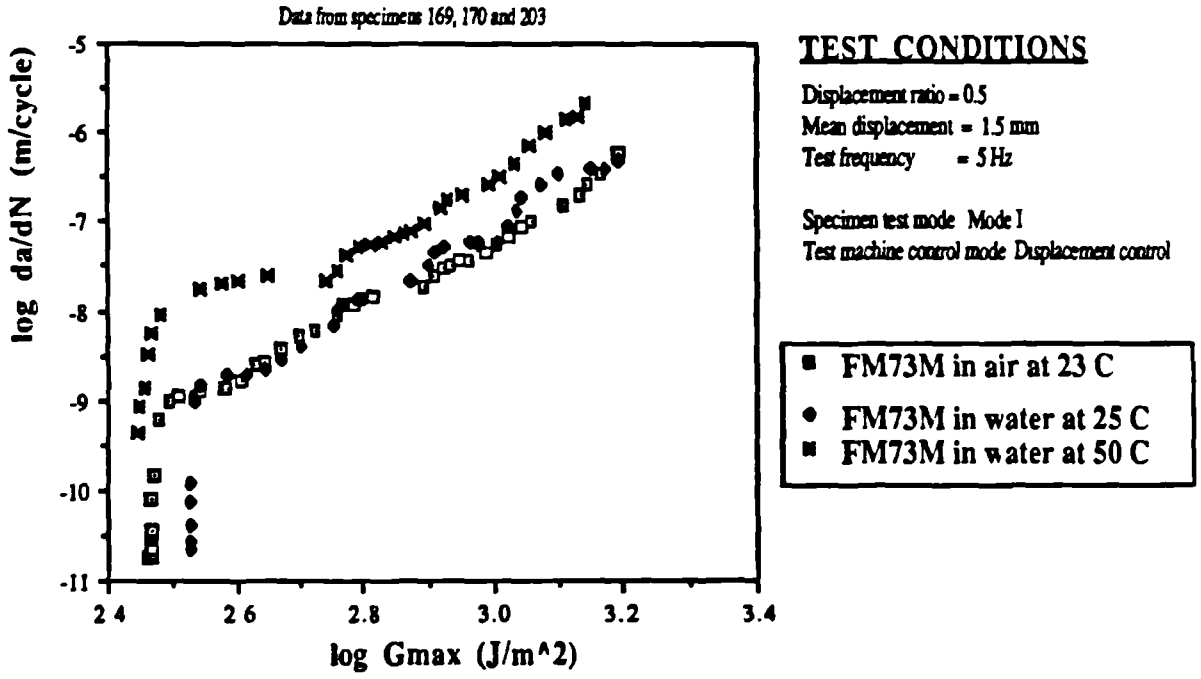


Figure 6.2a Influence of hot/wet environment (water) on the fatigue performance of a bonded joint
Note:- Substrate: thermosetting composite ("913C XAS"), Adhesive: Heat cure epoxy ("FM73M")

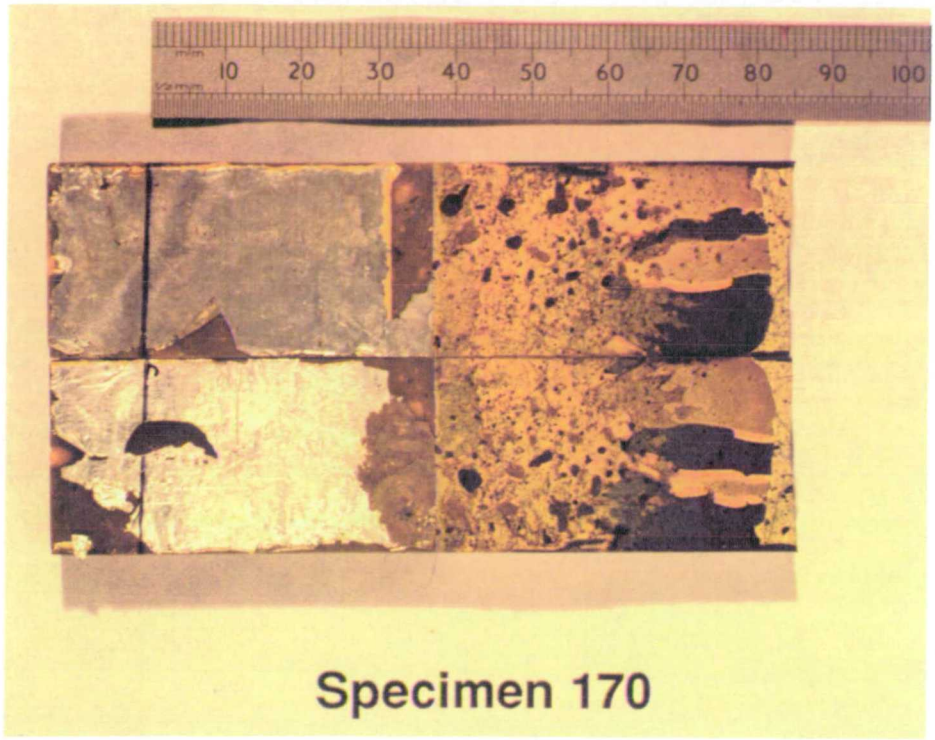


Figure 6.2b. Typical appearance of the fracture surfaces due to a fatigue crack propagating cohesively through a hot cure epoxy film adhesive (i.e "FM73M") bonding a thermosetting composite substrate. The joint was tested in water at 50 °C.

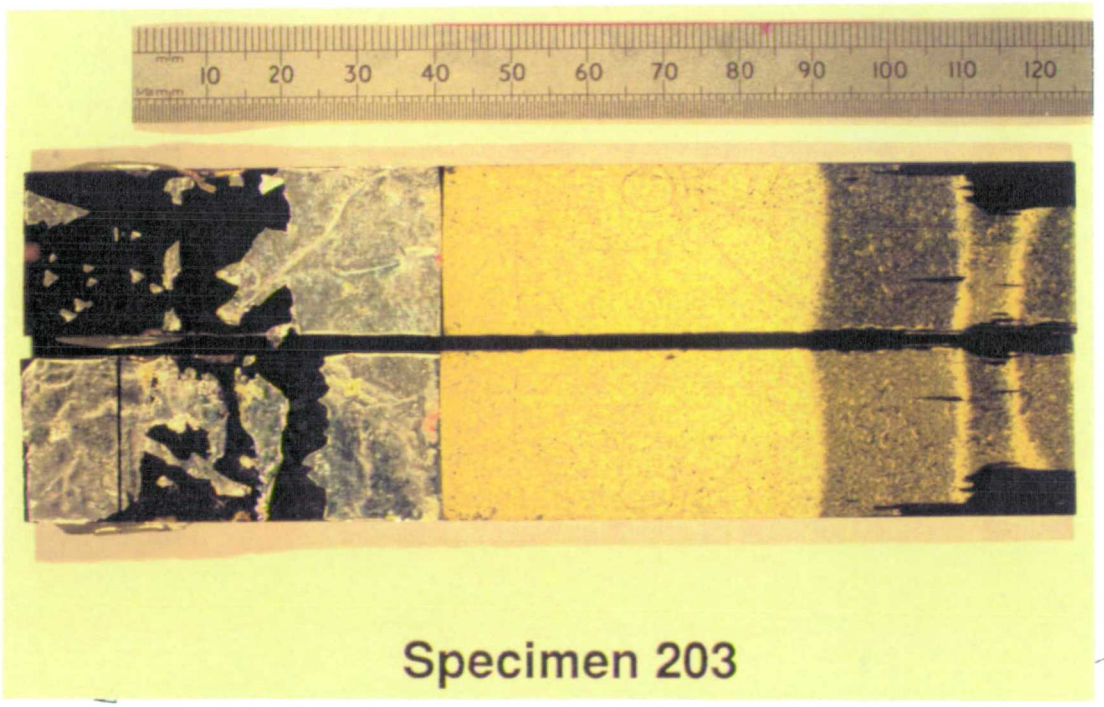


Figure 6.2c. Typical appearance of the fracture surfaces due to a fatigue crack propagating cohesively through a hot cure epoxy film adhesive (i.e "FM73M") bonding a thermosetting composite substrate. The joint was tested in air at 23 °C and 50% R. H.

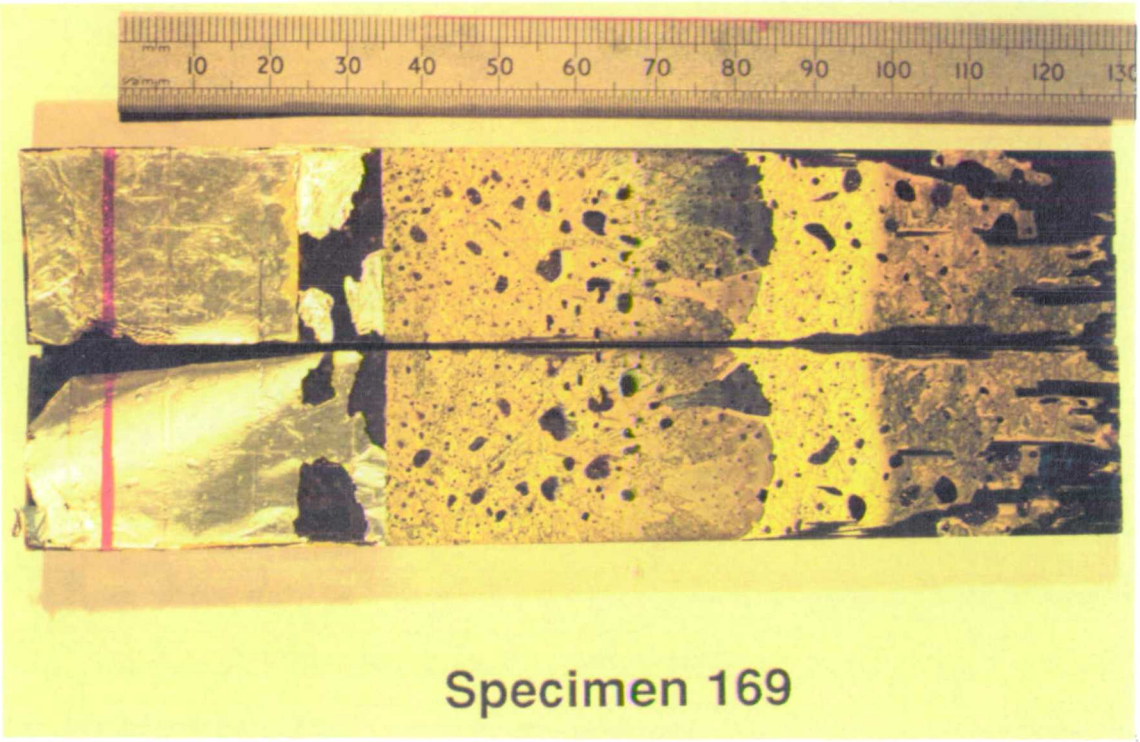


Figure 6.2d. Typical appearance of the fracture surfaces due to a fatigue crack propagating cohesively through a hot cure epoxy film adhesive (i.e "FM73M") bonding a thermosetting composite substrate. The joint was tested in water at 25 °C.

6.2.4. Influence of the Substrate Employed on the Fatigue Performance of the Hot-cure Film Adhesive Tested in Dry Air and in Water at 25 °C and 50 °C.

Thermoplastic composite substrates are chemically different from thermosetting composite substrates. Hence both materials may have different resistance to water especially at the interface between the substrate and the adhesive. Therefore, tests were carried out to study the influence of water and temperature on the fatigue performance of a film adhesive when it was used in bonding a thermoplastic composite compared with when it was used for bonding a thermosetting composite.

Figures 6.3a and 6.3b show that, for the same value of G_{max}, the crack growth rate in the thermoplastic composite joint was faster than in the thermosetting composite joint when tests were performed in water at 25 °C and 50 °C.

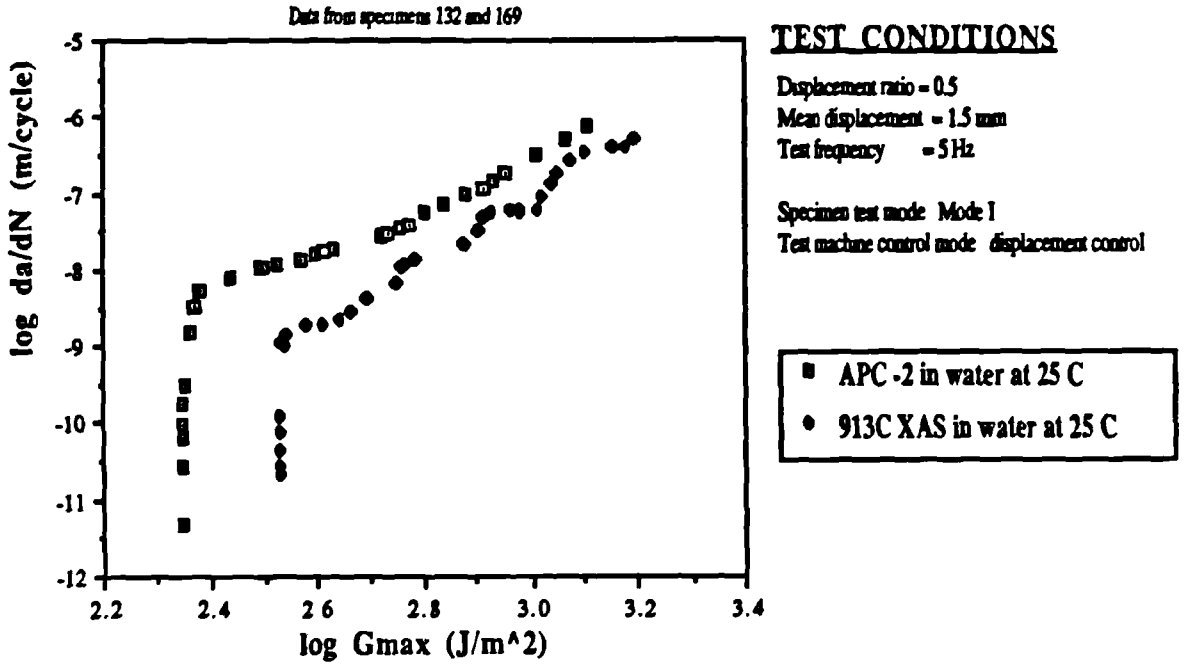


Figure 6.3a. Influence of the type of substrate on the fatigue performance of a bonded joint tested in water at 25 C. (Note:- Adhesive: Heat cure epoxy, "FM73M").

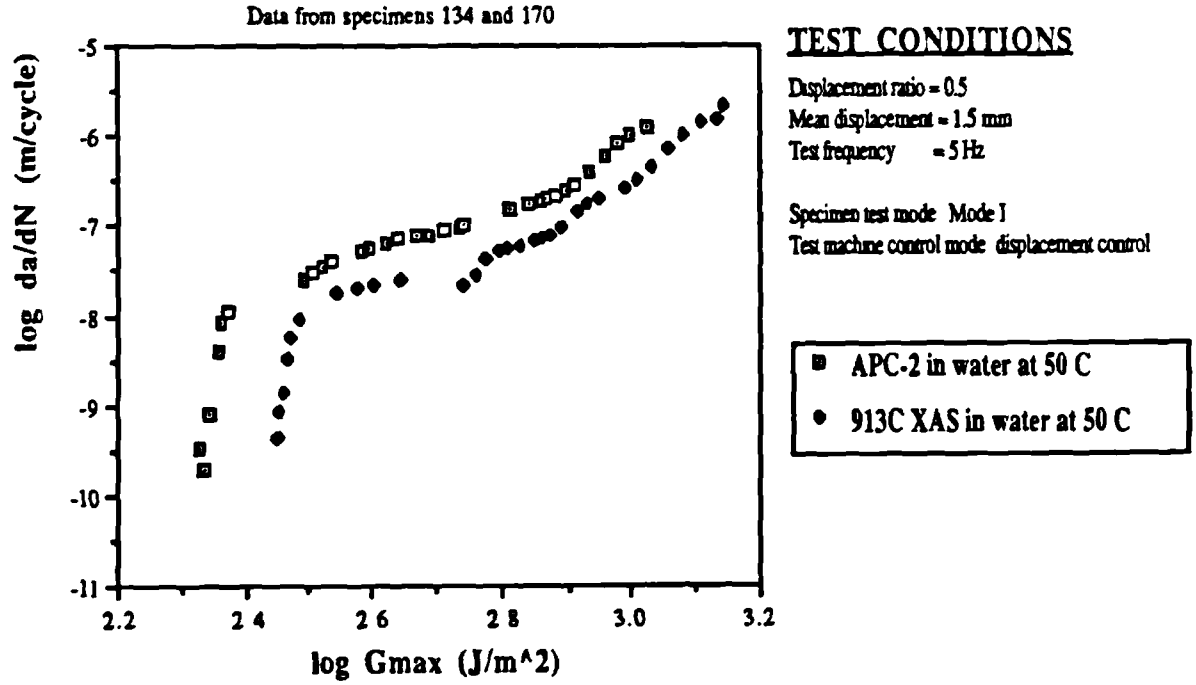


Figure 6.3b. Influence of the type of substrate on the fatigue performance of a bonded joint tested in water at 50 C. (Note:- Adhesive: Heat cure epoxy, "FM73M").

As can be seen from the fracture surfaces shown in Figures 6.3c and 6.3d, the thermoplastic composite joints tested in water at 25 °C and 50 °C failed due to a combination of regions of cohesive failure through the adhesive and interfacial failure along the adhesive/substrate interface. The regions of interfacial failure increased with increased temperature. Figures 6.3e and 6.3f show the fracture surfaces of the thermosetting composite joints tested in water at 25 °C and 50 °C. Figure 6.3e shows that the locus of failure was cohesive through the adhesive when the thermosetting composite joint was tested in water at 25 °C. Figure 6.3f shows that considerable interfacial failure occurred when the thermosetting composite joint was tested in water at 50 °C although the degree of interfacial failure in the thermosetting composite joint (see Figure 6.3f) was lower that for the thermoplastic composite joint (see Figure 6.3d).

Figure 6.3g shows that when the tests were performed in air at 23 °C, the locus of failure was cohesive through the adhesive and the type of substrate had no significant effect on the fatigue performance of the bonded joint. The results from Figure 6.3g indicate that it is the degree of instability of the adhesive/substrate interface which is the major factor responsible for the crack growing faster in the thermoplastic composite joint compared with the thermosetting composite joint when both joints were tested in water at 25 °C and 50 °C.

These results imply that in the presence of water, the degree of stability of the adhesive/substrate interface is greater in the thermosetting composite than the thermoplastic composite. Also from the Table 6.2, it can be seen that the reduction in the values of W_{Al} for the thermoplastic composite substrates (i.e APC-2) is significantly lower than for the thermosetting composite substrates (i.e 913C XAS) indicating that the interface of the thermosetting substrate/epoxy adhesive is more stable. The above thermodynamic calculations predict that all the interface investigated should remain stable in the presence of water since W_{Al} is positive in all the cases considered. However, as mentioned earlier, these calculations are an approximate guide to interfacial stability because they take no account of interfacial forces arising from primary bonds, acid-base interactions or mechanical interlocking.

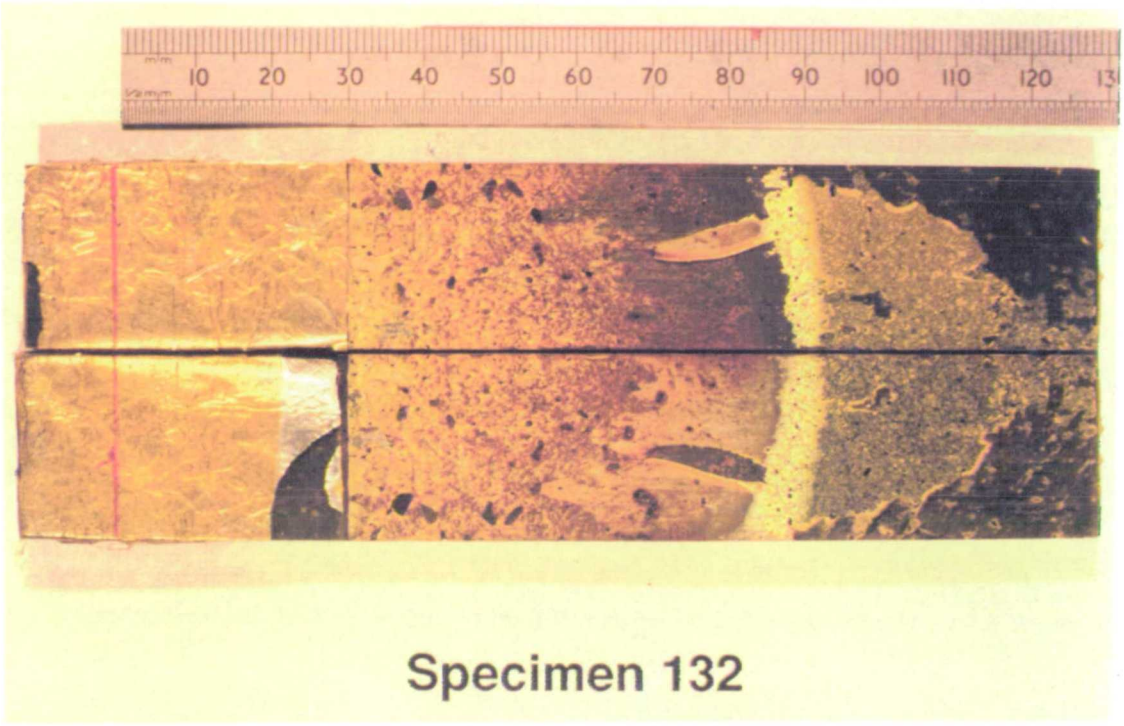


Figure 6.3c. Typical appearance of the fracture surfaces due to a fatigue crack propagating cohesively through a hot cure epoxy film adhesive (i.e "FM73M") bonding a thermoplastic composite substrate. The joint was tested in water at 25 °C.

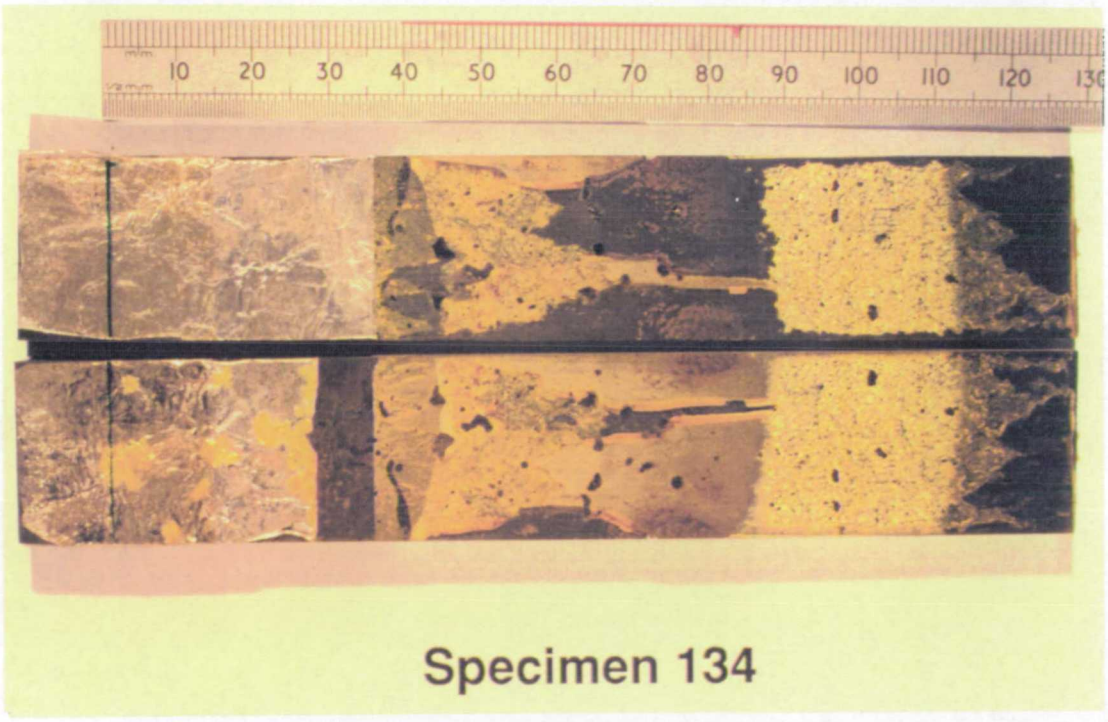


Figure 6.3d. Typical appearance of the fracture surfaces due to a fatigue crack propagating cohesively through a hot cure epoxy film adhesive (i.e "FM73M") bonding a thermoplastic composite substrate. The joint was tested in water at 50 °C.

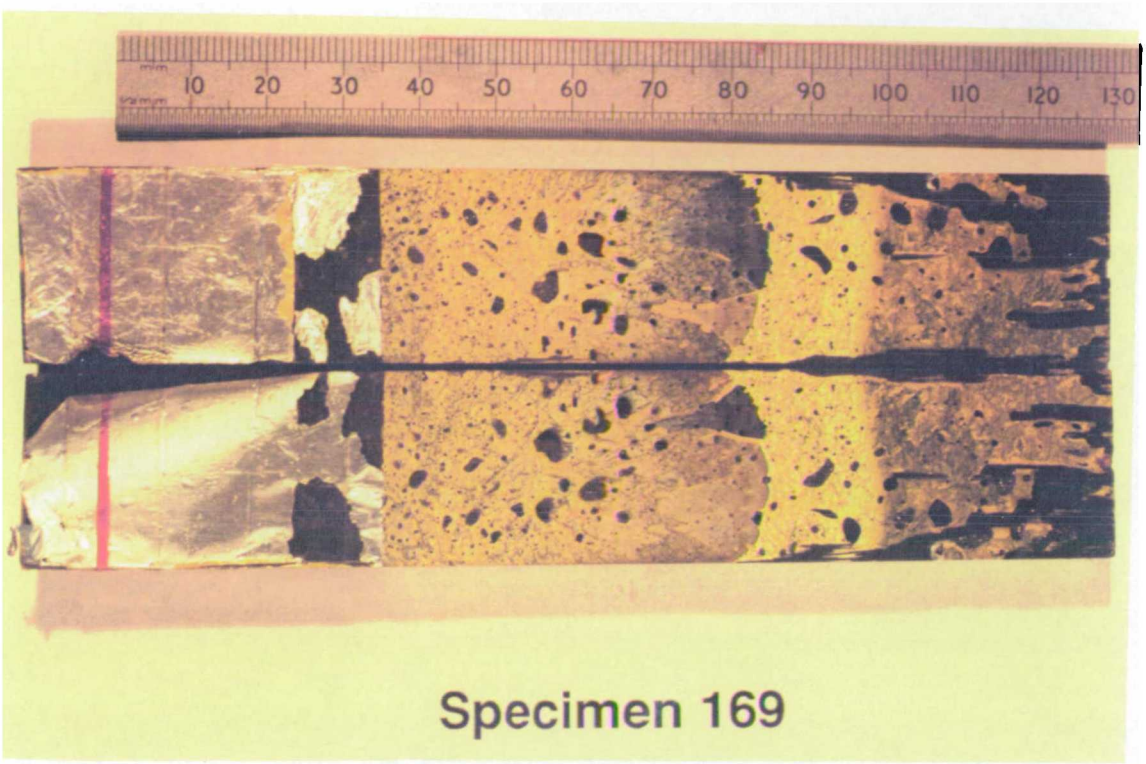


Figure 6.3e. Typical appearance of the fracture surfaces due to a fatigue crack propagating cohesively through a hot cure epoxy film adhesive (i.e "FM73M") bonding a thermosetting composite substrate. The joint was tested in water at 25 °C.

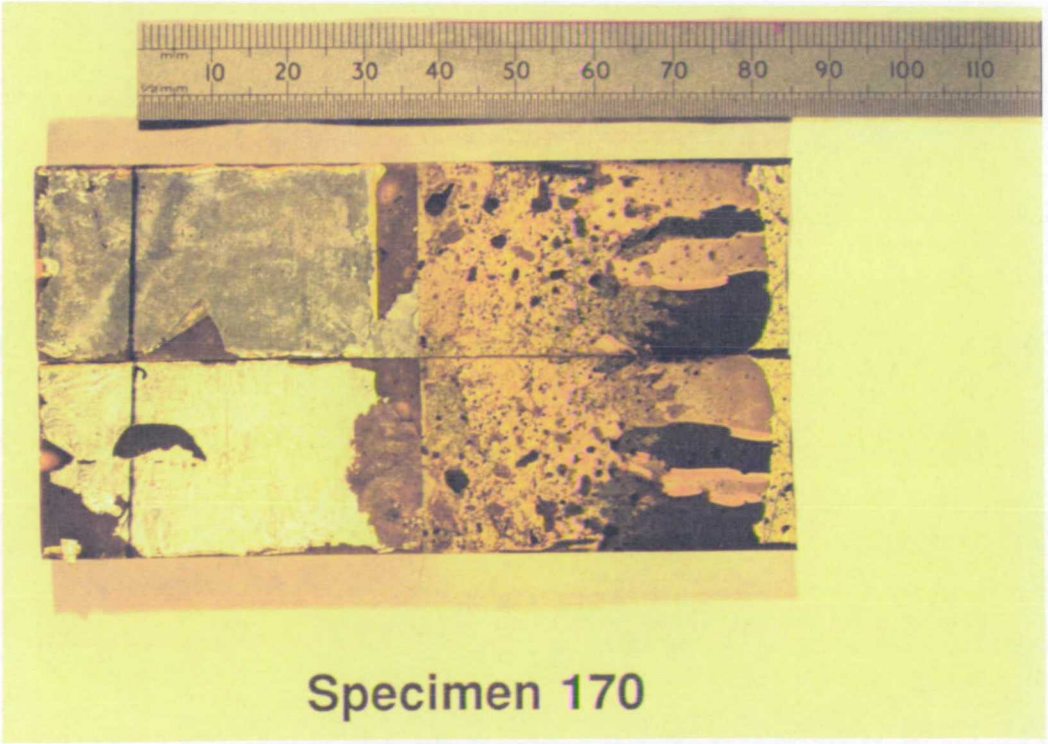


Figure 6.3f. Typical appearance of the fracture surfaces due to a fatigue crack propagating cohesively through a hot cure epoxy film adhesive (i.e "FM73M") bonding a thermosetting composite substrate. The joint was tested in water at 50 °C.

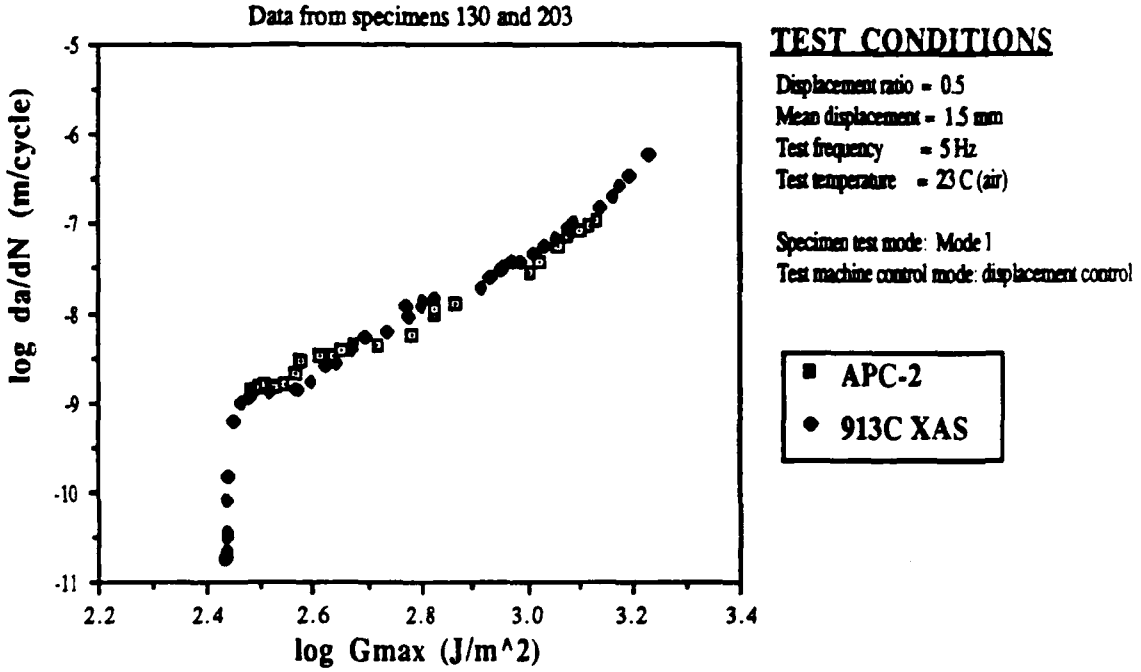


Figure 6.3g. Influence of the type of substrate on the fatigue performance of a bonded joints when tests were performed in dry air. (note:- Adhesive heat cure epoxy, "FM73M")

6.3 CONCLUSIONS

The main conclusions from the results presented in this chapter are:

(1) The fatigue tests carried out in distilled water at 25 °C and 50 °C, showed that in the cases where the locus of failure was cohesive through the adhesive layer, the value of the threshold fracture energy of the adhesive was higher than that obtained from testing in dry air at 23 °C. This was because the water interacted physically with the adhesive causing plasticization at the crack tip and thereby increasing the apparent toughness of the adhesive.

(2) The interface between a thermosetting composite ("913C XAS") and a cold-cure adhesive ("9309.3NA") did not breakdown during the entire period (2 months) of fatigue testing in water at 25 °C and 50 °C and the locus of failure was cohesive through the adhesive. Also at the early stages of testing in water, it was observed that the crack grow rate in the adhesive was the same in air and in water at 25 °C and 50 °C. However, after prolonged testing the plasticization of the adhesive by water resulted in higher threshold fracture energy values from tests in water than from tests in air.

(3) Similarly, at the early stages of testing, the crack growth rates in a thermosetting composite substrate bonded with a hot cure adhesive were the same in air at 23 °C and water at 25 °C and the locus of joint failure was cohesive through the adhesive. Also, due to the effects of plasticization, the threshold fracture energy of the adhesive was higher for tests in water at 25 °C than in air at 23 °C.

(4) The interface between the thermosetting composite and the heat cure adhesive was unstable during fatigue testing in water at 50 °C. Hence the crack growth rate was faster than in air at 23 °C and water at 25 °C.

(5) The interface between a thermoplastic composite (913C XAS) and the heat cure epoxy adhesive (FM73M) was found to be unstable during the fatigue testing in water at 25 °C and 50 °C. The locus of joint failure was a combination of cohesive and interfacial failure and the crack growth rates were much higher than those obtained from similar tests using thermosetting composite substrates.

CHAPTER SEVEN

SCANNING ELECTRON MICROSCOPY STUDIES

7.1 INTRODUCTION

This chapter discusses the use of the scanning electron microscopy (SEM) technique to study and understand the mechanisms of crack growth in adhesive joints. Mechanisms such as the direction of crack propagation, the influence of the rubber particles on the fracture and fatigue performance and the influence of the polyester mat-carrier are of particular interest. The usefulness of the SEM technique is its ability to focus on a region of interest at a low magnification and then, in a step-wise manner increase the magnification to reveal the characteristic features of the fracture process in more detail. However, some caution was exercised before generalising the information obtained from a single picture since a picture taken from a specific region does not provide the full details of the failure mechanism by any means.

As a results, efforts were made to study different sections of the fracture surfaces by dividing it into three different zones namely zones I, II and III as shown in Figure 7.1. Zone I represents the region where the crack growth rate is assumed to be negligible (i.e the near threshold region). Zone II represents the region where the relationship between log da/dN and log G_{max} is assumed to be linear (i.e the linear region II). Zone III represents the region where the monotonic loading value of G_{max} (i.e G_{1c}) dominates the overall crack growth rate (i.e the near fracture region). The information obtained from these different zones are compared and general conclusions were made only when certain features were seen often enough to be considered as characteristic features of the fracture or fatigue crack growth process.

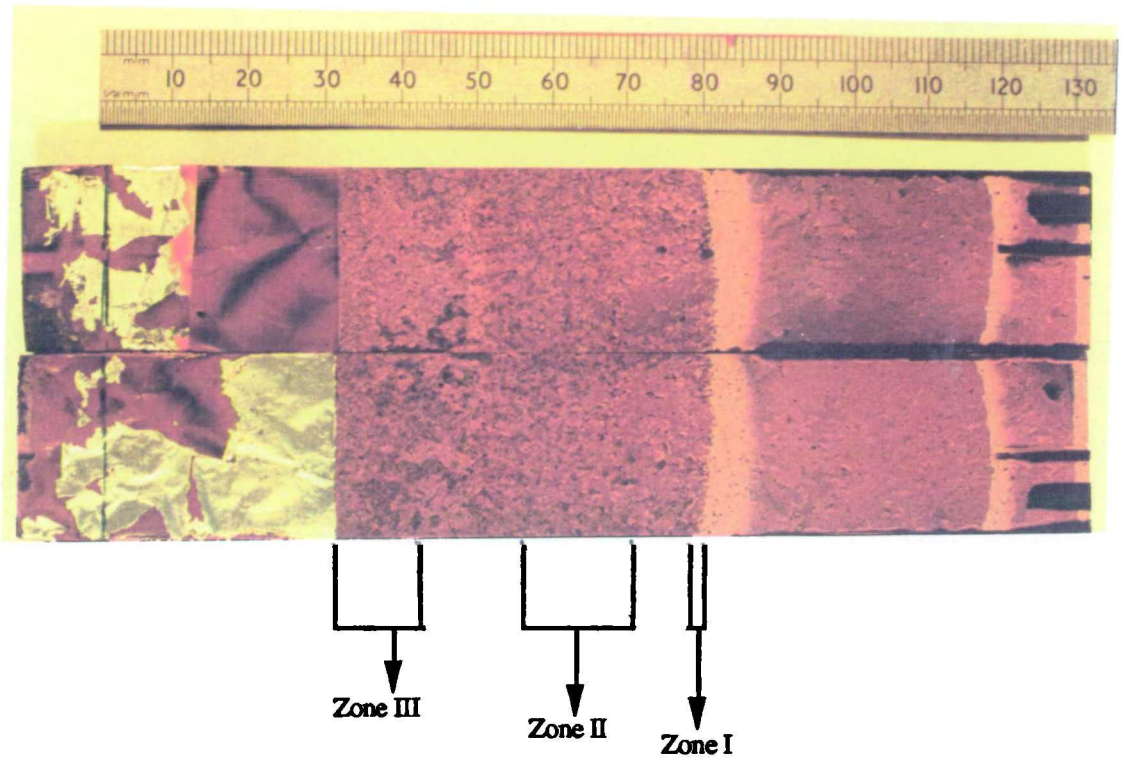


Figure 7.1. Division of the fracture surface of a DCB joint into three zones.
Notes: Zone I = area corresponding to the near threshold region of growth curve (see Figure 8.7);
Zone II = area corresponding to the linear region II part of growth curve;
Zone III = area corresponding to the fast fracture region of growth curve;

7.2 EXPERIMENTAL TECHNIQUE

The SEM equipment used in this work was the "JSM 5300" (1991). The debonded surfaces to be examined were cut to 2x2 cm sizes suitable for mounting on the SEM specimen holder. A sputter coater ("Edward 5150 A") was used to deposit a layer of gold all over the sample. The gold coating was typically 100 Å to 200 Å thick. After sputtering, a small amount of silver paint was applied between the specimen and the aluminium stub to improve the conductivity and to hold the specimen on the stub. A quick examination of the effectiveness of the coating process could be made by visual observation of the sample, which showed a the discolouration of the adhesive from its original colour to a gold/green colour when successful coating was achieved. The surfaces of the debonded specimen were then examined using the secondary electron image at an acceleration voltage of 15 kV and working distance of 20mm.

7.3 RESULTS AND DISCUSSION

7.3.1 Cold Cure Epoxy Paste Adhesive ("9309.3NA")

Figure 7.2a shows the typical appearance of the debonded surface obtained from a constant rate of displacement test carried out on the cold cure epoxy paste adhesive ("9309.3NA") bonding the thermosetting composite. The locus of failure was cohesive through the adhesive layer and the direction of crack growth is shown by the arrow. The figure reveals several characteristic features such as river markings or plastic flow lines, ridges and depressions, short fibres, voids and spherical glass beads and it was observed that these features were common to all the three zones (see Figure 7.1). Figures 7.2b - 7.2e show magnified views of selected regions from Figure 7.2a.

As can be seen from these figures, there are ridges and circular depressions caused by void growth and coalescence as the crack grows through the adhesive layer (Kinloch 1989). The ridges and voids scatter light and give rise to the stress whitening regions which were visually observed on the fracture surfaces as plastic flow lines. Figures 7.2f and 7.2g show a magnified view of other characteristic features on the debonded surface which include the 0.5mm glass beads used to control the thickness of the adhesive layer, voids left by entrapped air bubbles during the curing of the adhesive and the short fibres which are included by the manufacturer to control the viscosity and improve the mechanical properties of the adhesive at high temperatures. Figures 7.3a to 7.3c show the typical appearance of zones I, II & III (see Figure 7.1) of a surface from a fatigue test. The figures also show characteristic features that are similar to those observed from static testing such as plastic flow lines, ridges and depressions, voids, glass beads and short asbestos fibres. However, a comparison of Figures 7.2a with 7.3a show that the plastic flow lines obtained from the fatigue test are generally smaller in size than those obtained from static testing. Also by comparing Figure 7.3a with 7.3b and 7.3c, it was observed that as the fatigue crack growth rate decreased the size of the plastic flow lines decreased accordingly.

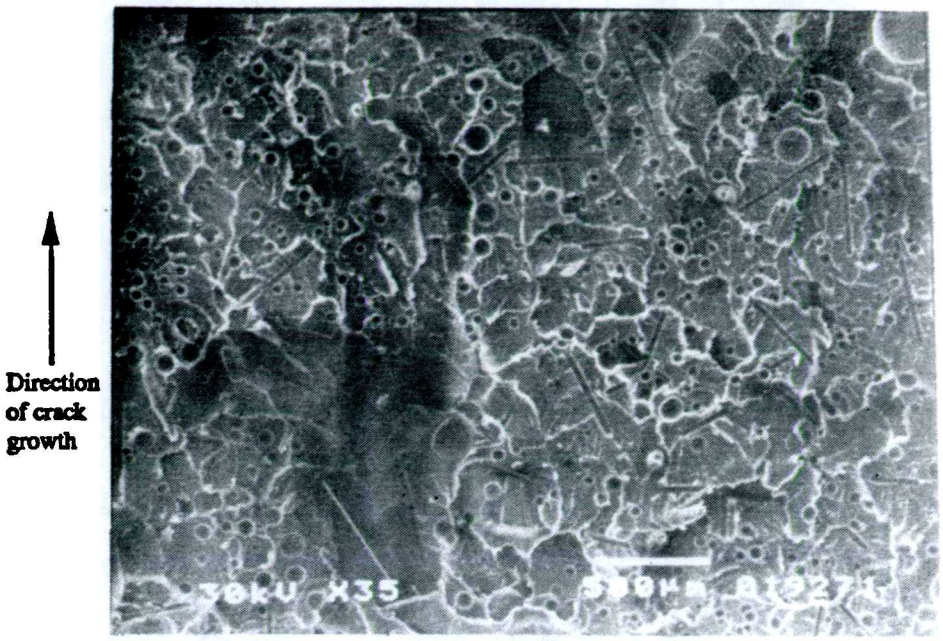


Figure 7.2a. Typical scanning electron micrographs of fracture surfaces obtained from performing a constant rate of displacement test on the cold cure epoxy paste adhesive bonding a thermosetting composite. It shows characteristic features such as plastic flow lines, ridges and depressions, short asbestos fibres and voids (x35).

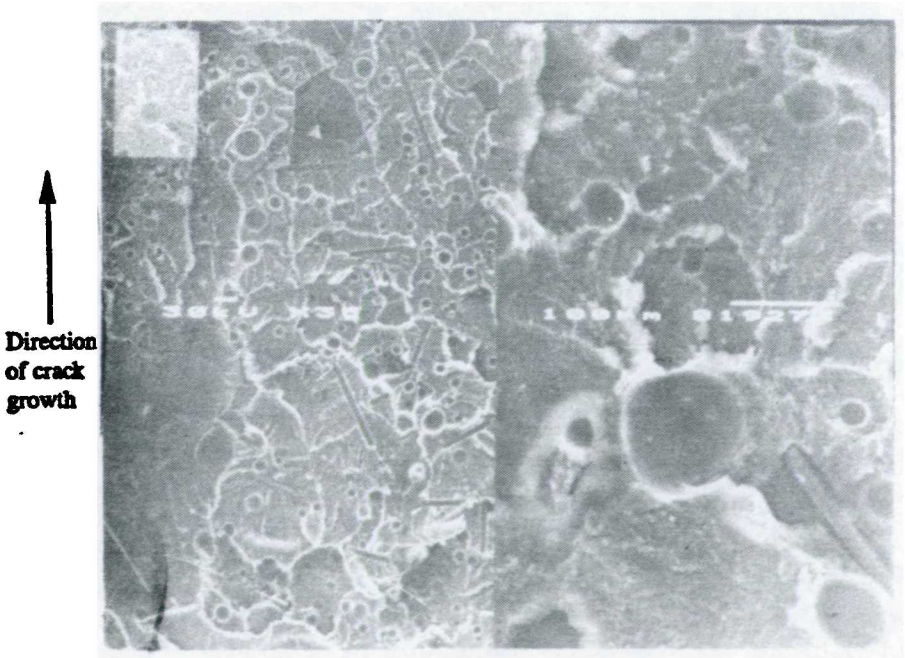


Figure 7.2b. A magnified view of a selected region (i.e the rectangular box) on Figure 7.2a showing the plastic flow lines, voids, ridges and depressions (x150).

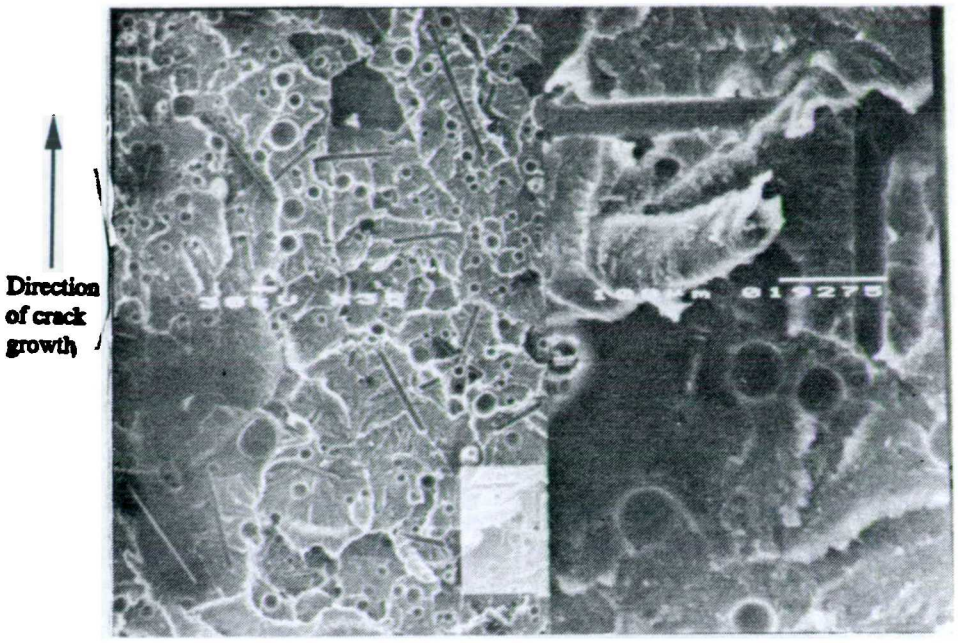


Figure 7.2c. A magnified view of another selected region (i.e the rectangular box) on Figure 7.2a showing the plastic flow lines, voids, ridges and depressions similar to those observed in Figure 7.2b (x150).

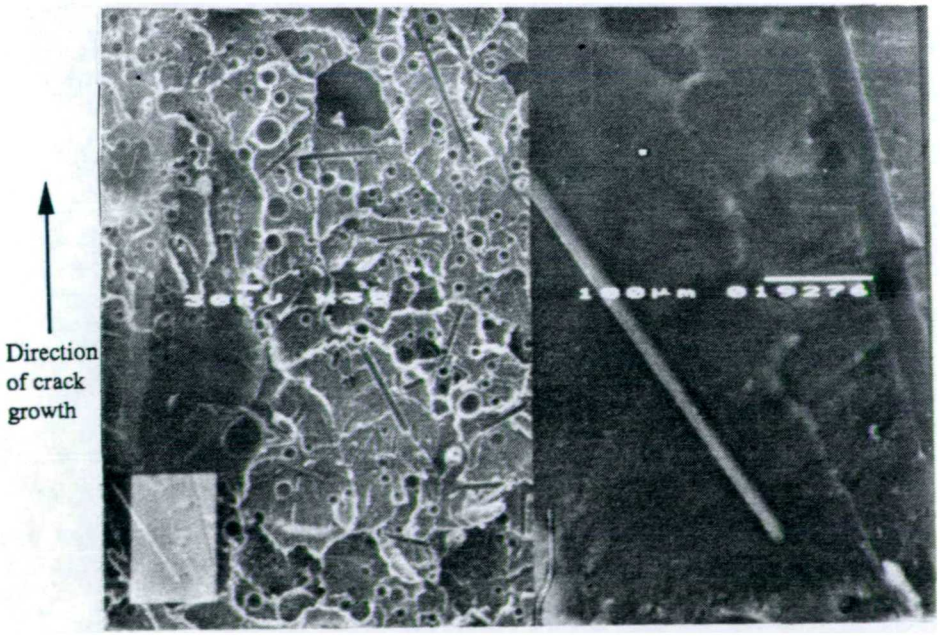


Figure 7.2d. A magnified view of another selected region (i.e the rectangular box) on Figure 7.2a showing the plastic flow lines, voids, ridges and depressions similar to those observed in Figures 7.2b and 7.2c (x150).

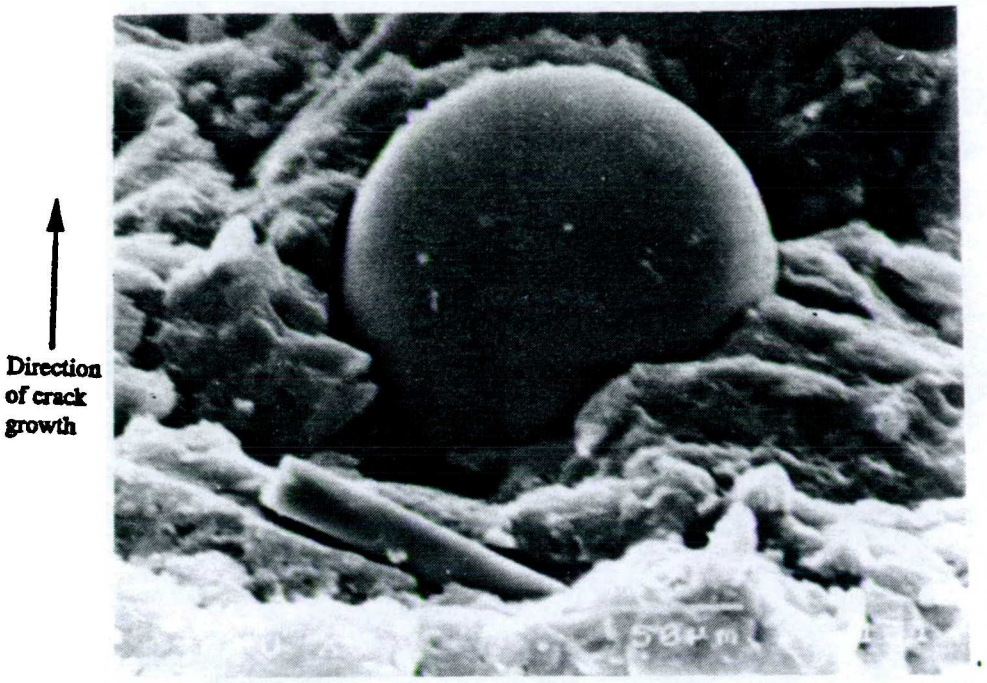


Figure 7.2e. Typical scanning electron micrograph of the glass beads used to control the thickness of the adhesive layer (x500).

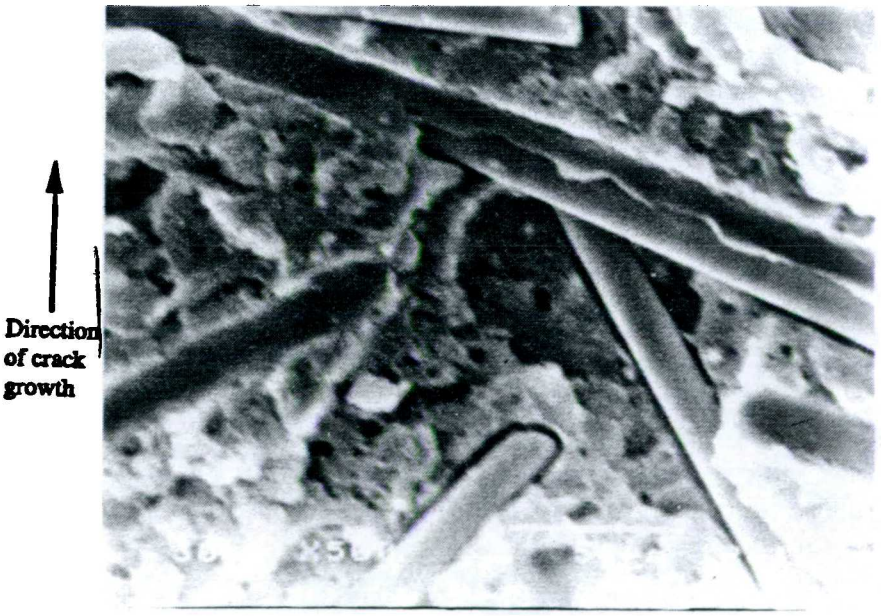


Figure 7.2f. Typical scanning electron micrograph of short fibre which were included by the manufacturers to control the viscosity and improve the mechanical properties of the adhesive at high temperature. The figure also shows the voids left by the entrapped air bubbles during the curing of the adhesive (x500).

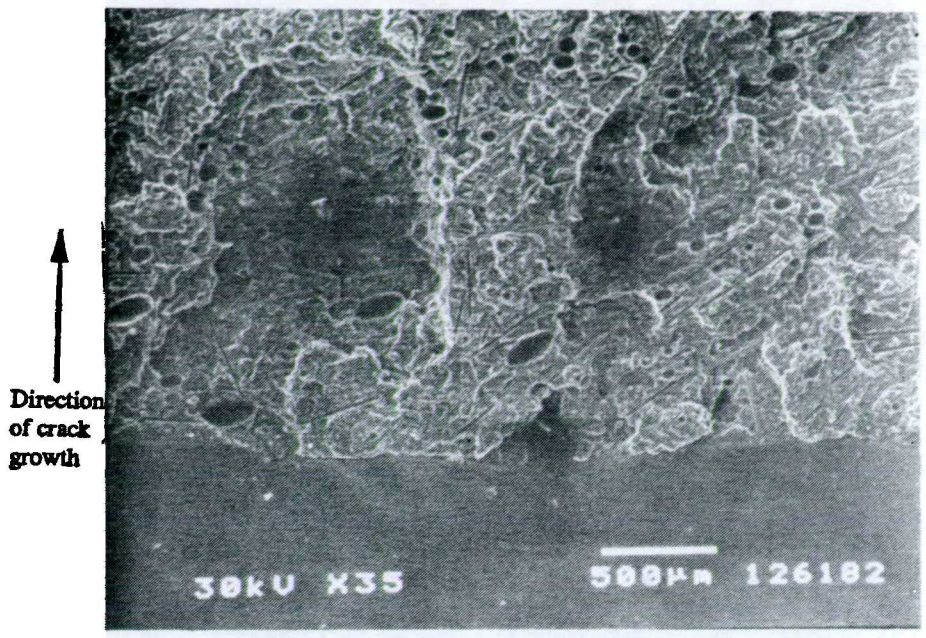


Figure 7.3a. Typical scanning electron micrograph of the Zone III part of the fracture surfaces (see Figure 7.1) when a fatigue test was carried out on the cold cure epoxy paste adhesive bonding a thermosetting fibre-polymer composite (x35).

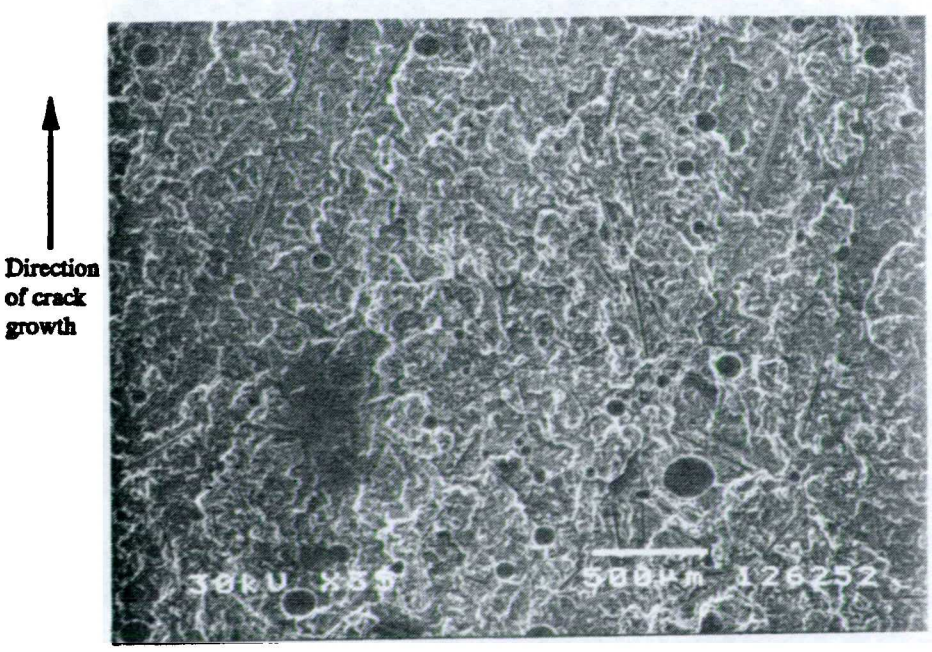


Figure 7.3b. Typical scanning electron micrograph of the Zone II part of the fracture surfaces (see Figure 7.1) when a fatigue test was carried out on the cold cure epoxy paste adhesive bonding a thermosetting fibre -polymer composite (x35).

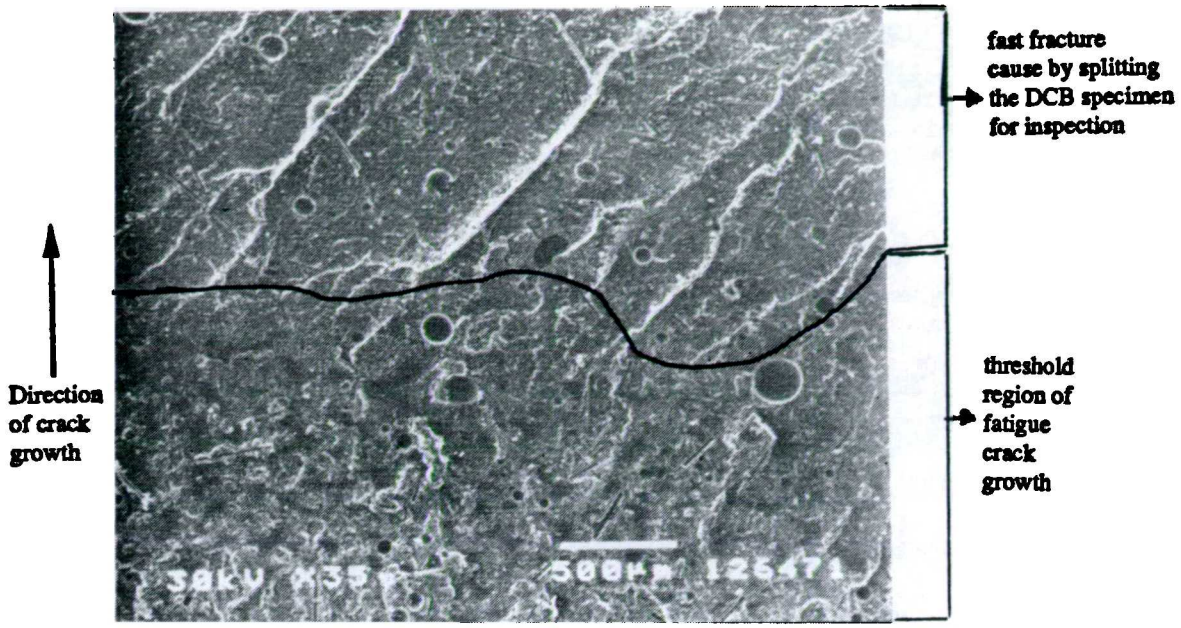


Figure 7.3c. Typical scanning electron micrograph of the Zone I part of the fracture surfaces (see Figure 7.1) when a fatigue test was carried out on the cold cure epoxy paste adhesive bonding a thermosetting fibre -polymer composite (x35). From Figure 7.3a to 7.3c, it can be seen that as the fatigue crack growth rate decreased, the size of the plastic flow lines decreased accordingly.

7.3.2 Hot Cure Epoxy Film Adhesive with a Mat-Carrier

Figure 7.4a shows the typical appearance of the fracture surface obtained from a constant rate of displacement test carried out on the hot cure epoxy film adhesive ("FM73M") bonding the thermosetting composite. The locus of failure was again cohesive through the adhesive layer and the direction of crack growth is shown by the arrow. The figure reveals characteristic features such as plastic flow lines, voids due to entrapped air bubbles during the curing of the adhesive, and the polyester mat-carrier, which controls the thickness of the adhesive layer. Figures 7.4b to 7.4e are magnified views of selected area on Figure 7.4a and the general conclusion drawn from these figures is that there is very little damage to the mat-carrier during static testing. In particular, Figure 7.4b shows that the mat carrier debonds from the adhesive with very little damage to the carrier itself. Thus, the failure of "FM73M" under static testing conditions are via the process of shear yielding of the adhesive matrix and the debonding of the

interface between the mat-carrier and the adhesive. Figure 7.5a illustrates the appearance of a typical debonded surface obtained from the fatigue test and it shows characteristic features similar to Figure 7.4a. Figures 7.5b to 7.5e show magnified views of a selected region in Figure 7.5a. They demonstrate that there was considerable tearing and damage of the mat-carrier compared with that observed from the statically tested joints, especially when comparing Figure 7.4b (static test) with 7.5b (dynamic test). These observations are consistent with those reported by Jablonski et al (1980) where SEM photomicrographs of fracture surfaces of a rubber modified epoxy film adhesive showed that there was significant damage to the mat-carrier after fatigue testing, but no damage was observed on the mat carrier after static testing. Hence, from the present investigation and from results obtained from previous work (section 5.5.5) it can be concluded that the influence of the mat-carrier is a major factor responsible for the good fatigue resistance of the hot cure epoxy film adhesive possibly to the extent of accounting for the observation that its fatigue performance is now superior to that of the cold cure epoxy paste adhesive. Notwithstanding the fact that the latter has a higher static fracture energy (i.e 5.7 kJ/m^2) compared with the former (i.e 2.93 kJ/m^2).



Figure 7.4a. Typical scanning electron micrograph of fracture surfaces obtained from performing a constant rate of displacement test on the hot cure epoxy film adhesive bonding a thermosetting composite. The figure shows characteristic features such as polyester mat carrier, plastic flow lines and voids (x35).

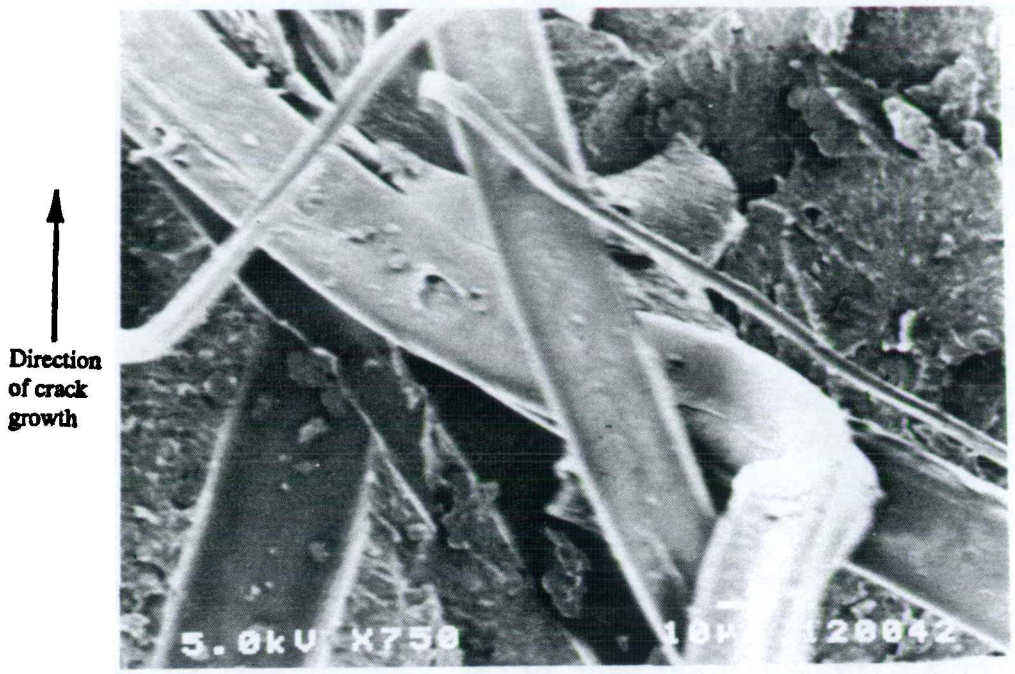


Figure 7.4b. Typical scanning electron micrograph showing a magnified view of the mat carrier (x750).

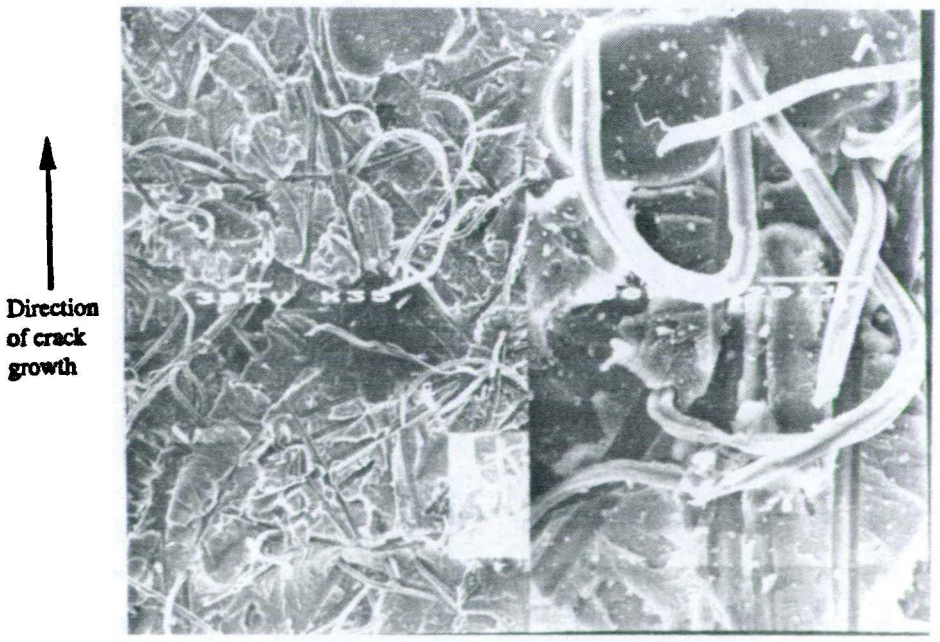


Figure 7.4c. A magnified view of a selected region (i.e the rectangular box) on Figure 7.4a showing that the fracture surface is dominated by interfacial failure between the carrier and the adhesive (x150).

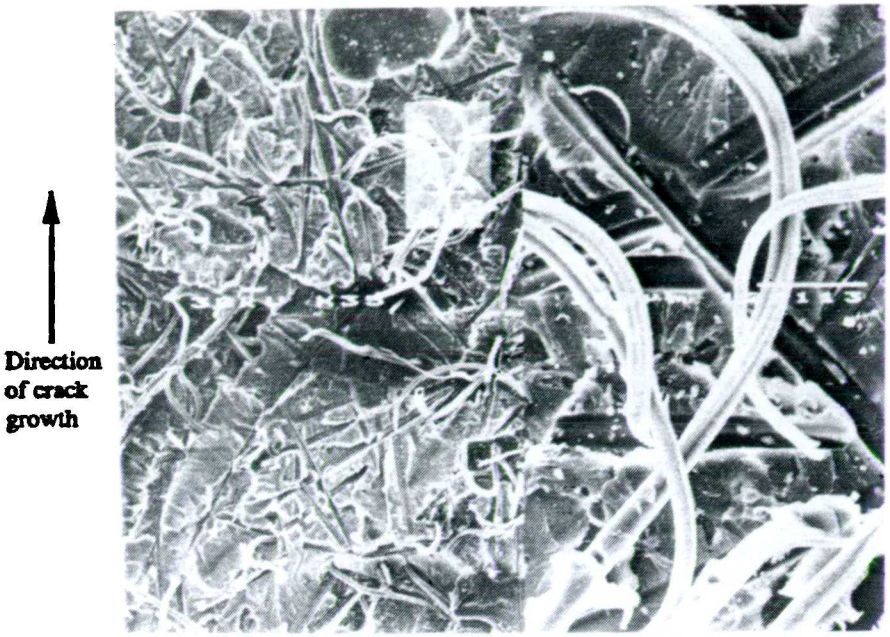


Figure 7.4d. A magnified view of another selected region (i.e the rectangular box) on Figure 7.4a also showing that the fracture surface is dominated by interfacial failure between the carrier and the adhesive (x150).

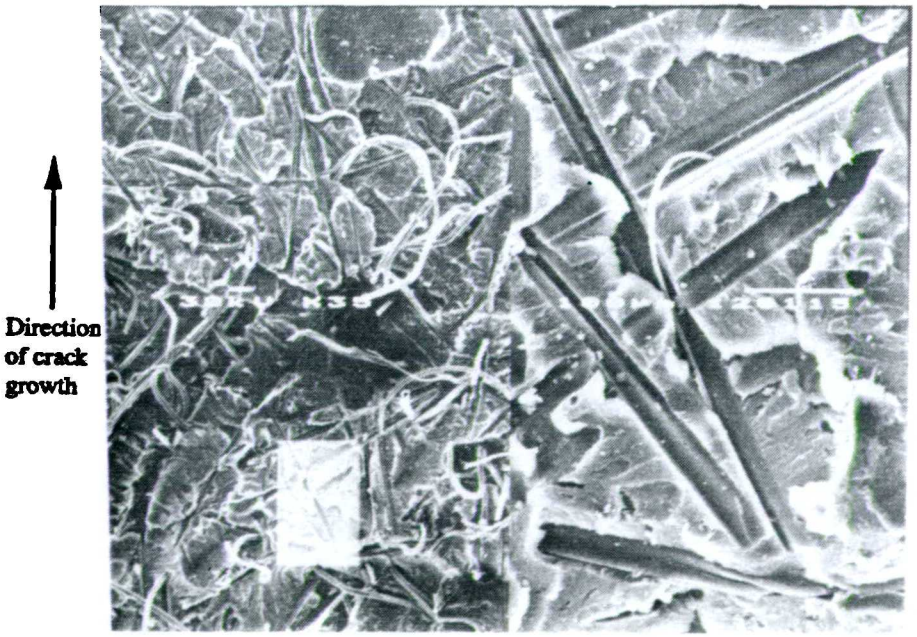


Figure 7.4e. A magnified view of another selected region (i.e the rectangular box) on Figure 7.4a also showing that the fracture surface is dominated by interfacial failure between the carrier and the adhesive (x150).

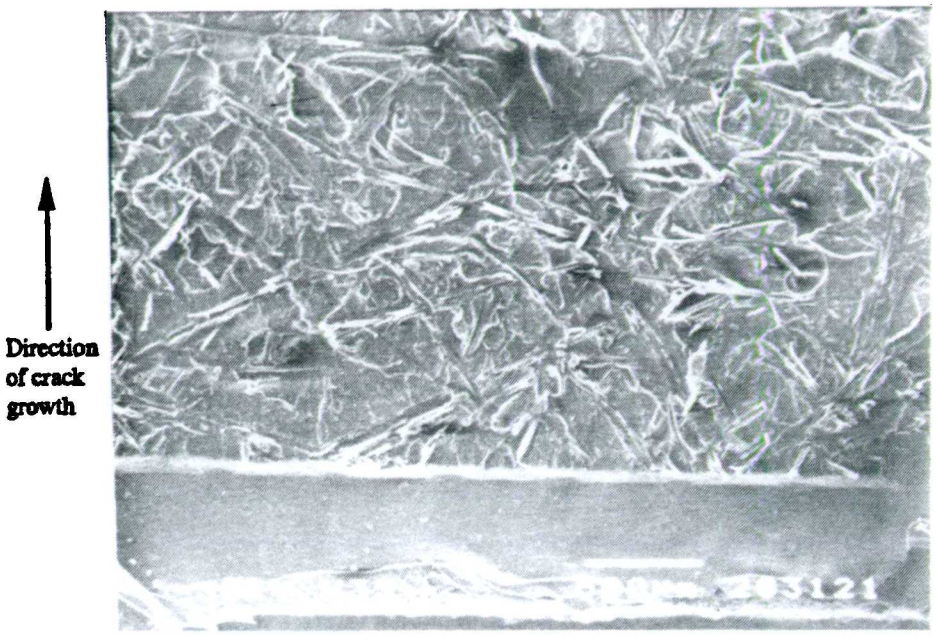


Figure 7.5a. Typical scanning electron micrographs of fractured surfaces obtained from performing a fatigue test on the hot cure epoxy film adhesive bonding a thermosetting composite. The figure shows characteristic features (x35) similar to those observed from static testing, such as polyester mat carrier, plastic flow lines and voids.

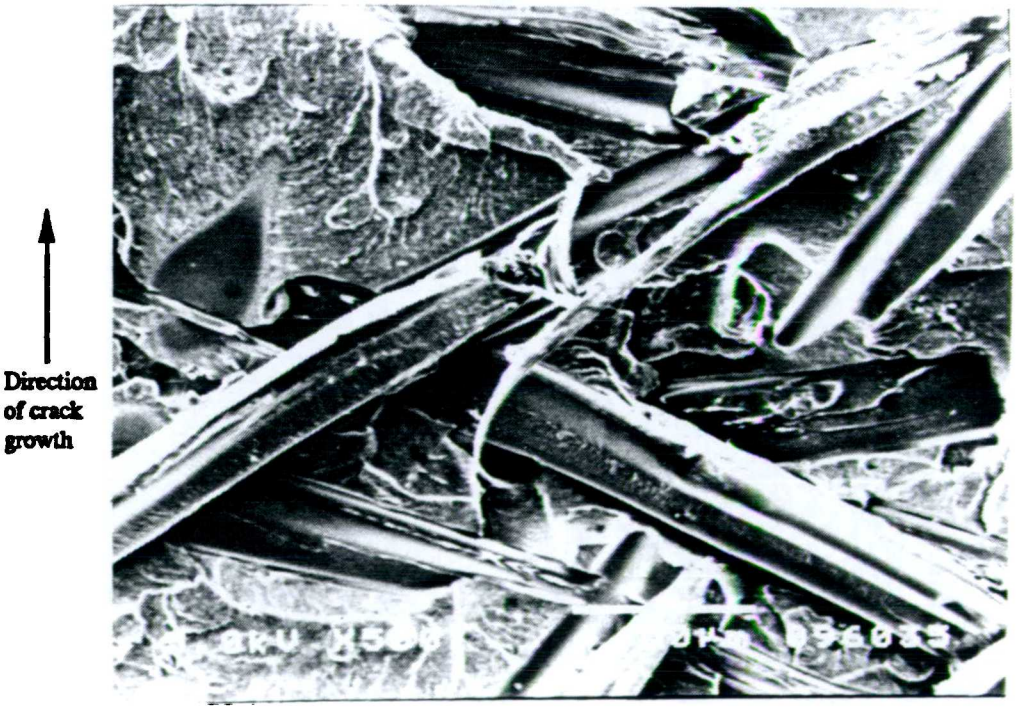


Figure 7.5b. Typical scanning electron micrograph showing a magnified view of the amount of damage to the mat carrier due fatigue crack growth (x500).



Figure 7.5c. A magnified view of a selected region (i.e the rectangular box) on Figure 7.5a showing that there is considerable damage to the mat carrier compared with the case for static loading (x150).

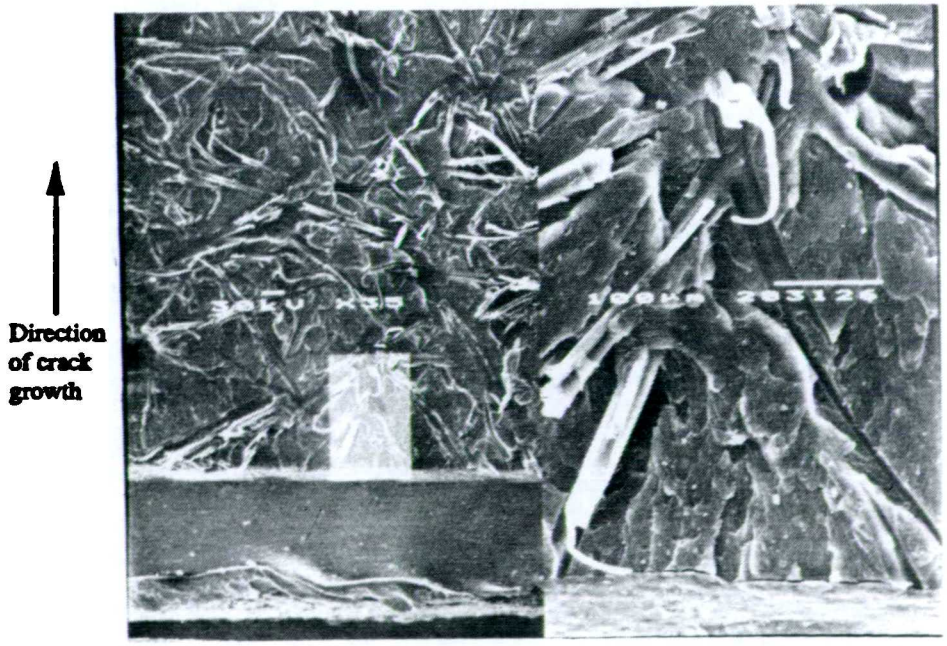


Figure 7.5d. A magnified view of another selected region (i.e the rectangular box) on Figure 7.5a also showing that there is considerable damage to the mat carrier compared with the case for static loading (x150).

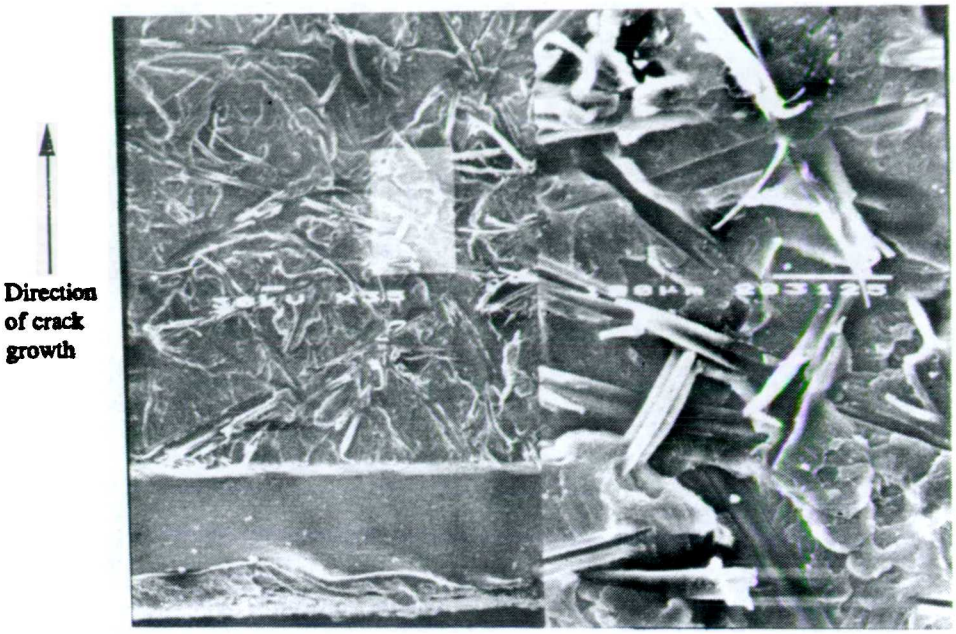


Figure 7.5e. A magnified view of another selected region (i.e the rectangular box) on Figure 7.5a also showing that there is considerable damage to the mat carrier compared with the case for static loading (x150).

7.4 CONCLUSIONS

The main conclusions from this chapter are:

(1) When the locus of failure was cohesive through the adhesive layer, the SEM photomicrographs of fracture surfaces of the cold cure epoxy paste adhesive used in bonding the thermosetting composite revealed that:

(i) The characteristic features on the surface include river markings, ridges and depressions, short fibres, voids and the spherical glass beads which were added to control the adhesive layer thickness.

(ii) The sizes of the plastic flow lines on the debonded surfaces from static tests were much larger than those typically observed from fatigue testing. The size of the plastic flow lines decreased as the crack growth rate decreased.

(2) When the locus of failure was cohesive through the adhesive layer, the SEM photomicrographs of fracture surfaces of the hot cure epoxy film adhesive used in bonding the thermosetting composite revealed that:

(i) There is very little damage to the mat-carrier during static testing and fracture occurs through the mechanism of localised shear yielding in the epoxy matrix and the interfacial debonding of the mat-carrier and the adhesive.

(ii) There was significant damage to the mat-carrier during fatigue testing and fracture occurs through the mechanism of localised shear yielding in the epoxy matrix and extensive damage to the mat-carrier.

CHAPTER EIGHT

PREDICTION OF THE SERVICE LIFE OF BONDED JOINTS.

8.1 INTRODUCTION

8.1.1 Background

The ultimate goal of studying the fatigue crack propagation behaviour is to be able to predict the service life of any engineering component with confidence, and avoid catastrophic failures. Therefore one of the principal objectives of this work was to investigate the possibility of using the collected fatigue data to predict the lifetime of a bonded joint. It is believed that such a prediction will facilitate the development of a soundly based quality control test method and the quantitative prediction of the lifetimes of bonded joints in their service conditions.

In Chapters Five and Six the fatigue data were presented and it was shown that the results could be characterised using a modified form of the Paris law, from which the material constants D and n were obtained. In this chapter a technique for estimating the lifetime of real bonded component will be established. Firstly an attempt will be made to show that the service life of a double cantilever beam specimen can be predicted from a knowledge of the linear region II constants (D and n), the geometrical dimensions of the specimen and the compliance calibration curve for the substrate. The compliance curve can be obtained from either a constant crosshead rate experiment or by using finite element analysis. Secondly it will be demonstrated that the constants D and n are independent of the geometry of the specimen by using them to predict the service life of single lap joints. Such joints are generally believed to have high peel

stresses at the end of the bond overlap (Hart -Smith 1973, Adams 1974) and the results from these theoretical studies will be compared with the results from real bonded components using the experimental data obtained from the DCB and single lap joints.

8.1.2 Service Life Design Philosophies

The problem of ensuring satisfactory fatigue performance of components and bonded components continues to be a major consideration in design studies. Three main design philosophies have been put forward. The first two philosophies are referred to as the "safe-life" and the "fail-safe" (Maxwell 1971). The "safe-life" approach is broadly based on the concept that significant fatigue damage will not develop during the service life of a structure, while, in contrast, the "fail-safe" approach recognises that some significant fatigue damage may develop in the later stages of the life of a structure. The "fail-safe" philosophy then recommends that allowances should be made to ensure that the growth of such cracks do not have a significant effect on the performance of the structure, before they are detected during routine inspections for cracks. The basic requirements for the "fail-safe" approach were defined by Maxwell (1971) to be: (i) a crack missed at one inspection should not cause failure before the next, and (ii) the presence of the crack shall not cause the residual strength of the component to be less than 80% of its designed ultimate value.

The third design philosophy is known as the "damage-tolerant" design philosophy (USAF 1974) which is based on the assumption that newly manufactured structures will always have inherent flaws and the task is to predict the service life from the inherent flaw size. The "damage-tolerant" design approach differs from the "fail safe" approach in that it goes much further to model the minimum allowable flaw size as the largest size of any defect naturally present in the material, instead of some arbitrarily specified flaw size as is the case for the "fail-safe" approach. It then proceeds to discover whether this flaw size will grow to a critical size to cause failure during the expected life of the structure. The choice of any of the above design philosophies is dependent on the design engineer and the requirements of the project.

Which ever design philosophy is assumed, the development of any rational fatigue life prediction method for a material must involve:

(a) an experimental observation of the degree of fatigue damage,

(b) a formulation of a fatigue damage model,

(c) the use of the model to predict the service life of the material, and

(d) an experimental verification of the life prediction model.

8.1.3. Selection of Minimum and Maximum Permissible Crack Sizes for the Prediction of Service Life.

The essence of studying the fatigue crack growth rate based on the damage tolerance approach is to be able to determine how long it takes a crack to grow from a certain crack size to the maximum permissible size at which failure of the component is assumed. The initial crack size should be reliably detected using non destructive inspection (NDI) techniques and other methods previously discussed in section 3.9. It should be remembered that the initial flaw size cannot be zero because real components and structures will always contain discontinuities such as voids, flaws and damaged regions. The choice of the maximum permissible crack size is dependent on a variety of considerations among which may include the need to avoid fast fracture or collapse, the need to restrict crack growth so that repairs remain practicable, or the need not to exceed a specified value of stress intensity factor or strain energy release rate (e.g K_{th} or G_{th}).

8.1.4. Fatigue Crack Initiation and Propagation Lifetimes

The determination of the service life of an adhesive used in bonding any engineering component requires a knowledge of the fatigue crack initiation and propagation lifetimes. The initiation life of an adhesively bonded joint is the number of cycles required to initiate the growth of a crack, whilst the propagation life is the number of cycles required to propagate a crack from a known crack size to a predetermined critical crack size. The total fatigue life of the bonded joint is the sum of the initiation and propagation times. There is no simple or clear

delineation of the boundary between fatigue crack initiation and propagation but it is generally acknowledged (Kinloch 1983) that crack initiation is governed by the molecular theory of fracture which is based on the energy required to break the bonds present in the adhesive (Tomkins 1966). On the other hand crack propagation is governed by fracture mechanics arguments based on the propagation of existing flaws or defects, which are assumed to be in the form of a crack.

Considering the crack initiation process then, very little is known about how the breaking of primary covalent bonds or secondary van der Waal bonds present in the adhesive contributes to the fatigue crack initiation life in polymers. Some authors (e.g., Chudnovsky 1984) have suggested a thermodynamic approach to the above problem by treating the crack initiation process as a form of local instability so that a framework can be proposed to establish a law for crack initiation. The success of this approach has yet to be established.

Experimentally, however, the contribution of initiation time to the service life of a bonded structure depends on the magnitude of the loads applied to the joint. If at the beginning of an experiments the maximum load applied to the joint is just less than the critical load required to cause fast fracture (i.e P_{max} = 60-90% $P_{critical}$), then the fatigue life will be dominated mainly by the crack propagation life and the crack initiation time will be negligible.

In contrast, if at the beginning of the experiment the maximum load applied is very close to the corresponding load required for the near threshold region of crack growth, then the fatigue life of the joint will be dominated by the crack initiation life. In the present investigation the crack initiation process has been reduced to a minimum by using an initial maximum load of about 60 to 95% of the load required to cause fast fracture. This leads to the number of cycles to failure obtained from the test being mainly associated with the crack propagation stage.

8.2 PREDICTION OF THE SERVICE LIFE USING THE CRACK GROWTH RATE MODEL

In section 2.5 two crack growth laws based on the crack growth rate model were suggested for characterising the fatigue behaviour of adhesively bonded joints. For the region where the relationship between da/dN and G_{max} was linear, the equation suggested was:

$$\frac{da}{dN} = D(G_{max})^n \tag{8.1}$$

while the expression for the full fatigue curve covering regions I, II and III was given as:

$$\frac{da}{dN} = DG_{max}^n \left(\frac{1-\left(\frac{G_{th}}{G_{max}}\right)^{D_1}}{1-\left(\frac{G_{max}}{G_{1c}}\right)^{D_2}} \right) \tag{8.2}$$

Now, the concept of predicting the service life of an adhesively bonded joint using the crack growth rate model is based on the fact that the designer may start from a knowledge of the material constants D and n (equation 8.1) or D, n, D_1, D_2, G_{th} and G_{1c} (equation 8.2). Next the details of the specimen geometry and loading and testing conditions are used to calculate the value of G_{max} to be substituted into either equation 8.1 or 8.2. The service life of the bonded joint can then be estimated by integrating these equations, using computerised numerical methods. In the next two sections, it will be demonstrated how a knowledge of the values of D, n, D_1, D_2, G_{th} and G_{1c} (obtained by curve-fitting the sigmoidal shape of the da/dN versus G_{max} curve) enable the service life of any bonded joint subjected to mode I loading to be predicted. Firstly, an attempt will be made to predict the service life of a DCB joint from a knowledge of the material constants previously obtained from the fatigue tests. The predicted results will then be compared with the data previously generated from the experiments. This

exercise should obviously give a useful assessment of the accuracy of the crack growth laws used to describe the form of da/dN versus G_{max} relationships. These results are presented in section 8.3.

Secondly the fatigue service life of a different specimen geometry namely a single lap joint will be predicted. The ability to use the material constants generated from a pure mode I test to predict the service life of single lap joints arises from the fact that detailed analyses (Adams 1974, 1990, Hart-Smith 1973,1985) have shown that single lap joints prepared in accordance with the ASTM D1002-72 standard will fail due to the peel (tensile) stresses generated at the ends of the overlap, rather than due to shear stress concentrations. Indeed, the predictive model based on the crack growth rate law can be used for any specimen geometry, provided the value of G_{max} can be deduced for that geometry. Therefore, in the present investigation, a method has been proposed for the calculation of the value of G_{max} generated as a result of the peel stresses at the end of the overlap of a single lap joint. The value of G_{max} is then substituted into either equation 8.1 or 8.2 to predict the service life of the joint. The results are presented in section 8.4.

8.3 MODELLING AND PREDICTING THE FATIGUE BEHAVIOUR OF THE DCB JOINTS

8.3.1 Adaptation of the Crack Growth Rate Model to the DCB Specimen Geometry

In order to successfully model the fatigue failure of a DCB joint equations 8.1 and 8.2 have to be adapted to the specimen geometry by deriving a method whereby G_{max} can be calculated without having to perform a fatigue experiment. It should be noted that without experimental data from a fatigue test, the value of G_{max} is difficult to estimate because at least one of the variables required for substitution into any of equations 5.8 to 5.11 will be unknown. If for example, experiments were performed under a constant displacement amplitude, the value of

P_{max} will be unknown. Therefore, a method has to be found by which P_{max} can be substituted without a knowledge of the actual values from a fatigue test. One such method is to substitute the value of the specimen compliance (i.e $C = \delta_{max}/P_{max}$) in the place of P_{max}. Equations 8.1 and 8.2 have been modified and adapted to the DCB joint. When the value of G_{max} is estimated using the compliance equation (equation 5.9) in which P_{max} has been substituted for by C/δ_{max}, and the resulting equation is:

$$G_{max} = \frac{\delta_{max}^2}{2B\,C^2} \cdot \frac{dC}{da} \tag{8.3}$$

When equation 8.3 is substituted into equation 8.1 and integrated, the resulting equation is:

$$N_f = \frac{1}{D}\left(\frac{2B}{\delta_{max}^2}\right)^n \int_{a_i}^{a_f} \left(\frac{C^2}{\left(\frac{dC}{da}\right)}\right)^n \tag{8.4}$$

where

C = specimen compliance

B = width of specimen

δ_{max} = maximum displacement during fatigue cycling

N_f = number of cycles to complete failure (i.e the service life of the adhesive)

D and n are linear region II constants

Similarly, when the full characterisation expression (equation 8.2) is modified, the resulting equation upon substituting for G_{max} (using equation 8.3) and then integrating is:

$$N_f = \int_{a_i}^{a_f} \frac{\left(1 - \left(\frac{\delta_{max}^2}{2B\,G_{1c}} \frac{1}{C^2} \frac{\partial C}{\partial a}\right)^{D_2}\right)}{D\left(\frac{\delta_{max}^2}{2B} \frac{1}{C^2} \frac{\partial C}{\partial a}\right)^n \left(1 - \left(\frac{2B\,G_{th}}{\delta_{max}^2} C^2 \frac{1}{\frac{\partial C}{\partial a}}\right)^{D_1}\right)} \qquad (8.5)$$

where the constants D_1 and D_2 are obtained as will be described later in section 8.3. Similarly when the value of G_{max} was estimated using the displacement equation (equation 5.11) in which P_{max} has been substituted for by C/δ_{max}, and the resulting equation is:

$$G_{max} = \frac{3F}{2B(a+\chi h)Z} \cdot \frac{\delta_{max}^2}{C} \qquad (8.6)$$

And the resulting upon substitution into equation 8.1 and integration is:

$$N_f = \frac{1}{D}\left(\frac{2Z\,B}{3F\,\delta_{max}^2}\right)^n \int_{a_i}^{a_f} C^n (a + \chi h)^n \qquad (8.7)$$

where

C = specimen compliance

δ_{max} = maximum displacement during fatigue cycling

N_f = number of cycles to complete failure (i.e the service life of the adhesive)

D = Paris law coefficient

n = Paris law exponent

B = width of specimen

a_i = initial crack length

a_f = final crack length

F, Z = are correction factors as described in section 4.2.

And when the full characterisation expression (equation 8.2) is modified the resulting equation after integrating is:

$$N_f = \int_{a_i}^{a_f} \frac{\left(1 - \left(\left(\frac{3F\,\delta_{max}^2}{2z\,B\,G_{ic}}\right)\left(\frac{1}{C(a+\chi h)}\right)\right)^{D_2}\right)}{D\left(\left(\frac{3F}{2z}\frac{\delta_{max}^2}{B}\right)\left(\frac{1}{C(a+\chi h)}\right)\right)^{a}\left(1 - \left(\left(\frac{2z\,B\,G_{th}}{3F\,\delta_{max}^2}\right)(C(a+\chi h))\right)^{D_1}\right)} \qquad (8.8)$$

The integration of equations 8.4, 8.5, 8.7 and 8.8 may be carried out using Simpson's rule, or any other mathematical integration method. However the main problem involved with solving these equations is how to get the compliance function C = f(a) without the need to perform a fatigue test on a DCB joint. Two options are available. One option is to use finite element analysis to get the compliance function C=f(a). The other option is to obtain the compliance function C= f(a) from the constant rate of displacement test results. Finally, when the function C = f(a) is known, it is then necessary to ensure that the compliance function obtained from these two methods is equivalent to that obtained from a fatigue experiment.

8.3.2. Variables Affecting the Compliance Curve of a DCB Joint.

From Equation 4.17, it can be seen that the variables that may influence a compliance calibration curve of a DCB joint are the specimen width and thickness and the specimen axial modulus. A conversion factor that corrects for the effect of changes in specimen geometry, fibre/matrix volume fraction and the type of substrate on a compliance calibration curve has been deduced from Equation 4.17 using as an example a case involving a compliance calibration curve generated from FE analysis compared with a curve generated from a fatigue

experiment. The resulting equation is:

$$C_2 = C_1\left(\frac{B_1 h_1^2}{B_2 h_2^2 q}\right)\left(\frac{E_1}{E_2}\right) \tag{8.9}$$

where

subscript 1 = theoretical values used in FE analysis

subscript 2 = experimental measurement during fatigue testing

C = compliance of specimen

E = modulus of specimen

B = width of specimen

h = thickness of specimen

and

$$q = \frac{(\text{no of plies})_2}{(\text{no of plies})_1} \tag{8.10}$$

Tests were performed on a DCB bonded joint to test for the effectiveness of the correction expressed in equation 8.9. A finite element programme (ABAQUS) was used to generate a compliance calibration curve. Figure 8.1 shows the compliance curve from a fatigue test compared with a theoretical curve generated use finite element analysis. The two curves are very different because of the difference in the above mentioned variables. Figure 8.2 shows the effect when the correction suggested in equation 8.9 was applied. As can be seen from Figure 8.2 the application of equation 8.9 corrects for the compliance calibration curve obtained using the finite element theoretical results so that it is in good agreement with the experimental curve. This means that the curve-fitting equation of the corrected curve generated from finite element can be used in equations 8.4, 8.5, 8.7 and 8.8.

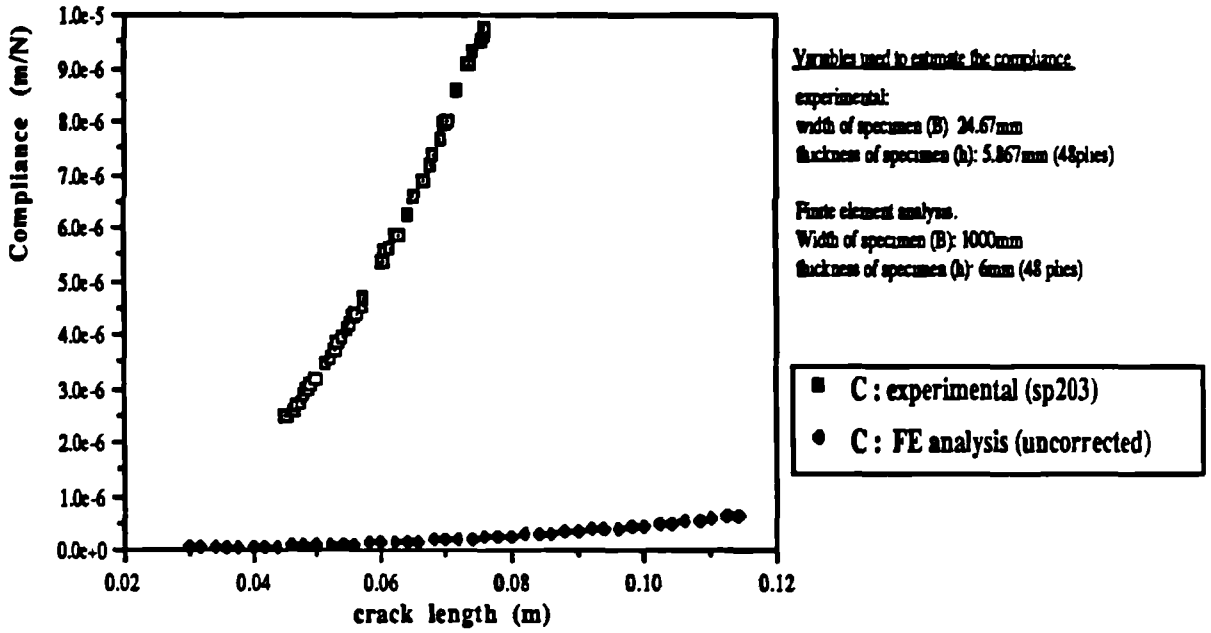


Figure 8.1. Comparison of the compliance calibration curve generated from an experiment with that generated from finite element analysis when suggested corrections in equation 8.7 were not applied. (Substrate 913C XAS-5-34%, adhesive FM73M).

In addition, there was the need to check for the effects of creep (or stress relaxation) on the substrate modulus during fatigue testing since this factor has not been accounted for in equation 8.9. The effect of creep on the substrate modulus will be more pronounced at low frequencies since at relatively high frequencies, the load will be removed before the material has time to creep, and any accumulated creep strain will be too low to affect the compliance of the specimen. Hence, to test for the effect of creep on the substrates used in the present investigation, results from tests at a frequency of 1 Hz were analysed. The substrate modulus was estimated using equation 4.19 and plotted against the number of cycles of testing. As can be seen from Figure 8.3, there are no signs of any significant drop in in the modulus of the specimen during the entire testing period of over 1.8 million cycles (i.e 20 days). These observations are in agreement with similar findings by Talreja (1980) and O' Brien (1991) in which they observed no significant loss in modulus of a composite material during fatigue testings.

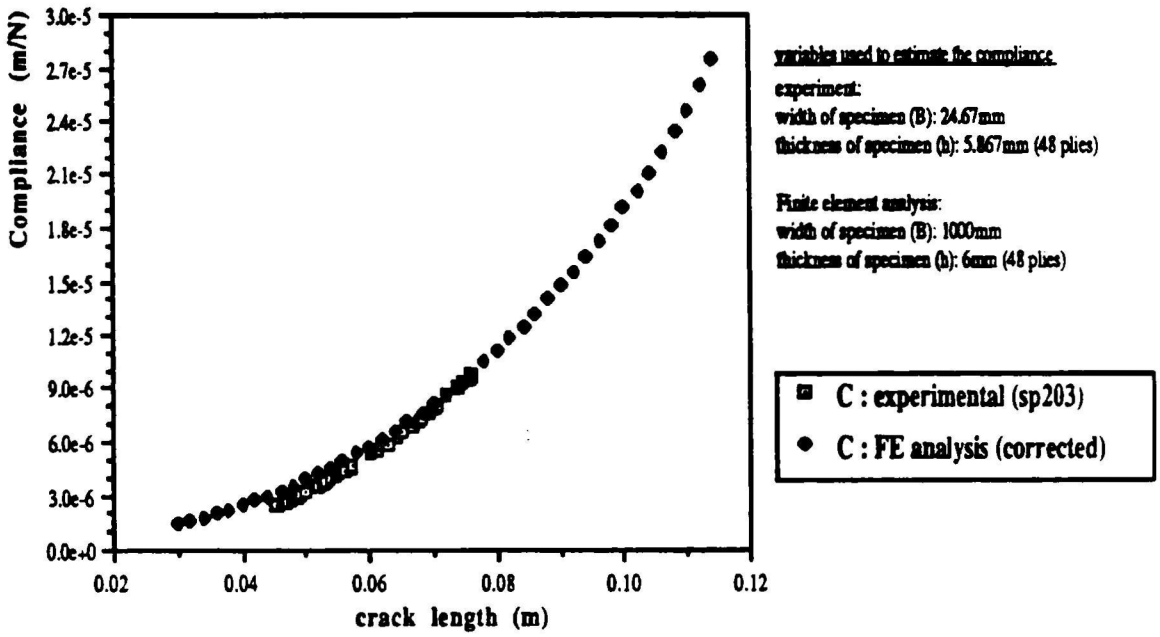


Figure 8.2. Comparison of the compliance calibration curve generated from an experiment with that generated from finite element analysis when suggested corrections in equation 8.7 were applied. (Substrate 913C XAS-5-34%, adhesive FM73M).

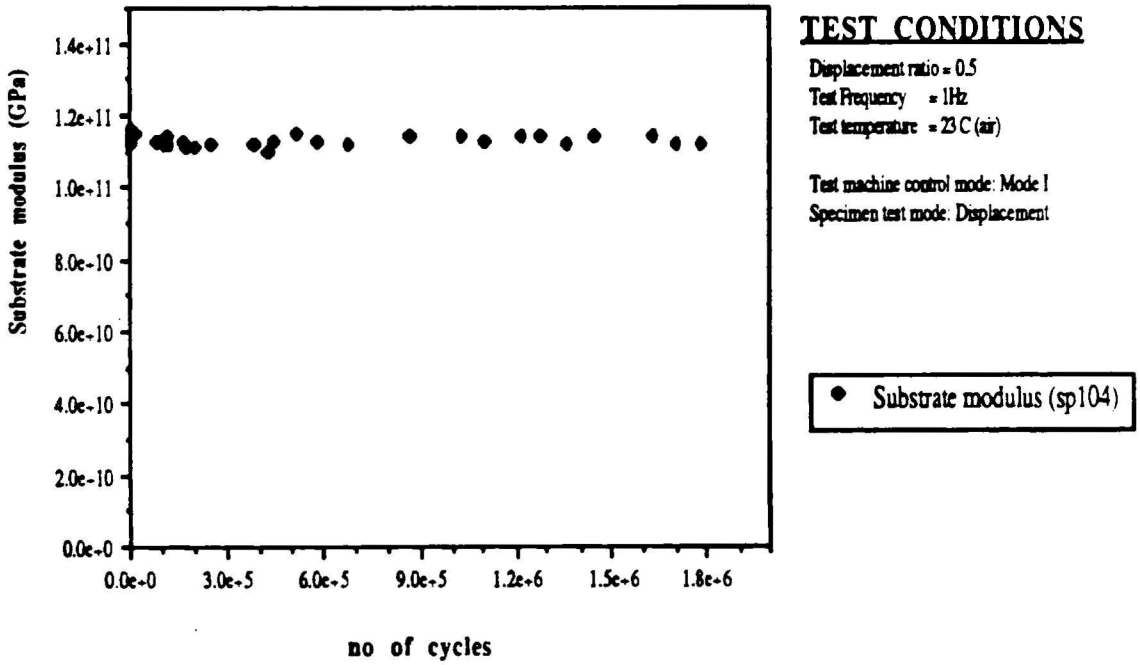


Figure 8.3. Variation of substrate modulus with the number of fatigue cycles. (Substrate 913C XAS-5-34%, adhesive FM73M).

In order to verify further that the effect of creep on the substrate modulus is negligible, the compliance calibration curve generated from a static test was compared with that from a fatigue test. As can be seen from Figure 8.4, the two curves are the same thus demonstrating that the effect of creep was negligible.

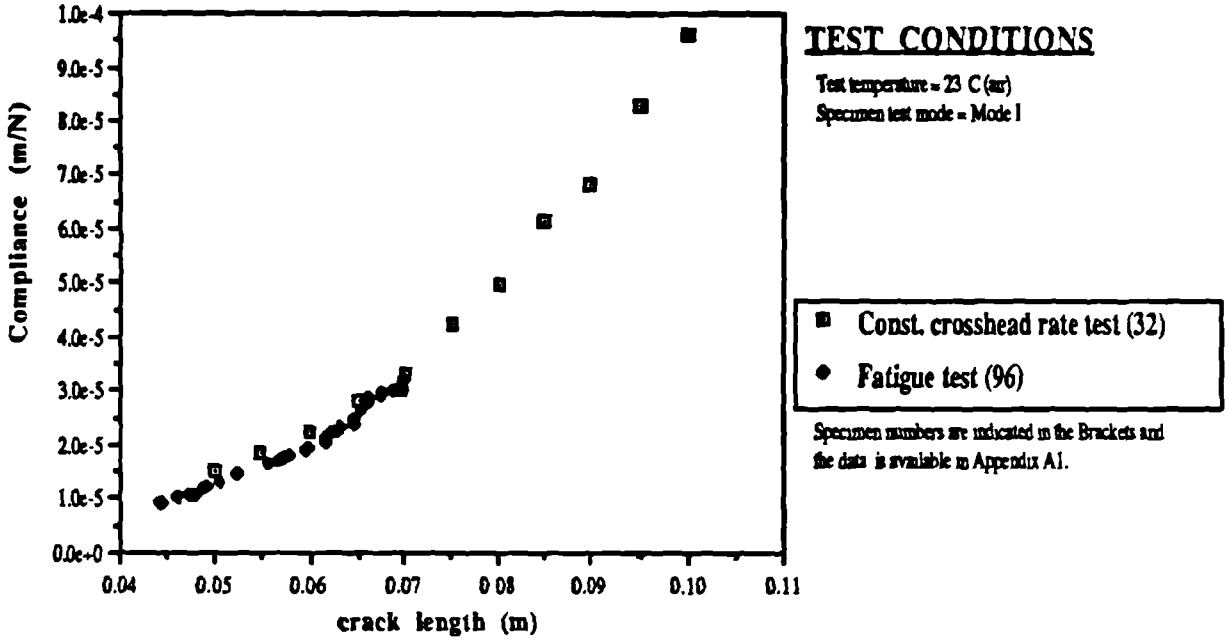


Figure 8.4. Effect of the type of loading on the compliance compliance of a bonded joint. (Substrate 913C XAS-5-34%, adhesive FM73M).

8.3.3 Modelling the Fatigue Crack Growth Law

8.3.3.1 The Hot Cure Epoxy Film Adhesive Bonding the Thermosetting CFRP.

Figure 8.5 shows the comparison of the modelled growth curve with the curve obtained from experimental observations of the fatigue performance of a DCB bonded joint made from using a hot cure epoxy film adhesive to bond a thermosetting CFRP. The predicted curve was obtained using equation 8.1 which assumes that the entire fatigue life of the bonded joint can be predicted by the linear region II equation. As was discussed in section 8.3.1, the value of G_{max} in equation 8.1 was substituted for by either equation 8.3 or 8.6.

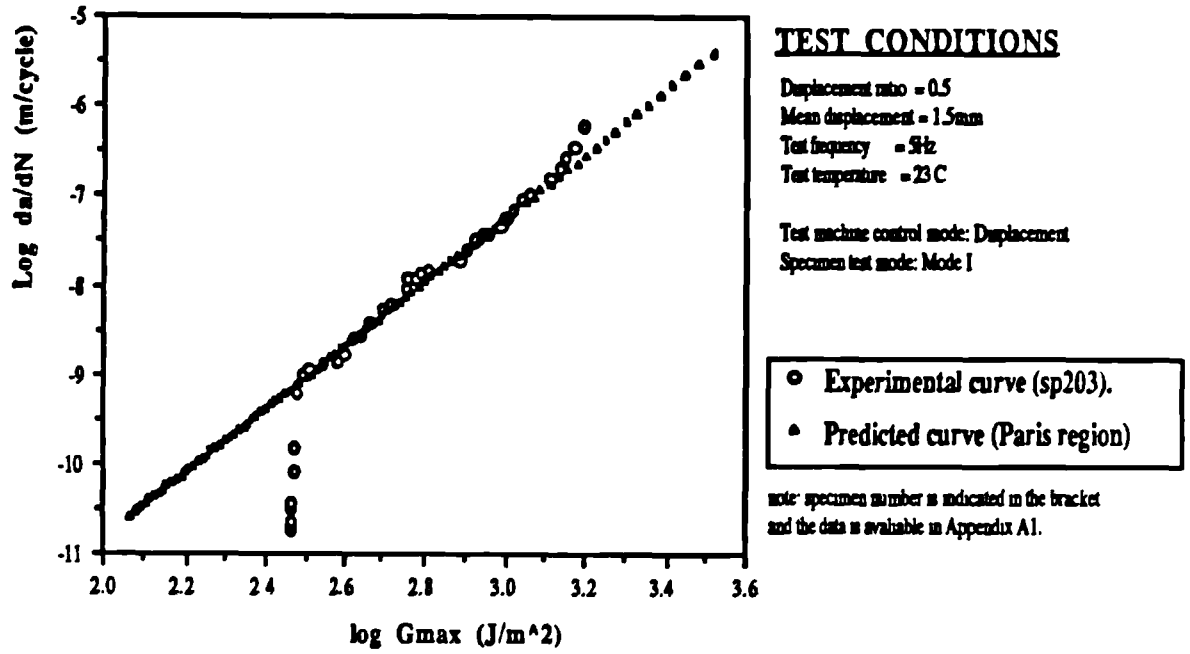


Figure 8.5. Comparison of the crack growth curve observed from experiments on a bonded DCB joint with the growth curve predicted using the linear equation (i.e equation 8.1). (note: Substrate 913C XAS-5-47%, adhesive FM73M).

The values of the linear region II constants D and n used in the equation were 1.903 x 10^{-18} m/cycle and 3.59. These values were the average values obtained for the hot cure adhesive when tests were carried out at a displacement ratio of 0.5 (section 5.6). As Figure 8.5 shows, there is good agreement between the experimental and the modelled curves in the linear region (i.e region II). As was discussed in section 2.4, the main disadvantage of using the linear region II equation (equation 8.1) is that the equation completely ignores the fatigue performance of the adhesive in the near threshold region and the predicted service life will be an underestimation of the actual service life of the bonded joint. For this reason, the use of an expression which fully characterises the fatigue behaviour of the bonded joint over the three regions of growth (i.e Equation 8.2) was recommended by Ewalds (1984) and Martin (1990) The constants D_1 and D_2 may be obtained by fitting equation 8.2 to the experimental data. Figure 8.6 shows how equation 8.2 may be used to evaluate D_1 and D_2 by a trial and error method. The results revealed that for mode I fatigue testing, the best fit is obtained when D_1 = 10, D_2 =1.

Figure 8.7 shows the comparison of the predicted growth curve with the experimental curve when equation 8.2 was used and the value of G_{max} was obtained using equation 8.3. The values of D and n were the same as used previously (i.e Figure 8.5) and were 1.903×10^{-18} and 3.59 respectively. The value of G_{th} and G_{1c} were 0.28 and 2.93 kJ/m^2. From Figure 8.7, it can be seen that using equation 8.2 in the place of equation 8.1 results in the avoidance of the problem involved in underestimating the actual service life of the bonded joint in the near threshold region. However it should be realised that equation 8.2 is only usable if the values of G_{th} and G_{1c} are known.

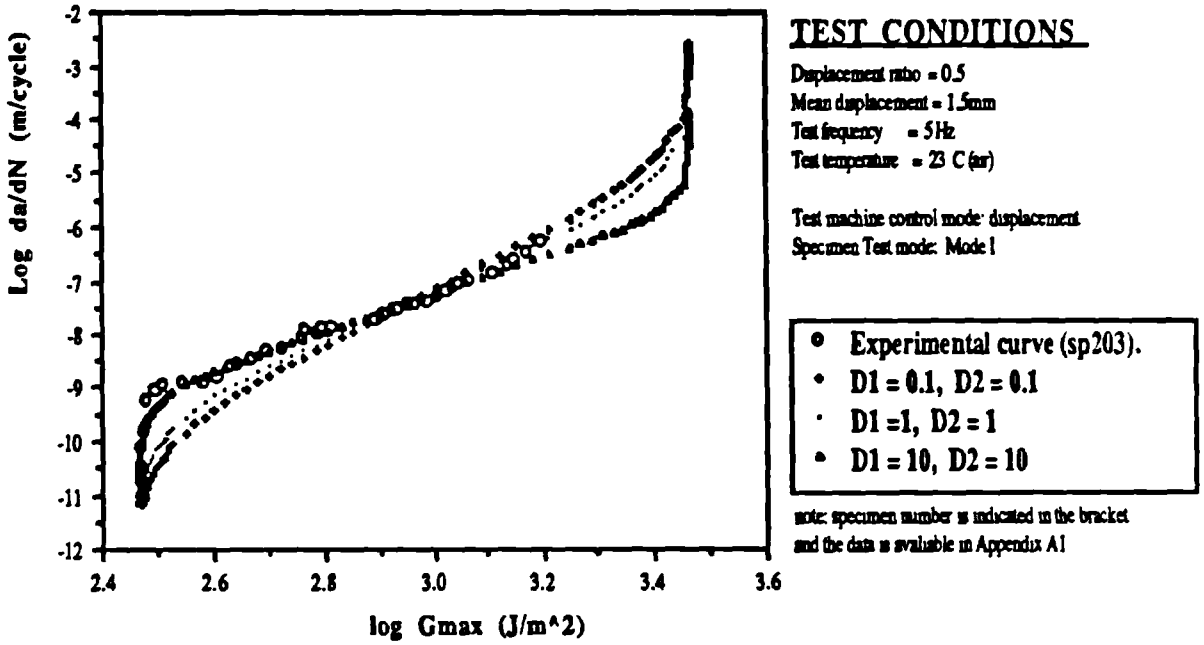


Figure 8 6. A method of obtaining the constants D1 and D2 by fitting equation 8.2 to the experimental data (Substrate: 913C XAS-5-34%, Adhesive: FM73M).

The value of D_2 has been chosen for convenience as it was experimentally impossible to obtain growth curves above 10^{-5} m/cycle in the near fast fracture region. The use of the more sophisticated experimental techniques such as a video recorder or data-logger could reveal the true shape of the curve in this region. Therefore, in the present investigation, it was assumed for convenience that the shape of the curve in the near fracture region should be very much similar to that in the near threshold region. Hence the value of D_2 in equation 8.2 was assumed

to be equal to that of D_1.

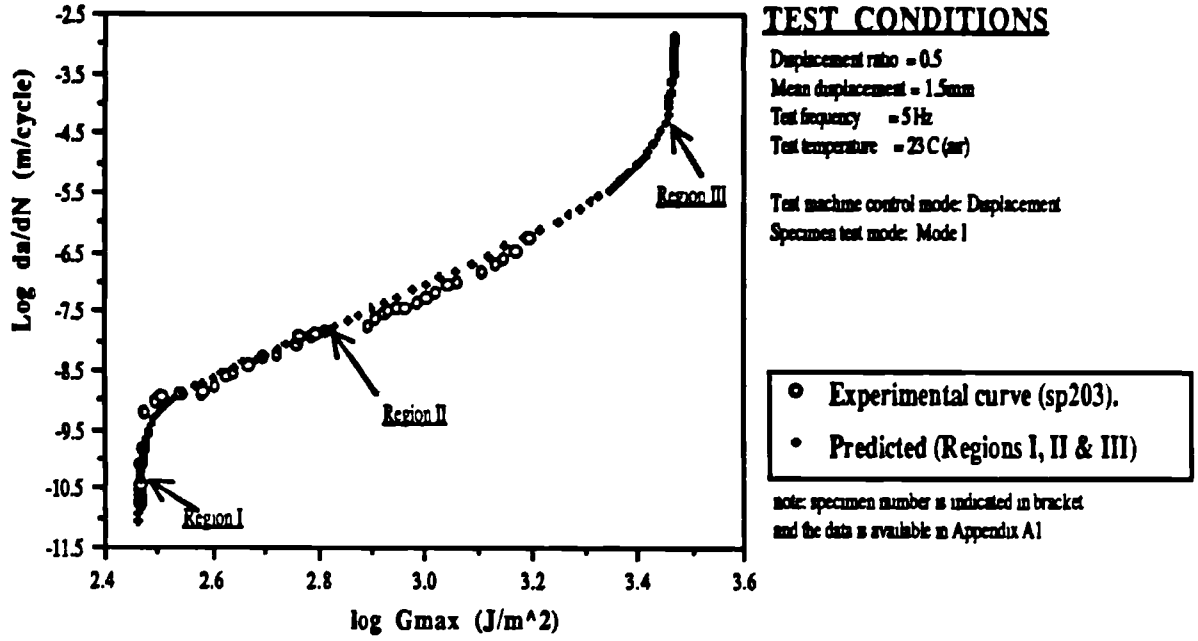


Figure 8.7. Comparison of the observed crack growth rate from a bonded DCB joint with a growth curve predicted using the 'three region prediction equation' (equation 8.2), in which D1 = 10 and D2 = 1. (note: substrate 913C XAS-5-47%, adhesive FM73M).

Figure 8.8 shows the comparison between the experimental and theoretical curves when $D_1 = D_2 = 10$. If Figure 8.8 is compared to Figure 8.7, it can be seen that Figure 8.8 shows a better agreement between the experimental and predicted curves especially in the linear region of the growth curve. There is a slight deviation of the experimental data points from linearity at the upper part of Figure 8.8 and it is believed that the deviation may be due to scatter and not necessarily an indication of the boundary between regions II and III.

More experimental data points are needed from the near fracture region in order to obtain the real value of D_2. Figure 8.9 shows that good agreement of results are also obtainable when the value of G_{max} was estimated from the corrected displacement equation (equation 8.6) and substituted into equation 8.2.

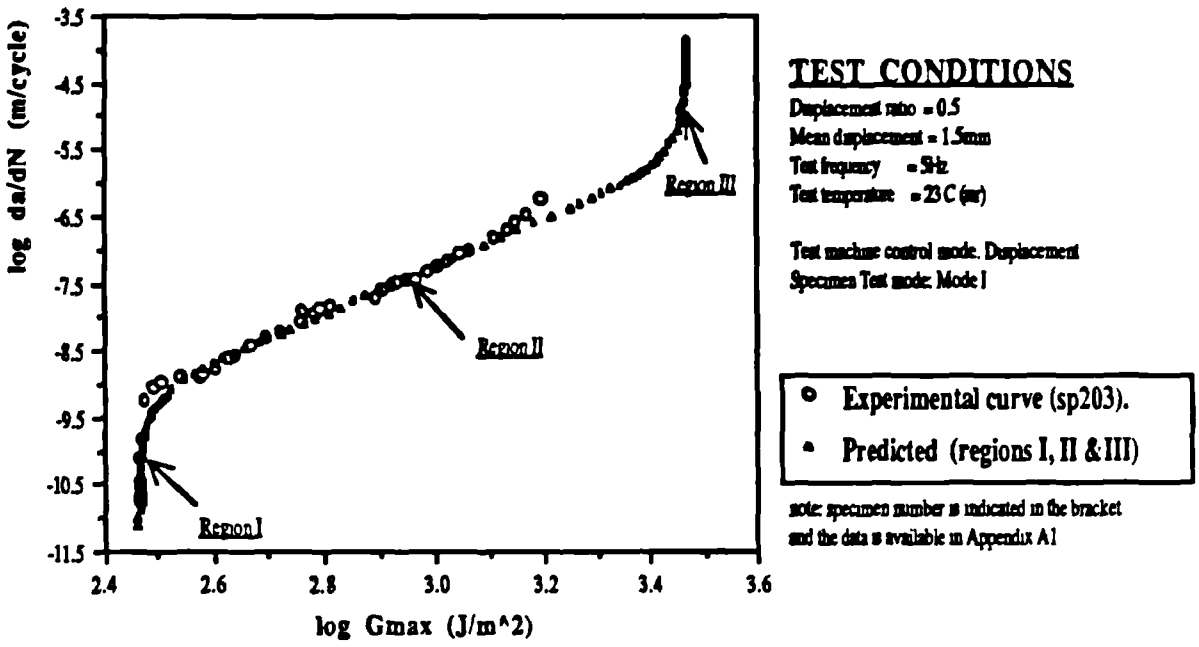


Figure 8.8. Comparison of the observed crack growth rate from a bonded DCB joint with a growth curve predicted using the 'three region prediction equation' (equation 8.2), in which D1 = 10, D2 = 10. (note: substrate 913C XAS-5-47%, adhesive FM73M).

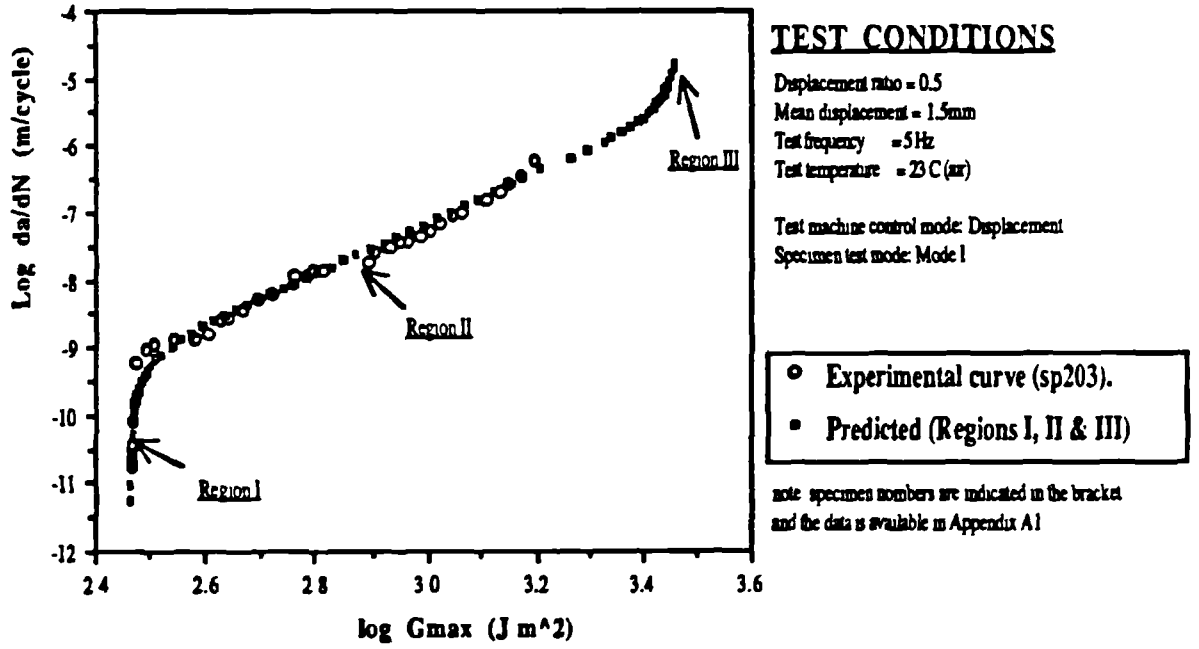


Figure 8.9 Comparison of the observed crack growth rate from a bonded DCB joint with a growth curve predicted using equation 8.2, in which D1 = 10, D2 = 10. (note: substrate 913C XAS-5-47%, adhesive FM73M)

8.3.3.2. The Cold Cure Epoxy Paste Adhesive Bonding the Thermosetting CFRP.

Figure 8.10 shows the comparison of the predicted growth curve with the curve obtained from experimental observations of the fatigue performance of a DCB bonded joint made from using a cold cure epoxy paste adhesive to bond a thermosetting CFRP. The figure was obtained when the full characterisation equation (equation 8.2) was used to predicted the crack growth rate. The values of D and n are 2.42×10^{-16} and 3.15, the values of G_{1c} and G_{th} are 5.70 and 0.15 kJ/m^2 and the values of the constants D_1 and D_2 were obtained from the fixing of arbitrary values into equation 8.2 to fit the experimental data as was described in the previous section. Similarly the best curve-fit was obtained when $D_1 = 10$ and $D_2 = 10$. As was explained earlier, the value of D_2 is chosen for convenience because it was experimentally impossible to obtain the growth curves in the near fast fracture region.

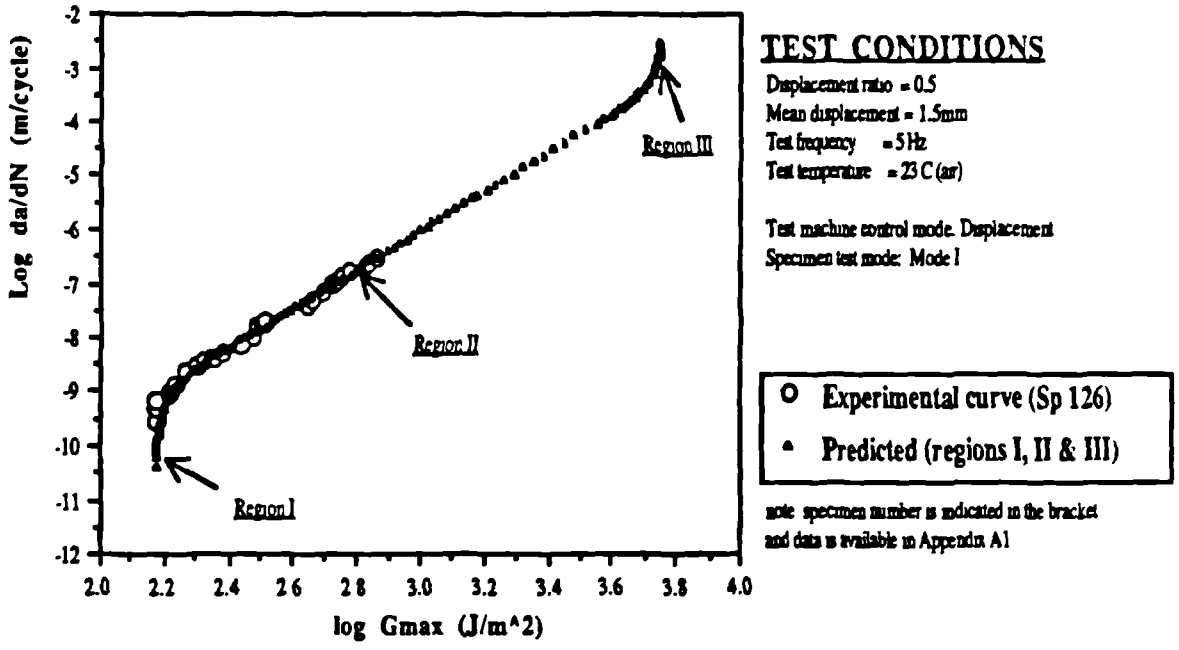


Figure 8.10 Comparison of the observed crack growth rate from a bonded DCB joint with a growth curve predicted using the 'three region prediction equation' (equation 8.2) in which D1 = 10 and D2 = 10 (Note Substrate 913CXAS-5-47%, adhesive 9309.3NA).

8.3.4. Predicting the G_{max} versus N Relationship

The crack growth rate model can also be used to predict the relationship between G_{max} and the number of cycles to complete failure over predetermined crack lengths in a DCB joint. A computer program has been written in Pascal to obtain G_{max} from equation 8.3 and then solve the integration of equation 8.2 to obtain the value of N_f for a DCB joint as a function of G_{max}.

Figure 8.11 shows a comparison of the predicted results and experimental observations on a G_{max} -N curve for a cold cure epoxy paste adhesive bonding a thermosetting CFRP. The value of the constants D, n, D_1, D_2, G_{th} and G_{1c} for the adhesive were calculated as described in section 8.3. As can be seen from the figure, the predicted and experimental results are in very good agreement.

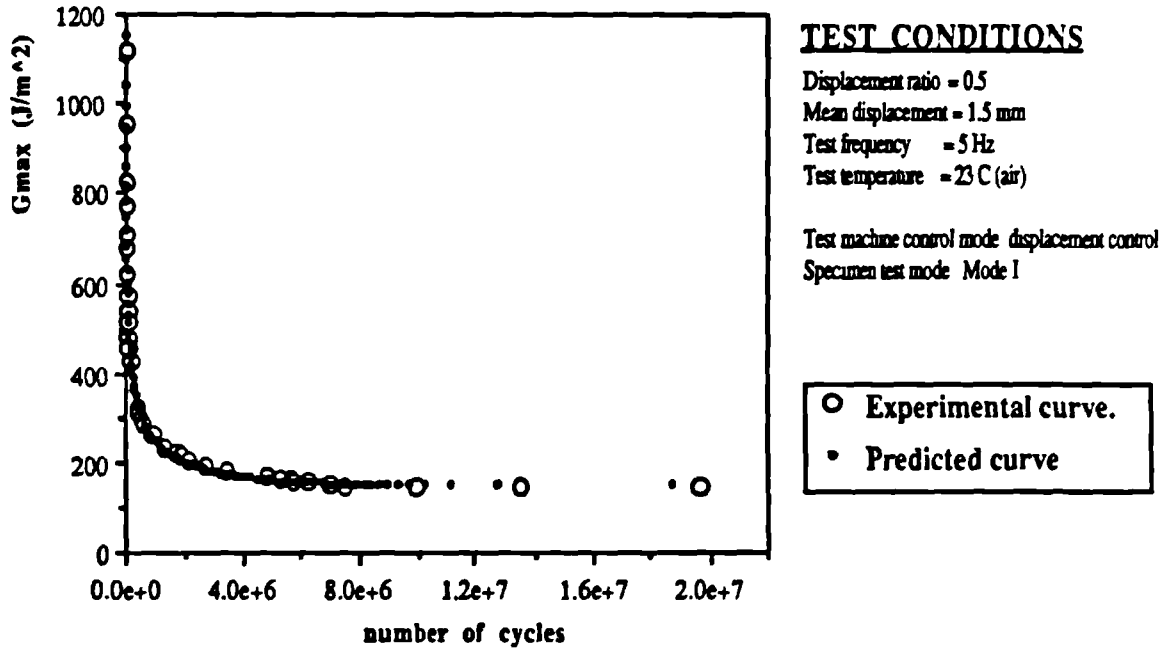


Figure 8.11. Predicting the Gmax versus N relationship using the 'three region prediction equation' (equation 8.2) (Note: Substrate 913C XAS-5-47%, adhesive 9309.3NA).

8.4. THE PREDICTION OF FATIGUE FAILURE IN SINGLE LAP JOINTS

8.4.1. Introduction:

In section 8.3 the crack growth rate equation has been used to model and predict the service life of bonded DCB joints and attention was drawn to the fact that the da/dN vs G_{max} curves are material property curves, and are not dependent on the specimen geometry. The main purpose of this section is to investigate the prediction of the service life of a single lap joint using these growth rate curves generated from the DCB specimen geometry. However, before the crack growth rate model can be successfully applied, a method needs to be available by which the maximum value of the mode I strain energy release rate in a single lap joint, (i.e $(G_{max})_{SLJ}$), can be estimated.

8.4.2. Estimating the Value of $(G_{max})_{SLJ}$ for Single Lap Joints.

A single lap joint prepared in accordance with ASTM D 1002 (1972) specification is shown in Figure 8.12. Since the single lap joint is one of the most common type of joints used in testing and design, considerable work has been reported on the stress distribution in this type of joint. Some authors (Hart-Smith 1973, Adams 1974, Adams 1989, Allman 1976 and Guess 1977) have worked on the relationship between the peel and shear stresses in single lap joints. In all cases, detailed analyses have revealed that if the joints were prepared in accordance with the ASTM D 1002 standard, the failure of the joint is not caused by the shear stresses but by the high peel (i.e., tensile) stresses at the ends of the joint overlap. Thus these results showed that although it appears that these joints are loaded in pure shear, there are bending moments due to the offset of the load line which causes high peel stresses at the end of the bonded overlap. The maximum peel stress and bending moment at the end of the bond overlap have been determined by Hart-Smith (1973,1985). Hart-Smith's method of determining the bending moment was later modified by Adams (1990) to give a more accurate result. From a knowledge of the bending moment at the crack tip of thin cracked laminates, Williams (1988) proposed a very powerful method, by using the simple beam theory, to estimate the mode I strain energy release

rate, G_{max}. The method of analysis proposed by Williams is applicable to the mode I debonding process in single lap joints since the bending moments at the end of the overlap are acting in opposite directions causing the adhesive to peel apart (Figure 8.13).

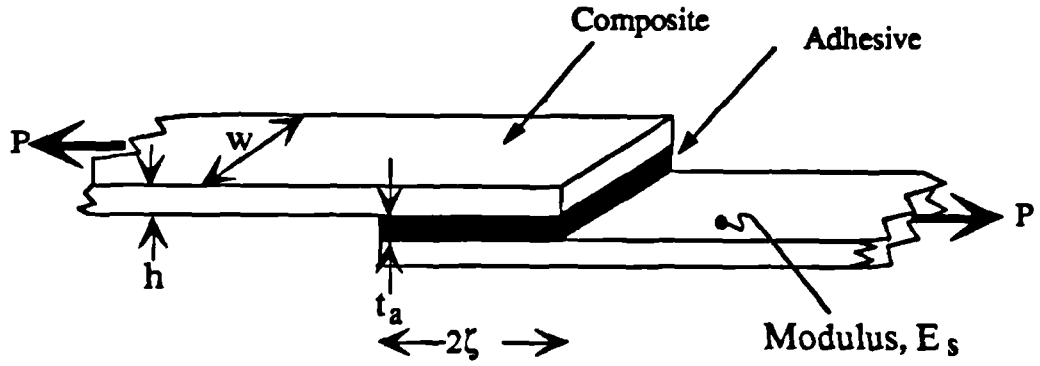


Figure 8.12 The single lap joint specimen geometry

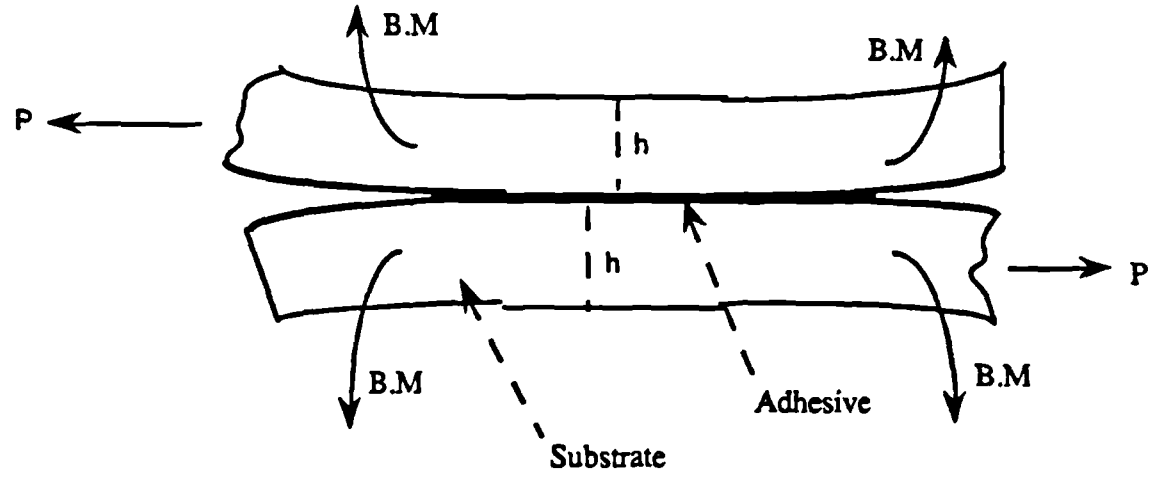


Figure 8.13. Bending moments (B.M) acting at the ends of the overlap of a single lap joint

Now the Williams method for estimating the strain energy release rate may be combined with the Hart-Smith and Adams methods for calculating bending moments to estimate the strain energy release rate, $(G_{max})_{SLJ}$ in a single lap joint due to the presence of the bending moments

at the end of the overlap. The contributions of the above authors are presented in Appendix D and the resulting equation for estimating the strain energy release rate in single lap joints is:

$$(G_{max})_{SLJ} = \left(\frac{12}{E_s h^3}\right)\left(\frac{T(h+t_a)}{2}\right)^2\left(\frac{1}{(1+\varepsilon\varsigma)^2}\right) \qquad (8.11)$$

where:

T = applied load per unit width

h = thickness of the substrate

t_a = thickness of the adhesive

E_s = modulus of the substrate

ς = half the bonded overlap in the direction of the applied load

and:

$$\varepsilon = \left(\frac{T}{X}\right)^{1/2} \qquad (8.12)$$

and where:

$$X = \frac{E_s h^3}{12(1-\mu^2)} \qquad (8.13)$$

and where:

E_s = modulus of the substrate

h = thickness of the substrate

μ = Poissons ratio of the substrate

If it is assumed that crack grows through a single lap joint in a plane parallel to the loading direction, the growth of such crack by a length 'a' at both ends of the overlap will change the overlap length from '2ς' to '$(2\varsigma - 2a)$'. Hence equation 8.11 becomes:

$$(G_{max})_{SLJ} = \left(\frac{12}{E_s h^3}\right)\left(\frac{T(h+t_a)}{2}\right)^2\left(\frac{1}{(1+\varepsilon(\zeta - a))^2}\right) \qquad (8.14)$$

8.4.3. Prediction of the Service Life of Single Lap Joint using the Crack Growth Rate Model.

8.4.3.1 Introduction

By using the crack growth rate models the service life of single lap joints may be predicted from a knowledge of the following variables.

G_{max} : the estimated mode I fracture energy (equation 8.14)

a_{si} : the initial flaw size

a_{sf} : the final flaw size

D and n : the Paris constants for pure Mode I fatigue failure

D_1 and D_2 : the curve fitting constants obtained from the three region prediction equation

Since the constants D, n, D_1 and D_2 are independent of the specimen geometry, it is possible to use the values which have been obtained from the experiments using the DCB geometry (section 8.3). However before any predictions can be made values of the initial and final flaw sizes in the lap joints are required.

8.4.3.2. Estimating the Initial Flaw Size.

In this work it has been assumed that the initial flaw size in single lap joints is the Griffith flaw size and its value is given by the equation:

$$a_{si} = \frac{E_a G_{1c}}{\pi \sigma_a^2} \qquad (8.15)$$

Where

G_{1c} = mode I fracture energy of the adhesive

E_a = modulus of the adhesive

σ_a = the tensile strength of the adhesive obtained by substituting the critical value of the static fracture load into the expression for estimating peel stress which was proposed by Hart-Smith (1985) as:

$$\sigma_a = \frac{P_{1c}(h+t_a)}{2B(1+\varepsilon\zeta)} \cdot \left(\frac{E_a}{2t_a X} \right)^{1/2} \qquad (8.16)$$

where

P_{1c} = the critical value of the static fracture

B = width of the specimen, and

all other variables are as defined in equations 8.11 and 8.13 and 8.15

For the hot cure epoxy film adhesive bonding the thermosetting CFRP, the critical value of the static fracture load obtained from the constant rate of displacement test was 10 kN. When this value was substituted into equation 8.15, the value of the initial flaw size was estimated as 560 μm. This appears to be a reasonable value for several reasons.

Firstly, Kinloch (1983) while using the experimental data obtained by Radford (1971), deduced by using equation 8.15 that the intrinsic flaw size, a_0, in an epoxy resin containing rigid particulate fillers can be as high as 500 μm. Secondly, the hot cure epoxy film adhesive ("FM73M") is manufactured with a polyester mat-carrier which has the multiple purpose of serving as a control for the adhesive layer thickness and as an escape guide for residual solvents and other related gases release during the curing of the adhesive. The combination of the effect of the mat-carrier and the gas bubbles entrapped in epoxy resin adhesives during curing will result in the presence voids after curing and Wood et al. (1991) have shown that such voids may be as large as 400 to 500 μm.

8.4.3.3. Final Flaw Size:

From experimental observations, it was found that during fatigue cycling in a load control mode, the crack growth rate increases as the crack grows and the value of the applied fracture energy will increase from its initial value, G_{max}, to the critical value, G_{1c}, when the specimen finally fails. The final flaw size, a_{sf}, at which the specimen fails can be obtained by rearranging equation 8.14 to give:

$$a_{sf} = \left(\varsigma - \left(\frac{\left(\frac{3(T(h+t_a))^2}{E_s h^3 G_{1c}} \right)^{1/2} - 1}{\varepsilon} \right) \right) \qquad (8.17)$$

It should be noted that the value of a_{sf} can never exceed, of course, the overlap length. The fact that the crack does indeed grow substantially during the fatigue test can be demonstrated by the significant increase in the compliance of the lap joint during the test. For example, the compliance typically increased by about 20% over 2.5 x 10^5 cycles (as shown in Figure 8.14).

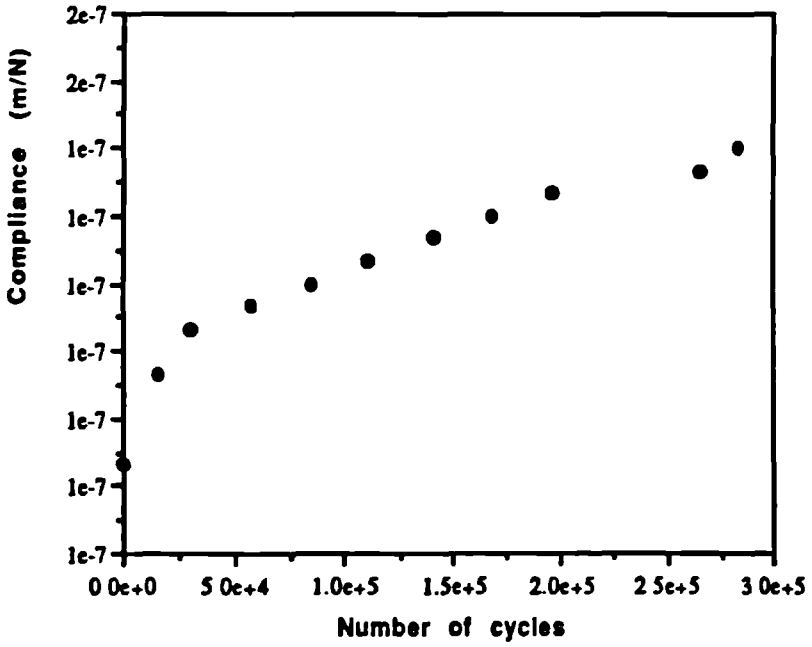


Figure 8.14 Variation of the compliance with the number of cycles as a crack grows from an initial size of 0.56mm to a final size of 9.75mm in a single lap joint (Substrate 913C XAS-5-47%, adhesive FM73M).

This is in broad agreement with the work of Jemian and Ventrice (1969) who found out that when a crack to grew from 0.56mm to about 10mm in a single lap joint made from aluminium substrate bonded with a hot cure epoxy adhesive, the compliance of the joint increased by about 35%.

8.4.4. Crack Growth Rate Equations for Predicting the Service Life of Single Lap Joints

The service life of single lap joints can be determined in two ways. Firstly, if may be assumed that the linear region II equation can be used to describe the crack growth rate behaviour and hence from equations 8.1 and 8.14 (with $G_{max} = (G_{max})_{SLJ}$) and integrating:

$$N_f = \frac{1}{D}\left(\frac{3(T(h+t_a))^2}{E_s h^3}\right)^{-n} \int_{a_{si}}^{a_{sf}} \left(1+\varepsilon(\varsigma - a)\right)^{2n} da \qquad (8.18)$$

which after integration gives:

$$N_f = \frac{1}{D}\left(\frac{3(T(h+t_a))^2}{E_s h^3}\right)^{-n}\left(\frac{1}{\varepsilon(2n+1)}\right)\left(\left(1+\varepsilon(\varsigma - a_s)\right)^{2n+1} - \left(1+\varepsilon(\varsigma - a_{sf})\right)^{2n+1}\right) \qquad (8.19)$$

Where D and n are the linear region II constants which may be obtained from experiments on any specimen geometry. In this work, these values were obtained from fatigue tests on the DCB specimens. Secondly, the full fatigue curve characterisation model (equation 8.2) may be assumed for the crack growth behaviour and, similarly, from equations 8.2 and 8.14:

$$N_f = \int_{a_{si}}^{a_{sf}} \frac{D G_{1c}^{D_2} \left[E_g h^3 (1+\varepsilon(\zeta - a))^2 \right]^{n-D_2}}{\left[3(T(h+t_g))^2 \right]^{n-D_1}} \cdot \frac{\left[G_{1c} E_g h^3 (1+\varepsilon(\zeta - a))^2 - 3(T(h+t_g))^2 \right]^{D_2}}{\left[3(T(h+t_g))^2 - G_{th} E_g h^3 (1+\varepsilon(\zeta - a))^2 \right]^{D_1}} \qquad (8.20)$$

where the values of D_1 and D_2 may also be obtained from a DCB specimen as was described in section 8.3.

8.4.5. Experimental Investigation of the Fatigue Performance of Single Lap Joints.

In order to investigate the accuracy of equations 8.19 and 8.20, experimental data from the single lap joint were obtained from bonding the thermosetting CFRP using the hot cure epoxy film adhesive. The samples were prepared in accordance with the ASTM D1002 (1972) recommendations. The experiments were carried out in load control at a stress ratio of 0.5 and and at room temperature, since the values of the material constants D, n, D_1, D_2, G_{th} and G_{1c} are dependent on the stress ratio (or displacement ratio) and the testing environment (Chapters Five and Six) and the values under these test conditions have been ascertained. For every value of the maximum load applied, a corresponding number of cycles to failure were noted and a graph of the maximum load versus the number of cycles to failure was plotted.

8.4.6. Comparison of the Experimental Observations from SLJ Tests with the Predicted Results.

At the beginning of a prediction exercise for single lap joints, the following details are available:

(a) an equation to predict the service life (e g equation 8.19 or 8.20),

(b) the material constants D, n which may have been obtained from experiments on the DCB joints by curve fitting the linear region II part of the growth curve, and

(c) the values of the material constants G_{1c} and G_{th} obtained from static and fatigue tests.

(d) the values of material constants D_1 and D_2 obtained by curve-fitting regions I & III part of the growth curve (section 8.3).

(e) the details of the materials and specimen geometry .

In the next two sections, predictions will be carried out using the material constants obtained from a thermosetting CFRP bonded with a hot cure epoxy film adhesive. The values of the material constants are $D = 1.903 \times 10^{-18}$ (m/cycle) $n = 3.59$, $D_1 = 10$, $D_2 = 10$, $G_{th} = 0.28$ kJ/m^2 and $G_{1c} = 2.93$ kJ/m^2. Further comparison of the theoretical predictions with experimental data are discussed.

8.4.6.1 Predicted Lifetimes Using the Linear Region II Model.

If it is assumed that the linear region II model may be used to model the service life of the single lap joint, then provided the peel stresses in the joint dominate the failure, the service life of the joints, N_f, can be predicted using equation 8.19. Figure 8.15 shows a comparison of the predicted N_f of cycles with the experimental results of a P_{max} - N_f curve. As can be seen, the two curves are in good agreement in the region where the value of the maximum applied load, P_{max}, was in the range between 60 and 95% of the maximum load at fracture.

However, as the load decreased below this range, the number of cycles to failure experimentally measured became increasingly greater than that predicted for the same value of P_{max}. This observed trend of an underestimation of the service life of the bonded joint at relatively low values of P_{max} may be due to several reasons. Firstly, as was mentioned earlier in section 8.1.4, when the value of P_{max} is much lesser than P_{1c} (and much closer to the corresponding load required for the near threshold region) the influence of the crack initiation time on the total fatigue life of the bonded joint becomes increasingly significant. Hence, because the crack initiation time has not been adequately accounted for in this region, the use of the crack growth rate model to predict the service life of the bonded joint may result in a low value of N_f. Secondly, as was discussed in section 2.4, the use of the linear region II equation

may result in an underestimation of the predicted service life of a bonded joint because the equation ignores the near threshold region of crack growth. For this reason, an attempt will be made in the next section to check whether this problem can be minimised by using the 'full characterisation model' (i.e equation 8.20).

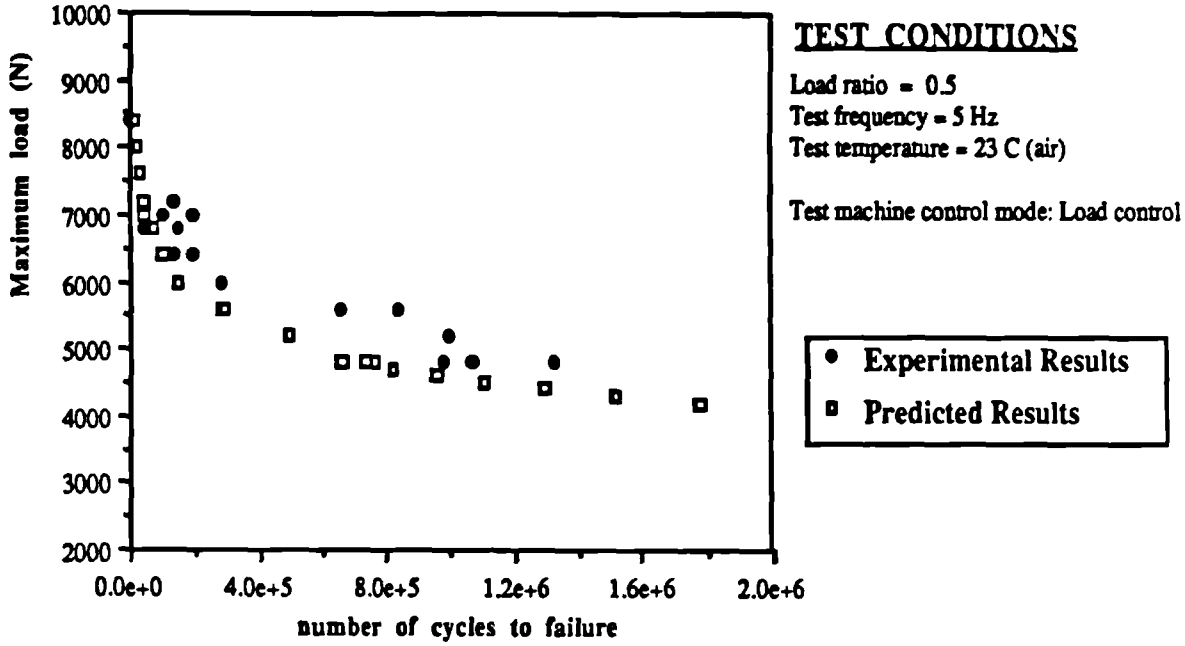


Figure 8.15. Comparison of the number of cycles to failure observed from a single lap joint with the predicted results using the linear region II constants obtained from a DCB joint. (Note: Substrate 913C XAS-5-47%, adhesive FM73M).

8.4.6.2 Predictions Using the 'Full Characterisation Model'

If it is assumed that the the full characterisation model may be used to model the service life of the single lap joint, then provided the peel stresses in the joint dominate the failure, then the service life of the joints, N_f, can be predicted using equation 8.20. Figure 8.16 shows a comparison of the predicted service life with the experimental results for a P_{max} - N_f curve. As can be seen, the two curves are in good agreement in the region where the value of the maximum applied load, P_{max}, was in the range between 60 and 95% of the maximum load at fracture.

A comparison of Figures 8.15 and 8.16 shows that the use of the full characterisation model

gives more accurate predictions. However, the use of the full characterisation model has not completely solved the problem of minimising the degree of scatter at low levels of applied maximum load. The predicted values of N_f using the model (equation 8.20) are greater than those experimentally measured unlike when the linear region II model was used (i.e where the calculated value of N_f was smaller). Since the experimental and predicted curves shown in Figure 8.16 were obtained at load levels between 50 and 90% of the maximum load at fracture, it is difficult to know whether this observation at low load levels is due to experimental scatter.

Figure 8.17 shows a comparison of the experimental data with the predicted results when the predictions were made when relatively high maximum loads were applied (i.e P_{max} = 90% of P_{max} at fracture) to when relatively low loads were applied (i.e P_{max} close to corresponding value for the near threshold region). As can be seen from the figure, more experimental data is needed in the near threshold region before accurate conclusions can be made on the differences in the predicted and experimental results at low levels of P_{max}. This is obviously an area for further study.

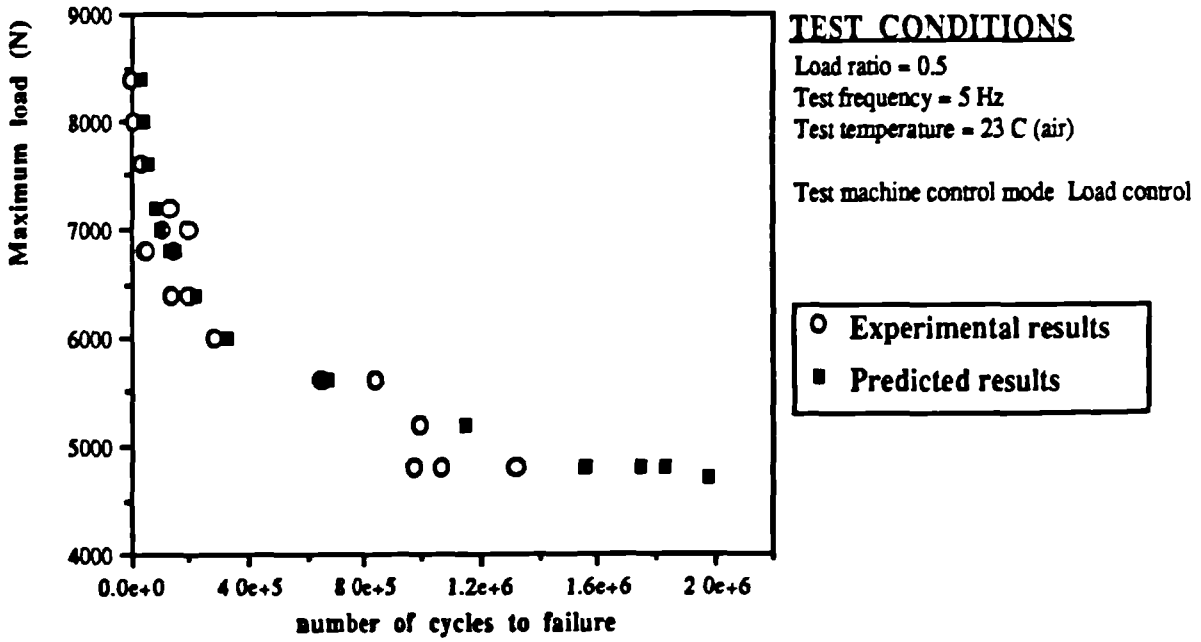


Figure 8.16 Comparison of the number of cycles to failure observed from a single lap joint with the predicted results obtained by substituting the material constants from a bonded DCB joint test into equation 8.20 (Note:- Sub. 913C XAS, adhesive FM73M)

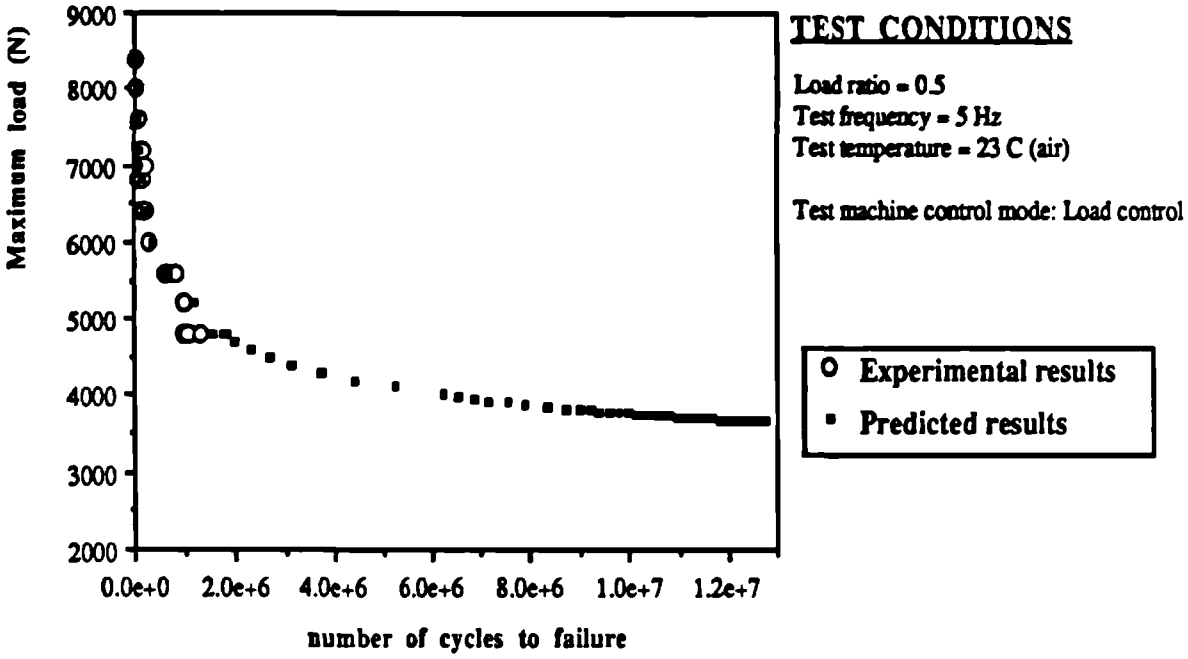


Figure 8.17. Comparison of the number of cycles to failure observed from a single lap joint with the predicted results. (Note: Substrate 913C XAS-5-47%, adhesive FM73M).

8.5. FURTHER PREDICTIONS OF THE FATIGUE LIFETIME OF SINGLE LAP JOINTS

8.5.1. Introduction

One of the main advantages of the models described above is that they can also be used to predict the effects of geometrical parameters such as the thicknesses of the substrate and the adhesive and the length of the bonded overlap. The predictions are made using equation 8.20.

8.5.2 Effect of the Overlap Length

Figure 8.18 shows that as the overlap increases, the corresponding number of cycles to failure would be predicted to increase accordingly. These observations are also consistent with theoretical predictions by Hart-Smith (1985) but he only considered the static strength. The present work is the first to predict the fatigue behaviour. Furthermore, Figure 8.19 shows that a similar experimental trend has indeed been observed from work on the effect of the overlap carried out by Althof (1966).

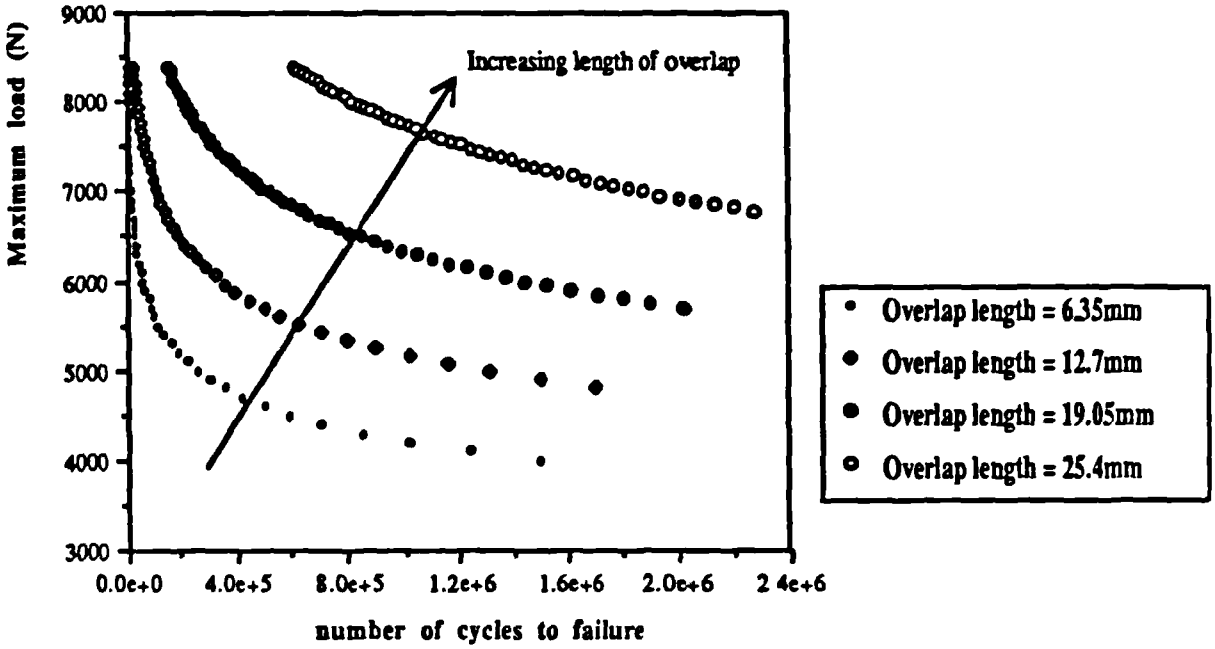


Figure 8.18 Predictions of the effect of changes in the length of overlap on the service life of single lap joints (Note: Substrate 913C XAS-5-34%, adhesive FM73M).

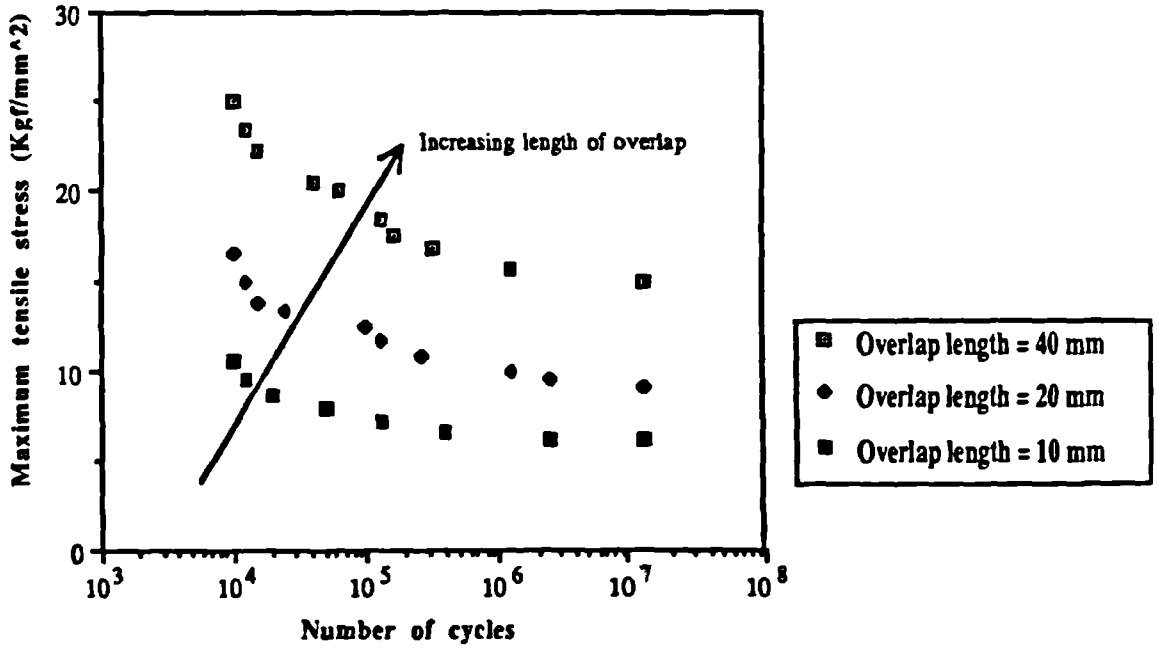


Figure 8.19 Influence of changes in the length of overlap on the service life of bonded joints (Adapted from Althof (1966) Note: Substrate Stainless steel, adhesive Epoxy-Phenol i e "Hidux 1197A"

8.5.3. Effect of Substrate Thickness:

Figure 8.20 shows that as the substrate thickness increases, the number of cycles to failure of the joint would also be predicted to increase. No experimental work to compare this prediction could be found. This is an obvious area for further study.

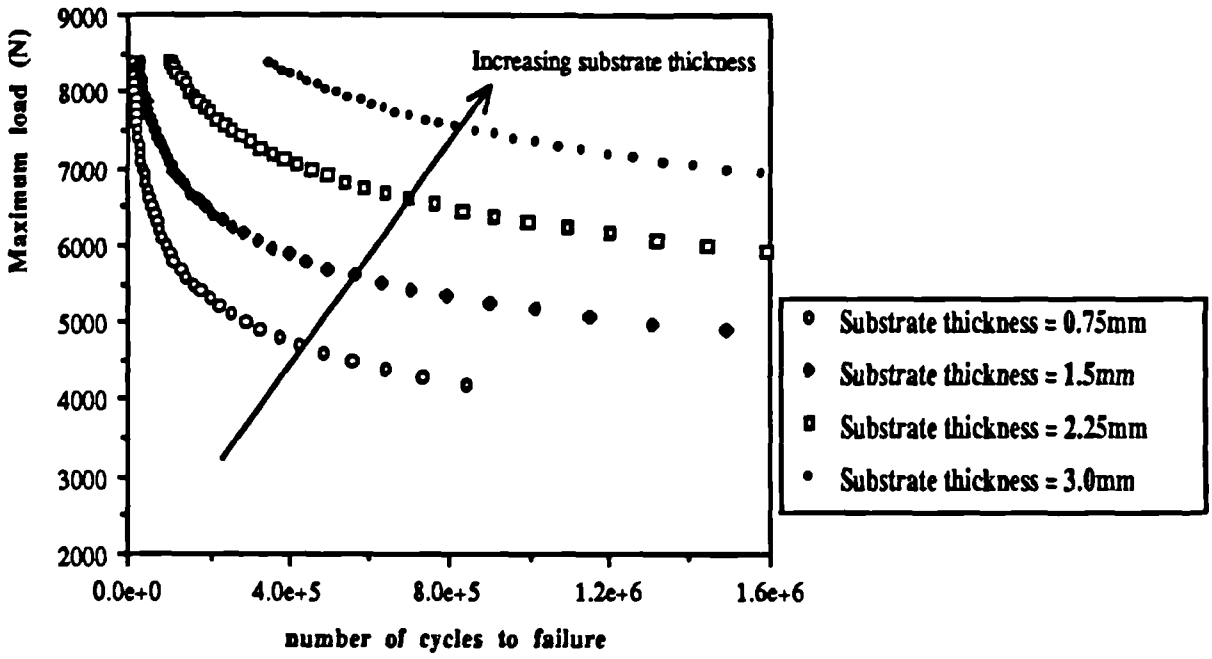


Figure 8.20. Predictions of the effect of changes in substrate thickness on the service life of single lap joints. (Note: Substrate 913C XAS-5-34%, adhesive FM73M).

8.5.4. Effect of Adhesive Thickness.

Figure 8.21 shows that as the adhesive layer thickness increases, the predicted number of cycles to failure of the joint now decreases. This predictions are supported by work carried out by Crocombe et al (1987) in which it was observed that the strength of single lap joints made from aluminium substrate bonded with a cold cure paste adhesive ("9309.3NA") decreased with increasing adhesive thickness. Furthermore, theoretical predictions by Hart-Smith's (1985) have also revealed that an increase in the adhesive thickness results in an increase in the peel stresses at the end of the bonded overlap, thereby reducing the service life of the bonded joint.

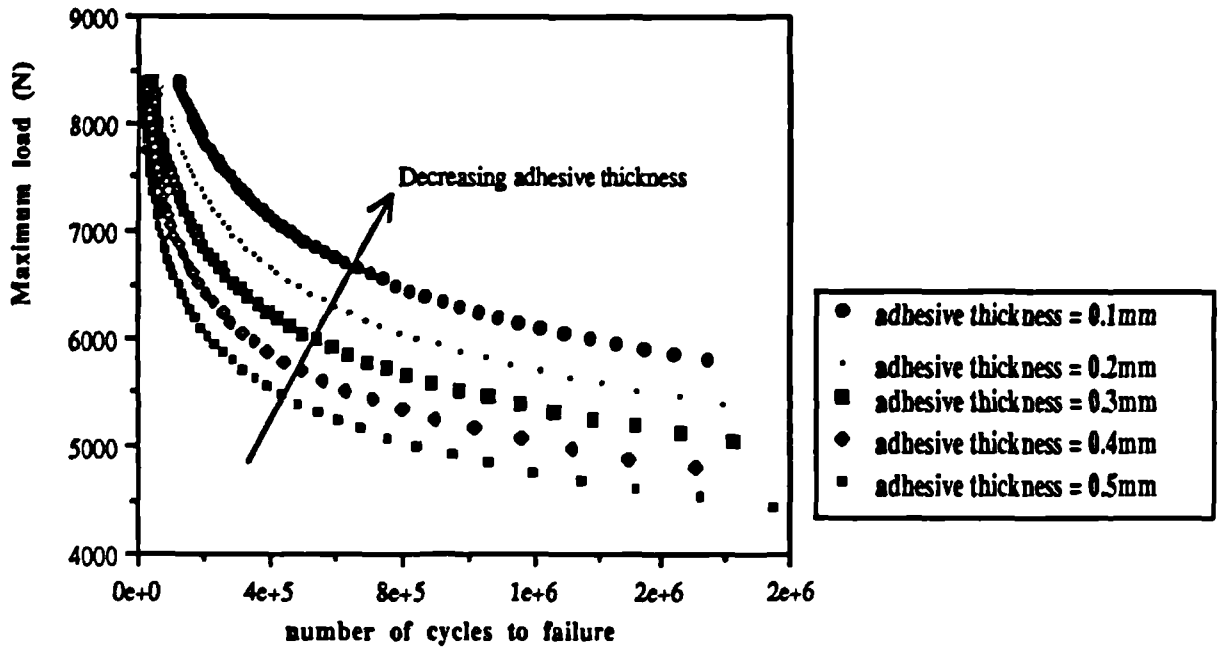


Figure 8.21. Prediction of the effect of changes in the thickness of the adhesive on the service life of single lap joints. (Note: Substrate 913C XAS-5-34%, adhesive FM73M).

8.6. CONCLUSIONS

The main conclusions from this chapter are:

(1) Crack growth rate models have been developed and used to predict the service life of a bonded DCB joint. For the successful use of the models the following steps were taken;

(i) A finite element package was used estimate a compliance calibration (i.e C vs a) curve of the specimen.

(ii) A correction factor has been suggested by which the compliance calibration curve generated from finite element analysis can be made equivalent to that generated from the fatigue experiments. A polynomial curve-fitting equation of the compliance calibration curve was then undertaken.

(iii) Empirical models (equations 8.1 and 8.2) were calculated from the experimental crack growth curves (i.e da/dN versus G_{max} curves) to obtain the material constants. The equations from the compliance calibration curves were substituted into the empirical model equations and the service life, N_f, of the bonded joints were deduced by simple numerical integration methods. This exercise validated the modelling of the fatigue crack growth behaviour.

(2) The service life of single lap joints have been predicted by using the crack growth rate models via the following steps;

(i) The value of the mode I strain energy release rate that is applied to a single lap joint, $(G_{max})_{SLJ}$ during longitudinal tensile loading has been estimated.

(ii) Methods of estimating the initial and final flaw sizes in single lap joints subjected to fatigue cycling have been deduced.

(iii) From a knowledge of the material properties (i.e D, n, D_1, D_2, G_{th} and G_{1c}) obtained from the DCB fatigue tests, the service life of single lap joints has been successfully predicted using the crack growth rate models. The predicted results are in good agreement with the experimental observations.

(3) The effects of substrate thickness, adhesive thickness and the length of overlap on the service life of single lap joints has also been predicted. The results revealed that:

(i) As the overlap length increases, the corresponding number of cycles to failure increases.

(ii) As the substrate thickness increases, the number of cycles to failure of the joint increases.

(iii) As the adhesive layer thickness increases, the number of cycles to failure of the joint decreases.

CHAPTER NINE

SUMMARY OF THE MAIN CONCLUSIONS

From the work described in the previous chapters the following main conclusions may be drawn:

(1) Static tests (i.e constant rate of displacement tests) were performed on the bonded joints because the data was needed for use as reference point for determining the maximum and minimum loads and displacements during fatigue testing. It has been shown that the correction factors are needed for the simple beam method of analysis in order to obtain accurate values of the adhesive fracture energy, G_{1c}. The results from the static tests revealed that (i) the fracture energy, G_{1c}, of the hot cure epoxy film adhesive "FM73M" is 2.93 ± 0.3 kJ/m^2 whilst for the cold-cure epoxy paste adhesive "9309.3NA" is 5.70 ± 0.4 kJ/m^2 and (ii) the fracture energy of an adhesive is independent of the thickness and type of fibre-composite substrate provided the locus of failure is cohesive through the adhesive layer.

(2) The best method of characterising the fatigue performance of bonded joints is by relating the crack growth rate, da/dN, to the maximum value of the strain energy release rate, G_{max}; such that the fatigue data are presented as plots of log da/dN against log G_{max}. This method is superior to other common forms of data presentation for several reasons. Firstly, the da/dN versus G_{max} curve is independent of the geometry of the test specimen. It should be noted that other forms of data presentation such as plots of applied stress versus the number of cycles to failure or plots of G_{max} versus the number of cycles to failure are dependent on the specimen geometry. Secondly, by using G_{max} instead of the strain energy release rate range, ΔG, any errors in the

analysis of the data which may be due to the effects of facial interference can be eliminated.

(3) The fatigue tests carried out in air at 23 °C and 50% relative humidity revealed that :

(i) The crack growth rate in the hot cure epoxy film adhesive (i.e "FM73M") is slower than in the cold cure epoxy paste adhesive (i.e "9309.3NA") at a given value of G_{max} and the threshold value G_{th} for the "FM73M" adhesive is higher than for the "9309.3NA" adhesive. These observations are in direct contrast to the static test results which showed that the "9309.3NA" adhesive has a higher fracture energy than the "FM73M" adhesive.

(ii) When fatigue tests are carried out under displacement control, the displacement ratio is the only loading condition that affects fatigue crack propagation. It was observed that as the displacement ratio increases, then the crack growth rate decreases, for a given value of G_{max}. Other loading conditions such as the mean displacement, frequency (i.e between 1 and 5 Hz), and the type and thickness of the substrate did not significantly affect the fatigue performance of the adhesive joints.

(4) Comparing the results from the fatigue tests carried out in air (i.e at 23 °C and 50% R.H) with those obtained from testing in water at 25 °C and 50 °C revealed that the adhesive/substrate interface remained intact during the fatigue testing of the following adhesive/substrate combinations; (i) the thermosetting composite bonded with the cold cure epoxy paste adhesive and tested in air at 23 °C and in water at 25 °C and 50 °C, (ii) the thermosetting composite bonded with the hot cure epoxy film adhesive and tested in air at 23 °C and in water at 25 °C and (iii) the thermoplastic composite bonded

with the hot cure epoxy film adhesive and tested in air at 23 °C. In all these cases, the threshold value, G_{th}, of the adhesive tested in water was higher than that obtained from testing in air. This was considered to be due to plasticization of the adhesive at the crack tip. However, it was observed that the adhesive/substrate interface was unstable and failed for other adhesive/substrate combinations, e.g. the thermoplastic composite bonded with the epoxy film adhesive and tested in water at 23 °C and 50 °C. In such circumstances, the locus of joint failure was by a combination of cohesive and interfacial failure and the crack growth rates were for higher than those previously observed from similar tests using the adhesive/substrate combinations mentioned in (i), (ii), and (iii) above.

(5) Surface examination using, scanning electron microscopy (SEM), of the debonded surfaces when the locus of failure was cohesive through the cold-cure epoxy paste adhesive (i.e "9309.3NA") revealed characteristic features such as plastic flow lines, ridges and depressions, short fibres, voids and spherical glass beads (which has been added to control the adhesive layer thickness). The plastic flow lines observed from the static tests were larger in size than those typically obtained from the fatigue tests. It was also observed that, during fatigue testing, the size of the plastic flow lines decreased as the crack growth rate decreased.

(6) Surface examination, using scanning electron microscopy (SEM), of the debonded surfaces when the locus of failure was cohesive through the hot-cure epoxy film adhesive (i.e"FM73M") revealed that the influence of the mat-carrier is a major factor and is responsible for the good fatigue resistance of the hot-cure epoxy film adhesive. Indeed , the presence of the mat carrier may account for the observation that the fatigue performance of this adhesive is superior to that of the cold cure epoxy paste adhesive, even though the latter has a higher (static) fracture energy than the former.

(7) The service life of bonded joints can be predicted by (i) using an empirical model to describe the crack growth curves and so obtain material constants such as D, n, D_1, D_2 and G_{th} (see Chapter Eight), (ii) calculating the initial and final permissible flaw sizes, (iii) calculating the value of G_{max} from the loading conditions for the bonded joint of interest, and (iv) substituting all the above mentioned parameters into a predictive model which has been developed and enables the service life, N_f, of the bonded joint to be determined. This procedure has been successfully used for modelling the fatigue performance of bonded DCB joints. Finally, and most importantly in order to verify that the constants (i.e D, n, D_1, D_2 and G_{th}) obtained from a da/dN versus G_{max} curve are independent of the specimen geometry and to further test the predictive model, these constants have been successfully used to predict the service life of single lap joints. The predicted results were found to be in good agreement with experimental observations.

(8) The predictive model has also been used to examine the effects of substrate thickness, adhesive thickness and length of overlap on the service life of single lap joints. The results obtained showed that (i) as the overlap length increases, the corresponding number of cycles to failure increases, (ii) as the substrate thickness increases, the number of cycles to failure of the joint increases and (iii) as the adhesive layer thickness increases, the number of cycles to failure of the joint decreases.

CHAPTER TEN

PROPOSALS FOR FUTURE WORK

The present research work has established methods based upon a continuum fracture mechanics approach for assessing the performance and predicting the service life of adhesively bonded fibre-composite joints. In order to further contribute to the establishment of a design criteria for predicting the service life of bonded fibre composite joints, the following suggestions are recommended for future work:

(1) In the present research, the fatigue tests, like most other similar experiments to date, were conducted by subjecting the bonded joints to constant amplitude cyclic load or displacement fluctuations. Although fatigue data generated from such tests are sometimes useful, the majority of engineering structures are subjected to complex fluctuating-load environments. Unfortunately, the effects of variable amplitude loading on the fatigue life of bonded joints are presently not well established. Thus, it will be of importance to conduct research in this area.

(2) In Chapter Four, attempts were made to reinforce the relatively thin composite substrates with steel plates in order to minimise the specimen displacement and enable fatigue testing at higher frequency. However, it was found that the surface treatment technique employed was insufficient to prevent debonding at the interface between the steel and the adhesive. Therefore, it is recommended that future work should be directed towards the improving the surface treatment technique for adhesive bonding of steel.

(3) Ideally, fatigue crack growth is a prime candidate for automation. The experiments are tedious, require continuous monitoring and must be performed with a high degree of accuracy. In addition, some fatigue experiments such as threshold testing can last for weeks, or even months. Hence, for future work, the automation of fatigue crack growth experiments on bonded joints is highly recommended since it offers the possibility of a large return on the initial investment both in terms of reduction in man hours and increasing the accuracy of the results obtained.

(4) The total fatigue life of a bonded joint is the sum of the crack initiation and propagation times. Although, it is generally acknowledged that the crack initiation life is governed by the molecular theory of fracture, which is based on the energy required to break the bonds present in the adhesive (Kinloch 1983), there is very little known about how the breaking of primary covalent bonds or secondary van der Waal bonds present in the adhesive contribute to the crack initiation time. Again, this is obviously an area for further study.

(5) In the present research work, a complete format has been presented for assessing the fatigue performance of adhesively bonded fibre composite joints. However as mentioned earlier, because fatigue test experiments such as threshold testing can last for months, attention was mainly focussed on mode I loading of the test specimen in air and in a hostile environment such as water. Although the fracture and crack growth analysis procedures for mode I loading are identical to those of modes II, III and mixed modes, different numbers and material constants may apply. Hence, it is recommended that for future work experiments should be carried out in order to obtain the numerical values of the material constants for the other different modes of loading.

(6) In Chapter Six, it was observed from the fatigue tests results that the threshold value, G_{th}, of the adhesive tested in water was higher than that obtained from testing in air. This was considered to be due to the plasticization of the adhesive at the crack tip. However, it was noticed that the plasticization of the adhesive occurred after prolonged testing (about 2 days) and not immediately after immersing the bonded joint in water. At the moment no possible explanation could be found for this most interesting observation. This is obviously another area where further work is needed.

(7) The material constants D, n, D_1, D_2, G_{th} obtained from the empirical models proposed in the present work for characterising fatigue crack growth in bonded joints were only obtained for one value of the displacement ratio. Thus, when a fatigue test is carried out at a different displacement ratio, a new set of material constants may have to be obtained. Therefore, it will be interesting in a future investigation to develop an empirical model that covers all values of the displacement ratio, so that the material constants obtained from such a model are independent of the loading conditions applied to the specimen.

(8) In Chapter Eight, a model was suggested and used to predict the effect of the substrate thickness on the service life of single lap joints. The predictions indicate that, as the substrate thickness increases, the number of cycles to failure of the joint should increase accordingly. However, no experimental work to test this prediction could be found. Therefore, in a future investigation it is recommended that experiments should be undertaken to validate this prediction and so further validate the model developed in the present work.

APPENDIX

data from specimen no. 3

	Column 1	Column 2	Column 3	Column 4	Column 5	Column 6	Column 7	Column 8	Column 9	Column 10	Column 11	Column 12	Column 13	Column 14
1	A	P	d	F	Z	dC/dd	Gc(area)	Gc(comp)	Gc U D	Gc C D	Gc C L	Gc U L	E Up	E Cp
2	(mm)	(N)	(mm)				(KJ/m 2)	(KJ/m 2)	(KJ/m 2)	(KJ/m 2)	(KJ/m 2)	(KJ/m 2)	(GPa)	GPa)
3									4	5	6	7		
4	35 00	306 00	11 60	0 8207	0 8497	2 84E 03		5 72	6 55	5 35	5 47	4 91	90 77	128 91
5	40 00	273 00	14 80	0 8160	0 8500	3 54E 03	5 86	5 68	6 52	5 38	5 43	5 11	94 75	126 81
6	45 00	243 00	17 50	0 8211	0 8558	4 29E 03	5 08	5 45	6 10	5 11	5 31	5 12	101 55	130 54
7	50 00	220 00	20 00	0 8195	0 8556	5 07E 03	5 18	5 28	5 91	5 01	5 23	5 18	106 11	131 24
8	55 00	207 00	25 30	0 8073	0 8463	5 89E 03	5 43	5 43	6 15	5 24	5 40	5 55	109 25	129 49
9	60 00	188 00	28 50	0 8100	0 8485	6 75E 03	4 92	5 14	5 77	4 96	5 23	5 45	114 35	132 31
10	65 00	173 00	32 70	0 8045	0 8440	7 65E-03	5 24	4 93	5 62	4 87	5 08	5 42	118 61	131 18
11	70 00	175 00	40 90	0 7886	0 8147	8 59E-03	5 83	5 66	6 60	5 70	5 69	6 43	117 78	125 42
12	75 00	172 00	47 70	0 7478	0 7972	9 57E 03	5 65	6 09	7 06	6 09	6 06	7 13	122 09	125 05
13	80 00	170 00	55 20	0 7239	0 7773	1 06E-02	5 96	6 59	7 57	6 52	6 46	7 92	126 55	124 50
14	90 00	145 00	63 00	0 7269	0 7788	1 27E-02	6 15	5 77	6 65	5 78	5 87	7 29	132 76	127 59
15	95 00	138 00	70 10	0 7166	0 7698	1 39E-02	5 80	5 69	6 58	5 73	5 80	7 36	135 46	127 32
16	100 00	128 00	72 90	0 7279	0 7787	1 51E-02	5 28	5 15	5 93	5 20	5 41	6 80	138 72	130 62
17	105 00	125 00	82 70	0 6980	0 7535	1 63E-02	5 63	5 47	6 36	5 54	5 59	7 38	140 43	126 82
18	110.00	120 00	88.80	0 6854	0 7426	1 75E-02	5 60	5 43	6 33	5 51	5 53	7 46	142 75	126 04
							Mean = 5 54	Mean = 5 61	Mean = 6 38	Mean = 5 46	Mean = 5 57	Mean = 6 30		
							SD = 0 36	SD = 0 38	SD = 0 51	SD = 0 45	SD = 0 36	SD = 1 03		

Table A1. Mode I fracture data obtained from a DCB joint made from a thermoplastic composite substrate (i.e "APC-2") bonded with a two-part cold-cure epoxy paste adhesive (i.e "9309.3NA").

Notes:
The table shows that the "corrected" load and displacement methods (i.e Equations 4.15 and 4.16) are in good agreement with one another and with the area and compliance methods (i.e Equations 4.1 and 4.3).

width of the DCB specimen, B = 23.23 mm
thickness of a fibre-composite arm, h = 1.625 mm (12 plies)
L_2 (as shown in Figure 4.4) = 10.30 mm
L_1 (as shown in Figure 4.4) = 9.58 mm

All symbols and abbreviations shown in above columns are as defined in the nomenclature.

data from specimen no. 19

	Column 1	Column 2	Column 3	Column 4	Column 5	Column 6	Column 7	Column 8	Column 9	Column 10	Column 11	Column 12
1	A	P	d	f	z	dC/dd	Gc(area)	Gc(comp)	Gc - U - D	Gc - I - D	Gc - L - L	Gc - U - L
2	(mm)	(N)	(mm)				(KJ/m^2)	(KJ/m^2)	(KJ/m^2)	(KJ/m^2)	(KJ/m^2)	(KJ/m^2)
3												
4	50.00	245.00	21.60	0.8105	0.8485	3.76E-03		4.88	6.86	5.84	5.82	5.24
5	55.00	227.00	25.40	0.8063	0.8455	5.02E-03	5.70	5.58	6.79	5.83	5.90	5.44
6	60.00	209.00	28.90	0.8063	0.8456	6.16E-03	5.41	5.81	6.52	5.65	5.85	5.49
7	65.00	200.00	34.40	0.7901	0.8325	7.19E-03	6.09	6.21	6.86	5.95	6.07	5.90
8	70.00	182.00	38.20	0.7902	0.8322	8.11E-03	5.96	5.80	6.44	5.62	5.76	5.67
9	75.00	176.00	44.50	0.7721	0.8172	8.93E-03	5.94	5.97	6.77	5.91	5.98	6.09
10	80.00	165.00	49.30	0.7670	0.8126	9.63E-03	5.76	5.66	6.50	5.78	5.89	6.09
11	85.00	163.00	57.10	0.7425	0.7921	1.02E-02	5.99	5.87	7.09	6.21	6.23	6.70
12	90.00	162.00	64.00	0.7202	0.7733	1.07E-02	5.74	6.07	7.57	6.60	6.64	7.42
							Mean = 5.82	Mean = 5.76	Mean = 6.83	Mean = 5.93	Mean = 6.01	Mean = 6.00
							SD = 0.21	SD = 0.38	SD = 0.34	SD = 0.30	SD = 0.27	SD = 0.68

Table A2. Mode I fracture data obtained from a DCB joint made from a thermosetting composite substrate (i.e "913C XAS-5-47%") bonded with a two-part cold-cure epoxy paste adhesive (i.e "9309.3NA").

Notes:
Comparison with Table A3 shows that "9309.3NA" has a higher fracture energy, G_{1c}, than "FM73M" (see Figure 4.10). Also comparison with Table A1 shows that the fracture energy of the adhesive is independent of the type of substrate (see Figure 4.12).

width of the DCB specimen, B = 23.15 mm
thickness of a fibre-composite arm, h = 1.72 mm (12 plies)
L_2 (as shown in Figure 4.4) = 10.36 mm
L_1 (as shown in Figure 4.4) = 9.50 mm

All symbols and abbreviations shown in above columns are as defined in the nomenclature.

data from specimen no. 2B

	Column 1	Column 2	Column 3	Column 4	Column 5	Column 6	Column 7	Column 8	Column 9	Column 10	Column 11	Column 12
1	A	P	a	f	z	dC/da	Gc(area)	Gc(comp)	Gc U D	Gc L D	Gc L I	Gc U I
2	(mm)	(N)	(mm)				(kJ/m^2)	(kJ/m^2)	(kJ/m^2)	(kJ/m^2)	(kJ/m^2)	(kJ/m^2)
3												
4	31.00	240.00	6.90	0.8702	0.8775	2.55E-03		3.12	3.45	3.11	3.02	2.75
5	36.00	210.00	8.80	0.8733	0.8886	3.33E-03	2.84	3.14	3.30	2.99	3.06	2.84
6	41.00	178.00	10.70	0.8776	0.8965	4.22E-03	2.91	2.86	2.98	2.72	2.81	2.64
7	46.00	165.00	13.90	0.8674	0.8914	5.20E-03	3.03	3.03	3.20	2.93	2.96	2.86
8	51.00	140.00	16.10	0.8710	0.8956	6.28E-03	2.68	2.86	2.96	2.72	2.83	2.75
9	56.00	140.00	19.10	0.8676	0.8937	7.45E-03	2.29	3.13	3.07	2.83	3.08	3.05
10	61.00	126.00	23.00	0.8584	0.8869	8.71E-03	3.48	2.96	3.05	2.82	2.91	2.93
11	66.00	118.00	27.20	0.8491	0.8797	1.01E-02	3.05	3.00	3.12	2.89	2.94	3.01
12	71.00	110.00	31.60	0.8402	0.8725	1.15E-02	3.15	2.98	3.14	2.91	2.91	3.03
13	76.00	100.00	34.60	0.8419	0.8738	1.31E-02	2.77	2.80	2.92	2.71	2.74	2.87
14	81.00	95.00	40.10	0.8286	0.8629	1.47E-02	3.10	2.84	3.02	2.80	2.76	2.94
15	86.00	90.00	43.80	0.8274	0.8616	1.64E-02	2.36	2.85	2.94	2.73	2.77	2.97
16	91.00	84.00	48.80	0.8139	0.8503	1.83E-02	3.44	2.76	2.95	2.74	2.85	2.90
17	96.00	83.00	56.70	0.7988	0.8361	2.02E-02	2.69	2.98	3.15	2.91	2.81	3.15
18	101.00	80.00	62.40	0.7875	0.8282	2.22E-02	2.75	3.04	3.17	2.93	2.85	3.24
19	106.00	73.00	65.30	0.7931	0.8324	2.43E-02	2.86	2.77	2.89	2.68	2.62	2.97
							Mean = 2.89	Mean = 2.94	Mean = 3.08	Mean = 2.83	Mean = 2.85	Mean = 2.93
							SD = 0.34	SD = 0.13	SD = 0.15	SD = 0.12	SD = 0.13	SD = 0.15

Table A3. Mode I fracture data obtained from a DCB joint made from a thermosetting composite substrate (i.e "913C XAS-5-47%") bonded with a one-part hot-cure epoxy film adhesive (i.e "FM73M").

Notes
Comparison with Table A2 shows that "9309.3NA" has a higher fracture energy than "FM73M" (see Figure 4.10). Also comparison with Tables A4 and A5 shows that the *fracture energy of the adhesive is independent of the thickness* of substrate (Figure 4.13).

Notes:
width of the DCB specimen, B = 23.36 mm
thickness of a fibre-composite arm, h = 1.49 mm (12 plies)
L_2 (as shown in Figure 4.4) = 10.68 mm
L_1 (as shown in Figure 4.4) = 9.87 mm

All symbols and abbreviations shown in above columns are as defined in the nomenclature.

data from specimen no. 60

	Column 1	Column 2	Column 3	Column 4	Column 5	Column 6	Column 7	Column 8	Column 9	Column 10	Column 11	Column 12
1	A	P	δ	F	λ	dC/dδ	GC(area)	GC((comp)	GC U D	GC L D	GC C L	GC U L
2	(mm)	(N)	(mm)				(kJ/m^2)	(kJ/m^2)	(kJ/m^2)	(kJ/m^2)	(kJ/m^2)	(kJ/m^2)
3												
4	50.00	325.00	9.00	0.9284	0.9399	1.13E-03		2.63	3.86	3.32	3.24	2.20
5	55.00	299.00	10.10	0.9325	0.9443	1.33E-03	2.60	2.61	3.62	3.16	3.25	2.28
6	60.00	277.00	11.50	0.9341	0.9463	1.57E-03	2.62	2.65	3.50	3.08	3.26	2.31
7	65.00	259.00	12.80	0.9363	0.9486	1.87E-03	2.95	2.57	3.25	2.88	3.07	2.20
8	70.00	241.00	15.60	0.9304	0.9444	2.22E-03	3.58	2.83	3.54	3.16	3.24	2.37
9	80.00	200.00	18.20	0.9356	0.9488	3.08E-03	2.78	2.71	3.00	2.71	2.87	2.14
10	85.00	181.00	20.40	0.9342	0.9478	3.59E-03	3.46	2.58	2.87	2.60	2.62	1.98
11	95.00	175.00	26.60	0.9258	0.9412	4.78E-03	2.74	3.21	3.23	2.95	2.98	2.31
12	100.00	165.00	28.00	0.9249	0.9404	5.43E-03	3.02	3.25	3.16	2.89	2.91	2.27
							Mean = 2.99	Mean = 2.78	Mean = 3.33	Mean = 2.97	Mean = 3.04	Mean = 2.22
							S.D. = 0.35	S.D. = 0.26	S.D. = 0.32	S.D. = 0.23	S.D. = 0.22	S.D. = 0.12

Table A4. Mode I fracture data obtained from a DCB joint made from a thermosetting composite substrate (i.e "913C XAS-5-47%") bonded with a one-part hot-cure epoxy film adhesive (i.e "FM73M").

Notes:
Comparison with Tables A3 and A5 shows that the fracture energy of the adhesive is independent of the thickness of substrate (see Figure 4.13).

width of the DCB specimen, B = 22.74 mm
thickness of a fibre-composite arm, h = 2.81 mm (18 plies)
L_2 (as shown in Figure 4.4) = 11.01 mm
L_1 (as shown in Figure 4.4) = 9.61 mm

All symbols and abbreviations shown in above columns are as defined in the nomenclature.

data from specimen no. 32

	Column 1	Column 2	Column 3	Column 4	Column 5	Column 6	Column 7	Column 8	Column 9	Column 10	Column 11	Column 12
1	A	P	a	F	Z	dC/da	Gc(area)	Gc(comp)	Gc - U - D	Gc - C - D	Gc - C - L	Gc - U - L
2	(mm)	(N)	(mm)				(kJ/m^2)	(kJ/m^2)	(kJ/m^2)	(kJ/m^2)	(kJ/m^2)	(kJ/m^2)
3												
4	50.00	440.00	6.70	0.9483	0.9550	5.99E-04		2.59	3.95	3.56	3.30	1.52
5	55.00	405.00	7.50	0.9518	0.9589	7.63E-04	2.62	2.80	3.70	3.19	3.30	1.56
6	60.00	375.00	8.50	0.9534	0.9611	9.41E-04	2.82	2.96	3.56	3.10	3.30	1.59
7	65.00	338.00	9.50	0.9549	0.9629	1.13E-03	3.08	2.89	3.31	2.91	3.09	1.52
8	70.00	327.00	10.80	0.9550	0.9634	1.34E-03	2.43	3.20	3.38	2.99	3.30	1.65
9	80.00	271.00	13.50	0.9552	0.9641	1.79E-03	3.32	2.94	3.07	2.75	2.88	1.48
10	85.00	248.00	15.10	0.9546	0.9638	2.04E-03	3.45	2.75	2.93	2.64	2.65	1.37
11	95.00	237.00	19.70	0.9496	0.9601	2.57E-03	2.83	3.23	3.29	2.99	3.00	1.59
12	100.00	224.00	21.50	0.9492	0.9598	2.86E-03	3.05	3.21	3.23	2.94	2.94	1.58
							Mean = 2.95	Mean = 2.95	Mean = 3.38	Mean = 2.98	Mean = 3.08	Mean = 1.54
							SD = 0.34	SD = 0.22	SD = 0.31	SD = 0.22	SD = 2.24	SD = 0.08

Table A5. Mode I fracture data obtained from a DCB joint made from a thermosetting composite substrate (i.e "913C XAS-5-47%") bonded with a one-part hot-cure epoxy film adhesive (i.e "FM73M").

Notes:
Comparison with Tables A3 and A4 shows that the fracture energy of the adhesive is independent of the thickness of substrate.

width of the DCB specimen, B = 22.38 mm
thickness of a fibre-composite arm, h = 3.71 mm (24 plies)
L_2 (as shown in Figure 4.4) = 11.46 mm
L_1 (as shown in Figure 4.4) = 9.61 mm

All symbols and abbreviations shown in above columns are as defined in the nomenclature.

Specimen number 92

	1	2	3	4	5	6	7	8	9
1	crack length	no of cycles	max load	min load	log Gmax (displ	log Gmax (com)	log da/dN	Z	F
2	a	N	Pmax	Pmin				correction	correction
3	(m)		(N)	(N)	(kJ/m^2)	(kJ/m^2)	(m/cycle)	factor	factor
4									
5	0 06330	4950	213 00	14 00	2 841	3 031		0 9783	0 9750
6	0 06602	15178	190 00	11 00	2 878	2 971		0 9801	0 9770
7	0 06804	24158	181 50	10 00	2 848	2 954		0 9813	0 9784
8	0 06903	30298	166 50	10 00	2 805	2 889	0 821	0 9819	0 9790
9	0 07017	45660	160 00	10 00	2 782	2 863	-7 985	0 9826	0 9797
10	0 07128	61958	151 00	9 50	2 752	2 821	-7 448	0 9831	0 9803
11	0 07176	89140	146 00	9 50	2 741	2 806	-7 561	0 9833	0 9806
12	0 07296	166712	142 00	9 50	2 717	2 778	-7 658	0 9839	0 9812
13	0 07777	372154	123 50	9 00	2 635	2 686	-7 684	0 9859	0 9835
14	0 07849	413520	117 50	8 50	2 610	2 623	-7 743	0 9862	0 9838
15	0 08024	502128	112 00	9 50	2 581	2 579	-7 785	0 9868	0 9845
16	0 08134	558330	108 00	10 50	2 561	2 544	-7 844	0 9872	0 9849
17	0 08374	825388	102 50	10 50	2 528	2 488	-8 112	0 9879	0 9857
18	0 08429	914058	101 50	11 50	2 522	2 478	-8 238	0 9881	0 9859
19	0 08464	1245923	101 00	11 50	2 518	2 470	-8 486	0 9882	0 9860
20	0 08531	1407066	97 50	10 50	2 500	2 434	-8 635	0 9884	0 9862
21	0 08578	1684092	96 50	11 00	2 493	2 422	-8 733	0 9885	0 9864
22	0 08661	1840098	94 50	9 50	2 481	2 397	-8 708	0 9888	0 9867
23	0 08661	2118292	95 50	12 50	2 485	2 406	-8 825	0 9888	0 9867
24	0 08691	2553456	93 50	11 50	2 475	2 385	-8 805	0 9888	0 9868
25	0 08781	2984362	89 50	8 50	2 452	2 338	-8 768	0 9891	0 9870
26	0 08892	3495256	88 50	9 50	2 443	2 316	-8 738	0 9894	0 9873
27	0 09044	3879938	88 50	10 50	2 437	2 297	-8 737	0 9897	0 9878
28	0 09108	4706562	87 50	9 50	2 430	2 278		0 9899	0 9879
29	0 09145	5156830	86 50	8 50	2 423	2 262		0 9900	0 9880
30	0 09199	5583554	83 50	7 00	2 406	2 223		0 9901	0 9882

Table A6. Mode I fatigue data obtained from a DCB joint made from a thermosetting composite substrate (i.e "913C XAS-5-47%") bonded with a one-part hot-cure epoxy film adhesive (i.e "FM73M").

Notes:
Comparison with Table A9 shows the effect of displacement ratio and with Table A11 shows the effect of the type of adhesive.

thickness h = 3 84 mm (24 plies)
width B = 24 26 mm
L_1 (Figure 4.4) = 11.03 mm
L_2 (Figure 4.4) = 9.25 mm
frequency, f = 1 Hz
DR = 0 1
MD = 3 4 mm
Test temperature = 23 °C (air)
Test machine control mode. Displ.

All symbols and abbreviations shown are as defined in the nomenclature.

Specimen number 98

	1	2	3	4	5	6	7	8	9
1	crack length	no of cycles	max load	min load	log Gmax (displ)	log Gmax (corr)	log da/dN	Z	F
2	a	N	Pmax	Pmin				correction	correction
3	(m)		(N)	(N)	(kJ/m^2)	(kJ/m^2)	(m/cycle)	factor	factor
4									
5	0.04457	4950	350.00	137.00	3.145	3.117		0.9705	0.9716
6	0.04513	15178	320.00	124.00	3.092	3.058		0.9727	0.9735
7	0.04726	24158	302.00	117.00	3.058	3.023		0.9741	0.9748
8	0.04778	39298	294.50	114.00	3.043	3.008	7.063	0.9747	0.9753
9	0.04962	45646	274.00	106.50	3.004	2.959	-7.233	0.9757	0.9761
10	0.04818	61958	260.00	103.50	2.978	2.921	-7.412	0.9762	0.9766
11	0.05055	80140	242.00	96.00	2.935	2.883	7.494	0.9777	0.9779
12	0.05221	100712	220.00	88.00	2.881	2.828	-7.607	0.9793	0.9793
13	0.05570	372154	193.50	80.00	2.809	2.765	7.852	0.9820	0.9818
14	0.05674	413520	187.50	78.50	2.778	2.778	7.870	0.9826	0.9825
15	0.05718	502120	182.00	76.00	2.765	2.761	-7.953	0.9831	0.9828
16	0.05796	566330	179.50	75.00	2.751	2.765	8.004	0.9836	0.9832
17	0.05878	626308	166.50	67.50	2.707	2.736	8.236	0.9848	0.9842
18	0.05982	914056	163.00	67.00	2.696	2.721	8.273	0.9847	0.9843
19	0.06185	1245823	156.50	64.00	2.667	2.721	-8.453	0.9858	0.9852
20	0.06178	1407066	150.00	63.00	2.646	2.688	-8.533	0.9857	0.9852
21	0.06226	1664002	143.50	60.00	2.626	2.658	8.566	0.9860	0.9855
22	0.06306	1840060	142.00	59.00	2.616	2.663	-8.683	0.9863	0.9858
23	0.06326	2116262	139.00	55.50	2.596	2.631	-8.694	0.9864	0.9859
24	0.06443	2563456	133.00	56.00	2.579	2.635	-8.768	0.9870	0.9864
25	0.06463	2864362	129.00	52.00	2.561	2.606	-8.866	0.9871	0.9865
26	0.06532	3485256	122.00	50.00	2.536	2.578	8.906	0.9874	0.9868
27	0.06612	3878030	118.00	48.00	2.506	2.542	8.974	0.9877	0.9871
28	0.06622	4706582	112.00	44.00	2.493	2.521	-9.020	0.9877	0.9871
29	0.06736	5156630	106.50	43.50	2.477	2.524	-8.977	0.9882	0.9876
30	0.06754	5563564	106.00	43.50	2.470	2.515	-8.950	0.9883	0.9876
31	0.06767	6018468	107.00	43.00	2.466	2.518	-8.913	0.9883	0.9877
32	0.06873	6467765	106.50	43.00	2.457	2.506	-8.972	0.9887	0.9881
33	0.06932	6871068	106.00	43.00	2.451	2.533	9.027	0.9888	0.9883
34	0.06964	7300230	106.00	43.00	2.449	2.530	9.115	0.9890	0.9884
35	0.06962	7775390	106.00	43.00	2.444	2.535	9.301	0.9891	0.9884
36	0.06962	8187836	104.00	42.00	2.440	2.526	9.692	0.9891	0.9884
37	0.06962	9074032	100.50	41.00	2.425	2.496	-10.437	0.9891	0.9884
38	0.06964	9612411	100.00	41.00	2.423	2.493	10.305	0.9891	0.9884
39	0.06964	9934782	100.00	41.00	2.423	2.493	9.998	0.9891	0.9884
40	0.06966	10318284	100.00	41.00	2.423	2.493	9.758	0.9891	0.9885
41	0.06966	10364133	100.00	41.00	2.423	2.493	-9.758	0.9891	0.9885
42	0.06966	10563211	99.00	40.00	2.416	2.486	-9.723	0.9891	0.9885
43	0.06966	10741357	99.00	41.00	2.416	2.486	9.877	0.9891	0.9885
44	0.06966	10811271	99.00	41.00	2.416	2.486	-10.035	0.9891	0.9885
45	0.07001	10833211	99.00	41.00	2.413	2.478		0.9891	0.9885
46	0.07001	10966327	99.00	41.00	2.413	2.478		0.9891	0.9885
47	0.07001	11811294	99.00	41.00	2.413	2.478		0.9891	0.9885

Table A7. Mode I fatigue data obtained from a DCB joint made from a thermosetting composite substrate (i.e "913C XAS-5-47%") bonded with a one-part hot-cure epoxy film adhesive (i.e "FM73M").

Notes:
Comparison with Table A9 shows the effect of frequency (see Figure 5.5) and with Table A13 shows the effect of the substrate thickness (see Figure 5.10a)

thickness h = 3.71 mm (24 plies)
width B = 24.00 mm
L_1 (Figure 4.4) = 11.11 mm
L_2 (Figure 4.4) = 9.25 mm
frequency, f = 5 Hz
DR = 0.5
MD = 2.4 mm
Test temperature = 23 °C (air)
Test machine control mode: Displ.

All symbols and abbreviations shown are as defined in the nomenclature.

Specimen number 98

	1	2	3	4	5	6	7	8	9
1	crack length	no of cycles	max load	min load	log Gmax (displ)	log Gmax (corr)	log da/dN	Z	F
2	a	N	Pmax	Pmin				correction	correction
3	(m)		(N)	(N)	(kJ/m^2)	(kJ/m^2)	(m/cycle)	factor	factor
4									
5	0 08056	860	212 50	90 20	3 193	3 118		0 9787	0 9712
6	0 08196	1422	208 40	88 40	3 178	3 136		0 9776	0 9722
7	0 08268	1820	205 20	86 40	3 167	3 138		0 9779	0 9727
8	0 08331	3187	196 70	82 80	3 146	3 115	-6 113	0 9783	0 9731
9	0 08416	4262	192 20	80 30	3 132	3 111	-6 385	0 9787	0 9736
10	0 08465	5961	186 90	78 00	3 117	3 097	-6 434	0 9780	0 9739
11	0 08519	8713	179 40	74 90	3 096	3 072	-6 558	0 9792	0 9743
12	0 08726	14985	173 50	72 90	3 071	3 078	-6 691	0 9802	0 9755
13	0 08786	22581	169 00	70 90	3 057	3 063	-6 821	0 9805	0 9758
14	0 08878	37621	164 90	69 30	3 042	3 055	-6 902	0 9808	0 9763
15	0 08906	36078	161 60	67 60	3 032	3 043	-7 075	0 9810	0 9765
16	0 09206	80644	145 80	60 70	2 972	2 990	-7 217	0 9823	0 9780
17	0 09276	91719	141 80	58 00	2 957	2 974	-7 203	0 9826	0 9783
18	0 09289	101519	140 30	56 90	2 952	2 967	-7 203	0 9826	0 9784
19	0 09408	113331	135 90	55 80	2 933	2 952	-7 208	0 9831	0 9789
20	0 09447	119994	135 20	55 50	2 929	2 951	-7 191	0 9832	0 9791
21	0 09742	167877	125 60	50 50	2 885	2 915	-7 358	0 9842	0 9803
22	0 09780	189199	123 60	47 40	2 876	2 901	-7 470	0 9843	0 9804
23	0 09837	197795	120 20	46 20	2 861	2 883	-7 511	0 9845	0 9807
24	0 09884	263913	114 20	45 50	2 836	2 842	-7 680	0 9847	0 9808
25	0 09950	285490	112 80	42 90	2 828	2 836	-7 674	0 9849	0 9811
26	0 10131	339618	108 20	42 30	2 802	2 811	-7 662	0 9854	0 9816
27	0 10204	382354	106 30	41 30	2 792	2 800	7 644	0 9856	0 9821
28	0 10287	427515	103 70	40 30	2 777	2 783	-7 728	0 9859	0 9824
29	0 10359	458702 00	103 40	40 70	2 773	2 785	-7 803	0 9861	0 9826
30	0 10481	530710 00	100 80	39 90	2 757	2 768	-7 910	0 9864	0 9830
31	0 10491	603948 00	96 90	37 90	2 739	2 735	-7 902	0 9864	0 9830
32	0 10502	692582 00	93 10	35 70	2 722	2 700		0 9865	0 9831
33	0 10676	778678 00	89 90	33 90	2 691	2 683		0 9874	0 9842
34	0 10903	872840 00	86 00	31 30	2 671	2 647		0 9875	0 9843

Table A8. Mode I fatigue data obtained from a DCB joint made from a thermosetting composite substrate (i.e "913C XAS-5-47%") bonded with a one-part hot-cure epoxy film adhesive (i.e "FM73M").

Notes:
Comparison with Tables A9 and A10 shows the effect of mean displacement (see Figure 5.8a).

thickness h = 3.79 mm (24 plies)
width B = 24.01 mm
L_1 (Figure 4.4) = 11.04 mm
L_2 (Figure 4.4) = 9.15 mm
frequency, f = 1 Hz
DR = 0.5
MD = 7.2 mm
Test temperature = 23 °C (air)
Test machine control mode: Displ.

All symbols and abbreviations shown are as defined in the nomenclature.

Specimen number 99

	1	2	3	4	5	6	7	8	9
1	crack length	no of cycles	max load	min load	log Gmax (displ)	log Gmax (corr)	log da/dN	Z	F
2	a	N	Pmax	Pmin				correction	correction
3	(m)		(N)	(N)	(kJ/m^2)	(kJ/m^2)	(m/cycle)	factor	factor
4									
5	0 04416	3700	338 50	121 50	3 183	3 031		0 9700	0 9711
6	0 04488	8200	328 00	112 50	3 162	3 038		0 9711	0 9720
7	0 04576	12100	315 00	108 25	3 136	3 041		0 9723	0 9731
8	0 04604	14200	308 00	104 50	3 121	3 028	-6 748	0 9727	0 9734
9	0 04720	19900	288 00	97 75	3 084	3 021	-6 802	0 9741	0 9747
10	0 04788	24000	278 00	94 50	3 063	3 015	-6 848	0 9749	0 9754
11	0 04808	27500	271 50	92 50	3 050	3 003	-6 948	0 9752	0 9756
12	0 04884	36500	254 75	87 00	3 015	2 978	-7 084	0 9761	0 9765
13	0 05161	77200	223 25	76 00	2 935	2 949	-7 242	0 9788	0 9788
14	0 05224	86500	215 00	73 25	2 913	2 934	-7 251	0 9784	0 9793
15	0 05272	97700	210 50	72 00	2 900	2 930	-7 313	0 9798	0 9797
16	0 05314	108700	204 50	70 00	2 884	2 916	-7 370	0 9801	0 9800
17	0 05368	120500	198 50	68 50	2 865	2 911	-7 451	0 9807	0 9806
18	0 05480	165200	188 00	64 50	2 834	2 888	-7 656	0 9814	0 9812
19	0 05524	185200	184 50	63 50	2 822	2 883	-7 744	0 9818	0 9815
20	0 05544	205800	180 00	62 25	2 810	2 866	-7 852	0 9818	0 9817
21	0 05582	247200	173 00	59 75	2 789	2 844	-7 988	0 9823	0 9820
22	0 05622	294000	168 75	58 00	2 778	2 835	-8 049	0 9825	0 9822
23	0 05652	338000	161 75	56 50	2 755	2 800	-8 066	0 9827	0 9823
24	0 05680	381800	161 00	56 50	2 751	2 803	-8 078	0 9828	0 9825
25	0 05748	421900	155 50	54 00	2 731	2 789	-8 051	0 9833	0 9828
26	0 05798	502700	149 50	52 00	2 710	2 766	-8 068	0 9836	0 9832
27	0 05828	517500	148 75	52 50	2 708	2 767	-8 038	0 9838	0 9833
28	0 05858	540600	147 50	52 00	2 700	2 766	-8 024	0 9838	0 9835
29	0 05878	564800	145 00	50 50	2 691	2 758	-8 057	0 9841	0 9837
30	0 05904	588500	144 00	50 50	2 686	2 757	-8 105	0 9843	0 9838
31	0 05922	619800	141 50	50 50	2 677	2 748	-8 183	0 9844	0 9839
32	0 05946	673900	140 25	49 00	2 671	2 744	-8 228	0 9845	0 9840
33	0 05964	706800	138 75	48 75	2 666	2 736	-8 312	0 9846	0 9841
34	0 06008	776000	136 00	47 50	2 653	2 730	-8 385	0 9848	0 9844
35	0 06016	846500	134 25	47 00	2 647	2 721		0 9849	0 9844
36	0 06036	886800	132 75	46 50	2 641	2 715		0 9850	0 9845
37	0 06046	930100	131 50	46 00	2 636	2 709		0 9851	0 9846

thickness h = 3 82 mm (24 plies)
width B = 24.00 mm
L_1 (Figure 4 4) = 11.11 mm
L_2 (Figure 4.4) = 9.20 mm
frequency, f = 1 Hz
DR = 0 5
MD = 2 4 mm
Test temperature = 23 °C (air)
Test machine control mode: Displ.

All symbols and abbreviations shown are as defined in the nomenclature.

Table A9. Mode I fatigue data obtained from a DCB joint made from a thermosetting composite substrate (i.e "913C XAS-5-47%") bonded with a one-part hot-cure epoxy film adhesive (i.e "FM73M").

Notes:
Comparison with Table A6 shows the effect of displacement ratio and with Table A7 shows the effect of frequency (see Figure 5.5).

Specimen number 99RE

	1	2	3	4	5	6	7	8
1	crack length	no of cycles	max load	min load	log Gmax (corr)	log da/dN	Z	F
2	a	N	Pmax	Pmin			correction	correction
3	(m)		(N)	(N)	(kJ/m^2)	(m/cycle)	factor	factor
4								
5	0 06186	400	263 00	114 00	2 960		0 9733	0 9687
6	0 06216	600	261 00	112 50	2 993		0 9738	0 9692
7	0 06394	900	258 50	110 50	3 097		0 9753	0 9708
8	0 06418	1100	255 00	109 00	3 097	-5 790	0 9755	0 9711
9	0 06520	2100	247 00	105 50	3 117	-6 111	0 9763	0 9720
10	0 06546	4100	237 00	100 50	3 082	-6 388	0 9765	0 9722
11	0 06636	5700	231 25	98 50	3 104	-6 513	0 9771	0 9730
12	0 06706	9200	223 00	95 50	3 095	-6 725	0 9776	0 9735
13	0 06726	11800	218 50	93 00	3 084	-6 773	0 9778	0 9737
14	0 06744	16200	210 50	88 75	3 056	-6 849	0 9779	0 9738
15	0 06864	21400	205 00	86 50	3 070	-6 896	0 9788	0 9748
16	0 06970	29400	196 75	83 50	3 054	-6 918	0 9793	0 9755
17	0 07334	72900	167 50	72 50	2 970	-7 170	0 9814	0 9778
18	0 07440	83900	164 50	71 00	2 965	-7 223	0 9820	0 9785
19	0 07474	92800	161 50	69 50	2 951	-7 253	0 9821	0 9787
20	0 07518	105000	157 75	68 00	2 934	-7 338	0 9824	0 9790
21	0 07554	110700	158 50	67 50	2 930	-7 442	0 9825	0 9792
22	0 07686	162300	147 00	64 00	2 882	-7 822	0 9832	0 9799
23	0 07716	175200	145 25	63 50	2 872	-7 857	0 9833	0 9800
24	0 07740	200700	141 75	62 00	2 852	-7 704	0 9834	0 9801
25	0 07850	251300	137 25	60 50	2 826	-7 770	0 9839	0 9807
26	0 07880	272300	135 50	60 00	2 815	-7 770	0 9840	0 9808
27	0 07976	325100	132 25	58 50	2 793	-7 808	0 9844	0 9813
28	0 08014	366800	129 50	57 25	2 774	-7 854	0 9846	0 9815
29	0 08068	410800	127 00	56 50	2 754	-7 860	0 9848	0 9818
30	0 08126	440700	125 25	55 75	2 741	-7 837	0 9850	0 9820
31	0 08188	486800	122 50	54 50	2 718	-7 816	0 9852	0 9823
32	0 08230	511300	121 50	54 00	2 709	-7 844	0 9854	0 9824
33	0 08282	534400	120 25	53 50	2 696	-7 842	0 9856	0 9827
34	0 08340	583100	118 25	52 50	2 677	-7 866	0 9858	0 9828
35	0 08374	620700	116 50	51 50	2 660	-7 939	0 9859	0 9830
36	0 08432	668300	115 00	51 00	2 643	-7 997	0 9861	0 9833
37	0 08508	752500	111 75	49 75	2 609		0 9864	0 9836
38	0 08540	790600	110 50	49 00	2 596		0 9865	0 9837
39	0 08710	1005900	105 25	47 25	2 527		0 9870	0 9843

thickness h = 3.82 mm (24 plies)
width B = 24.00 mm
L_1 (Figure 4 4) = 11.11 mm
L_2 (Figure 4.4) = 9.20 mm
frequency, f = 1 Hz
DR = 0 5
MD = 4 8 mm
Test temperature = 23 °C (air)
Test machine control mode: Displ.

All symbols and abbreviations shown are as defined in the nomenclature.

Table A10. Mode I fatigue data obtained from a DCB joint made from a thermosetting composite substrate (i.e "913C XAS-5-47%") bonded with a one-part hot-cure epoxy film adhesive (i.e "FM73M").

Notes:
Comparison with Tables A8 and A9 shows the effect of mean displacement (see Figure 5.8a).

Specimen number 105

	1	2	3	4	5	6	7	8	9
1	crack length	no of cycles	max load	min load	log Gmax (displ)	log Gmax (com)	log da/dN	Z	F
2	a	N	Pmax	Pmin				correction	correction
3	(m)		(N)	(N)	(kJ/m^2)	(kJ/m^2)	(m/cycle)	factor	factor
4									
5	0 06270	3988	166 50	6 50	2 699	2 857		0 9822	0 9802
6	0 06586	6890	147 00	6 50	2 630	2 751		0 9840	0 9821
7	0 06730	9390	135 50	7 50	2 588	2 681		0 9847	0 9828
8	0 06989	13687	122 50	7 50	2 532	2 598	-6 251	0 9859	0 9841
9	0 07263	20977	108 00	7 00	2.465	2.495	-6.363	0 9870	0 9852
10	0 07497	24601	104 50	6 00	2.441	2.473	-6 455	0 9878	0 9862
11	0 08378	71257	80 00	5 50	2 288	2 276	-6 830	0 9904	0 9889
12	0 08626	75062	78 50	5 50	2.270	2 272	-6 802	0 9910	0 9895
13	0 08743	86074	76 50	7 00	2.255	2.256	-6.890	0 9912	0 9898
14	0 08772	102487	70 50	6 00	2.218	2.187	-7 141	0.9913	0 9899
15	0 09063	153655	64 50	3 50	2.169	2 126	-7.296	0 9919	0 9905
16	0 09625	288033	59 50	3 50	2.113	2.090	-7 573	0 9928	0 9916
17	0 09686	332550	57.50	3 50	2.096	2 065	-7 644	0 9929	0 9917
18	0 09774	421943	56 50	3 50	2.085	2 055	-7.820	0 9931	0 9919
19	0 09784	507163	56 50	3 00	2.085	2.056	-8.157	0 9931	0 9919
20	0 09887	589954	56 00	3 00	2.078	2.055	-8.259	0 9932	0 9920
21	0 09966	784025	55 50	1.00	2.071	2 052	-8 533	0 9933	0 9922
22	0 09968	946852	55.50	1.00	2.071	2 053	-8.957	0 9933	0.9922
23	0 09974	1024242	55 00	1.00	2.067	2 045	-9.120	0 9933	0 9922
24	0 09981	1142356	54 50	1.00	2 063	2 038	-8.895	0 9934	0 9922
25	0 09983	1198016	54 00	1 00	2.058	2.030	-8.936	0 9934	0 9922
26	0 09989	1283866	54 00	1 00	2 058	2 030	-8 816	0 9934	0 9922
27	0.10034	1377746	53.50	2.00	2.053	2.025	-8.714	0 9934	0 9923
28	0 10038	1560186	53 50	2 00	2.052	2.025		0 9934	0 9923
29	0.10086	1631255	53 00	2.00	2.047	2.021		0 9935	0 9923
30	0.10094	1719408	53.00	2.00	2.046	2.021		0 9935	0 9924

thickness h = 3 76 mm (24 plies)
width B = 24.54 mm
L_1 (Figure 4.4) = 11.03 mm
L_2 (Figure 4 4) = 9 15 mm
frequency, f = 1 Hz
DR = 0 1
MD = 2.4 mm
Test temperature = 23 °C (air)
Test machine control mode: Displ.

All symbols and abbreviations shown are as defined in the nomenclature.

Table A11. Mode I fatigue data obtained from a DCB joint made from a thermosetting composite substrate (i.e "913C XAS-5-47%") bonded with a one-part hot-cure epoxy film adhesive (i.e "FM73M").

Notes:
Comparison with Table A6 shows the effect of the type of adhesive.

Specimen number 122

	1	2	3	4	5	6	7	8	9
1	crack length	no of cycles	max load	min load	log Gmax (displ)	log Gmax (corr)	log da/dN	Z	F
2	a	N	Pmax	Pmin				correction	correction
3	(m)		(N)	(N)	(kJ/m^2)	(kJ/m^2)	(m/cycle)	factor	factor
4									
5	0.04183	2700	733.00	165.00	3.135	3.139		0.9713	0.9758
6	0.04298	10000	668.00	143.00	3.083	3.070		0.9742	0.9778
7	0.04474	18000	644.50	137.50	3.056	3.054		0.9766	0.9787
8	0.04587	26300	604.50	130.50	3.022	3.008	0.758	0.9778	0.9807
9	0.04714	34200	588.00	126.50	2.998	2.983	0.868	0.9792	0.9817
10	0.04907	45000	566.50	123.00	2.975	2.962	7.025	0.9811	0.9831
11	0.04988	57000	541.50	118.50	2.961	2.952	7.209	0.9818	0.9838
12	0.05068	81000	517.50	114.00	2.928	2.920	7.389	0.9824	0.9841
13	0.05129	100200	503.00	111.50	2.911	2.903	-7.525	0.9829	0.9845
14	0.05231	141000	480.00	109.50	2.895	2.892	7.663	0.9837	0.9851
15	0.05400	300000	480.00	84.50	2.787	2.779	7.764	0.9868	0.9870
16	0.05483	446500	387.00	84.00	2.780	2.784	-7.875	0.9865	0.9874
17	0.05564	597500	388.00	83.00	2.781	2.787	7.988	0.9870	0.9882
18	0.05630	672000	380.00	82.50	2.748	2.757	-8.052	0.9877	0.9884
19	0.05641	848000	364.50	80.00	2.713	2.711	8.210	0.9882	0.9888
20	0.05272	1271300	329.00	84.00	2.988	2.974	-8.359	0.9892	0.9897
21	0.05432	1587200	318.50	82.00	2.944	2.881	-8.432	0.9898	0.9902
22	0.05544	2078300	306.50	81.00	2.625	2.648	8.497	0.9902	0.9906
23	0.05712	2818700	286.00	80.50	2.602	2.640	-8.614	0.9907	0.9910
24	0.05851	3500000	268.50	81.50	2.583	2.633	8.757	0.9911	0.9913
25	0.05983	4063000	273.00	82.00	2.556	2.618	-8.842	0.9915	0.9917
26	0.07000	5004000	265.00	79.00	2.539	2.586	-8.957	0.9918	0.9918
27	0.07000	5511900	250.00	78.00	2.526	2.577	-8.996	0.9918	0.9919
28	0.07131	6047700	252.50	76.00	2.516	2.560	9.048	0.9919	0.9920
29	0.07187	6403400	247.00	74.00	2.504	2.548	9.155	0.9921	0.9921
30	0.07200	7595000	242.00	75.00	2.492	2.540	9.302	0.9922	0.9923
31	0.07200	8463100	241.00	75.00	2.490	2.538	9.627	0.9922	0.9923
32	0.07274	8885000	240.50	74.00	2.489	2.537	9.819	0.9923	0.9923
33	0.07277	9747700	240.50	74.00	2.488	2.537	-10.269	0.9923	0.9923
34	0.07278	10668000	240.00	73.00	2.488	2.536	10.435	0.9923	0.9923
35	0.07283	11471300	240.00	74.00	2.488	2.536	-10.602	0.9923	0.9923
36	0.07285	12503300	239.50	73.00	2.487	2.535	-10.748	0.9923	0.9923
37	0.07288	14497800	239.50	73.00	2.487	2.535	-10.993	0.9923	0.9923
38	0.07287	16632100	239.50	73.00	2.487	2.535		0.9923	0.9923
39	0.07290	18235500	239.00	73.00	2.486	2.533		0.9923	0.9923
40	0.07290	19113400	238.50	72.50	2.485	2.531		0.9923	0.9923

Table A13. Mode I fatigue data obtained from a DCB joint made from a thermosetting composite substrate (i.e "913C XAS-5-47%") bonded with a one-part hot-cure epoxy film adhesive (i.e" FM73M").

Notes:

Comparison with Table A7 shows the effect of substrate thickness (see Figure 5.10a) and with Table A16 shows the effect of the type of substrate (see Figure 5.11a).

thickness h = 7.88 mm (48 plies)
width B = 22.69 mm
L_1 (Figure 4.4) = 13.16 mm
L_2 (Figure 4.4) = 9.22 mm
frequency, f = 5 Hz
DR = 0.5
MD = 1.5 mm
Test temperature = 23 °C (air)
Test machine control mode: Displ.

All symbols and abbreviations shown are as defined in the nomenclature.

Specimen number 119

	1	2	3	4	5	6	7	8	9
1	crack length	no of cycles	max load	min load	log Gmax (displ)	log Gmax (com)	log da/dN	Z	F
2	a	N	Pmax	Pmin				correction	correction
3	(m)		(N)	(N)	(kJ/m^2)	(kJ/m^2)	(m/cycle)	factor	factor
4									
5	0 07160	1588	361 30	4 90	2 790	2 766		0 9915	0 9914
6	0 07260	21220	339 10	4 00	2 758	2 746		0 9917	0 9916
7	0 07310	26447	330 00	2 40	2 743	2 741		0 9919	0 9918
8	0 07360	36620	325 80	4 00	2 734	2 742	7 210	0 9920	0 9919
9	0 07430	47842	317 30	4 10	2 720	2 743	7 185	0 9922	0 9920
10	0 07550	66358	312 70	4 30	2 708	2 759	-7 225	0 9924	0 9923
11	0 07606	78428	299 60	5 10	2 686	2 734	-7 307	0 9925	0 9924
12	0 07650	82530	297 10	4 80	2 680	2 736	-7 336	0 9926	0 9925
13	0 07710	101550	290 70	5 00	2 667	2 730	-7 441	0 9928	0 9926
14	0 07780	114647	284 20	5 10	2 655	2 722	-7 498	0 9929	0 9927
15	0 07934	178600	266 50	4 80	2 619	2 690	-7 594	0 9932	0 9930
16	0 08282	388123	232 20	3 40	2 544	2 606	-7 875	0 9938	0 9936
17	0 08414	417436	227 50	4 80	2 528	2 596	-7 865	0 9940	0 9938
18	0 08456	487530	223 40	4 80	2 519	2 582	-7 949	0 9941	0 9938
19	0 08466	561958	219 40	5 20	2 510	2 567	-8 151	0 9941	0 9939
20	0 08658	642258	203 50	5 40	2 469	2 507	-8 292	0 9944	0 9941
21	0 08678	916810	202 20	5 10	2 465	2 502	-8 290	0 9944	0 9941
22	0 08860	1348346	189 40	3 30	2 429	2 445	-8 356	0 9947	0 9944
23	0 08956	1741475	178 90	-1 10	2 397	2 389	-8 438	0 9949	0 9946
24	0 09162	2133126	172 80	-1 40	2 378	2 353	-8 530	0 9951	0 9948
25	0 09274	2599025	169 30	-1 50	2 364	2 328	-8 742	0 9952	0 9949
26	0 09340	2725223	167 30	-1 60	2 358	2 312	-8 716	0 9953	0 9950
27	0 09348	3818192	164 70	-1 10	2 349	2 297	-8 768	0 9953	0 9950
28	0 09350	3440775	162 20	-1 10	2 342	2 284	-8 765	0 9953	0 9950
29	0 09488	3883441	161 50	-1 00	2 335	2 265	-8 753	0 9954	0 9951
30	0 09712	4770520	156 20	5 00	2 318	2 215	8 745	0 9956	0 9953
31	0 09870	6054710	152 20	-7 20	2 295	2 151	8 824	0 9958	0 9955
32	0 09936	6602926	151 30	-2 10	2 289	2 133		0 9959	0 9955
33	0 10098	8240655	139 40	5 10	2 248	2 020		0 9960	0 9957
34	0 10228	9241562 00	137 60	-4 50	2 236	1 968		0 9961	0 9958

thickness h = 7 55 mm (48 plies)
width B = 22 80 mm
L_1 (Figure 4 4) = 13 02 mm
L_2 (Figure 4.4) = 9 25 mm
frequency, f = 5 Hz
DR = 0.1
MD = 1 5 mm
Test temperature = 23 °C (air)
Test machine control mode: Displ.

All symbols and abbreviations shown are as defined in the nomenclature.

Table A12. Mode I fatigue data obtained from a DCB joint made from a thermosetting composite substrate (i.e "913C XAS-5-47%") bonded with a one-part hot-cure epoxy film adhesive (i.e "FM73M").

Notes:
Comparison with Table A13 shows the effect of displacement ratio (see Figure 5.7a).

Specimen number 125

	Column 1	Column 2	Column 3	Column 4	Column 5	Column 6	Column 7	Column 8	Column 9
1	crack length	no of cycles	max load	min load	log Gmax (displ)	log Gmax (corr)	log da/dN	Z	F
2	a	N	Pmax	Pmin				correction	correction
3	(m)		(N)	(N)	(kJ/m^2)	(kJ/m^2)	(m/cycle)	factor	factor
4									
5	0.04064	912	666.20	254.10	3.161	2.729		0.9917	0.9936
6	0.05258	1600	646.40	236.20	3.135	2.819		0.9930	0.9954
7	0.06306	2978	562.30	210.10	3.003	2.874		0.9943	0.9957
8	0.06400	5978	526.40	193.10	3.029	2.866	-6.041	0.9955	0.9967
9	0.06652	10000	467.00	170.00	2.949	2.817	-6.082	0.9970	0.9986
10	0.06824	12000	454.00	165.60	2.932	2.811	-6.130	0.9982	0.9988
11	0.06248	12000	446.80	161.80	2.911	2.846	6.138	0.9991	0.9996
12	0.06306	16160	410.40	151.20	2.876	2.815	6.274	0.9996	0.9998
13	0.06470	18040	400.10	144.20	2.851	2.805	6.308	0.9999	0.9994
14	0.06668	22310	384.70	138.30	2.828	2.876	-6.564	0.9993	0.9998
15	0.06834	34634	346.20	123.20	2.766	2.823	6.714	0.9912	0.9914
16	0.06864	43320	322.60	114.10	2.730	2.778	6.818	0.9915	0.9917
17	0.07101	63060	303.00	108.00	2.696	2.745	6.938	0.9919	0.9920
18	0.07306	76636	284.80	100.10	2.663	2.709	7.060	0.9921	0.9923
19	0.07306	87033	271.30	94.20	2.637	2.668	-7.170	0.9924	0.9924
20	0.07418	104250	267.20	90.50	2.606	2.632	-7.237	0.9926	0.9927
21	0.07624	122610	248.00	86.70	2.567	2.618	7.268	0.9928	0.9929
22	0.07618	136500	242.20	83.00	2.572	2.596	-7.344	0.9931	0.9930
23	0.07756	175762	230.10	78.00	2.542	2.562	-7.497	0.9933	0.9933
24	0.08169	300146	202.70	68.90	2.467	2.477	-7.782	0.9941	0.9940
25	0.08266	466060	187.60	67.40	2.452	2.458	-7.836	0.9942	0.9941
26	0.08387	630300	182.20	65.80	2.436	2.439	-7.910	0.9944	0.9942
27	0.08467	801866	180.00	63.90	2.421	2.423	-8.108	0.9945	0.9944
28	0.08581	843516	170.20	60.50	2.393	2.381	8.300	0.9947	0.9945
29	0.08675	1342176	174.60	67.00	2.380	2.386	-8.685	0.9948	0.9948
30	0.08684	1748736	174.00	66.20	2.378	2.383	-8.826	0.9948	0.9947
31	0.08748	2341866	173.60	67.40	2.374	2.382	-9.246	0.9948	0.9947
32	0.08788	3639824	173.20	64.00	2.373	2.381	-8.887	0.9948	0.9947
33	0.08788	4414678	172.60	63.40	2.371	2.358	-9.918	0.9948	0.9947
34	0.08789	5364088	172.20	66.40	2.370	2.356	-10.318	0.9948	0.9948
35	0.08778	6188988	170.60	61.80	2.368	2.348	-10.613	0.9948	0.9948
36	0.08778	7838112	168.40	60.70	2.360	2.337	-10.888	0.9949	0.9948
37	0.08772	8788047	168.00	60.40	2.358	2.329	-11.165	0.9949	0.9948
38	0.08772	9875878	168.00	62.40	2.356	2.327	-11.212	0.9949	0.9948
39	0.08773	10881232	168.00	48.20	2.355	2.327	11.068	0.9949	0.9948
40	0.08774	12785568	168.40	48.20	2.355	2.328	-10.936	0.9949	0.9948
41	0.08774	13965888	168.20	48.20	2.355	2.326	-10.885	0.9949	0.9948
42	0.08778	14113122.00	168.00	48.20	2.353	2.324	-10.850	0.9949	0.9948
43	0.08780	16146322.00	168.00	48.40	2.352	2.322		0.9949	0.9948
44	0.08781	17416896.00	168.20	48.20	2.351	2.320		0.9949	0.9948
45	0.08784	17943821.00	168.20	48.20	2.351	2.320		0.9949	0.9948

Table A14. Mode I fatigue data obtained from a DCB joint made from a thermosetting composite substrate (i.e "913C XAS-5-47%") bonded with a two-part cold-cure epoxy paste adhesive (i.e "9309.3NA").

Notes
Comparison with Table A15 shows the effect of testing in water (see Figure 6.1a).

thickness h = 7.67 mm (48 plies)
width B = 22.20 mm
L_1 (Figure 4.4) = 13.05 mm
L_2 (Figure 4.4) = 9.22 mm
frequency, f = 5 Hz
DR = 0.5
MD = 1.5 mm
Temperature = in water at 25 °C
Test machine control mode: Displ.

All symbols and abbreviations shown are as defined in the nomenclature.

Specimen number 128

	1	2	3	4	5	6	7	8	9
1	crack length	no of cycles	max load	min load	log Gmax (displ)	log Gmax (corr)	log da/dN	Z	F
2	a	N	Pmax	Pmin				correction	correction
3	(m)		(N)	(N)	(kJ/m^2)	(kJ/m^2)	(m/cycle)	factor	factor
4									
5	0.06000	000	600.30	261.30	2.049	2.067		0.9880	0.9878
6	0.06040	5030	537.00	232.20	2.000	2.050		0.9877	0.9884
7	0.06100	13320	480.00	208.00	2.017	2.052		0.9888	0.9893
8	0.06314	18650	456.40	198.20	2.007	2.065	-6.546	0.9893	0.9897
9	0.06400	24000	429.40	187.30	2.002	2.038	-6.656	0.9898	0.9903
10	0.06600	30000	416.10	181.30	2.033	2.025	-6.689	0.9902	0.9906
11	0.06714	36647	398.20	168.20	2.793	2.779	-6.776	0.9907	0.9908
12	0.06900	51414	394.10	158.80	2.787	2.763	6.875	0.9913	0.9914
13	0.07064	63000	340.40	151.70	2.731	2.736	-6.961	0.9917	0.9918
14	0.07100	72730	340.20	140.10	2.714	2.720	-7.021	0.9919	0.9920
15	0.07314	86430	320.70	140.00	2.681	2.693	-7.103	0.9923	0.9924
16	0.07404	116000	300.00	134.00	2.657	2.666	7.303	0.9926	0.9925
17	0.07800	140000	293.10	120.70	2.628	2.644	-7.399	0.9929	0.9929
18	0.08100	304347	254.60	100.30	2.604	2.618	-7.721	0.9940	0.9938
19	0.08200	442436	229.00	90.70	2.489	2.508	-7.742	0.9942	0.9941
20	0.08334	519000	223.60	86.30	2.476	2.488	7.816	0.9943	0.9941
21	0.08434	586662	218.30	83.00	2.460	2.477	-8.011	0.9944	0.9943
22	0.08664	662040	203.40	80.40	2.418	2.437	-8.140	0.9947	0.9946
23	0.08820	1318343	187.00	78.00	2.373	2.390	-8.269	0.9951	0.9949
24	0.09002	1746823	178.00	76.30	2.344	2.358	-8.385	0.9952	0.9950
25	0.09110	1867400	176.00	74.30	2.337	2.361	-8.406	0.9953	0.9951
26	0.09272	2154815	166.10	70.50	2.313	2.330	-8.461	0.9955	0.9952
27	0.09374	2711823	162.70	68.70	2.292	2.306	-8.518	0.9956	0.9953
28	0.09620	3472823	152.50	61.20	2.254	2.268	-8.650	0.9958	0.9956
29	0.09820	4021000	144.50	58.50	2.223	2.238	-8.877	0.9960	0.9958
30	0.09940	5267970	142.50	58.30	2.216	2.228	-8.896	0.9960	0.9958
31	0.09996	5697790	140.50	57.50	2.207	2.220	9.008	0.9961	0.9958
32	0.09940	6774150	140.30	58.00	2.206	2.222	-8.033	0.9961	0.9958
33	0.09960	6230740	138.70	56.40	2.203	2.218	-9.013	0.9961	0.9958
34	0.09994	7017712	133.70	53.00	2.183	2.183	-9.152	0.9961	0.9958
35	0.10104	7470840	132.10	53.30	2.173	2.181	-9.330	0.9962	0.9960
36	0.10150	8060710	131.10	53.00	2.166	2.178	-9.649	0.9963	0.9960
37	0.10180	13626705	130.50	53.00	2.165	2.177		0.9963	0.9961
38	0.10200	19703467	130.00	53.00	2.162	2.176		0.9963	0.9961
39	0.10210	24370000	130.00	53.00	2.162	2.176		0.9963	0.9961

Table A15. Mode I fatigue data obtained from a DCB joint made from a thermosetting composite substrate (i.e "913C XAS-5-47%") bonded with a two-part cold-cure epoxy paste adhesive (i.e "9309.3NA").

Notes:
Comparison with Table A13 shows the effect of type of adhesive (see Figure 5.9a) and with Table A14 shows the effect of testing in water (see Figure 6.2a).

thickness h = 7.95 mm (48 plies)
width B = 23.36 mm
L_1 (Figure 4.4) = 13.23 mm
L_2 (Figure 4.4) = 9.25 mm
frequency, f = 5 Hz
DR = 0.5
MD = 1.5 mm
Test temperature = 23 °C (air)
Test machine control mode: Displ.

All symbols and abbreviations shown are as defined in the nomenclature.

Specimen number 130

	1	2	3	4	5	6	7	8	9
1	crack length	no of cycles	max load	min load	log Gmax (displ)	log Gmax (com)	log da/dN	Z	F
2	a	N	Pmax	Pmin				correction	correction
3	(m)		(N)	(N)	(kJ/m^2)	(kJ/m^2)	(m/cycle)	factor	factor
4									
5	0 04186	2300	625 00	126 00	3 208	3 064		0 9730	0 9779
6	0 04252	5600	606 50	115 00	3 189	2 910		0 9739	0 9786
7	0 04302	15000	574 00	106 00	3 154	2 803		0 9758	0 9799
8	0 04432	22000	550 00	98 00	3 132	2 755	6 964	0 9764	0 9803
9	0 04555	30100	541 00	99 00	3 116	2 718	-7 022	0 9770	0 9813
10	0 04607	40000	527 00	97 00	3 100	2 575	-7 091	0 9784	0 9817
11	0 04685	51700	506 50	90 50	3 077	2 539	-7 130	0 9793	0 9824
12	0 04774	61900	492 00	90 00	3 058	2 272	7 256	0 9801	0 9830
13	0 04920	87600	464 00	87 00	3 022	2 258	-7 435	0 9815	0 9840
14	0 04953	107600	461 50	85 00	3 008	2 250	-7 541	0 9818	0 9842
15	0 05482	402000	356 00	74 00	2 869	2 247	-7 894	0 9856	0 9871
16	0 05547	522700	328 00	68 00	2 829	2 240	-7 971	0 9860	0 9874
17	0 05588	591300	327 00	67 00	2 825	2 226	8 025	0 9862	0 9876
18	0 05720	846500	302 00	62 00	2 782	2 194	8 247	0 9869	0 9882
19	0 06067	1352600	271 00	57 00	2 717	2 179	-8 359	0 9883	0 9893
20	0 06144	1736100	251 00	53 00	2 676	2 174	-8 378	0 9889	0 9897
21	0 06207	2121100	240 00	52 00	2 653	2 174	8 413	0 9892	0 9899
22	0 06330	2288500	233 50	49 00	2 634	2 166	8 470	0 9896	0 9903
23	0 06489	2556000	226 00	47 00	2 610	2 147	-8 476	0 9902	0 9908
24	0 06581	2967600	211 50	48 00	2 577	2 136	-8 534	0 9905	0 9911
25	0 06643	3387800	208 50	44 00	2 567	2 106	-8 589	0 9907	0 9912
26	0 06730	3869500	200 00	41 00	2 544	2 089	-8 619	0 9910	0 9914
27	0 06800	4331900	194 00	40 00	2 527	2 087	8 632	0 9912	0 9916
28	0 06839	4738300	191.00	40 00	2 518	2 091	-8 628	0 9913	0 9917
29	0 06909	5254700	188 50	42 00	2 509	2 091	-8 619	0 9915	0 9919
30	0 06975	5812200	186 50	42 00	2 500	2 088	-8 627	0 9917	0 9920
31	0 07048	6443900	182 00	42 00	2 486	2 078	8 668	0 9919	0 9922
32	0 07123	6467900	182 00	42 00	2 482	2 075		0 9921	0 9924
33	0 07165	6952900	180 00	42 00	2 475	2 060		0 9922	0 9924
34	0 07177	7701400	180 00	42 00	2 474	2 048		0 9922	0 9925

Table A16. Mode I fatigue data obtained from a DCB joint made from a thermoplastic composite substrate (i.e "APC-2" bonded with a one-part hot-cure epoxy film adhesive (i.e "FM73M").

Notes:
Comparison with Table A13 shows the effect of type of substrate (see *Figure* 5.11a).

thickness h = 6 34 mm (48 plies)
width B = 21.50 mm
L_1 (Figure 4 4) = 12.52 mm
L_2 (Figure 4.4) = 9.36 mm
frequency, f = 5 Hz
DR = 0.5
MD = 1.5 mm
Test temperature = 23 °C (air)
Test machine control mode: Displ.

All symbols and abbreviations shown are as defined in the nomenclature.

Specimen number 132

	1	2	3	4	5	6	7	8	9
1	crack length	no of cycles	max load	min load	log Gmax (displ)	log Gmax (corr)	log da/dN	Z	F
2	a	N	Pmax	Pmin				correction	correction
3	(m)		(N)	(N)	(kJ/m^2)	(kJ/m^2)	(m/cycle)	factor	factor
4									
5	0.04580	2156	836.80	303.10	3.216	3.291		0.9788	0.9818
6	0.04720	2778	788.00	286.20	3.178	3.266		0.9803	0.9829
7	0.04866	4243	713.60	260.00	3.126	3.193		0.9816	0.9838
8	0.04932	5467	684.20	248.80	3.106	3.184	0.131	0.9822	0.9843
9	0.05137	8078	644.10	233.90	3.066	3.137	0.292	0.9836	0.9856
10	0.05306	13140	581.60	212.60	3.011	3.068	0.466	0.9849	0.9864
11	0.05518	26423	521.70	190.90	2.951	2.996	0.748	0.9862	0.9874
12	0.05582	32627	507.10	181.80	2.929	2.980	-0.848	0.9866	0.9878
13	0.05636	38833	494.90	175.00	2.912	2.965	-0.931	0.9868	0.9880
14	0.05646	51376	486.40	167.40	2.902	2.929	7.903	0.9870	0.9880
15	0.05694	74306	438.90	154.00	2.841	2.875	-7.136	0.9880	0.9893
16	0.06144	99798	406.20	146.50	2.806	2.836	7.264	0.9892	0.9900
17	0.06224	132500	384.20	138.80	2.777	2.797	-7.408	0.9895	0.9901
18	0.06320	164478	373.90	134.00	2.760	2.781	-7.488	0.9899	0.9904
19	0.06420	181178	367.90	126.30	2.736	2.762	7.534	0.9903	0.9907
20	0.06493	211788	348.40	124.70	2.722	2.736	7.568	0.9906	0.9909
21	0.06912	411820	290.80	100.70	2.639	2.631	7.730	0.9918	0.9920
22	0.07000	462060	282.30	100.60	2.618	2.618	-7.767	0.9920	0.9922
23	0.07060	524066	283.50	102.20	2.600	2.598	7.799	0.9922	0.9924
24	0.07226	631982	260.30	97.10	2.572	2.642	-7.886	0.9926	0.9927
25	0.07483	868143	246.00	88.20	2.520	2.498	7.943	0.9931	0.9932
26	0.07666	984176	237.70	84.80	2.496	2.481	-7.973	0.9935	0.9936
27	0.08010	1360906	218.20	76.80	2.438	2.413	8.101	0.9941	0.9940
28	0.08363	1866318	193.70	66.00	2.378	2.330	-8.291	0.9948	0.9948
29	0.08412	2258188	191.30	66.00	2.370	2.331	-8.477	0.9947	0.9948
30	0.08474	2762343	188.30	66.40	2.363	2.325	-8.633	0.9948	0.9947
31	0.08507	4518828	186.60	63.90	2.353	2.308	9.493	0.9948	0.9947
32	0.08631	8648078	184.40	63.00	2.348	2.304	-9.758	0.9948	0.9947
33	0.08630	7058578	184.20	63.00	2.348	2.304	-10.036	0.9948	0.9948
34	0.08548	7806482	184.10	62.50	2.347	2.304	-10.181	0.9948	0.9948
35	0.08548	9274998	184.10	65.00	2.347	2.304	-10.507	0.9948	0.9948
36	0.08550	12185000	184.00	65.00	2.347	2.303	-11.318	0.9948	0.9948
37	0.08552	13464125	183.80	60.00	2.346	2.303		0.9948	0.9948
38	0.08553	16124133.00	183.80	60.00	2.346	2.303		0.9948	0.9948
39	0.08554	17431600.00	183.40	40.70	2.346	2.301		0.9948	0.9948

Table A17. Mode I fatigue data obtained from a DCB joint made from a thermoplastic composite substrate (i.e "APC-2") bonded with a one-part hot-cure epoxy film adhesive (i.e "FM73M").

Notes:
Comparison with Tables A16 and A20 shows the effect of testing in water at 25 °C (see Figure 6.3a).

thickness h = 6.16 mm (48 plies)
width B = 23.96 mm
L_1 (Figure 4.4) = 12.35 mm
L_2 (Figure 4.4) = 9.15 mm
frequency, f = 5 Hz
DR = 0.5
MD = 1.5 mm
Test temperature = water at 25 °C
Test machine control mode: Displ.

All symbols and abbreviations shown are as defined in the nomenclature.

Specimen number 134

	1	2	3	4	5	6	7	8	9
1	crack length	no of cycles	max load	min load	log Gmax (displ)	log Gmax (corr)	log da/dN	Z	F
2	a	N	Pmax	Pmin				correction	correction
3	(m)		(N)	(N)	(kJ/m^2)	(kJ/m^2)	(m/cycle)	factor	factor
4									
5	0.04670	1910	661.40	196.00	3.122	3.075		0.9799	0.9826
6	0.04770	2606	631.00	186.50	3.095	3.048		0.9806	0.9832
7	0.04986	4046	584.50	169.00	3.047	3.009		0.9827	0.9847
8	0.05074	4686	563.80	162.30	3.026	2.990	-5.919	0.9833	0.9852
9	0.05186	5668	540.80	155.30	2.999	2.971	-5.951	0.9842	0.9858
10	0.05277	6614	524.10	150.10	2.981	2.955	-5.988	0.9848	0.9863
11	0.05381	8018	506.80	143.60	2.960	2.936	-6.225	0.9853	0.9867
12	0.05462	10030	494.50	137.20	2.936	2.913	-6.409	0.9859	0.9872
13	0.05568	14220	480.30	132.80	2.912	2.894	-6.545	0.9866	0.9878
14	0.05623	17118	463.30	129.00	2.896	2.879	-6.614	0.9868	0.9879
15	0.05690	19918	442.30	123.90	2.881	2.867	-6.670	0.9872	0.9882
16	0.05748	22780	432.70	121.40	2.868	2.856	-6.702	0.9875	0.9884
17	0.05786	24868	427.60	120.40	2.860	2.853	-6.736	0.9877	0.9886
18	0.05853	28068	414.20	116.40	2.843	2.833	-6.770	0.9880	0.9889
19	0.05907	37160	362.20	110.40	2.812	2.806	-6.825	0.9888	0.9893
20	0.05962	50630	344.60	96.50	2.740	2.732	-6.984	0.9897	0.9903
21	0.06000	71870	344.20	82.50	2.734	2.745	-7.025	0.9900	0.9905
22	0.06000	78070	328.20	81.10	2.712	2.707	-7.043	0.9901	0.9906
23	0.06010	86670	316.70	80.00	2.696	2.694	-7.095	0.9908	0.9910
24	0.06067	98630	304.60	86.20	2.648	2.674	-7.096	0.9908	0.9912
25	0.06720	117346	290.70	83.10	2.641	2.651	-7.124	0.9912	0.9916
26	0.06810	134945	280.20	78.60	2.628	2.631	-7.166	0.9915	0.9918
27	0.06972	154218	268.70	75.90	2.595	2.618	-7.248	0.9919	0.9921
28	0.07034	162536	266.70	74.20	2.586	2.618	-7.268	0.9921	0.9923
29	0.07230	221346	242.30	68.20	2.536	2.582	-7.401	0.9928	0.9927
30	0.07306	246946	230.80	66.30	2.523	2.551	-7.453	0.9927	0.9928
31	0.07464	271995	231.90	64.10	2.506	2.563	-7.518	0.9931	0.9931
32	0.07510	295255	225.40	62.00	2.491	2.536	-7.606	0.9932	0.9932
33	0.08036	536330	180.80	46.70	2.371	2.411	-7.942	0.9941	0.9941
34	0.08120	730804	177.60	46.50	2.359	2.407	-8.078	0.9943	0.9942
35	0.08166	922618	177.60	47.10	2.356	2.408	8.401	0.9943	0.9943
36	0.08223	1348600	173.80	42.80	2.343	2.396	-9.104	0.9944	0.9944
37	0.08266	2043666	167.80	37.00	2.328	2.373	9.490	0.9945	0.9944
38	0.08275	4266940	170.30	39.30	2.334	2.388	-9.700	0.9945	0.9944
39	0.08282	6610336	168.30	37.40	2.331	2.388		0.9945	0.9944
40	0.08323	7810218	166.20	31.90	2.319	2.388		0.9946	0.9945
41	0.08360	8952967	164.80	27.40	2.314	2.366		0.9946	0.9945

Table A18. Mode I fatigue data obtained from a DCB joint made from a thermoplastic composite substrate (i.e "APC-2") bonded with a one-part hot-cure epoxy film adhesive (i.e "FM73M").

Notes:
Comparison with Tables A21 shows the effect of testing in water at 50 °C (see Figure 6.3b).

thickness h = 6.13 mm (48 plies)
width B = 24.05 mm
L_1 (Figure 4.4) = 12.38 mm
L_2 (Figure 4.4) = 9.20 mm
frequency, f = 5 Hz
DR = 0.5
MD = 1.5 mm
Test temperature = water at 50 °C
Test machine control mode: Displ.

All symbols and abbreviations shown are as defined in the nomenclature.

Specimen number 187

	1	2	3	4	5	6	7	8	9
1	crack length	no of cycles	max load	min load	log Gmax (displ)	log Gmax (corr)	log da/dN	Z	F
2	a	N	Pmax	Pmin				correction	correction
3	(m)		(N)	(N)	(kJ/m^2)	(kJ/m^2)	(m/cycle)	factor	factor
4									
5	0.04437	330	646.50	152.00	3.066	2.720		0.9785	0.9787
6	0.04563	828	601.00	161.90	3.026	2.918		0.9770	0.9807
7	0.04780	1278	582.30	161.00	3.000	2.674		0.9800	0.9823
8	0.04943	1800	563.40	148.90	2.975	2.866	6.824	0.9817	0.9836
9	0.04974	2460	546.20	147.70	2.960	2.817	6.756	0.9818	0.9836
10	0.05147	3060	517.60	144.10	2.927	2.811	6.840	0.9833	0.9848
11	0.05328	5530	492.60	138.20	2.895	2.946	6.120	0.9846	0.9858
12	0.05528	10040	448.00	130.30	2.843	2.915	6.318	0.9858	0.9868
13	0.05692	12580	431.60	127.00	2.823	2.895	-6.411	0.9863	0.9872
14	0.05732	16060	411.20	123.10	2.795	2.878	-6.514	0.9870	0.9878
15	0.05784	18040	403.30	121.30	2.784	2.823	-6.552	0.9873	0.9881
16	0.05967	24760	378.10	117.00	2.748	2.778	-6.614	0.9888	0.9887
17	0.06020	28410	368.00	113.20	2.733	2.745	-6.666	0.9884	0.9890
18	0.06070	31180	361.40	110.60	2.721	2.706	-6.704	0.9886	0.9892
19	0.06106	36460	353.00	107.00	2.705	2.668	-6.766	0.9891	0.9896
20	0.06304	46330	340.30	103.00	2.684	2.632	-6.888	0.9896	0.9899
21	0.06469	66590	319.00	101.00	2.647	2.610	7.074	0.9902	0.9905
22	0.06561	77760	311.00	97.10	2.633	2.600	7.154	0.9905	0.9908
23	0.06647	81561	302.00	94.50	2.617	2.662	-7.234	0.9907	0.9909
24	0.06737	110400	293.10	91.10	2.598	2.477	-7.382	0.9910	0.9912
25	0.06867	144010	280.70	85.90	2.574	2.468	-7.575	0.9913	0.9915
26	0.06957	166600	271.70	82.30	2.556	2.439	-7.733	0.9916	0.9917
27	0.07208	305460	242.00	73.20	2.495	2.423	7.926	0.9922	0.9923
28	0.07362	557736	234.00	70.60	2.474	2.381	8.103	0.9926	0.9926
29	0.07503	856070	224.20	66.50	2.448	2.366	8.312	0.9928	0.9929
30	0.07523	1032020	221.30	67.00	2.442	2.363	8.478	0.9928	0.9928
31	0.07663	1415113	210.70	66.00	2.436	2.362	-8.692	0.9931	0.9931
32	0.07671	1618888	206.60	67.50	2.466	2.361	-8.885	0.9932	0.9932
33	0.07710	2312260	206.60	67.40	2.402	2.360	8.043	0.9933	0.9933
34	0.07742	3106500	201.30	65.00	2.392	2.360	-8.328	0.9934	0.9933
35	0.07778	4873982	197.70	61.70	2.383	2.348	8.671	0.9934	0.9934
36	0.07779	5400372	194.80	60.50	2.378	2.337	-8.677	0.9934	0.9934
37	0.07807	6662478	194.70	60.50	2.378	2.328	8.686	0.9935	0.9934
38	0.07819	7526816	193.30	49.60	2.371	2.327	8.678	0.9936	0.9936
39	0.07872	9667782	189.30	47.00	2.362	2.327		0.9936	0.9936
40	0.07882	9100316	188.40	47.40	2.360	2.326		0.9937	0.9934
41	0.07896	9878420	188.10	47.00	2.358	2.326		0.9937	0.9936

Table A19. Mode I fatigue data obtained from a DCB joint made from a thermosetting composite substrate (i.e 913C XAS-5-47%) bonded with a two-part cold-cure epoxy paste adhesive (i.e "9309.3NA").

Notes:

thickness h = 7.35 mm (48 plies)
width B = 23.45 mm
L_1 (Figure 4.4) = 12.81 mm
L_2 (Figure 4.4) = 9.12 mm
frequency, f = 5 Hz
DR = 0.5
MD = 1.5 mm

Test temperature = water at 50 °C
Test machine control mode: Displ.

All symbols and abbreviations shown are as defined in the nomenclature.

Specimen number 100

	1	2	3	4	5	6	7	8	9
1	crack length	no of cycles	max load	min load	log Gmax (dapt)	log Gmax (exam)	log da/dN	Z	F
2	a	N	Pmax	Pmin				correction	correction
3	(m)		(N)	(N)	(kJ/m^2)	(kJ/m^2)	(m/cycle)	factor	factor
4									
5	0.04858	1858	813.20	285.90	3.259	3.291		0.9808	0.9828
6	0.05010	2600	785.20	229.90	3.232	3.256		0.9822	0.9838
7	0.05048	3126	772.40	224.00	3.222	3.192		0.9826	0.9841
8	0.05084	5208	731.80	211.90	3.194	3.184	-8.303	0.9828	0.9844
9	0.05100	6897	716.40	208.00	3.178	3.137	-8.410	0.9834	0.9848
10	0.05274	8885	697.40	199.10	3.154	3.066	-8.404	0.9842	0.9854
11	0.05460	14615	627.60	180.00	3.100	2.996	-8.473	0.9853	0.9864
12	0.05607	18200	604.40	174.00	3.074	2.969	-8.668	0.9862	0.9871
13	0.05748	24462	581.40	168.20	3.047	2.946	-8.738	0.9870	0.9877
14	0.05781	29864	580.80	164.10	3.036	2.929	-8.872	0.9870	0.9878
15	0.05831	35714	566.70	161.60	3.021	2.875	-7.047	0.9874	0.9881
16	0.05871	43037	543.40	158.20	3.000	2.836	-7.214	0.9878	0.9883
17	0.05928	51952	511.80	154.30	2.970	2.787	-7.227	0.9879	0.9885
18	0.05967	62400	513.40	148.00	2.978	2.761	-7.241	0.9880	0.9886
19	0.06007	75010	487.00	143.10	2.962	2.752	7.218	0.9882	0.9887
20	0.06103	93400	466.30	134.50	2.923	2.736	-7.270	0.9888	0.9893
21	0.06241	98510	466.80	132.40	2.912	2.631	-7.330	0.9892	0.9896
22	0.06301	112100	452.40	130.20	2.901	2.618	-7.490	0.9894	0.9898
23	0.06364	150700	428.80	125.10	2.875	2.588	-7.667	0.9897	0.9900
24	0.06703	369860	369.80	107.00	2.788	2.662	7.877	0.9906	0.9910
25	0.06817	442060	356.80	104.80	2.768	2.498	-7.933	0.9911	0.9913
26	0.06848	514785	352.60	106.70	2.760	2.481	-7.986	0.9912	0.9914
27	0.06921	567806	346.30	104.30	2.750	2.413	-8.168	0.9914	0.9916
28	0.07006	830730	317.00	93.90	2.698	2.338	8.391	0.9919	0.9920
29	0.07220	1378934	290.80	81.10	2.668	2.331	8.536	0.9922	0.9922
30	0.07292	1842334	286.60	80.20	2.643	2.326	8.648	0.9924	0.9924
31	0.07383	2270200	270.00	82.90	2.613	2.306	8.726	0.9926	0.9926
32	0.07402	3177840	264.30	76.00	2.602	2.304	8.726	0.9926	0.9926
33	0.07760	4062040	230.00	72.50	2.540	2.304	8.843	0.9934	0.9933
34	0.07767	4208810	230.20	71.50	2.535	2.304	8.997	0.9934	0.9933
35	0.07773	4600250	233.00	70.70	2.530	2.304	9.065	0.9934	0.9933
36	0.07778	4991274	233.00	69.90	2.526	2.303	9.814	0.9934	0.9933
37	0.07782	5611046	232.70	69.90	2.526	2.303	-10.117	0.9934	0.9933
38	0.07786	6877458	232.30	69.60	2.527	2.303	10.374	0.9934	0.9933
39	0.07790	7311050	231.90	69.90	2.526	2.301	-10.575	0.9934	0.9933
40	0.07792	8000460	231.70	69.30	2.526	2.526	-10.661	0.9934	0.9933
41	0.07794	10406784	231.50	69.10	2.525	2.525		0.9934	0.9933
42	0.07797	12003467	231.20	68.70	2.524	2.524		0.9934	0.9933
43	0.07801	16003784	230.80	68.40	2.523	2.523		0.9934	0.9933

Table A20. Mode I fatigue data obtained from a DCB joint made from a thermosetting composite substrate (i.e 913C XAS-5-47%) bonded with a one-part hot-cure epoxy film adhesive (i.e "FM73M").

Notes:
- thickness h = 7.42 mm (40 plies)
- width B = 24.81 mm
- L_1 (Figure 4.4) = 13.06 mm
- L_2 (Figure 4.4) = 9.16 mm
- frequency, f = 5 Hz
- DR = 0.5
- MD = 1.5 mm

Test temperature = water at 25 °C
Test machine control mode: Displ.

All symbols and abbreviations shown are as defined in the nomenclature.

Specimen number 170

	1	2	3	4	5	6	7	8	9
1	crack length	no of cycles	max load	min load	log Gmax (displ)	log Gmax (calm)	log da/dN	Z	F
2	a	N	Pmax	Pmin				correction	correction
3	(m)		(N)	(N)	(kJ/m^2)	(kJ/m^2)	(m/cycle)	factor	factor
4									
5	0.04136	1764	848.00	216.50	3.204	3.115		0.9720	0.9783
6	0.04378	2200	812.70	207.40	3.169	3.127		0.9755	0.9788
7	0.04418	2613	793.70	201.30	3.156	3.115		0.9760	0.9792
8	0.04480	2990	778.20	198.20	3.143	3.110	5.686	0.9769	0.9799
9	0.04536	3298	766.60	182.20	3.133	3.107	5.829	0.9775	0.9803
10	0.04636	3880	736.30	184.20	3.111	3.093	5.858	0.9788	0.9811
11	0.04780	5217	706.00	172.30	3.082	3.078	-6.006	0.9800	0.9822
12	0.04872	6246	676.80	162.30	3.058	3.067	6.133	0.9809	0.9829
13	0.04944	6298	647.90	150.90	3.034	3.029	6.334	0.9816	0.9834
14	0.05020	10066	621.50	144.20	3.011	3.006	-6.490	0.9821	0.9838
15	0.05060	13670	606.70	136.60	2.992	2.986	6.582	0.9827	0.9843
16	0.05254	20048	566.30	126.70	2.952	2.950	6.895	0.9838	0.9853
17	0.05366	26870	540.00	120.90	2.930	2.934	6.770	0.9846	0.9858
18	0.05411	30730	526.80	117.60	2.918	2.923	-6.848	0.9850	0.9861
19	0.05524	42176	506.30	112.00	2.902	2.908	-7.011	0.9857	0.9867
20	0.05580	51447	491.10	108.10	2.875	2.884	-7.090	0.9861	0.9870
21	0.05646	58629	478.70	106.30	2.862	2.868	7.125	0.9864	0.9873
22	0.05720	66765	466.00	104.00	2.848	2.858	7.189	0.9868	0.9876
23	0.05780	81283	451.80	101.70	2.829	2.837	7.217	0.9871	0.9878
24	0.05878	94000	437.40	97.80	2.810	2.819	7.243	0.9876	0.9883
25	0.05942	110256	424.60	95.00	2.793	2.801	-7.298	0.9879	0.9885
26	0.06074	129462	412.20	91.80	2.773	2.781	-7.366	0.9884	0.9890
27	0.06140	144000	402.20	87.60	2.759	2.778	-7.636	0.9887	0.9892
28	0.06200	164013	387.30	84.90	2.748	2.753	-7.652	0.9890	0.9895
29	0.06302	372710	326.40	66.40	2.645	2.647	-7.886	0.9904	0.9907
30	0.06390	466300	306.60	66.30	2.602	2.620	-7.864	0.9913	0.9915
31	0.07000	516240	294.20	63.30	2.578	2.607	-7.882	0.9918	0.9919
32	0.07264	617560	277.40	60.00	2.543	2.571	-7.744	0.9923	0.9923
33	0.07630	862784	248.70	48.70	2.483	2.501	-8.043	0.9929	0.9928
34	0.07676	1012864	240.70	48.00	2.467	2.477	-8.240	0.9930	0.9929
35	0.07620	1268163	236.80	44.80	2.463	2.478	-8.488	0.9931	0.9930
36	0.07658	1403215	236.80	46.70	2.466	2.470	8.857	0.9931	0.9931
37	0.07697	1882642	234.00	42.50	2.458	2.463	9.083	0.9932	0.9931
38	0.07716	2303756	232.70	40.40	2.446	2.458	-8.363	0.9932	0.9932
39	0.07730	3044244	231.80	40.80	2.444	2.457		0.9933	0.9932
40	0.07734	4481700	231.30	40.10	2.443	2.456		0.9933	0.9932
41	0.07740	6351656	230.80	33.80	2.442	2.454		0.9933	0.9932
42	0.07743	8705136	230.60	26.00	2.441	2.454		0.9933	0.9932
43	0.07747	7860486	230.30	27.10	2.441	2.453		0.9933	0.9932
44	0.07749	8877703	230.20	26.00	2.440	2.453		0.9933	0.9932
45	0.07752	10663846	229.90	26.10	2.440	2.452		0.9933	0.9932
46	0.07756	12945033	229.70	26.40	2.439	2.452		0.9933	0.9933
47	0.07760	15007236	229.50	26.00	2.438	2.451		0.9933	0.9933

Table A21. Mode I fatigue data obtained from a DCB joint made from a thermosetting composite substrate (i.e 913C XAS-5-47%) bonded with a one-part hot-cure epoxy film adhesive (i.e "FM73M").

Notes:

thickness h = 7.61 mm (46 plies)
width B = 25.16 mm
L_1 (Figure 4.4) = 13.04 mm
L_2 (Figure 4.4) = 9.11 mm
frequency, f = 5 Hz
DR = 0.5
MD = 1.5 mm
Test temperature = water at 50 °C
Test machine control mode: Displ.

All symbols and abbreviations shown are as defined in the nomenclature.

Specimen number 202

	1	2	3	4	5	6	7	8	9
1	crack length	no of cycles	max load	min load	log Gmax (disp)	log Gmax (comp)	log da/dN	Z	F
2	a	N	Pmax	Pmin				correction	correction
3	(m)		(N)	(N)	(kJ/m^2)	(kJ/m^2)	(m/cycle)	factor	factor
4									
5	0.04540	1000	700.40	252.40	3.247	3.250		0.0770	0.0007
6	0.04632	2420	707.80	262.40	3.224	3.245		0.0788	0.0016
7	0.04674	3143	740.50	274.40	3.209	3.229		0.0793	0.0017
8	0.04746	3900	733.00	260.20	3.190	3.229	0.235	0.0800	0.0023
9	0.04787	5077	697.00	256.30	3.171	3.193	0.456	0.0804	0.0028
10	0.04870	6000	671.00	245.00	3.147	3.178	0.593	0.0812	0.0032
11	0.04918	10002	666.00	230.40	3.134	3.164	0.706	0.0818	0.0035
12	0.04966	15200	627.00	220.00	3.109	3.138	0.818	0.0821	0.0038
13	0.05139	20261	670.20	218.60	3.092	3.088	0.907	0.0833	0.0040
14	0.05157	33041	562.00	200.70	3.047	3.077	7.046	0.0837	0.0052
15	0.05268	40140	530.00	190.00	3.022	3.066	7.158	0.0844	0.0057
16	0.05321	57500	522.20	190.70	3.006	3.031	7.262	0.0846	0.0058
17	0.05368	68000	507.20	184.10	2.988	3.015	7.344	0.0850	0.0062
18	0.05407	89037	486.00	177.00	2.964	2.988	-7.426	0.0855	0.0066
19	0.05526	102000	474.50	172.20	2.950	2.978	7.431	0.0859	0.0068
20	0.05577	125022	461.10	168.10	2.934	2.960	7.496	0.0862	0.0072
21	0.05636	140003	463.00	167.00	2.923	2.961	-7.523	0.0866	0.0074
22	0.05714	161400	441.10	161.30	2.906	2.936	7.603	0.0868	0.0078
23	0.05740	186120	439.00	160.30	2.902	2.918	7.729	0.0871	0.0078
24	0.05820	200400	372.00	137.00	2.813	2.825	7.848	0.0884	0.0098
25	0.05884	420864	301.10	121.00	2.700	2.804	7.871	0.0887	0.0082
26	0.05160	473040	366.00	120.10	2.704	2.788	7.931	0.0900	0.0085
27	0.05237	530400	343.00	121.00	2.704	2.774	7.972	0.0902	0.0087
28	0.05781	583730	341.00	124.20	2.700	2.775	8.053	0.0904	0.0088
29	0.05460	647300	320.70	118.00	2.721	2.737	8.223	0.0901	0.0084
30	0.05497	844548	304.70	100.40	2.667	2.695	8.283	0.0902	0.0085
31	0.05651	1343007	291.00	100.70	2.666	2.670	8.430	0.0907	0.0010
32	0.05776	1720032	270.00	101.70	2.642	2.642	8.588	0.0911	0.0013
33	0.05810	1906836	270.00	99.00	2.637	2.621	8.668	0.0912	0.0014
34	0.05910	2500023	260.00	90.20	2.606	2.595	8.782	0.0916	0.0017
35	0.07015	5271170	261.00	83.10	2.564	2.571	8.863	0.0918	0.0018
36	0.07044	5863670	240.00	80.40	2.570	2.560	8.877	0.0918	0.0018
37	0.07102	6703534	233.10	82.00	2.543	2.517	8.991	0.0922	0.0023
38	0.07308	8704270	220.70	80.30	2.500	2.462	9.048	0.0926	0.0026
39	0.07456	9870670	210.10	77.20	2.483	2.468	9.022	0.0926	0.0028
40	0.07571	10803702	210.30	77.70	2.477	2.463	9.223	0.0931	0.0030
41	0.07580	10941274	207.70	77.00	2.471	2.442	9.029	0.0931	0.0030
42	0.07586	10003460	206.70	77.50	2.469	2.438	10.003	0.0931	0.0031
43	0.07589	11721007	206.50	77.10	2.468	2.438	10.456	0.0931	0.0031
44	0.07591	12041223	206.40	76.70	2.468	2.438	-10.514	0.0931	0.0031
45	0.07593	13000300	206.20	76.60	2.467	2.437	10.637	0.0931	0.0031
46	0.07597	13610670	206.00	77.00	2.466	2.436	10.695	0.0931	0.0031
47	0.07600	15000350	206.00	76.30	2.466	2.436	-10.736	0.0931	0.0031
48	0.07602	15340453	206.00	76.00	2.466	2.436	-10.747	0.0931	0.0031
49	0.07606	20011070	206.50	76.20	2.466	2.436	-10.738	0.0931	0.0031
50	0.07608	21000007	206.40	76.30	2.465	2.436		0.0931	0.0031
51	0.07611	23000400	206.10	76.00	2.464	2.433		0.0931	0.0031
52	0.07612	23000104	206.00	76.00	2.464	2.433		0.0931	0.0031

Table A22. Mode I fatigue data obtained from a DCB joint made from a thermosetting composite substrate (i.e 913C XAS-5-47%) bonded with a one-part hot-cure epoxy film adhesive (i.e "FM73M").

Notes:

- **thickness h = 5.87 mm (48 plies)**
- **width B = 24.67 mm**
- **L_1 (Figure 4.4) = 12.19 mm**
- **L_2 (Figure 4.4) = 9.17 mm**
- **frequency, f = 5 Hz**
- **DR = 0.5**
- **MD = 1.5 mm**

Test temperature = 23 °C (air)

Test machine control mode: Displ.

All symbols and abbreviations shown are as defined in the nomenclature.

Specimen number 283

	1	2	3	4	5	6	7	8
1	crack length	no of cycles	max. load	min. load	log Gmax (displ)	log da/dN	Z	F
2	a	N	Pmax	Pmin			correction	correction
3	(m)		(N)	(N)	(kJ/m^2)	(m/cycle)	factor	factor
4								
5	0.05196	460	480.70	163.60	2.837		0.9842	0.9859
6	0.05444	803	462.30	160.00	2.807		0.9858	0.9871
7	0.05463	1290	420.60	155.90	2.765		0.9860	0.9872
8	0.05522	1690	443.50	153.80	2.765	-5.713	0.9863	0.9875
9	0.05604	1990	435.50	151.50	2.773	-5.860	0.9868	0.9879
10	0.05683	2378	431.30	150.20	2.765	-5.894	0.9872	0.9882
11	0.05742	3070	425.90	149.10	2.757	-6.115	0.9875	0.9884
12	0.05784	4928	418.40	145.70	2.745	-6.340	0.9877	0.9886
13	0.05854	6367	410.60	144.70	2.736	-6.466	0.9880	0.9889
14	0.05924	8270	404.60	142.70	2.726	-6.612	0.9883	0.9891
15	0.05980	11380	398.60	140.90	2.717	-6.800	0.9886	0.9893
16	0.06028	19260	390.70	139.70	2.708	-7.027	0.9888	0.9895
17	0.06050	27490	381.70	138.30	2.695	-7.165	0.9889	0.9896
18	0.06229	43620	370.00	133.80	2.673	-7.322	0.9896	0.9902
19	0.06348	90410	354.40	129.90	2.649	-7.477	0.9900	0.9905
20	0.06422	126063	344.50	126.80	2.634	-7.669	0.9903	0.9908
21	0.06549	175353	334.50	122.80	2.615	-7.929	0.9907	0.9911
22	0.06659	389975	316.30	117.90	2.586	-8.241	0.9911	0.9914
23	0.06784	572262	303.80	114.90	2.564	-8.527	0.9914	0.9917
24	0.06802	1314828	290.30	113.90	2.543		0.9915	0.9918
25	0.06828	1898088	281.00	111.40	2.528		0.9916	0.9918
26	0.06832	2735303.00	275.00	106.90	2.518		0.9916	0.9918

Notes:

thickness h = 6.15 mm (48 plies)
width B = 24.30 mm
L_1 (Figure 4.4) = 12.13 mm
L_2 (Figure 4.4) = 9.10 mm
frequency, f = 5 Hz
DR = 0.5
MD = 1.5 mm
Test temperature = 23 °C (air)
Test machine control mode: Displ.

All symbols and abbreviations shown are as defined in the nomenclature.

Table A23. Mode I fatigue data obtained from a DCB joint made from a thermosetting composite substrate (i.e "913C XAS-5-47%") bonded with a one-part hot-cure epoxy film adhesive with no mat-carrier (i.e "FM73").

Specimen number 284

	1	2	3	4	5	6	7	8
1	crack length	no of cycles	max load	min load	log Gmax (displ)	log da/dN	Z	F
2	a	N	Pmax	Pmin			correction	correction
3	(m)		(N)	(N)	(kJ/m^2)	(m/cycle)	factor	factor
4								
5	0 04534	1978	617 20	180 99	3 019		0 9795	0 9815
6	0 04611	2381	570 90	166 40	2 971		0 9793	0 9821
7	0 04662	2745	553 00	160 00	2 954		0 9798	0 9825
8	0 04812	3096	536 00	155 10	2 932	-5 535	0 9812	0 9835
9	0 04893	3387	523 60	150 70	2 917	-5 547	0 9820	0 9841
10	0 05040	3630	508 20	146 70	2 899	-5 545	0 9831	0 9850
11	0 05089	4070	494 00	142 80	2 882	-5 683	0 9835	0 9852
12	0 05141	4430	485 40	141 10	2 871	-5 818	0 9839	0 9856
13	0 05212	5027	474 00	137 50	2 856	-6 292	0 9844	0 9860
14	0 05257	5650	466 90	134 90	2 847	-6 327	0 9847	0 9862
15	0 05329	9950	427 60	123 80	2 806	-6 425	0 9852	0 9866
16	0 05602	14980	402 30	115 60	2 784	-6 548	0 9868	0 9879
17	0 05681	19460	390 50	111 80	2 747	-6 983	0 9872	0 9882
18	0 05802	27320	378 20	108 10	2 727	-7 298	0 9878	0 9887
19	0 05920	79430	345 40	99 40	2 682	-7 556	0 9893	0 9901
20	0 06184	182886	319 80	92 40	2 637	-7 765	0 9904	0 9909
21	0 06304	392200	310 60	96 20	2 617	-8 001	0 9899	0 9904
22	0 06428	491338	291 50	83 70	2 584	-8 112	0 9903	0 9908
23	0 06530	584736	300 00	83 30	2 581	-8 262	0 9907	0 9911
24	0 06553	685713	290 50	83 10	2 581	-8 494	0 9908	0 9911
25	0 06597	1035168	285 70	80 70	2 567		0 9909	0 9912
26	0 06656	1382078	284 90	83 10	2 563		0 9911	0 9914
27	0 06730	2127778	272 40	80 30	2 540		0 9913	0 9916

Notes:
thickness h = 6 09 mm (48 plies)
width B = 24 58 mm
L_1 (Figure 4 4) = 12 35 mm
L_2 (Figure 4 4) = 0 16 mm
frequency, f = 5 Hz
DR = 0 5
MD = 1.5 mm
Test temperature = 23 °C (air)
Test machine control mode: Displ.

All symbols and abbreviations shown are as defined in the nomenclature.

Table A24. Mode I fatigue data obtained from a DCB joint made from a thermosetting composite substrate (i.e "913C XAS-5-47%") bonded with a one-part hot-cure epoxy film adhesive with no mat-carrier (i.e "FM73").

APPENDIX B

EFFECTIVE MODULUS OF A DCB BONDED JOINT

The effective stiffness, Φ, of a sandwich beam may be estimated from an expression of the form (Williams 1980):

$$\Phi = \frac{Bd^3}{12} \cdot E_s \left\{ 4 - 4\left(\frac{E_s - E_a}{E_s}\right)\left(\left(1 - \frac{h_2}{d}\right)^3 - \left(\frac{h_1}{d}\right)^3\right) - \frac{\left[3\left(1 - \left(\frac{E_s - E_a}{E_s}\right)\left(\left(1 - \frac{h_2}{d}\right)^2 - \left(\frac{h_1}{d}\right)^2\right)\right)^2\right]}{\left[1 - \left(\frac{E_s - E_a}{E_s}\right)\left(1 - \left(\frac{h_1}{d} + \frac{h_2}{d}\right)\right)\right]} \right\} \qquad (B1)$$

For the case applied to the DCB joint the above variables are defined as:

B = width of specimen

h_1 = thickness of the lower arm of the substrate

h_2 = thickness of the upper arm of the substrate

t_a = thickness of the adhesive

E_s = substrate modulus

E_a = adhesive modulus and

d = the thickness of the DCB specimen (i.e $h_1 + h_2 + t_a$)

For a typical case of an epoxy film adhesive (e.g "FM73M") bonding a thermoplastic substrate (e .g "APC-2") when the thickness of the arms of the DCB specimen are equal, the numerical values of the above variables are

Es = 125 GPa, Ea = 3 Gpa, B = 25 mm, $h_1 = h_2 = 1.5$ mm, and $t_a = 0.5$ mm.

And when the above variables are substituted into Equation B1, Then $\Phi = 7.1139$

Now the stiffness of composite substrate, Φ_s, is given by the expression

$$\Phi_s = E_s I = \frac{BE_s(h_1 + h_2)^3}{12} \qquad (B2)$$

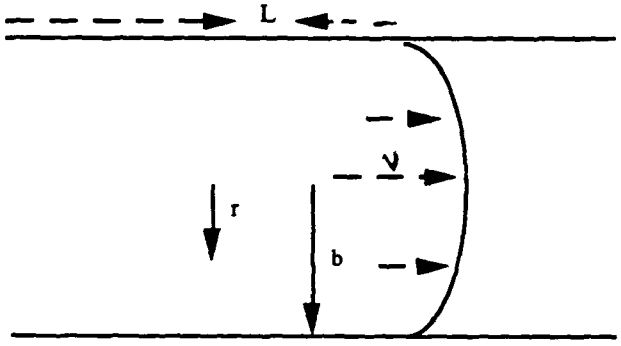
substituting the relevant values, $\Phi_s = 7.031$

Hence the stiffness of the DCB bonded joint is greater the stiffness of the composite substrate by 1.18%. The above calculation are consistent with the experimental observations reported in section 4.3.2. By using equation 4.19 to analyse the experimental data, the average value of the specimen modulus was 128.46 GPa while the modulus of the composite was given (ICI 1988) as 125 GPa. This corresponds to a difference of 2.76%.

APPENDIX C

SPEED OF WATER ALONG THE DIRECTION OF CRACK PROPAGATION

The velocity profile of a liquid (water) flowing into the crack tip plastic zone between two parallel fibre-polymer composite plates (assuming the composite material is impermeable to water) is given by:



$$v = \frac{P}{4\eta L} \cdot (2b^2 - 2r^2) \qquad (C1)$$

where

P = Pressure of flow

η = viscosity of water

b = half the size of the crack tip opening displacement given by:

$$b = \frac{G_{1c}}{\sigma_y} \tag{C2}$$

where G_{1c} is the fracture energy of the adhesive and σ_y is the adhesive yield stress.

The amount of water flowing per unit width per unit time, φ, is given by:

$$\varphi = \frac{P}{4\eta L} . (2b^2 - 2r^2) \tag{C3}$$

The total flow per unit time in the full width of crack opening displacement, ϕ, is given by:

$$\phi = \frac{P}{4\eta L} . \int_0^b (2b^2 - 2r^2)\, dr \tag{C4}$$

integrating

$$\phi = \frac{Pb^3}{3\eta L} \tag{C5}$$

for a liquid flowing between two parallel plates

$$P = \frac{2\gamma}{2b} \tag{C6}$$

where γ = the interfacial tension between the liquid and the crack face. If it is assumed that the crack face is of high energy, then γ is the surface free energy between the water and the adhesive.

Substituting Equation C5 into C4:

$$\phi = \frac{\gamma b^2}{3\eta L} \qquad \text{(C7)}$$

However

$$\phi = \frac{dx}{dt} . 2B \qquad \text{(C8)}$$

where dx/dt is the speed of the liquid along the crack.

Hence

$$\frac{dx}{dt} = \frac{\gamma b}{6\eta L} \qquad \text{(C9)}$$

substituting the following numerical values into Equation C9,

i.e G_{1c} = 5.72 kJ/m^2, σ_y = 31 MPa, γ = 27.92 x 10^{-3} J/m^2 (Kodokian 1989), η = 0.894 Pa.s (i.e for water at 25 ^oC), L = 84.67 x10^{-3} (i.e crack length at near threshold region).

$$\frac{dx}{dt} = 5.67 \times 10^{-6} \text{ m/s}$$

The above estimated value of dx/dt was much greater than the da/dt even at the beginning of the fatigue test when da/dt is highest (i.e da/dt from specimen number 125 = 4.55 x 10^{-6} m/s). Hence the speculation that the crack may be moving cohesively at a faster rate than the rate of water ingression into the plastic zone cannot be justified.

APPENDIX D

ESTIMATION OF THE SERR FROM A SINGLE LAP JOINTS

The maximum value of the peel stress at the end of the overlap in a Single Lap Joint was determined by Hart -Smith (1985) as:

$$\sigma_{max} = M_e \left(\frac{E_a}{2\, t_a\, X}\right)^{1/2} \qquad \text{(D1)}$$

where

E_a = modulus of the adhesive

t_a= thickness of the adhesive layer

and the value of the bending stiffness X and bending moment M_e are obtained from the equations below

$$X = \frac{E_s\, h^3}{12(1-\mu^2)} \qquad \text{(D2)}$$

where

E_s = modulus of the substrate

h = thickness of the substrate

μ = poissons ratio of the substrate

and

$$M_e = 0.5\,K\,T\,(h+t_a) \qquad (D3)$$

where

T = applied tensile load per unit width

c = half the bonded overlap in the direction of the applied load

and

K is the bending moment factor given by

$$K = \frac{1}{\left(1 + \varepsilon c + \frac{\varepsilon^2 c^2}{6}\right)} \qquad (D4)$$

where

$$\varepsilon = \left(\frac{T}{X}\right)^{1/2} \qquad (D5)$$

The bending moment factor, K, (equation 8.21) was later modified by Adams (1990) to give a more accurate result closer to similar results obtained by finite element analysis. Adams 'bending moment factor' is given as:

$$K = \frac{1}{1 + \varepsilon c} \qquad (D6)$$

equation 8.20 was substituted into 8.23 to give:

$$M_e = \frac{T\,(h + t_a)}{2\,(1 + \varepsilon c)} \qquad (D7)$$

Williams (1988) proposed a very powerful method using the simple beam theory to estimate the mode I fracture energy, G_{max}, from a knowledge of the bending moment at the crack tip of cracked laminates made from thin sheets. Since the beam theory analysis applied to composite laminate have also been found to be adaptable to bonded composite joints, Williams equation can be used to estimate the fracture energy in a Single Lap Joint due to the presence of bending moments at the end of the overlap.

By Williams equation,

$$G_{max} = \left(\frac{6}{B^2 E_s}\right)\left(\frac{h_1^3}{h_2^3\,(h_1^3 + h_2^3)}\right)\left(M_2 - \left(\frac{h_2}{h_1}\right)^3 M_1\right)^2 \qquad (D8)$$

where

h_1 and h_2 = the thicknesses of the upper and lower substrate

M_1 and M_2 = bending moment in the upper and the lower substrate

E_s = modulus of the substrate

B = width of the substrate

If $h_1 = h_2$, then $M_1 = M_2$, and equation 8.25 simplifies to become:

$$G_{max} = \frac{12\,M^2}{B^2\,E_s\,h^3} \qquad (D9)$$

equation 8.24 is substituted into equation 8.26 to give:

$$G_{max} = \frac{12}{E_s\,h^3}\left(\frac{T\,(h + t_a)}{2}\right)^2\left(\frac{1}{(1+\varepsilon c)^2}\right) \qquad (D10)$$

REFERENCES

Adams & Peppiatt (1974) — Adams, R. D., and Peppiatt N. A., (1974), "Stress analysis of single lap joints", Journal of Strain Analysis, vol 9, no.3.

Adams et al (1987) — Adams D. F., Zimmerman R. S., and Odom E. M., 1987) "Frequency and load ratio effects on the critical strain energy release rate thresholds of graphite/epoxy composites", Toughened Composites, ASTM STP 937, Norman J. Johnston Ed. pp 242-259.

Adams (1989) — Adams, R. D., (1989), "Strength predictions for lap joints, especially with composite adherends. A Review", J. Adhesion, vol 30, pp. 219-242.

Adams (1990) — Zhao X., and Adams R. D., (1990), "A new method for determining the Bending Moment Factors in Single Lap Joints", Proceedings on Adhesion, Plastic and Rubber Institute, 4th International Conference, Cambridge, England.

Allman (1976) — Allman D.J., (1976), "A theory for elastic stresses in adhesively bonded joints", Royal Aircraft Establishment, TR76024.

Althof (1966) — Althof W., (1966), "The strength of bonded single lap metal joints subjected to fatigue loading at room temperature and at 100°C", DLR-FB 66-47, Royal Aircraft Establishment Library Translation No. 1207.

Arad (1971) — Arad S., Radon J. C., and Culver L. E., (1971), Journal of Mechanical Engineering Science, vol 13, pp 75-81.

ASME (1986), — American Society for Mechanical Engineers, (1986), "Rules for In-service inspection of nuclear power plant components", Boiler Pressure Vessels Code, Section XI, USA.

ASTM E-399 (1981) — ASTM E-399 81, (1981), "Plain strain fracture toughness of metallic materials"

ASTM E647-88 — ASTM E 647-88 (1988), "Standard test method for measurement of fatigue crack growth rates".

ASTM D1002-72 — ASTM D1002-72 (*Reapproved* 1983) "*Standard test method for* strength properties of adhesives in shear by tension loading (metal to metal)".

Bathias & Laskimi (1985) — Bathias C., and Laskimi A., (1985) "Delamination threshold and loading effect in fiber glass epoxy composite" Delamination and Debonding of Materials, ASTM STP 876, pp 217-237.

Backlund (1982) — Backlund J., Blom A. F., and Beevers C. J., (1982), "Fatigue threshold fundamentals and Engineering applications" Engineering Materials Advisory Services Ltd, Chamelon Press, London.

Barsom (1973) — Barsom J. M., (1973), "Fatigue crack growth under variable amplitude loading in ASTM A514 Grade B Steel", ASTM STP 536.

Barsom (1987) Rolfe S. T., and Barsom J. M., (1987), Fracture and fatigue control in structures, Applications of fracture mechanics, Prentice Hall inc., Englewood Cliffs, New Jersey.

Bascom et al (1976) Bascom W. D., and Cottington R. L., (1976), J. Adhesion, 7, pp 333.

Beaumont (1985) Ogin, S. L., Smith P. A., and Beaumont, P. W. R., (1985), "Matrix cracking and stiffness reduction during fatigue of $(0/90)_s$ GFRP laminate", Comp. Sci. and Tech., 22, pp 23-31.

Beaumont (1986a) Evans A. G., Ahmad A. B., Gilbert D. G., and Beaumont P. W. R., (1986a), Acta Metall., 34, pp 79.

Beaumont (1986b) Poursartip,A., and Beaumont, P. W. R., (1986b), "The fatigue damage mechanics of carbon fibre composite laminates: II-life prediction", Composite Science and Tech., 25, p 283-299.

Berry (1963) Berry J. P., (1963), J. Polym. Sci., A1, pp 993.

Boogaart (1966) Van de Boogaart A., (1966), "Physical basis of yield and fracture", Inst. Phys. London, pp 167.

Bradley et al (1980) Bradley W. L., Schapery R. A., and DEvitt D. F., (1980), J. Comp. Mat., 14, pp 270.

Brinson & Sancaktar (1980) Brinson H. F., and Sancaktar E., (1908), "The viscoelastic shear behaviour of structural adhesives", Adhesion and Adsorption of Polymers", L. H. Lee Ed., Polymer Science & Technology Series, 12-A, Plenum Pub. pp 279-300.

Brinson et al (1975) Brinson H. F., Renieri M. P., and Herakovich C. T., (1975), "Rate and time dependent failure of structural adhesives" ASTM STP 593, pp 177-199.

Broek (1986) Broek D., (1986), Elementary Engineering Fracture Mechanics, Kulwer Academic Publishers, Lancaster, U.K.

Broek (1989) Broek D., (1986), The practical use of Fracture Mechanics, Kulwer Academic Publishers, Lancaster, U.K.

Broutman (1965) Broutman L. J., and McGarry F. J., (1965), J. Appl. Polym. Sci., 9, pp 585.

Broxterman (1989) Phillips P. G., and Broxterman W. E., (Aug. 1989) "Adhesive and sealants in autos to grow at 250% of GNP" Adhesives Age, pp 38

BSI (1980) British Standard Institution, PD 6493 (1980), "Guidance on some methods for the derivation of Acceptance levels for defects in fusion welded joints".

Bucknall (1972) Bucknall C. B., Clayton D., and Keast W. E., (1972), J. Mater. Sci., 7, pp 1443.

Cardrick (1986) Cardrick A. W., Maxwell R. D. J., and Morrow S. M., (1986), "How future UK. military aircraft will be designed for tolerance to fatigue damage", Fatigue of Engineering Materials and structures, Mechanical Engineering Publications.

CEGB (1986) Central Electricity Generating Board, May 1986, Report R/H/R6, Rev 3, U.K., "Assessment of the integrity of structures containing defects".

Chen et al (1987) Chen N. N. S., Niem P. I. F., and Lee R. C., (1987), "Fatigue behaviour of adhesively bonded joints", J. ASdhesion, vol 21, pp 115-128.

Ciba Geigy (1988) Ciba Geigy (1988), Private communication: Bonded Structures Division, Ciba Geigy Plastics and Additives Co., Cambridge, UK.

Chudnovsky (1984) Chudnovsky A., (1984), NASA Contractor Report, 174634.

Clark (1992) Clark S., (1992), "An introduction to the altrasonic inspection of composites" Proceedings of a Course on Non Distructive Testing of Composite Materials held at Imperial College Centre for Composite Materials, 28th -30th Jan. 1992.

Comyn (1983) Comyn J., (1983), Durability of structural adhesives, A. J. Kinloch Ed., Applied Sci. Pub., Barking, Essex.

Comyn (1987) Comyn J., Brewis D. M., Tredwell S. T., (1987), J. Adhesion, 21, pp 59.

Comyn (1989) Comyn J., (1989), "A review of certain recent work on the durability of alumminium alloy bondedwith epoxide and phenolic adhesives", J. Adhesion, vol 29, pp 121-130.

Crocombe (1987) Crocombe A. D., (1987), "The effect of the adhesive thickness on the strength of a bonded joint", Adhesion 12, Ed. K. W. Allen, Elsevier Applied Sci.Pub., pp176-192.

Culver (1974) Radon C. M., Arad J. C., and Culver L. E., (1974), Engineering Fracture Mechanics, 6, pp 195-208.

Cynamid (1988) Cynamid (1988), Private communication: American Cynamid Co.Maryland, U. S. A.

Donaldson & Mall (1989) Donaldson S. L., and Mall S., (1989) "Delamination growth in graphite/epoxy composite subjected to mode III loading", Journal of Reinforced Plastics and Composites, vol 8, pp 91-103.

Davidson (1990) Davidson B. D., (1990), "An analytical investigation of delamination front curvature in DCB specimens", J. Comp. Materials, vol 24, pp 1124-1137.

Davis (1990) Davis R. D. (1990), "The durability of adhesively bonded aluminium alloy", Ph.D Thesis, Mech. Engin. Dept, Imperial College London.

De Vreis et al (1977) De vries K. L., Bennett S. J., and Anderson G. P., (1977), Analysis and Testing of Adhesive Bonds, Academic Press, New York, pp 58.

Djavanroodi (1989) Djavanroodi F., (1989), "Creep and Creep-Fatigue crack growth ", Ph.D Thesis, Mech. Engin. Dept, Imperial College London.

Donald (1982) Donald A. M., and Kramer E. J., (1982), J. Mater. Sci., 17, pp 1871.

ECCS (1985) European Convention for Constructional Steelwork, (1985 Oct), "Recommendations for fatigue design of steel structures", Technical Committee 6-Fatigue, ICOM 150.

Elber (1976) Elber W., (1976), "Equivalent constant amplitude concept for crack growth under spectrum loading", ASTM STP 595, Fatigue crack growth under spectrum loads, pp 236-250.

Ewalds (1984) Ewalds H. L., and Wanhill R. J. H., (1984), Fracture Mechanics, pp 174, Edward Anold (Publishers) Ltd., Baltimore, Maryland, 21202 USA.

Everett et al (1985) Everett Jr. R. A., and Johnson W. S., (1985), Delamination and Debonding of Materials, ASTM STP 876, W. S. Johnson Ed., Phil., pp 267-281

Everett et al (1987) Everett Jr. R.A., Johnson W.S., Mangalgiri P. D., (1987) "Effect of adherend thickness and mixed mode loading on the debond growth in adhesively bonded composite joints", J. Adhesion, vol 23, pp 263-288.

Feddersen et al (1973) Feddersen C. E., and Davies K. B., (1973) "Evaluation of fatigue crack growth rates by polynimial curve fitting", Int. Journal of Fracture, 9, pp 116

Forman (1967) Forman R. G., Kearing V. E., Engle R. M., (1967), Trans. ASME, Journal of Basic Engineering, vol 89, pp 459-464.

Gent et al (1971) Gent A. N., and Kinloch A. J., (1971), J. Polymer Sci., A2, 9, pp 659.

Gibala (1982) Gibala R., Serrano A. M., and Welsch G. E., (1982), Polymer Engineering Sci., 22, pp 934.

Grant FH15 (1988) Grant FH15 (1988), Grant instruments LTD., Barrington, Cambridge, CB2 5QZ, England.

Griffith (1921) Griffith A. A., (1921), "The phenomina of Rupture and flaws in solids", Phil. Trans. Roy. Soc., A221, pp163 - 197.

Gorbatkina (1991) Gorbatkina J. A., and Shaidurova N. K., (1991), "Effect of Aging in water on the strength of fibre-polymer systems", J. Adhesion, vol 35, pp 203-215.

Guess et al (1977) Guess T. R., Allred R. E. and Gerstle F. P. Jr, (1977), "Comparison of lap shear specimens", Journal of Testing and Evaluation, vol 5, no 2, pp 84-93.

Hart-Smith (1973) Hart-Smith L. J., (1973), "Adhesively-bonded single lap joints", NASA Langley Research Centre Report, NASA CR 112236, Hampton, VA..

Hart-Smith (1985) — Hart-Smith L. J., (1985), "Designing to minimise peel stresses in adhesively bonded joints", Delamination and Debonding of materials, ASTM STP 876, W. S., Johnson Edition, American Society for Testing Materials, Philadelphia, pp 238-266.

Hart-Smith (1985a) — Hart-Smith L. J., (April 1985) "Bonding aircraft does work", Adhesives Age, pp 24 -26.

Hunston (1983) — Kinloch A. J., Shaw S. J., Tod D. A., and Hunston D. L., (1983) Polym, 24, pp 1341.

Hwang et al (1986) — Hwang W., and Han K.S., (1986), Journal of Composite Materials, vol 20.

Hwang et al (1986) — Hwang W., and Han K.S., (1986), Composite Materials, Fatigue and Fracture, Second volume, ASTM STP 1012, Paul Lagace Ed., pp 87-102.

Hysol (1988) — Hysol (1988), Private communication: Hysol Aerospace and Industrial Division, Pittburg, U.S. A.

ICI (1988) — ICI (1988), Private communication: Advanced Materials Business Group, ICI, Welwyn Garden City, UK.

Irwin (1964) — Irwin G. R., (1964), Applied Mats. Res., 3, pp 65.

Jablonski (1980) — Jablonski D. A., (1980), "Fatigue crack growth in structural adhesives", J. Adhesion, vol II, pp 125-143.

Jemian & Ventrice (1969) — Jemian W. A., and Ventrice M. B., (1969), "The fracture toughness of adhesively bonded joints", J. Adhesion, vol 1, pp 190-207.

JSM 5300 (1991) — JEOL JSM 5300, (1991), JEOL (U.K) LTD., JOEL House, Silver court, Watchmead. Welwyn, Garden City, Herts.

Johnson (1983) — Johnson W. S., (1983), "Modelling Stiffness loss in Boron/Aluminium laminates below the fatigue limit", Long Term Behaviour of Composites, ASTM STP 813, T. K. O' Brien Ed. American Society for Testing Materials, pp 160-176.

Johnson & Mall (1988) — Johnson W. S., and Mall S., (1988), "Debonding characteristics of adhesively bonded woven kevlar composites", ASTM STP 981, W. S. Johnson edition, pp 194-206.

JWES (1980) — Japan Welding Engineering Society, (1976), 1st Revision 1980, "Method of assessment of defects in fusion welded joints with respect to brittle fracture".

Kambour (1973) — Kambour R. P., (1973), J. Polym. Sci, Macromol. Rev., 7.

Kenig at al (1989) — Kenig S., Dodiuk H., and Sharon G., "Effect of loading rate and temperature on the mechanical properties of structural adhesives containing a carrier" J. Adhesion, !1989), vol 31, pp 21-31.

Kilik et al (1989) — Kilik R., and Davis R., (1989), "Mechanical properties of adhesives filled with metal powders", Int. Journal of Adhesion and Adhesives, vol. 9, pp 224-228.

Kinloch et al (1973a) — Kinloch A. J., and Andrews E. H., (1973), Proc. Roy. Soc., A332, pp 385.

Kinloch et al (1973b) — Kinloch A. J., and Andrews E. H., (1973), Proc. Roy. Soc., A332, pp 401.

Kinloch et al (1974) — Kinloch A. J., and Andrews E. H., (1974), J. Polymer Sci., Symp., 46, pp 1.

Kinloch (1983) — Kinloch A. J., and Young R. J., (1983), Fracture Behaviour of Polymers, Elsevier Applied Science Publishers, London.

Kinloch 1986) — Kinloch A. J., (1986), Strutural Adhesives in Engineering, A. J. Kinloch Ed., Elsevier Applied Sci. Pub., London, pp 127.

Kinloch (1987) — Kinloch A. J., (1987), Adhesion and Adhesives Science and Tech., Chapman and Hall Ltd, London.

Kinloch & Kodokian — Kinloch A. J. and Kodokian G. K. A, (1989), "The adhesive fracture energy of bonded thermoplastic fibre composite", J. Adhesion, vol 29, pp 193-218.

Kinloch (1989) — Kinloch A. J., (1989), "Comments on the fatigue performance of structural adhesives" J. Adhesion, vol 30, pp 83-84.

Klesnil (1972) — Klesnil M., Lukas P., (1972) Engineering fracture mechanics, vol 4, pp 77-92.

Kodokian (1989) — Kodokian G. K. A., (1989), "The adhesive bonding of thermoplastic composite", Ph.D thesis, Mech. Engin. Dept, Imperial College London.

Knauss (1973) — Knauss W. G., (1973), Appl., Mech., Rev., vol 26, pp 1-17.

Knauss (1991) — Knauss W. G., (1991), "The effect of scrim material on the elasticity of adhesives under tension" J. Adhesion, vol 33, pp 185.

Knott (1973) — Knott J. F., (1973), "Fundamentals of fracture machanics", Butterworths and co. Ltd, London.

Kramer & Henkee (1984) — Kramer E. J., and Henkee C. S., (1984), J. Polymer Sci., Polymer Physics Ed., 22, pp 721.

Kutz (1986) — Kutz M., (1986), Mechanical Engineers Handbook, Pub., John Wiley and Sons, New York.

Langer (1962) — Langer B. F., "Design of pressure vessels for low cycle fatigue ", J. Basic Engineering, 84, 3, pp 389.

Laskimi & Bathias (1985) — Bathias C., and Laskimi A., (1985) "Delamination threshold and loading efect in fiber glass epoxy composite" Delamination and Debonding of Materials, ASTM STP 876, pp 217-237.

Lee (1991) — Lee, L. J., Yang J. N., and Shey D. Y., (1991), "Prediction of the fatigue life for matrix dominate composite laminates", Proc. of the 8th Int. Conference on Composite Materials, S. W. Tsai., and G. S. Springer Ed., Honolulu, pp 38-L-1.

Liechti (1987) — Liechti K. M., and Lin C., (1987) "Similarity concepts in the fatigue fracture of adhesively bonded joints", J. Adhesion, vol 21, pp 1-24.

Liu (1961) — Liu H. W., (1961), "Crack propagation in thin metal sheets under repeated loading", Trans. ASME, (Ser D), 83, pp 23 - 31.

Luckyram & Vardy (1988) — Luckyram J., and Vardy A. E., (1988) "Fatigue performance of two structural adhesives", J. Adhesion, vol 26, pp 273-291.

Luckyram & Vardy (1989) — Luckyram J., and Vardy A. E., (1989) "Reply to comments on the Fatigue performance of two structural adhesives", J. Adhesion, vol 30, pp 85-86.

Mai et al (1979) — Mai Y-U, and Williams G., (1979), J. Material Sci., 14, pp 1933.

Mai et al (1985) — Mai Y-U., and Atkins A. G., (1985), Elastic Plastic Fracture, Ellis Horwood Pub. Ltd, Chichester, England.

Mall (1982) — Mall S., Johnson W. S., and Everett Jr. R. H., (1982), "Cyliic debonding in adhesively bonded composites', Adhesion Joints, K. L. Mittal Ed., Plenum Press, New York, pp 639-658.

Mall & Johnson (1985) — Mall S., and Johnson W. S., (1985), "A fracture mechanics approach to designing adhesively bonded joints" Delamination and Debonding of Materials, ASTM STP 876, W. S. Johnson Ed., Philadelphia, pp 189-199.

Mall & Johnson (1986) — Mall S., and Johnson W. S., (1986), "Characterization of mode I and mixed mode failure of adhesive bonds between composite adherends", ASTM STP 893, J. M. Whitney Ed., pp 322-334.

Mall & Yun (1987) — Mall S., and Yun K. T., (1987), "Effect of adhesive ductility on cyclic debond mechanism in composite to composite bonded joints", J. Adhesion, vol 23, pp 215-231.

Mall & Johnson (1988) — Mall S., and Johnson W. S., (1988), "Debonding characteristics of adhesively bonded woven kevlar composites", ASTM STP 981, W. S. Johnson edition, pp 194-206.

Mall et al (1988) — Mall S., and Kochhar N. K., (1988), "Characterisation of bebond growth mechanism in adhesively bonded composite under mode II static and fatigue loading", Eng. Frac. Mech., Vol 31, No 5, pp 747-758.

Mall et al (1989) — Mall S., Yun K., and Kochhar N. K., (1989), "Characterization of matrix toughness effect on the cyclic delamination growth in graphite fibre composites", Composite Materials: Fatigue and Fracture, Second Volume, ASTM STP 1012, Paul Laggace Ed., pp 296-310.

Mall & Ramamurthy (1989) — Mall S., and Ramamurthy G., (1989), "Effect of bond thickness on the fracture and fatigue strength of adhesively bonded composite joints", Int. Journal of Adhesion and Adhesives, vol 9, no 1, pp 33-37.

Martin & Murri (1990) — Martin, R. H., and Murri G. B., (1990), "Characterisation of Mode I and Mode II delamination growth and threshold in AS4/PEEK composites", Composite Materials: Testing and design, vol 9, ASTM STP 1059, S. P. Garbo Edition, American Society for Testing Materials, Philadelphia.

Maxwell (1971) — Maxwell, R. D. J., (1971 May), "The practical Implementation of fatigue requirements to military aircraft and helicopters in the United Kingdom", Proceedings of the 6th ICAF Symposium, Miami, NASA SP-309, pp 213-229.

Mayes (1988) — Mayes (1988), Private communication: W. H. Mayes and Sons LTD., (1988), Windsor, England.

McEvily (1959) — McEvily A. J., and Illg W., (1959), "A method for predicting the rate of fatigue crack propagation", ASTM STP 274, Fatigue of Aircraft Structures, pp 112 - 119.

McEvily (1983) — McEvily A. J., (1983), Fatigue Mechanisms: Advances in quantitative measurement of physical damage, ASTM STP 811, pp 283-312.

McMillan (1967) — McMillan J. C., and Pelloux R. M. N., (1967), "Fatigue crack propagation under program and random loads", ASTM STP 415.

Mostovoy (1975) — Mostovoy S., and Ripling E. J., (1975), Polymer Science and Technology B, 9B, Plenium Press, New York, pp 513-562.

Morgan (1977) — Morgan R. J., and O' Neal J. E., (1977), J. Mater. Sci, 12., pp 1966.

O'Brien et al (1989) — O'Brien T. K. O., and Martin R. H., (1989) 4th Tech. Conf.: Composite Materials and Systems, pp 257-267.

O' Brien et al (1991) — O'Brien T. K., Salpekar S. A., and Murri G. B., (1991), "Fatigue delamination onset prediction in unidirectional tapered laminates", Composite Materials: Fatigue and Fracture (Third Volume), ASTM STP 1110, T. K. O'Brien Ed., pp 312-339.

Orowan (1955) — Orowan E., (1955), "Energy criteria of fracture", Welding Journal, 34, pp 1575 - 1605.

Palmer (1980) — Charles W. J., and Palmer S. J., (1980), "Application of Structural adhesives in production", Adhesives and sealant division 3M (UK) Ltd. Swansea .

Parker et al (1982) — Parker B. M. and Waghorne R. M., (1982), J. Composite Materials, 13, pp 280.

Paris (1963) — Paris P. C., and Endogan F., (1963), "A critical analysis of crack growth laws", Trans. ASME, 85, pp528.

Paris (1972) Paris P. C., Bucci R, J., Wessel E. T., Clark W. G., and Mager T. R., (1972), "Extensive study of low fatigue crack growth rates in A533 and A508 steels", ASTM STP 513, American Society for Testing and Materials, Philadelphia, 1972.

Piggott (1991) Piggott M. R., and Lam P. W. K., (1991), "Fatigue and fracture processes in aligned carbon-epoxy laminates", Comp. Materials: Fatigue and Fracture (Third Vol.) ASTM STP 1110, T. K. O' Brien Ed., pp 686-695.

Pocius & Wenz (1985) Pocious A. V., and Wenz R. P., (1985), 30th National SAMPE symposium pp 1073.

Plumbridge (1972) Plumbridge W. J., (1972), J. Material Sci., 7, pp 939.

Prel et at (1989) Prel Y. J., Davis P., Benzeggagh M. L., and Charentenay F. X., (1989) Composite Materials Fatigue and Fracture, vol 2, ASTM STP 1012, Paul Laggace Ed., pp 251-268.

Radon (1984) Radon J. C., and Wachnicki C. R., Composites, (1984), vol 15, no. 3.

Radford (1971) Radford K. C., Journal of Material Science, (1971), , 6, pp 1286.

Reifnider (1986) Reifnider K. L., (1986), "Critical element concepts for residual strength and life prediction", Proc., 1st Conference of American Society for Comp., pp 387-403.

Ripling et al (1971) Ripling E. J., Mostovoy S., and Bersch C. F., (1971), J. Adhesion, 3, pp 145.

Ripling et al (1988) Ripling E. J., Crosley P. B., and Johnson W. S., (1988), "A comparison of pure mode I and mixed mode I & III cracking of an adhesive containing an open knit mat carrier" Adhesively Bonded Joints: Testing , Analysis and Design, ASTM STP 981, W. S. Johnson Ed., pp 163-182.

Roderick (1975) Roderick G. L., Everett Jr. R. A., and Crews Jr., (1975), "Debond propagation in carbon-reinforced metals", Fatigue of Composite Materials, ASTM STP 569,pp 295-306.

Rolfe (1977) Rolfe S. T., and Barsom J. M., (1977), Fracture and fatigue control in structures, Applications of fracture mechanics, Prentice Hall inc., Englewood Cliffs, New Jersey.

Sancaktar et al (1980) Sancaktar E., Dwight D. W., and Brinson H. F., (1980), "Failure Characteristics of Structural Adhesives" Adhesion and Adsorption of Polymers, L. H. Lee Ed., Plenum Pub. pp 141-164.

Sanders (1986) Sanders W. D., (Aug. 1986), "Bonding aircraft with wing panels improves weight and durability", Adhesives Age, pp 38 -40.

Schapery et al (1988) Schapery R. A., and Davidson B. D., (1988), "Effect of finite width on the deflection and energy release rate of an orthotropic double cantilever specimen", Journal of Composite Materials, vol 22, pp 640-656.

Schijve (1967)	Schijve J., (1967), Significance of fatigue cracks in micro-range and macro-range", ASTM STP 415.
Schmueser (1991)	Schmueser D. W, (1991), "A fracture mechanics approach to characterizing cyclic debonding of varied thickness adhesive joints to electroprimed steel surfaces", J. Adhesion, vol 36, pp 1-23.
Spicer (1990)	Spicer M., and Pankevicius E. R., Journal of Material Science, 25, pp 3079-3082.
Talreja (1980)	Talreja R., (1980), "Stiffness based fatigue damage characterisation of fibrous composite", Advances in Composite Materials, Ed. A. R. Bunsell, vol 2, Pergamon Press, Oxford.
Theocaris (1974)	Theocaris P. S., Paipetis S. A., and Tsangaris J. M., (1974), Polymer, 15, pp 441.
Thomas (1953)	Thomas A. G., and Rivlin R. S., (1953), J. Polymer Sci., 10, pp 291.
Tomkins (1966)	Tomkins B., (1966), "Physical basis of yield and fracture", Inst. Physics, London, pp 187.
Trintina (1972)	Trintina G. G., (1972), J. Comp. Mat., 6, pp 192.
USAF (1974)	USAF, (1974), July, Military Specification MIL-A-83444 "Airplane damage tolerance requirements".
vonEuw et at (1972)	vonEuw E. F. J., Hertzberg R. W., and Roberts R., (1972), "Delay effects in fatigue crack propagation", ASTM STP 513.
Walker (1970)	Walker E. K., (1970), "Effect of environments and complex load history on the fatigue life" ASTM STP 462, pp 1-14.
Weertman (1966)	Weertman J., (1966), International Journal of Fracture, vol 2, pp 460-467.
Weertman (1969)	Weertman J., (1969), International Journal of Fracture, vol 5, pp 13-15.
Wei et al (1974)	Wei R. P., and Shih T. T., (1974), "Delay in fatigue crack growth", International Journal of Fracture, 10, no 1.
Weitsman (1977)	Weitsman Y., (1977), J. Compos. Mater., 11, pp 378.
Westergaad (1939)	Westergaad H. M., (1939), "Bearing pressures and cracks", J. Applied Mechanics, A June, 46.
Willenborg et al (1971)	Willenborg J., Engle R. M., and Wood H. A., (1971), "A crack growth retardation model using an effective stress concept", AFFDL-TM-FBR-71-1.
Wheeler (1972)	Wheeler O. E., (1972), "Spectrum loading and crack growth, Trans., ASME (J. Basic Engng), 94, pp 181-186.

Whitcomb (1981) — Whitcomb J. D., (1981), Fatigue of Fibrous Composite Materials, ASTM STP 723, pp 48 - 63.

Whitcomb & Ramkumar (1985) — Whitcomb J. D., and Ramkumar R. L., (1985), "Characterisation of mode I and mixed mode delamination growth in T300/5208 graphite/epoxy",Delamination and Debonding of Materials, ASTM STP 876, W. S. Johnson Ed., Philadelphia, pp 315-335.

Williams (1980) — Williams J. G., (1980), Stress Analysis of Polymers, Ellis Horwood, Chichester, U.K.

Williams (1984) — Williams J. G., (1984), Fracture Mechanics of Polymers, Ellis Horwood, Chichester, U.K.

Williams (1987) — Williams J. G., (1987), "Fracture mechanics of polymers and adhesives", Fracture of non metallic Materials, Herrman K. P., and Larsson (eds), pp 227-255.

Williams (1988) — Williams, J. G., (1988), "On the calculation of strain energy release rates of cracked laminates", International Journal of Fracture, 36, pp 101-119.

Williams (1989) — Williams, J. G., (1989), "The fracture mechanics of delamination test", Journal of Strain Analysis, Vol 24, no 4.

Williams et al (1990) — Williams J. G., Hashemi S., and Kinloch A. J., (1990), "The analysis of interlaminar fracture in uniaxial fibre composites" Proc. R. Soc., London. A427, pp 173-199.

Winstone (1985) — Winstone M. R., Nikbin K. M., and Webster G. A. (1985), J. Mat. Sci., vol 20, pp 2471-2476.

Wood (1991) — Wood J. R., (1991), "Modelling the behaviour of gas bubbles in epoxy resin", Composite Design Manufac. and Application, Proceedings of the 8th International Conf. on Composite Materials, ICCM/8, Honolulu, July 15-19, 1991, Edited by Stephen Tsai and G. S. Springer, pp 10-m-3.

Young et al (1978) — Young R. J., Glenhill R. A., Kinloch A. J., and Yamini S., (1978), Polymer, 19, pp 574.

Young et al (1985) — Young R. J., Maxwell D., and Kinloch A. J., (1985), J. Material Sci., 4, pp 1276.